A&A, 685, A83 (2024)
https://doi.org/10.1051/0004-6361/202348438

Astronomy & Astrophysics

The *Gaia*-ESO Survey: Calibrating the lithium–age relation with open clusters and associations

II. Expanded cluster sample and final membership selection★,★★

M. L. Gutiérrez Albarrán[1], D. Montes[1], H. M. Tabernero[1,2], J. I. González Hernández[3,4], E. Marfil[1,5], A. Frasca[6], A. C. Lanzafame[7,6], A. Klutsch[8,6], E. Franciosini[9], S. Randich[9], R. Smiljanic[10], A. J. Korn[11], G. Gilmore[12], E. J. Alfaro[13], T. Bensby[16], K. Biazzo[17], A. Casey[20], G. Carraro[23], F. Damiani[15], S. Feltzing[16], P. François[22], F. Jiménez Esteban[14], L. Magrini[9], L. Morbidelli[9], L. Prisinzano[15], T. Prusti[21], C. C. Worley[19], S. Zaggia[18], and GES builders

(Affiliations can be found after the references)

Received 31 October 2023 / Accepted 27 January 2024

ABSTRACT

Context. The Li abundance observed in pre-main sequence and main sequence late-type stars is strongly age-dependent, but also shows a complex pattern depending on several parameters, such as rotation, chromospheric activity, and metallicity. The best way to calibrate these effects, and with the aim of studying Li as an age indicator for FGK stars, is to calibrate coeval groups of stars, such as open clusters (OCs) and associations.

Aims. We present a considerable target sample of 42 OCs and associations – with an age range from 1 Myr to 5 Gyr – observed within the *Gaia*-ESO survey (GES), and using the latest data provided by GES iDR6 and the most recent release of *Gaia* that was then available, EDR3. As part of this study, we update and improve the membership analysis for all 20 OCs presented in our previous article.

Methods. We perform detailed membership analyses for all target clusters to identify likely candidates, using all available parameters provided by GES, complemented with detailed bibliographical searches, and based on numerous criteria: from radial velocity distributions, to the astrometry (proper motions and parallaxes) and photometry provided by *Gaia*, to gravity indicators ($\log g$ and the γ index), [Fe/H] metallicity, and Li content in diagrams of (Li equivalent widths) EW(Li) versus $T_{\rm eff}$.

Results. We obtain updated lists of cluster members for the whole target sample, as well as a selection of Li-rich giant contaminants obtained as an additional result of the membership process. Each selection of cluster candidates was thoroughly contrasted with numerous existing membership studies using data from *Gaia* to ensure the most robust results.

Conclusions. These final cluster selections will be used in the third and last paper of this series, which reports the results of a comparative study characterising the observable Li dispersion in each cluster and analysing its dependence on several parameters, allowing us to calibrate a Li–age relation and obtain a series of empirical Li envelopes for key ages in our sample.

Key words. techniques: spectroscopic – stars: abundances – stars: activity – stars: late-type – stars: rotation – galaxies: clusters: general

1. Introduction

Lithium in the form of its main isotope ^{7}Li (henceforth Li) is mainly observable through the spectral resonance lines of neutral Li, forming a doublet at 6707.76 Å and 6707.89 Å (e.g., Pallavicini et al. 1992; Soderblom 2010; Lyubimkov 2016; Randich & Magrini 2021). Li is a very fragile element that is easily destroyed in stellar interiors, burning at temperatures above ∼2.5–3 × 10^6 K, which corresponds to the temperature at the base of the convective zone of a solar-mass star on the zero-age main sequence (ZAMS; e.g., Pallavicini et al. 1990; Siess et al. 2000; Magrini et al. 2021). As a result, Li is slowly being depleted and its surface abundance decreases over time in solar-type and lower-mass FGK stars. The depletion of Li in these stars is strongly mass (colour) and age dependent: Li depletion increases with decreasing mass at a given age, and the timescales for significant Li depletion typically range from 10–20 Myr in M-type stars to ∼100 Myr in K-type stars, and ∼1 Gyr in G-type stars (e.g., Jeffries et al. 2014; Soderblom et al. 2014; Lyubimkov 2016; Randich & Magrini 2021). For their part, Li-rich giants show an additional contribution of surface Li that can only be accounted for with non-standard mixing mechanisms (e.g., Casey et al. 2016; Lyubimkov 2016; Magrini et al. 2021). As it only survives in the outer layers of a star, Li is a very sensitive indicator of youth in late-type stars, a useful tracer of stellar evolution for pre-main sequence (PMS), main sequence (MS), and post-MS stars, and is also particularly relevant for the determination of the age of stellar open clusters (OCs) and associations (e.g., Sestito & Randich 2005; Bouvier et al. 2018; Dumont et al. 2021a,b; Randich & Magrini 2021). For

★ The full versions of the tables in Appendix C are available at the CDS via anonymous ftp to cdsarc.cds.unistra.fr (130.79.128.5) or via https://cdsarc.cds.unistra.fr/viz-bin/cat/J/A+A/685/A83

★★ Based on observations collected with ESO telescopes at the La Silla Paranal Observatory in Chile, for the *Gaia*-ESO Large Public Spectroscopic Survey (188.B-3002, 193.B-0936).

a more comprehensive overview of Li as an age indicator and the mechanics of Li depletion, we refer the reader to the introductory chapter of the published thesis of Gutiérrez Albarrán (2022) and all references therein.

The present work is the second of a series of three papers where we study Li as an age indicator for PMS and MS FGKM late-type stars, with the ultimate aim being to calibrate an empirical Li–age relation. In this paper, we describe an expanded sample of 42 OCs and associations covering an age range from 1 Myr to 5 Gyr, using data from the *Gaia*-ESO Survey (GES) and from the *Gaia* mission (both briefly discussed below). For all target clusters, we here constrain the cluster membership to obtain the final lists of candidate members for all target clusters, updating and expanding the work already published in Gutiérrez Albarrán et al. (2020, hereafter, Paper I). In Gutierrez Albarrán et al. (in prep., hereafter, Paper III), presented as a companion paper to the present work, we finally reach our objective of constraining an empirical Li–age relation by first presenting a comparative study to quantify the observable Li dispersion for all target clusters and to analyse its dependence on several GES parameters, finally obtaining a set of empirical Li envelopes for several key ages in our sample. The analyses and results of this work are additionally presented in full in the published thesis of Gutiérrez Albarrán (2022).

The *Gaia*-ESO Survey (GES – Gilmore et al. 2012, 2022; Randich et al. 2013, 2022; Hourihane et al. 2023)[1] is a large public spectroscopic survey that systematically covers all major components of the Milky Way and provides a homogeneous and ambitious overview of the distribution of the kinematics, dynamical structure, and chemical compositions in the Galaxy. The GES uses the multi-object spectrograph FLAMES (Fibre Large Array Multi Element Spectrograph) at the Very Large Telescope (VLT at ESO, Chile) to obtain high-resolution spectra (R = 50 000) with UVES (Ultraviolet and Visual Echelle Spectrograph), as well as medium-resolution spectra (R = 5000–20 000) with GIRAFFE (e.g., Smiljanic et al. 2014; Frasca et al. 2015; Lanzafame et al. 2015; Gilmore et al. 2022). The observations, which began in December 2011 and were completed in January 2018, provide high-quality, uniformly calibrated spectroscopy for about 10^5 stars and a sample of 65 (plus 18–20 archive) OCs and star forming regions of all ages, metallicities, and stellar masses (Bragaglia et al. 2022; Gilmore et al. 2022; Randich et al. 2022). In addition to measured spectra, this exploration uses well-defined samples from photometric surveys, such as VISTA (Sutherland et al. 2015), 2MASS (Skrutskie et al. 2006) and a variety of photometric surveys of OCs that cover all the major components of the Galaxy (Gilmore et al. 2012; Bragaglia et al. 2022).

Gaia (Gaia Collaboration 2016b)[2] is an ongoing, ambitious global space-astrometry ESA mission that launched in 2013 and started scientific operations in mid-2014. Initially a 5-yr mission, in 2018 the *Gaia* mission was extended to 2020, and currently *Gaia* has been firmly extended until the end of 2022, with indicative approval until the end of 2025 (Gaia Collaboration 2021). Its primary science goal is to chart a three-dimensional map of the Galaxy, providing photometry and astrometry of unprecedented precision for most stars brighter than G = 20 mag, and to obtain low- and medium-resolution spectroscopy data for most stars brighter than G = 17 mag (Gilmore et al. 2012; Gaia Collaboration 2016b). *Gaia* provides a large stellar census that allows an extensive overview of the origin, composition, formation, and evolution of the Galaxy, producing a stereoscopic dataset that includes positions, proper motions, parallaxes, radial velocities, brightness, and astrophysical parameters of about one billion stars and other astronomical objects in the Milky Way and throughout the Local Group.

Gaia, with its revolutionary high-precision astrometry and photometry, can be optimally complemented with GES and the superior spectroscopic capabilities of its large ground-based telescope to obtain high-quality data, providing a rich dataset yielding 3D spatial distributions, 3D kinematics, individual chemical abundances, and improved astrophysical parameters for all target objects (e.g., Gilmore et al. 2012; Beccari et al. 2018; Cantat-Gaudin et al. 2018; Randich et al. 2018; Soubiran et al. 2018; Cánovas et al. 2019; Bossini et al. 2019). We finish this introductory section by further acknowledging that, in our analysis, we also made use of several sets of rotational periods ($P_{\rm rot}$) provided by missions such as CoRoT, *Kepler*, K2, and TESS.

This paper is organised as follows. In Sect. 2, we describe the expanded cluster sample upon which we base our analysis. In Sect. 3, we discuss the expanded and improved membership cluster analysis, describing our selection criteria, which take into account radial velocities (RVs), *Gaia* astrometry and photometry, gravity indicators, metallicity, and Li content, as well as various comparisons with previous studies from the literature using *Gaia* data (Sect. 3.3). In Sect. 3.4, we additionally describe the selection process for Li-rich contaminants obtained as an additional result of the membership analyses. We present the final lists of candidate members for the results of this project in Sect. 5.

2. Data

2.1. GES data

The GES consortium is structured in 19 working groups (WGs), WG0 to WG18, organised in a workflow and dedicated to different survey tasks, from data flow implementation and target selection, to the homogenisation of recommended parameters and the determination of abundances, preparation and documentation, and, finally, the delivery of the external data products to both ESO and the public archive (e.g., Gilmore et al. 2012, 2022; Lanzafame et al. 2015; Sacco et al. 2015). Among these WGs, WG10 and WG11 are focused on the spectroscopic analysis of the GIRAFFE and UVES FGKM late-type stars, respectively (e.g., Gilmore et al. 2012; Sacco et al. 2015), while WG12 is dedicated to the analysis of PMS stars in the fields of young clusters using both UVES and GIRAFFE data. Each WG is divided into several nodes, providing internally consistent results with various approaches, models and methodology[3] (Smiljanic et al. 2014; Lanzafame et al. 2015; Gilmore et al. 2022). For more specific and extensive details on the methodology employed by each node, see Smiljanic et al. (2014, WG11), Lanzafame et al. (2015, WG12), and Gilmore et al. (2022, all WGs). In addition, for an in-depth overview of the GES consortium and the data reduction process for GES spectra, we further refer the reader to Paper I, and also to chapter 2 of the thesis and all references therein.

Six analysis cycles and internal data releases have been carried out by GES (from iDR1 to iDR6), including homogenised

[1] https://www.gaia-eso.eu/
[2] https://sci.esa.int/web/gaia

[3] Our UCM node is part of both WG11 and WG12, and we determined atmospheric parameters by employing the code STEPAR (Tabernero et al. 2019), based on equivalent widths (EWs) automatizing the use of MOOG code (Sneden et al. 2012) and measured with the automatic tool TAME (Tool for Automatic Measurement of Equivalent Widths – Kang & Lee 2012; Tabernero et al. 2019). Also see Paper I.

recommended astrophysical parameters and elemental abundances derived from all the observations collected until the completion of the survey in January 2018 (Randich et al. 2022). Subsequent public releases to the ESO archive include DR2 (published in July 2015), DR3 (December 2016 and May 2017), DR4 (December 2020), and, finally, DR6 was released to the public in July 2023[4]. iDR4, which was made available to the consortium in February 2016, was the data release we used in Paper I for our preliminary cluster membership analysis. For all the following analysis presented in this paper we used the data provided by the sixth and last internal data release of GES (iDR6)[5]. iDR6 is a full release, including all observations from the beginning of the Survey until its completion in January 2018 (Gilmore et al. 2022; Franciosini et al. 2022a; Randich et al. 2022). Similarly to iDR5, the same line list and grid of synthetic spectra used for iDR4 were employed in this final release. This final GES catalogue provides results for 114 325 targets and includes data on velocities, stellar parameters, and abundances for up to 32 elements (Randich et al. 2022).

The *Gaia* mission has also provided three data releases so far, from *Gaia* DR1 (released in September 2016) and *Gaia* DR2 (April 2018) to *Gaia* DR3, which was released in June 2022, following the *Gaia* Early Data Release 3 (EDR3)[6] (Gaia Collaboration 2016a, 2018b, 2021, 2023). Pending further approvals of mission extensions, additional releases will also take place, with *Gaia* DR5 being currently anticipated to contain all collected data. In combination with GES iDR6, for the present project we made use of the proper motions, parallaxes and photometry provided by the latest data release then available, namely, the first installment of the third intermediate data release, *Gaia* EDR3, which is based on the data of the first 34 months of the mission. *Gaia* EDR3 provides, with increased precision and accuracy, an updated source list, astrometry, and broad photometry in the G, G_{BP} and G_{RP} bands (Gaia Collaboration 2021).

2.2. Cluster sample

Our present sample from GES iDR6 includes 114 325 UVES and GIRAFFE spectra of 42 OCs ranging in ages from 1 Myr to 4.5 Gyr. Here below we list the changes and improvements of the updated and improved iDR6 sample used in this work, in contrast to our former iDR4 sample of only 20 OCs and associations, as used in Paper I:

- The number of stars in the current iDR6 sample is considerably larger than the 12 493 UVES and GIRAFFE spectra we had at our disposal for the preliminary cluster calibration results in Paper I. This larger number of stars in the fields of many of our sample clusters improved our membership analysis and increased the number of final candidates in more than one case.
- Several issues were also solved thanks to this larger sample, such as the fact that with our former iDR4 file only a few UVES Li values were listed for many of the intermediate-age and old clusters, especially in the 3000–4000 K temperature range (M-type stars, more difficult to measure in those age ranges)[7]. Thus, we had to make additional use of the individual Li measurements derived by the OACT (Osservatorio Astrofisico di Catania) node, adding to our sample a number of GIRAFFE stars that had no recommended EW(Li) values in the iDR4 file[8]. We note that, even considering the list of spectra that were deprecated in the working version of iDR6 released to the consortium in December 2020, we observed no such lack with our present sample, and our former member lists are as a result either typically enlarged, or at least stay with approximately the same number of candidate stars.
- In addition to the larger number of spectra overall, we now count with 86 OCs in the current iDR6, 48 more than in iDR4. Our former iDR4 sample offered a total of 38 clusters, 26 of them being OCs, and the remaining 12 of them being globular, which we discarded. We do not consider any iDR6 globular cluster in this updated analysis either, as Li cannot be used as a youth indicator in those cases.
- In our current iDR6 sample, the data for the OCs suffering from the contamination of nebular lines, which can affect the RV distributions and therefore the final membership analysis (e.g., Bonito et al. 2013, 2020), were corrected by recalculating the RVs and applying an alternative different sky background subtraction (Gilmore et al. 2022)[9]. Thus, we were able to add to our sample a number of young and intermediate-age clusters we had to formerly discard because they exhibited high differential nebulosity (such as NGC 2264, NGC 2451 A and B, NGC 3532, NGC 6530, and Trumpler 14[10]).
- Finally, in this study we focus on FGK stars, and so we discarded all stars with $T_{\rm eff}$ > 7500 K from the cluster sample in all cases. Given the nature of our membership criteria (see Sect. 3), for each cluster we also deprecated from our analysis all stars with no measurements of RVs (*VRAD* in the iDR6 file), either $T_{\rm eff}$ (*TEFF*) or the newly measured infrared photometric temperatures (*TEFF_IRFM*), and/or EW(Li) (be it the corrected *EW*s, *EWC_LI*, or the improved *EW*s with an additional veiling correction, taking into account the estimate of the continuum emission due to accretion, *EW_LI_UNVEIL*; e.g., Lanzafame et al. 2015).

Out of the 86 OCs measured in the iDR6 data, we discarded all clusters with less than 100 stars, in order to have a sufficient minimum number of stars in each cluster to ensure a statistically significant membership analysis. On the other hand, we did not take into account any old clusters in the iDR6 file with ages older than 2 Gyr, other than the ones we already analysed in

[4] DR6 data products available from the ESO Science Archive Portal at https://archive.eso.org/scienceportal/home?data_collection=GAIAESO&publ_date=2023-07-02

[5] iDR6 data products released to the GES consortium at http://ges.ast.cam.ac.uk/GESwiki/GeSDR6/DataProducts

[6] See https://www.cosmos.esa.int/web/gaia/earlydr3 and https://www.cosmos.esa.int/web/gaia/dr3 to access *Gaia* EDR3 and DR3, respectively.

[7] This was due to the homogenisation process in iDR4, as only WG11 and WG12 provided homogenised *EW*s, while WG10 provided only abundances. As a result, *EW*s for GIRAFFE stars in intermediate-age and old clusters were not available in this release, and in some cases, *EW*s for young clusters were also missing if the node values proved inconsistent, which happened especially for M-type stars in WG12.

[8] The iDR4 issues have since been overcome thanks to the new homogeneous analysis done in iDR6 (Gilmore et al. 2022; Randich et al. 2022).

[9] In general terms (this is by no means a straightforward method), an initial estimate would firstly be formed from the background emission affecting the spectrum of a target object, taking into account both astronomical and atmospheric sources. This estimated background spectrum would then be subtracted from the input science spectrum on a pixel by pixel basis, which gives rise an output spectrum consisting of emission from the science object alone.

[10] The reason why this improved sky background subtraction could not be done for earlier releases to the level iDR6 has finally achieved is that, the Survey being fiber-fed, subtraction of the nebular sky background is not a straightforward procedure (Bonito et al. 2020).

Table 1. Age estimates, reddening, distance to the Sun, and GES and *Gaia* membership studies from the literature for the 16 star forming regions and young clusters in our sample.

Cluster name	Age (Myr)	$E(B-V)$ [(a)] (dex)	Distance (kpc)	References Ages	References Distance	GES and *Gaia* membership studies
NGC 6530	1–2	0.44 ± 0.10	1.33	3, 4, 18, 19, 20, 33	18, 19, 20, 21	2, 3, 16, 18, 19, 22
ρ Oph	1–3	0.76 ± 0.13	0.13 ± 0.01	1, 2, 3, 4, 5, 33, 61	1, 2, 6	1, 2, 3, 6
Trumpler 14	1–3	0.61 ± 0.10	2.90	3, 4, 13, 33	13, 14	2, 3, 15, 17
Cha I	2	0.18 ± 0.08	0.16 ± 0.02	3, 4, 7, 8, 9, 33	7, 8, 10, 11	2, 3, 7, 8, 10, 11[(b)], 12
NGC 2244	4	0.49 ± 0.09	1.59	3, 23, 24, 33	21, 23, 24, 25	3, 15, 24, 26
NGC 2264	4	0.05 ± 0.05	0.76	2, 3, 4, 27, 28, 29, 30, 33	2, 15, 25, 28, 29	2, 3, 15, 31, 32
λ Ori	6	0.09 ± 0.04	0.41	3, 43	34	3, 15
Col 197	13	0.64 ± 0.07	0.80–0.90	3, 5, 13, 35, 36, 37	13, 25, 35, 36, 37	3, 15
γ Vel	10–20	0.04 ± 0.03	0.35–0.40	2, 3, 8, 10, 38, 39, 40, 41, 42	8, 10, 38, 40, 41, 42	2, 3, 8, 10, 38, 39, 40, 41, 42, 44, 45, 46
NGC 2232	18–32	0.04 ± 0.03	0.32	3, 5, 43, 47, 48, 64	13, 25, 48	3, 15, 43, 48
NGC 2547	20–45	0.06 ± 0.03	0.36 ± 0.02	2, 3, 5, 8, 32, 41, 42, 48, 49, 50, 51, 63, 64	2, 8, 41, 42, 48	2, 3, 8, 15, 32, 42, 48, 49, 52
IC 2391	36 ± 2 [(c)]	0.03 ± 0.01	0.16 ± 0.01	3, 48, 51, 53, 64	2, 48, 54, 55, 56	2, 3, 15, 49, 52, 62
IC 2602	35 ± 1 [(c)]	0.04 ± 0.02	0.15 ± 0.01	3, 5, 48, 51, 64	2, 48, 56	2, 3, 15, 49, 52, 62
IC 4665	38 ± 3 [(c)]	0.15 ± 0.02	0.36 ± 0.01	3, 5, 48, 51, 64	2, 48, 57, 58	2, 3, 15, 48, 49, 52, 62
NGC 2451 B	39 ± 1 [(c)]	0.10 ± 0.03	0.36	3, 42, 48, 49, 51, 59, 60	42, 48, 59	2, 3, 15, 42, 48, 49
NGC 2451 A	44 ± 2 [(c)]	0.02 ± 0.02	0.19	3, 42, 48, 49, 51, 59, 60	42, 48, 59	2, 3, 15, 42, 48, 49

Notes. [(a)]References for the $E(B-V)$ reddening adopted from Jackson et al. (2022) for all clusters. [(b)]GES studies that reference the clusters and/or study them without taking membership analysis primarily into account. [(c)]Updated cluster ages using *Gaia* data, as listed by Bossini et al. (2019).
References. For the cluster ages, reddening and distances shown here we chose the most recent or most robust estimates for each cluster, but several other studies are further cited here, and age estimates are additionally briefly discussed in the individual notes of Appendix A: (1) Rigliaco et al. (2016); (2) Spina et al. (2017); (3) Jackson et al. (2022); (4) Randich et al. (2020); (5) Romano et al. (2021); (6) Cánovas et al. (2019); (7) Spina et al. (2014a); (8) Sacco et al. (2015); (9) López Martí et al. (2013); (10) Frasca et al. (2015); (11) Roccatagliata et al. (2018); (12) Galli et al. (2021); (13) Sampedro et al. (2017); (14) Mel'nik & Dambis (2017); (15) Cantat-Gaudin et al. (2018); (16) Castro-Ginard et al. (2020); (17) Damiani et al. (2017); (18) Wright et al. (2019); (19) Damiani et al. (2019); (20) Prisinzano et al. (2005); (21) Kuhn et al. (2019); (22) Prisinzano et al. (2019); (23) Mužić et al. (2019); (24) Michalska (2019); (25) Kharchenko et al. (2005); (26) Carrera et al. (2019); (27) Arancibia-Silva et al. (2020); (28) Bonito et al. (2020); (29) Gillen et al. (2020); (30) Venuti et al. (2019); (31) Maíz Apellániz (2019); (32) Jackson et al. (2016); (33) Randich et al. (2022); (34) Dib et al. (2018); (35) Dias et al. (2019); (36) Bonatto & Bica (2010); (37) Vande Putte et al. (2010); (38) Jeffries et al. (2014); (39) Spina et al. (2014b); (40) Franciosini et al. (2018); (41) Beccari et al. (2018); (42) Franciosini et al. (2022b); (43) Binks et al. (2022); (44) Damiani et al. (2014); (45) Prisinzano et al. (2016); (46) Cantat-Gaudin et al. (2019); (47) Liu & Pang (2019); (48) Pang et al. (2021); (49) Randich et al. (2018); (50) Sestito & Randich (2005); (51) Bossini et al. (2019); (52) Bravi et al. (2018); (53) Dumont et al. (2021b); (54) Platais et al. (2007); (55) De Silva et al. (2013); (56) Smiljanic et al. (2011); (57) Martín & Montes (1997); (58) Jeffries et al. (2009); (59) Silaj & Landstreet (2014); (60) Netopil & Paunzen (2013); (61) Kiman et al. (2021); (62) Gómez Garrido (2015); (63) Oliveira et al. (2003), (64) Jeffries et al. (2023).

Paper I, due to the fact that the Li content in GKM-type stars is strongly depleted in old clusters[11]. We also only analysed four additional clusters in the 0.8–2 Gyr age range, as we already counted with nine old clusters in our first sample selection with ages 0.8–4.5 Gyr, and preferred rather to add more new young and intermediate-age clusters to our updated study, adding to the age ranges where Li is increasingly relevant for the analysis at hand. This criteria leaves us with a total of 42 clusters constituting our current sample, including seven star forming regions (1–6 Myr) and nine young clusters (10–50 Myr), along with 13 intermediate-age clusters (90–575 Myr), and 13 old clusters (0.7–4.5 Gyr).

A number of membership studies have already been conducted, with potential members identified for all 42 clusters selected in the present paper. These studies, particularly those who made use of GES data and specifically iDR6 data, were of great help to evaluate the goodness of our membership analysis by comparing our final candidates with previous membership lists. We show all these studies in Tables 1 and 2. We divided the sample clusters into groups according to age, and show them in two tables for convenience due to their length: Table 1 lists the young (1–50 Myr) clusters, while Table 2 lists the intermediate-age (50–700 Myr) and old clusters (>700 Myr). In the individual notes of Appendix A, where we detail all cluster membership results, we reference these studies in greater detail for each of the clusters. These tables also list the age estimates, distances and reddening values from the literature for all clusters, and we additionally refer to Table 3 for RVs from the literature, to Table 4 for proper motions (*pmra* and *pmdec*) and parallaxes (π) from *Gaia*, and to Table 5 for [Fe/H] metallicities from the literature.

[11] Furthermore, these clusters being so far, the already depleted GKM stars are also too faint to be observed by GES.

3. Updated membership analysis

To obtain final lists of candidate members for the 42 clusters in our sample, we conducted a homogeneous and coherent analysis of their membership according to several criteria, which we now detail below:

RV analysis (full description in Paper I and the published thesis). We studied the radial velocity distribution of each cluster with the aid of the RStudio environment for R by applying a two-sigma clipping procedure on the median, and then adopting a 2σ limit about the cluster mean yielded by the Gaussian fit to identify the most likely kinematic members. Depending on the specific cluster, this 2σ limit was sometimes enlarged to 3σ to further consider marginal members, as detailed in Appendix A. In Table 3 we show the fit parameters (mean values, associated dispersions and 2σ intervals) and the number of kinematic members resulting from the updated study of the distributions of RV for the cluster sample. We additionally report updated reference values estimated from the literature, and also present in the last two columns of the table the mean values and associated dispersions of all final members of each cluster, after

Table 2. Age estimates, reddening, distance to the Sun, and GES and *Gaia* membership studies from the literature for the 26 intermediate-age and old clusters in our sample.

Cluster name	Age (Myr)	$E(B-V)^{(a)}$ (dex)	Distance (kpc)	References Ages	References Distance	GES and *Gaia* membership studies
NGC 6405	94	0.14 ± 0.04	0.46	1, 2, 3	2, 3, 4, 5	1, 3, 6
Blanco 1	94 ± 5 [(c)]	−0.01 ± 0.03	0.23–0.24	1, 10, 15, 16, 17, 18, 53	17, 18	1, 18
NGC 6067	120	0.34 ± 0.04	1.4–1.7	1, 7, 8, 9, 10, 11	4, 5	1, 6, 11
NGC 6649	120	1.43 ± 0.05	1.8 ± 0.1	12, 13, 14	12, 14	1, 6
NGC 2516	125–138	0.11 ± 0.03	0.41	1, 9, 19, 21, 22	22, 23, 24	1, 6, 20, 22, 25, 26, 27, 28
NGC 6709	173 ± 34 [(c)]	0.27 ± 0.02	1.1	1, 10, 15, 29	4, 29	1, 6
NGC 6259	210	0.63 ± 0.09	1.9	1, 9, 30, 31	4, 29	1, 6
NGC 6705	280	0.40 ± 0.06	1.88	1, 9, 10, 26, 27	4, 24	1, 6, 26, 27, 32, 33, 34[(b)]
Berkeley 30	300	0.51 ± 0.04	4.7–4.9	1, 4, 10, 30	4, 30	1, 6
NGC 6281	314	0.18 ± 0.02	0.47–0.51	1, 24, 30, 36	4, 30, 36	1, 6
NGC 3532	399 ± 5 [(c)]	0.05 ± 0.02	0.48–0.49	1, 10, 15, 28, 35	4, 28	1, 6, 28, 36, 37
NGC 4815	560	0.70 ± 0.07	2.40–2.90	1, 26, 27, 31, 37	24, 37	1, 6, 26, 27, 32, 33, 34, 37
NGC 6633	575	0.15 ± 0.04	0.39	1, 26, 27, 31, 38	4, 24	1, 6, 20, 26, 27
NGC 2477	700	0.31	1.4	39	3, 4, 6, 12, 39	6, 40
Trumpler 23	800	0.68 ± 0.04	2.20	1, 26, 27, 31, 43	24, 43	1, 26, 27, 42
Berkeley 81	860 ± 100	0.85 ± 0.04	3.00	1, 10, 26, 27, 31, 34, 45	24, 45	1, 6, 26, 27
NGC 2355	900	0.13 ± 0.03	1.80 ± 0.07	1, 4, 10, 30	42	1, 6,
NGC 6802	900	0.79 ± 0.06	1.80	1, 10, 26, 27, 31, 44	24	1, 6, 26, 27, 44
NGC 6005	973 ± 4 [(c)]	0.49 ± 0.06	2.70	1, 15, 26, 27, 31	4, 24	1, 6, 26, 27
Pismis 18	1200 ± 400	+0.22 ± 0.04	2.20	27, 28, 31	24	1, 27, 28
Melotte 71	1294 ± 89 [(c)]	0.11	2.2–3.2	8, 15	4, 42	6
Pismis 15	1300	0.56 ± 0.05	2.6–2.9	1, 4, 30	4, 30	1, 6
Trumpler 20	1400	0.37 ± 0.03	3.00	1, 10, 26, 27, 41	24, 41	1, 6, 26, 27, 33, 41, 46
Berkeley 44	1600	0.90 ± 0.07	1.80–3.10	1, 10, 26, 27, 31, 47	24, 47	1, 6, 26, 27
NGC 2243	4000 ± 120	0.04 ± 0.04	4.50	1, 10, 27, 31, 48, 49, 50	24, 32, 49	1, 6, 27
M67	4000–4500	0.059	0.90	21, 38, 51, 52	4, 12	40

Notes. [(a)]References for the $E(B-V)$ reddening adopted from Jackson et al. (2022) for all clusters except for NGC 2477 Rain et al. (2021). [(b)]GES studies that reference the clusters and/or study them without taking membership analysis primarily into account. [(c)]Updated cluster ages using *Gaia* data, as listed by Bossini et al. (2019).

References. For the cluster ages, reddening and distances shown here we chose the most recent or most robust estimates for each cluster. Several other studies are further cited here, and age estimates are additionally briefly discussed in the individual notes of Appendix A. (1) Jackson et al. (2022); (2) Kılıçoğlu et al. (2016); (3) Gao (2018); (4) Kharchenko et al. (2005); (5) Mel'nik & Dambis (2017); (6) Cantat-Gaudin et al. (2018); (7) Frinchaboy & Majewski (2008); (8) Netopil et al. (2016); (9) Randich et al. (2020); (10) Romano et al. (2021); (11) Rangwal et al. (2019); (12) Dib et al. (2018); (13) Liu & Pang (2019); (14) Alonso-Santiago et al. (2020); (15) Bossini et al. (2019); (16) Pang et al. (2021); (17) Gillen et al. (2020); (18) Zhang et al. (2020); (19) Binks et al. (2022); (20) Randich et al. (2018); (21) Dumont et al. (2021b); (22) Franciosini et al. (2022b); (23) Jeffries et al. (2001); (24) Dias et al. (2002); (25) Jackson et al. (2016); (26) Jacobson et al. (2016); (27) Magrini et al. (2017); (28) Fritzewski et al. (2019); (29) Vande Putte et al. (2010); (30) Sampedro et al. (2017); (31) Magrini et al. (2018); (32) Magrini et al. (2014); (33) Tautvaišienė et al. (2015); (34) Magrini et al. (2015); (35) Dobbie et al. (2012); (36) Fritzewski et al. (2021); (35) Hetem & Gregorio-Hetem (2019); (36) Joshi et al. (2016); (37) Friel et al. (2014); (38) Sestito & Randich (2005); (39) Rain et al. (2021); (40) Jadhav et al. (2021); (41) Donati et al. (2014b); (42) Buckner & Froebrich (2014); (43) Overbeek et al. (2017); (44) Tang et al. (2017); (45) Donati et al. (2014a); (46) Smiljanic et al. (2016); (47) Hayes & Friel (2014); (48) Heiter et al. (2014); (49) Jacobson et al. (2011); (50) Friel & Janes (1993); (51) Pallavicini et al. (2005); (52) Richer et al. (1998), (53) Jeffries et al. (2023).

applying all membership criteria and concluding our membership analysis.

Gaia astrometry (Sect. 3.1). As the next step we reinforced the kinematic selection and obtain lists of probable astrometric members with the aid of the proper motions and parallaxes provided by *Gaia* EDR3, analysing the locus of probable members in *pmra*-versus-*pmdec* diagrams, and studying the parallax distributions with a Gaussian fit, similarly to the case of RVs. See Table 4 for the results of the study of parallax distributions for the cluster sample, including all fit parameters as well as the mean values and associated dispersions of all final candidates for each cluster, after applying all criteria.

Gaia photometry (Sect. 3.2). We also made use of *Gaia* EDR3 photometry to analyse the goodness of the astrometric candidates and discard field contaminants in G-versus-$G_{\rm BP-RP}$ colour-magnitude diagrams (CMDs).

Gravity indicators (full description in Paper I and the thesis). We used the Kiel ($\log g$-versus-$T_{\rm eff}$) diagram to identify and discard evolved outliers, such as Li-rich giant stars (see Sect. 3.4) and other field contaminants. For all clusters we made use of the PARSEC isochrones (Bressan et al. 2012), with $Z = 0.019$, and ages ranging from 50 Myr to 5 Gyr. In the case of young clusters, we mainly used the γ index defined by Damiani et al. (2014) to effectively discard giant contaminants as a first

Table 3. Fit parameters and RV members for the target star forming regions and OCs.

Cluster [a]	RV [b]	2σ clipping		2σ membership	No. RV	Final fit of member list	
	(km s $^{-1}$)	$\langle RV \rangle$ (km s $^{-1}$)	σ (km s $^{-1}$)	intervals	members	$\langle$RV$\rangle$ (km s $^{-1}$)	σ (km s $^{-1}$)
NGC 6530	-1.9 ± 7.2 (1)	0.3	2.1	[−3.8, 4.6]	477	0.0	2.5
ρ Oph	-7.0 ± 0.2 (2)	−6.4	2.1	[−10.6, −2.2]	48	−6.6	1.0
Trumpler 14	-10.5 ± 6.9 (3)	−7.9	2.9	[−13.7, −2.1]	231	−8.4	3.0
Cha I	14.6 ± 1.2 (4)	15.7	1.1	[13.5, 17.9]	102	15.6	1.1
NGC 2244	33.6 ± 0.7 (5)	30.7	2.7	[25.3, 36.1]	143	30.5	2.7
NGC 2264	20.2 ± 6.4 (3)	20.2	2.5	[15.2, 25.2]	618	19.9	2.2
λ Ori	27.5 ± 0.4 (5)	27.1	1.0	[25.1, 29.1]	208	27.3	1.0
Col 197	35.8 ± 2.3 (3)	20.8	1.1	[18.6, 23.0]	124	20.7	1.1
NGC 2232	25.4 ± 0.9 (3)	29.7	14.1	[−0.2, 56.2]	750	25.3	0.6
IC 2391	15.3 ± 0.2 (3)	15.4	2.3	[10.5, 19.7]	55	14.6	0.7
IC 2602	17.4 ± 0.2 (3)	13.2	10.2	[−8.0, 34.0]	309	17.5	0.6
IC 4665	-14.4 ± 0.8 (3)	−13.4	14.8	[−43.0, 16.2]	233	−14.0	0.7
NGC 6405	-9.2 ± 0.8 (6)	−9.0	6.5	[−22.0, 4.0]	251	−8.8	0.8
Blanco 1	5.8 ± 0.1 (6)	5.8	0.7	[4.4, 7.2]	141	5.8	0.6
NGC 6067	-39.9 ± 0.2 (1)	−38.1	3.3	[−44.7, −31.5]	209	−37.8	2.0
NGC 6649	-8.9 ± 0.5 (3)	−10.3	3.8	[−18.7, −1.9]	32	... [c]	...
NGC 2516	23.8 ± 0.2 (3)	23.6	0.7	[22.3, 25.1]	460	23.8	0.8
NGC 6709	-7.8 ± 5 (1)	−7.7	10.3	[−28.3, 12.9]	322	−9.4	0.7
NGC 6259	-32.8 ± 0.4 (3)	−32.2	3.3	[−38.8, −25.6]	125	−32.5	2.5
NGC 6705	36.0 ± 0.2 (3)	35.6	1.9	[31.8, 39.4]	391	35.4	1.8
Berkeley 30	... [d]	47.7	3.6	[40.5, 54.9]	78	48.1	3.0
NGC 6281	-5.0 ± 0.1 (3)	−4.8	1.9	[−8.6, −1.0]	82	−4.5	0.7
NGC 3532	5.4 ± 0.2 (3)	5.3	0.9	[3.5, 7.1]	518	5.4	0.9
NGC 4815	-29.8 ± 0.3 (3)	−29.0	3.4	[−36.4, −22.8]	68	−27.6	4.0
NGC 6633	-28.6 ± 0.1 (3)	−22.4	13.2	[−49.0, 0.0] [e]	617	−28.3	0.9
NGC 2477	7.9 ± 0.1 (3)	8.1	1.0	[6.1, 10.1]	86	7.2	2.1
Trumpler 23	-61.4 ± 0.5 (3)	−61.3	1.8	[−57.7, −64.9]	51	−62.0	1.5
Berkeley 81	50.0 ± 0.7 (3)	47.7	2.2	[43.3, 52.1]	69	48.2	0.3
NGC 2355	36.9 ± 0.7 (3)	36.2	0.9	[34.4, 37.0]	119	36.3	0.9
NGC 6802	11.8 ± 0.4 (3)	13.0	1.8	[9.6, 16.6]	77	12.0	0.7
NGC 6005	-25.6 ± 0.5 (3)	−25.5	3.2	[−31.9, −19.1]	174	−24.6	1.1
Pismis 18	-28.5 ± 0.6 (3)	−29.7	2.8	[−35.3, −24.1]	41	−28.2	0.8
Melotte 71	51.3 ± 0.4 (3)	51.6	0.7	[50.2, 53.0]	71	51.1	0.4
Pismis 15	36.3 ± 0.7 (3)	35.0	0.1	[32.6, 37.4]	93	35.2	0.8
Trumpler 20	-39.8 ± 0.2 (3)	−39.8	1.4	[−42.6, −37]	451	−40.0	1.2
Berkeley 44	-7.6 ± 0.4 (3)	−8.8	0.4	[−10.4, −7.2]	39	−8.8	0.7
NGC 2243	59.6 ± 0.5 (3)	59.5	0.6	[58.3, 60.7]	469	59.6	0.6
M67	34.1 ± 0.1 (3)	34.0	0.8	[32.4, 35.6]	110	33.9	0.8

Notes. [a] As stated earlier in the text, regarding the clusters γ Vel, NGC 2547 and NGC 2451 A and B, we directly used the selections obtained by several studies listed in Table 1. [b] References for the mean cluster RVs: (1) Conrad et al. (2017); (2) Rigliaco et al. (2016); (3) Soubiran et al. (2018); (4) López Martí et al. (2013); (5) Carrera et al. (2019); (6) Gaia Collaboration (2018b). [c] Final selection only consists of two members, final fit is not possible. [d] We could not find any prior RV measurements from the literature for this cluster. [e] The 2σ membership interval for this cluster has been obtained after excluding a large contaminant population in the middle of the distribution, as detailed in Appendix A.

step of the membership process. Regarding the order of criteria, for the young clusters we discarded all giant contaminants using the γ index before performing the RV and astrometric analyses, due to their appreciable field contamination.

Metallicity (full description in Paper I and the thesis). Using the spectroscopic index [Fe/H] as a proxy of metallicity, an analysis of the metallicity distributions for each cluster (including all stars in the field before applying any other membership criteria) provided further confirmation of the membership of the candidate selections, and it was also taken into account to identify occasional rogue outliers that had been missed with all prior criteria. In Table 5 we present the updated results of the study of metallicity for the cluster sample, including all fit parameters, as well as the mean values and associated dispersions of all final candidates after concluding the

Table 4. Fit parameters and parallax membership for the target star forming regions and OCs.

Cluster[(a)]	*pmra* [(b)]	*pmdec* [(b)]	Parallax (π) [(b)]	2σ clipping		2σ membership	Final fit of member list	
	(mas yr^{-1})	(mas yr^{-1})	(mas)	$\langle\pi\rangle$ (mas)	σ (mas)	intervals	$\langle\pi\rangle$ (mas)	σ (mas)
NGC 6530	1.32 ± 0.08 [(1)]	−2.07 ± 0.08 [(1)]	0.750 [(2)]	0.770	0.060	[0.65, 0.89]	0.769	0.062
ρ Oph	−1.70 ± 0.07 [(1)]	0.20 ± 0.07 [(1)]	7.692 [(1)]	7.237	0.120	[7.001, 7.481]	7.250	0.116
Trumpler 14	−6.54 ± 0.07 [(1)]	2.06 ± 0.07 [(1)]	0.340 [(1)]	0.390	0.050	[0.290, 0.490]	0.395	0.066
Cha I	−19.0 ± 5.00 [(3)]	2.00 ± 4.00 [(3)]	6.250 [(1)]	5.240	0.080	[5.080, 5.400]	5.247	0.087
NGC 2244	−1.70 ± 0.07 [(1)]	0.20 ± 0.07 [(1)]	0.590–0.710 [(1)]	0.670	0.060	[0.550, 0.790]	0.665	0.071
NGC 2264	−1.76 ± 0.08 [(1)]	−3.72 ± 0.07 [(1)]	1.250 [(1)]	1.380	0.040	[1.200, 1.600]	1.388	0.063
λ Ori	1.19 ± 0.51 [(4)]	−2.12 ± 0.39 [(4)]	2.462 ± 0.124 [(4)]	2.500	0.048	[2.404, 2.596]	2.492	0.060
Col 197	−5.81 ± 0.31 [(4)]	3.93 ± 0.39 [(4)]	1.135 [(1)]	1.020	0.050	[0.930, 1.130]	1.023	0.059
NGC 2232	−4.70 [(4)]	−1.80 [(4)]	3.067 ± 0.099 [(4)]	3.100	0.060	[2.980, 3.220]	3.111	0.058
IC 2391	−24.64 ± 0.88 [(4)]	23.32 ± 0.73 [(4)]	6.585 [(5)]	6.620	0.070	[6.490, 6.790]	6.613	0.086
IC 2602	−17.58 ± 0.83 [(4)]	10.70 ± 0.90 [(4)]	6.758 [(5)]	6.610	0.080	[6.460, 6.780]	6.629	0.084
IC 4665	−0.91 ± 0.28 [(4)]	−8.52 ± 0.28 [(4)]	2.872 [(5)]	2.900	0.060	[2.780, 3.020]	2.887	0.077
NGC 6405	1.31 ± 0.34 [(4)]	−5.85 ± 0.34 [(4)]	2.172 [(4)]	2.190	0.020	[2.150, 2.230]	2.185	0.022
Blanco 1	18.74 ± 0.43 [(4)]	2.60 ± 0.44 [(4)]	4.210 ± 0.120 [(4)]	4.200	0.070	[4.060, 4.340]	4.225	0.062
NGC 6067	−1.91 ± 0.12 [(4)]	−2.59 ± 0.12 [(4)]	0.443 ± 0.065 [(4)]	0.470	0.028	[0.416, 0.528]	0.472	0.024
NGC 6649	−0.01 ± 0.18 [(4)]	−0.06 ± 0.18 [(4)]	0.467 ± 0.087 [(4)]	0.491	0.060	[0.371, 0.611]	... [(c)]	...
NGC 2516	−4.75 ± 0.44 [(4)]	11.22 ± 0.35 [(4)]	2.417 ± 0.045 [(4)]	2.429	0.031	[2.367, 2.491]	2.428	0.033
NGC 6709	−1.76 ± 0.08 [(4)]	−3.72 ± 0.07 [(1)]	1.250 [(1)]	1.380	0.040	[1.200, 1.600]	0.916	0.033
NGC 6259	−1.02 ± 0.13 [(4)]	−2.89 ± 0.12 [(4)]	0.408 ± 0.057 [(4)]	0.432	0.061	[0.310, 0.550]	0.463	0.034
NGC 6705	−1.57 ± 0.16 [(4)]	−4.14 ± 0.17 [(4)]	0.427 ± 0.083 [(4)]	0.411	0.039	[0.333, 0.489]	0.404	0.054
Berkeley 30	−0.25 ± 0.17 [(4)]	−0.33 ± 0.13 [(4)]	0.164 [(4)]	0.209	0.138	[−0.074, 0.478]	0.201	0.144
NGC 6281	−1.86 ± 0.30 [(4)]	−4.02 ± 0.24 [(4)]	1.873 ± 0.080 [(4)]	1.880	0.030	[1.820, 1.940]	1.889	0.056
NGC 3532	−10.39 ± 0.40 [(4)]	5.18 ± 0.40 [(4)]	2.066 ± 0.062 [(4)]	2.086	0.025	[2.035, 2.136]	2.085	0.024
NGC 4815	−5.76 ± 0.11 [(4)]	−0.96 ± 0.10 [(4)]	0.261 ± 0.062 [(4)]	0.294	0.076	[0.142, 0.446]	0.294	0.084
NGC 6633	1.20 ± 0.33 [(4)]	−1.81 ± 0.30 [(4)]	2.525 ± 0.073 [(4)]	2.533	0.045	[−0.448, 3.432] [(d)]	2.545	0.051
NGC 2477	−2.45 ± 0.01 [(4)]	0.88 ± 0.01 [(4)]	0.665 ± 0.037 [(4)]	0.688	0.030	[0.628, 0.784]	0.694	0.029
Trumpler 23	−4.18 ± 0.12 [(4)]	−4.75 ± 0.11 [(4)]	0.352 ± 0.059 [(4)]	0.353	0.040	[0.273, 0.433]	0.347	0.043
Berkeley 81	−1.20 ± 0.16 [(4)]	−1.83 ± 0.16 [(4)]	0.254 ± 0.090 [(4)]	0.261	0.054	[0.153, 0.369]	0.263	0.048
NGC 2355	−3.80 ± 0.14 [(4)]	−1.09 ± 0.13 [(4)]	0.497 ± 0.056 [(4)]	0.530	0.022	[0.486, 0.574]	0.529	0.015
NGC 6802	−2.81 ± 0.11 [(4)]	−6.44 ± 0.13 [(4)]	0.309 ± 0.067 [(4)]	0.335	0.028	[0.279, 0.391]	0.349	0.053
NGC 6005	−4.01 ± 0.12 [(4)]	−3.81 ± 0.12 [(4)]	0.362 ± 0.060 [(4)]	0.390	0.051	[0.288, 0.492]	0.327	0.135
Pismis 18	5.66 ± 0.11 [(4)]	−2.29 ± 0.11 [(4)]	0.332 ± 0.052 [(4)]	0.349	0.022	[0.305, 0.393]	0.342	0.100
Melotte 71	−2.45 ± 0.12 [(4)]	4.21 ± 0.11 [(4)]	0.434 ± 0.056 [(4)]	0.443	0.026	[0.391, 0.495]	0.348	0.100
Pismis 15	−5.30 ± 0.10 [(4)]	3.33 ± 0.12 [(4)]	0.354 ± 0.049 [(4)]	0.387	0.061	[0.265, 0.509]	0.401	0.058
Trumpler 20	−7.09 ± 0.09 [(4)]	0.18 ± 0.09 [(4)]	0.251 ± 0.045 [(4)]	0.272	0.030	[0.212, 0.332]	0.285	0.048
Berkeley 44	0.01 ± 0.13 [(4)]	−2.83 ± 0.14 [(4)]	0.303 ± 0.060 [(4)]	0.322	0.042	[0.238, 0.406]	0.341	0.062
NGC 2243	−1.28 ± 0.13 [(4)]	5.49 ± 0.13 [(4)]	0.211 ± 0.060 [(4)]	0.225	0.052	[0.121, 0.329]	0.220	0.048
M67	−10.97 ± 0.24 [(4)]	−2.95 ± 0.24 [(4)]	1.135 ± 0.051 [(4)]	1.161	0.026	[1.110, 1.214]	1.162	0.026

Notes. [(a)]As stated earlier in the text, regarding the clusters γ Vel, NGC 2547 and NGC 2451 A and B, we directly used the selections obtained by several studies listed in Table 1. [(b)]References for the mean cluster proper motions (*pmra* and *pmdec*) and parallaxes: (1) Kuhn et al. (2019); (2) Wright et al. (2019); (3) López Martí et al. (2013); (4) Cantat-Gaudin et al. (2018); (5) Kounkel & Covey (2019). [(c)]Final selection only consists of two members, final fit is not possible. [(d)]The 2σ membership interval for this cluster has been obtained after excluding a large contaminant population in the middle of the distribution, as detailed in Appendix A.

membership analysis. We note that, in contrast to the study of RVs and parallaxes, we decided to adopt 3σ membership intervals, instead of a 2σ limit, as the starting point to identify the most likely metallicity members. We also note that we also accepted as final cluster candidates a number of marginal metallicity members deviating moderately from the starting 3σ limits, as they fully fulfilled the rest of criteria in our analysis. We refer the reader to the individual notes of Appendix A for more details on these marginal stars for each cluster, as well as listing, in the case of some of the clusters, a smaller number of stars that were similarly accepted as robust cluster members, despite having [Fe/H] values that deviated more appreciably from the 3σ limit. It is thus apt to note that, in contrast to the most robust criteria in our analysis (particularly *Gaia* astrometry and CMDs), we consider metallicity to be among our less restrictive criteria and selected the final cluster members accordingly. This takes into account the inherent higher uncertainties related to [Fe/H] values derived from GIRAFFE spectra, even after the improvements achieved for the iDR6 data (e.g., Spina et al. 2014b; Gilmore et al. 2022), as well as the fact that the variations in stellar abundances also depend on several astrophysical factors and processes, such as atomic diffusion or the influence of planets (e.g., Oh et al. 2018; Liu & Pang 2019; Yong et al. 2023). Finally, stellar Li itself also depends on metallicity (a dependence that will be further analysed in Paper III; e.g., Jeffries 2014; Randich & Magrini 2021; Martos et al. 2023), which makes it

Table 5. Fit parameters and metallicity membership for the target star forming regions and OCs.

Cluster [a]	[Fe/H]	References	3σ clipping		3σ membership	Final fit of member list	
	(dex)	[Fe/H]	$\langle$[Fe/H]$\rangle$ (dex)	σ (dex)	intervals [d]	$\langle$[Fe/H]$\rangle$ (dex)	σ (dex)
NGC 6530	−0.04 ± 0.01	1	0.00	0.08	[−0.24, 0.24]	−0.01	0.09
ρ Oph	−0.08 ± 0.02	2	0.02	0.09	[−0.25, 0.29]	−0.03	0.20
Trumpler 14	−0.03 ± 0.02	1	0.00	0.06	[−0.18, 0.18]	−0.02	0.07
Cha I	−0.07 ± 0.04	2, 3	−0.02	0.04	[−0.15, 0.10]	−0.04	0.05
NGC 2244	−0.23	4	−0.04	0.05	[−0.20, 0.11]	−0.05 [b]	0.05
NGC 2264	−0.06 ± 0.01	1, 2, 5	−0.03	0.06	[−0.21, 0.15]	−0.03	0.06
λ Ori	−0.01	4	−0.04	0.07	[−0.25, 0.17]	−0.03	0.06
Col 197	... [c]	...	0.02	0.06	[−0.16, 0.20]	0.01	0.06
NGC 2232	0.04 ± 0.01	4	0.02	0.04	[−0.15, 0.15]	0.00	0.05
IC 2391	−0.03 ± 0.02	1, 2, 6, 7, 8	−0.03	0.03	[−0.10, 0.10]	−0.03	0.09
IC 2602	−0.02 ± 0.02	2, 7, 8	0.00	0.07	[−0.21, 0.21]	0.00	0.07
IC 4665	0.00 ± 0.02	2	−0.01	0.09	[−0.19, 0.17]	0.00	0.01
NGC 6405	0.07 ± 0.03	9, 10	0.03	0.12	[−0.33, 0.39]	0.00	0.06
Blanco 1	0.00	9, 12	0.01	0.02	[−0.05, 0.07]	0.01	0.02
NGC 6067	0.20 ± 0.08	9, 11	0.11	0.09	[−0.16, 0.38]	0.07	0.10
NGC 6649	... [c]	...	0.03	0.19	[−0.54, 0.60]	... [e]	...
NGC 2516	−0.02 ± 0.01	5, 13	0.02	0.05	[−0.13, 0.17]	0.00	0.06
NGC 6709	... [c]	...	0.00	0.17	[−0.51, 0.51]	−0.08	0.07
NGC 6259	0.21 ± 0.04	11, 14	0.18	0.09	[−0.09, 0.45]	0.17	0.10
NGC 6705	0.16 ± 0.04	11, 13	0.06	0.08	[−0.18, 0.30]	0.06	0.08
Berkeley 30	0.10	15	−0.19	0.18	[−0.73, 0.35]	−0.20	0.19
NGC 6281	0.06	9, 17	0.07	0.20	[−0.53, 0.67]	0.08	0.15
NGC 3532	−0.07 ± 0.10	16	0.02	0.06	[−0.16, 0.20]	0.02	0.07
NGC 4815	0.11 ± 0.01	11, 13, 18	0.07	0.20	[−0.53, 0.67]	0.01	0.08
NGC 6633	−0.01 ± 0.11	11, 13, 19	−0.01	0.19	[−0.58, 0.56]	0.03	0.15
NGC 2477	0.07 ± 0.03	9, 17, 20	0.10	0.04	[−0.02, 0.22]	0.14	0.04
Trumpler 23	0.21 ± 0.04	11, 13, 21	0.16	0.10	[−0.14, 0.46]	0.19	0.07
Berkeley 81	0.22 ± 0.07	11, 13	0.18	0.11	[−0.15, 0.51]	0.18	0.10
NGC 2355	−0.11	4	−0.12	0.05	[−0.27, 0.03]	−0.13	0.05
NGC 6802	0.10 ± 0.02	11, 13, 22	0.03	0.15	[−0.42, 0.48]	0.05	0.13
NGC 6005	0.19 ± 0.02	11, 13	0.14	0.10	[−0.16, 0.44]	0.19	0.08
Pismis 18	0.22 ± 0.04	11, 13	0.06	0.11	[−0.27, 0.39]	0.13 [b]	0.02
Melotte 71	−0.27	9, 12	−0.33	0.24	[−1.08, 0.42]	−0.09	0.01
Pismis 15	0.01 ± 0.01	23	−0.10	0.22	[−0.76, 0.56]	−0.07	0.11
Trumpler 20	0.10 ± 0.05	11, 13	0.06	0.10	[−0.24, 0.36]	0.08	0.10
Berkeley 44	0.27 ± 0.06	11, 13	0.12	0.09	[−0.15, 0.39]	0.12	0.09
NGC 2243	−0.38 ± 0.04	11, 13, 17	−0.57	0.13	[−0.96, −0.18]	−0.61	0.13
M67	−0.01 ± 0.04	11, 17, 19, 24	0.00	0.05	[−0.15, 0.15]	0.00	0.05

Notes. [a]For γ Vel, NGC 2547 and NGC 2451 A and B, we used the selections listed in Table 1. [b]For these clusters, the final mean [Fe/H] values deviate more appreciably from the literature values. [c]We could not find any prior measurements from the literature for these clusters. [d]In the individual notes of Appendix A we also list the number of stars that we accepted as robust members despite deviating from these 3σ intervals. [e]Final selection only consists of two members, final fit is not possible.

References. Shown here are the most recent or robust estimates for each cluster, several studies are further cited in Appendix A: (1) Randich et al. (2018); (2) Spina et al. (2017); (3) Sacco et al. (2015); (4) Carrera et al. (2019); (5) Binks et al. (2022); (6) De Silva et al. (2013); (7) Dumont et al. (2021b); (8) Smiljanic et al. (2011); (9) Netopil & Paunzen (2013); (10) Kılıçoğlu et al. (2016); (11) Magrini et al. (2018); (12) Bossini et al. (2019); (13) Jacobson et al. (2016); (14) Casali et al. (2019); (15) Paunzen et al. (2010); (16) Fritzewski et al. (2019); (17) Heiter et al. (2014); (18) Friel et al. (2014); (19) Sestito & Randich (2005); (20) Rain et al. (2021); (21) Overbeek et al. (2017); (22) Tang et al. (2017); (23) Carraro et al. (2005); (24) Liu & Pang (2019).

important not to discard those cluster members that are iron-rich or iron-poor.

Li content (full description in Paper I and the thesis). Probable candidates fulfilling the rest of criteria were considered Li members according to their locus in the EW(Li)-versus-$T_{\rm eff}$ diagrams, using as guides the upper Li envelope of IC 2602 (35 Myr; Montes et al. 2001; López-Santiago et al. 2003), the upper (Neuhaeuser et al. 1997) and lower (Soderblom et al. 1993) envelopes of the Pleiades (78–125 Myr), and the upper envelope of the Hyades (750 Myr; Soderblom et al. 1993). As this work revolves around the calibration of Li and its observable dispersion, this is one of the final criteria so as to already count with a robust list of probable cluster members and add the least bias to our study. We refer to the individual notes of Appendix A to illustrate some examples of the bias that we could add by filtering

candidates on the basis of Li before other criteria. In addition, for the star forming regions in our sample we additionally considered as cluster candidates all kinematic and astrometric members that are strong accretors with Hα10% > 270–300 km s^{-1}, disregardless of their Li content (Frasca et al. 2015; Sacco et al. 2017; Bonito et al. 2020)[12]. This is due to the enhancement and/or underestimation that can be caused by strong accretion (for more details, see Paper III).

Other Gaia membership studies (Sect. 3.3). Finally, we made use of additional studies conducted from *Gaia* DR1, DR2 and EDR3 data (e.g., Cantat-Gaudin et al. 2018; Randich et al. 2018; Soubiran et al. 2018; Bossini et al. 2019; Jackson et al. 2022) to better confirm the robustness of our final candidate selections. These studies were also of great help to decide on the membership of marginal members according to one of more criteria.

In this work, we improve and update all criteria presented and described in Paper I (namely, the analysis of RV distributions, surface gravity indicators, Li content, metallicity and comparison with several *Gaia* studies from the literature), as well as using the astrometry and photometry from *Gaia* EDR3 as new criteria, upon which we further elaborate in Sects. 3.1 and 3.2 in this section below. We additionally note that in our final analysis we modify the order of the criteria applied in the membership analysis in some cases, as briefly mentioned above, and we also improve on several of our methods in comparison to our analysis in Paper I. A complete in-depth description of all updated and improved criteria in our final membership analysis can be found in Chapter 2 of the thesis, and we also refer the reader to the individual notes of Appendix A, where we offer a detailed discussion of the membership analysis for all clusters in the sample. Finally, we also refer to Appendix B, where we show the individual figures for each cluster corresponding to most of the membership criteria.

We also note that for all clusters, we identified and discarded a series of binary stars, both SB1 (single line spectroscopic binaries) and SB2/3/4 (double and multiple line spectroscopic binaries), which can add significant contamination to our analysis. SB1s were excluded from our kinematic analysis, as they can strongly affect the observed RV distributions, but we decided to include those SB1 stars that had not already been discarded after applying all kinematic and astrometric filters for the rest of our membership criteria, seeing as Li measurements are not affected by SB1 binaries, and they could still be of interest for our analysis. On the other hand, SB2/3/4s were fully discarded from our data sample for all clusters and membership cirteria. All binary stars were identified using the iDR6 data release metadata (via the column PECULI; e.g., Gilmore et al. 2022), as well as existing studies (Merle et al. 2017, 2020). SB1 and SB2/3/4 stars are listed in the long tables of Appendix C.

3.1. Proper motions and parallaxes

In our earlier cluster calibration work using iDR4 data as described in Paper I, we made use of several GES membership studies using *Gaia* DR1 and DR2 to reinforce our final candidate selections, thus making use in an indirect way of the precision and robustness of the data provided by *Gaia*. One of the main improvements of the present analysis is to use the proper motions and parallaxes provided by *Gaia* EDR3 to identify robust astrometric candidates among the kinematic selection.

[12] A tracer of accretion and youth indicator in young PMS stars, Hα10% refers to the width of the Hα emission line at 10% peak intensity.

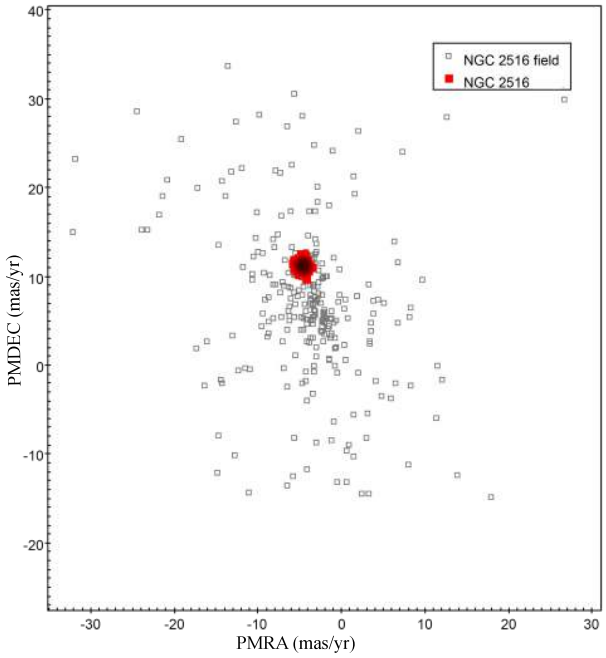

Fig. 1. *pmra*-versus-*pmdec* proper motion diagram showing the final candidate selection (red squares) for NGC 2516, a 125–138 Myr intermediate-age cluster.

In order to be able to use *Gaia* data for our cluster sample, we crossmatched the GES iDR6 files with *Gaia* EDR3 by making use of the CDS Upload X-Match functionality in TOPCAT[13], which allows users to join a local table with any table provided by VizieR[14], or SIMBAD[15] (Wenger et al. 2000; Taylor 2005). We chose a search radius of 5 arcsec for all clusters in our sample, and did not encounter any problems with duplicates. We then constrained all the *Gaia* measurements according to a series of quality indicators in order to ensure that the proper motions, parallaxes and photometry we used throughout the membership analysis are of sufficient quality regarding their precision, reliability and consistency (Lindegren 2018; Lindegren et al. 2018). We here used the renormalized unit weight error (RUWE – Lindegren et al. 2018; Gaia Collaboration 2021), only considering for the astrometric study of each cluster the stars with RUWE < 1.4 (Lindegren 2018; de la Torre Rojo 2020)[16] (also see Sect. 3.2 below for the quality indicators applied to *Gaia* photometry).

We studied the astrometric goodness of the kinematic members whose associated *Gaia* data fulfilled all these quality indicators by first plotting them in *pmra*-versus-*pmdec* diagrams and analysing the locus of probable members. As reference in order to identify this location for each cluster, we used the estimated proper motions from the literature listed in Table 4. As we can see in the example of Fig. 1 for intermediate-age cluster NGC 2516 (125–138 Myr), all astrometric members can be found clustered together in the expected location in the *pmra*-versus-*pmdec* diagram as estimated by the literature. This is one of our

[13] http://www.star.bris.ac.uk/~mbt/topcat/
[14] https://vizier.cds.unistra.fr/viz-bin/VizieR
[15] http://simbad.u-strasbg.fr/simbad/
[16] We refer to the following studies for more details on *Gaia* DR2 and EDR3 data processing and quality indicators (Cantat-Gaudin et al. 2018; Gaia Collaboration 2018a,b, 2021; Lindegren 2018; Lindegren et al. 2018; Randich et al. 2018; Riello et al. 2021; Torra et al. 2021).

most restrictive criteria, and so we discarded from our analysis all the kinematic members that strayed significantly from the expected locus. As a limit, we applied the criterion of studies such as Cantat-Gaudin et al. (2018) to select sources with proper motions within a maximum of 0.5 mas yr^{-1} of the centroid.

This criterion, combining precise measurements and accurate literature estimates, allowed us to optimally reinforce our list of kinematic members. We were also able to ascertain the astrometric membership of any marginal kinematic stars by studying their position in the proper motions diagrams, fully accepting them as potential candidates if they proved to be robust astrometric members. On the other hand, there were also a number of stars in each cluster to which we were not able to apply astrometric criteria, be it because there were no *Gaia* data available for those GES stars, or because the crossmatched *Gaia* data was filtered out with quality indicators. In those cases, we analysed the stars with the same criteria we used in Paper I (kinematics, gravity indicators, metallicity, and Li). We refer the reader to the individual notes of Appendix A for more details on the individual decisions for each cluster in these cases.

The next step in the astrometric analysis was to study the distributions of parallaxes (π) for each cluster. Similarly to the analysis of RV and metallicity distributions (as fully discussed in Paper I and the thesis), we fitted the initial parallax distributions for all clusters in the sample, making use of Gaussian curves, applying a 2σ clipping procedure on the median, and adopting a 2σ limit about the cluster mean yielded by the Gaussian fit to obtain the most likely parallax members. As was also the case with our RV and metallicity selections, we also considered a series of marginal parallax members that fully fulfilled the kinematic and proper motions criteria, and for these borderline members we similarly chose to enlarge the obtained 2σ intervals up to a certain threshold to assess them, typically resulting in a slightly larger 3σ interval (the exact value depends on each cluster, as is detailed in Appendix A).

In Table 4, we list all the mean parallax values, their associated dispersions and the resulting 2σ intervals for all 38 clusters analysed, alongside the estimated parallax values from the literature. The updated results for study of the distributions of RV and metallicity are also summarised in Tables 3 and 5, respectively (see Paper I and Chapter 2 of the thesis). As already discussed in Paper I for the kinematic analysis, the candidate selections for clusters γ Vel, NGC 2547 and NGC 2451 A and B were taken from several prior membership studies from the literature. However, in this case we also improved the final selections for these clusters by discarding several spurious stars that deviated appreciably in regards to our astrometry criteria. As in the case of RV and metallicity distributions (similarly further discussed in both Paper I and the published thesis), we also fitted the parallax distributions of our final lists of candidates for each cluster, and compared the obtained final central mean parallaxes and their associated dispersions with those available in the literature for each cluster, finding all of our final estimates to be in agreement. Figure 2 additionally shows an example of the parallax distribution analysis for intermediate-age cluster NGC 2516, comparing the initial fit following the 2σ clipping procedure, from which we obtain a preliminary 2σ membership interval, with the final distribution of the parallaxes for the final candidates for the cluster.

We consider astrometry to be one of the most restrictive criteria in our analysis due to its reliability and precision, and thus we fully discarded from our analysis all stars that proved to be non-members according to proper motions, and all stars that fulfilled the proper motions criterion but proved to be non-members according to the study of parallaxes were similarly fully discarded. In contrast to this, other criteria such as gravity indicators and metallicity being less robust, we chose not to make them as restrictive in order to obtain the most probable lists of candidate members (as discussed in more detail in both Paper I and Chapter 2 of the thesis).

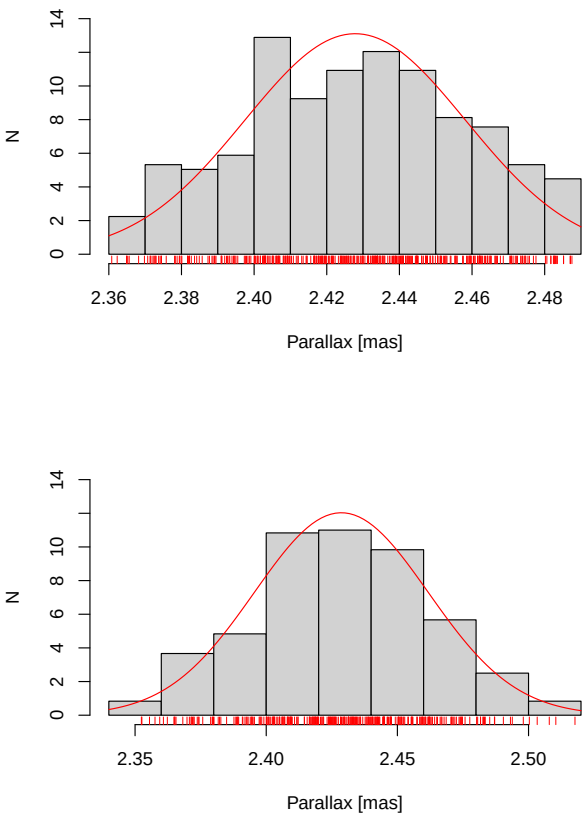

Fig. 2. Distributions of parallaxes and Gaussian fits for the intermediate-age cluster NGC 2516 (125–138 Myr). We display the histogram both for sources resulting from the 2σ clipping procedure on all the GES sources in this field (top panel), and for likely cluster members after applying all of our membership criteria (bottom panel).

3.2. Colour–magnitude diagrams

We made use of the photometry in the G, G_{BP}, and G_{RP} bands provided by *Gaia* EDR3 to reinforce the selections of kinematic and astrometric candidates and discard field contaminants by means of M_G-versus-G_{BP}–G_{RP} colour–magnitude diagrams (CMDs; e.g., Riello et al. 2021). The absolute magnitudes M_G were calculated using the apparent magnitudes G measured by *Gaia*, as well as the parallaxes (π) measured in milliarcseconds (mas). In addition to the criterion of RUWE < 1.4, already applied to astrometric criteria in Sect. 3.1, to ensure the most precise dataset possible, we used a series of additional quality indicators to the *Gaia* photometry, applying the following filters on the relative magnitude errors on the G, G_{BP} and G_{RP} photometric bands: $\sigma_G < 0.022$ mag, $\sigma_{RP} < 0.054$ mag, and $\sigma_{BP} < 0.054$ mag (Gaia Collaboration 2018a, 2021; Lindegren et al. 2018; Duque Arribas 2020; de la Torre Rojo 2020).

The use of *Gaia* photometry in CMDs offers a more precise and robust way to assess the membership of our astrometric candidates and discard field contaminants than criteria based

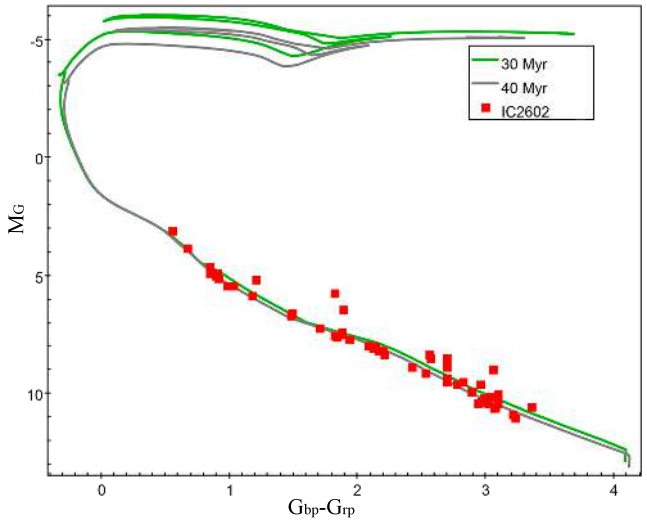

Fig. 3. CMD showing the final candidate selection (red squares) of IC 2602, a 35 Myr-old cluster. We overplot the PARSEC isochrones with $Z = 0.019$ for 30 Myr (green curve) and 40 Myr (grey curve).

on spectroscopic gravity indicators, such as the analysis of the potential candidate list in Kiel diagrams (the $T_{\rm eff}$-versus-$\log g$ plane), or using the γ index for the young clusters in the sample (both criteria are described in detail in Paper I and the thesis). The reason why Kiel diagrams prove to be less reliable is that $\log g$ values are generally less precise, and also scarcer in our sample, and so, we consider the analysis of CMDs to be a far more restrictive and reliable criterion than gravity indicators[17] (as further discussed in Paper I and Chapter 2 of the thesis). We encountered several cases, to give an example, where a target star fully fulfilled the CMD criterion but appeared to deviate more appreciably in the Kiel diagram, and in such cases we relied more heavily on our CMD analysis due to its superior precision and reliability. Similarly to the astrometric criteria described above, we fully discarded any astrometric candidates from the analysis when they deviated significantly from the expected trend in the CMD in a way that could not be explained by the existing inherent dispersion among the cluster members. We note, however, that most of our astrometric selections already being quite robust, these spurious astrometric candidates were not particularly common in our analysis.

For all clusters we made use of the PARSEC CMD isochrones (Bressan et al. 2012; de la Torre Rojo 2020)[18], choosing the *Gaia* EDR3 photometric system, for ages ranging from 1 Myr to 5 Gyr, and with a metal fraction of $Z = 0.019$ (except for the very low metallicity old cluster NGC 2243, where we used isochrones with $Z = 0.006$). We also took the interstellar reddening and extinction into account when obtaining the isochrones for each cluster age by applying the corresponding $A_{\rm V}$ (mag) extinction values. For each cluster, we calculated the $A_{\rm V}$ extinction in the V band by means of the expression $A_{\rm V} = 3.2E(B{-}V)$, using the $E(B{-}V)$ reddening given by (Jackson et al. 2022) and listed in Tables 1 and 2. As an example, in Fig. 3 we present the CMD for the cluster IC 2602, a 35 Myr old young cluster, while the CMDs for all clusters in the sample are shown in Appendix B.

3.3. Comparison with Gaia studies

As part of the preliminary work on the membership analysis of the 42 OCs in the sample, we did an extensive research on each cluster, and listed all available membership studies from the literature that included lists of candidates. In Appendix A we delve in detail on the comparisons between all these membership studies and our own final cluster selections. Among these, several membership studies were particularly relevant for our work, conducted from *Gaia* DR1 (Randich et al. 2018), DR2 (Cantat-Gaudin et al. 2018; Soubiran et al. 2018; Bossini et al. 2019) and EDR3 data (Jackson et al. 2022).

We adopted the ages revised by Bossini et al. (2019) for nine of our sample clusters, and the RVs from Soubiran et al. (2018) for 28 of them, as reported in Tables 1 and 2 for the ages, and Table 3 for the RVs, respectively. We also observed that, judging by the measured *Gaia* ages by Bossini et al. (2019), as well as the empirical Li envelopes constructed by using our cluster candidates (see Paper III) it is possible that some of the former age estimates for the preselected intermediate-age and old clusters could be overestimates – NGC 6005, for example, had a former age estimate of 1.2 Gyr, while Bossini et al. (2019) gives a lower age of 973 ± 5 Myr, which is more in accordance with the Li envelope of our candidate selection. However, we note that we also decided not to use the age estimates by Bossini et al. (2019) for two clusters (NGC 2516 and NGC 6633). The reason for this is that we believe these ages to be overestimates as well, judging by both more recent age estimations, and once again our own candidate selections and obtained empirical Li envelopes (see Appendix A for more details on the sample cluster ages).

We used the other three studies cited above (Cantat-Gaudin et al. 2018; Randich et al. 2018; Jackson et al. 2022) as an additional tool to assess our own selections after concluding all membership analyses and applying all the criteria discussed in this section. All these works were of great aid to confirm and reinforce the robustness of our final candidate selections, and were also markedly useful to aid in the confirmation of marginal members in those cases when the membership criteria were not sufficient to fully confirm their membership to the clusters. For the preliminary work published in Paper I, we mainly made use of the first two studies, conducted from *Gaia* DR1 and DR2 (Cantat-Gaudin et al. 2018; Randich et al. 2018), and for the final version of this work extensive use was made of the data in Jackson et al. (2022) in order to asses our final member selections. We also note the interest of later membership studies that were published after the completion of the present work Franciosini et al. (2022a), Prisinzano et al. (2022).

Jackson et al. (2022) combined GES iDR6 spectroscopic data with the astrometry provided by *Gaia* EDR3 to assign membership probabilities for a target sample of 63 OCs (including 39 out of 42 of the clusters in our sample (all except for NGC 2477, Melotte 71 and M67), as well as 7 globular clusters. Out of 43211 targets, Jackson et al. (2022) listed 13985 as highly probable cluster members, with $P > 0.9$, and an average membership probability of 0.993. Similarly to Cantat-Gaudin et al. (2018), the membership selection is purely kinematic and independent of photometry and chemistry and the final selection catalogues from both studies can be successfully combined with other photometric and spectroscopic criteria from GES.

For each of the clusters considered in these studies, see the individual notes in Appendix A for in-depth details regarding the

[17] Similarly to surface gravity indicators, [Fe/H] metallicity is not as robust a criterion as kinematics, astrometry and CMDs, as the [Fe/H] values derived from GIRAFFE spectra are widely dispersed and subject to larger uncertainties.

[18] http://stev.oapd.inaf.it/cgi-bin/cmd

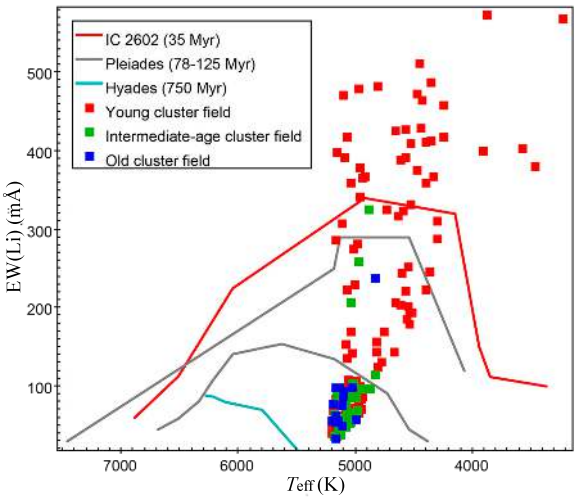

Fig. 4. EW(Li)-versus-$T_{\rm eff}$ diagram for the Li-rich giant outliers in the field of the young (red squares), intermediate-age (green squares), and old clusters (blue squares). Also shown are the upper envelope of EW(Li) for IC 2602 (35 Myr, red), the upper and lower envelopes of the Pleiades (78–125 Myr, grey), and the upper envelope of the Hyades (750 Myr, turquoise).

comparison between the candidates listed in these *Gaia* studies and our final member selections. In the tables described in Appendix C we also include for reference these *Gaia* membership selections alongside the columns listing the results of our membership analysis criteria.

3.4. Identification of Li-rich giant contaminants

As discussed in more detail in Paper I, gravity indicators help identify giant contaminants in the field of the clusters by plotting the sample stars in the Kiel diagram and the (γ, $T_{\rm eff}$) plane. Given their interest[19] (e.g., Smiljanic et al. 2018; Magrini et al. 2021), as a parallel result of the membership analysis we also listed some of these outliers for future study, specifically potential Li-rich giants with A(Li) > 1.5. We consider as likely giants any source with $\log g < 3.5$ (Spina et al. 2014a, 2017) and/or with $\gamma > 1.01$ (Damiani et al. 2014; Sacco et al. 2015; Casey et al. 2016; Spina et al. 2017). We also consider Li-rich giants to have $T_{\rm eff} < 5200$ K (Casey et al. 2016; Spina et al. 2017) and, in the case of stars in the field of young clusters, a lack of Hα emission, given that this is a youth indicator for PMS stars (Casey et al. 2016). In Figs. 4 and 5 we show all Li-rich giant outliers obtained in the field of each of the 42 clusters in our sample as a result of the membership analysis in diagrams of EW(Li), $\log g$, and γ as a function of $T_{\rm eff}$, for both the young clusters and the intermediate-age and old clusters in the sample. All Li-rich giants are also listed in Tables 6 and 7 in Sect. 4, as well as in the long tables of Appendix B.

We note that the classification of Li-rich giant stars in this work is only preliminary. We find a large number of potential Li-rich giants in the field of some clusters (e.g., IC 2602) and, while these stars fulfil the adopted criteria ($T_{\rm eff} < 5200$ K and A(Li) > 1.5), given the rare nature of these objects, further confirmation would be required to accept them as bona fide

[19] Comprising 1–2% of FGK giants and supergiants, most are still not well understood, requiring non-standard evolution models to account for the fresh Li detected on their surface (see the thesis and references therein).

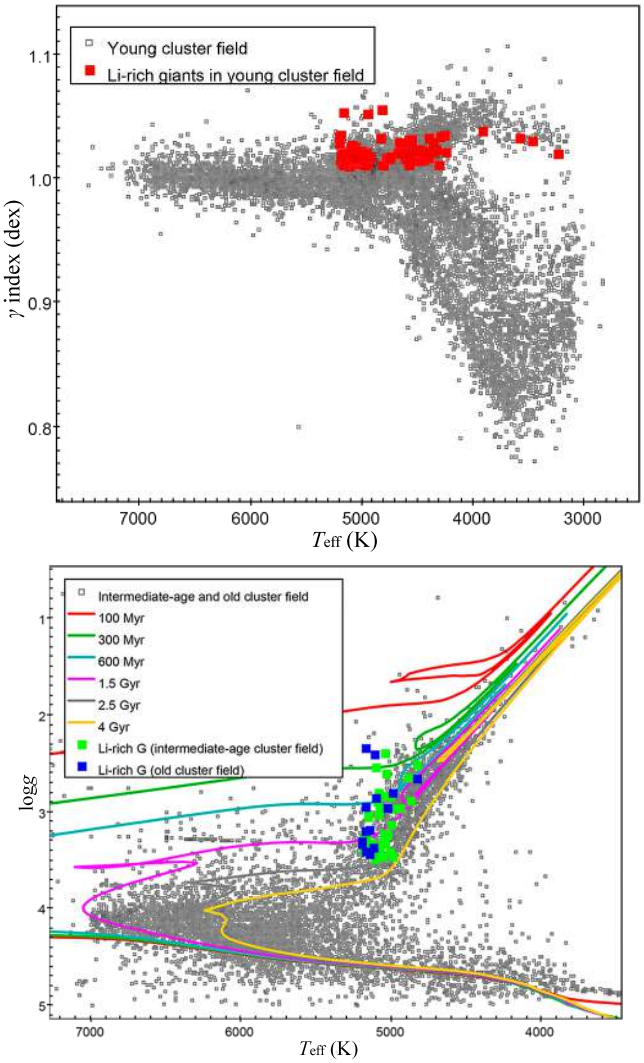

Fig. 5. γ index and $\log g$ as a function of $T_{\rm eff}$ for the Li-rich giant outliers (red squares) in the field of the young (top), and intermediate-age (green squares), and old (blue squares) clusters (bottom).

Li-rich giants. It is also worth noting that we selected all Li-rich giant outliers according to the filters on gravity criteria (γ index for young clusters, and $\log g$ for intermediate-age and old clusters) detailed above. In the case of several clusters, we do find some inconsistencies when plotting Li-rich giant outliers in CMDs, with the preselected Li-rich giants sometimes appearing to be non-giants according to photometric data. We detail these instances in the individual notes of Appendix A. For the moment, we decided to limit our classification of Li-rich giant contaminants to gravity indicators, as was also done in all cited instances in the literature, but this issue does reinforce the necessity to further confirm the goodness of all selected Li-rich giant outliers in this study.

4. Cluster member selections

We finish this section with the final results from the membership analysis of all 42 sample clusters, as summarised in Table 6. For each cluster, we report *i*) the number of stars from the iDR6 sample observed with both UVES and GIRAFFE; *ii*) those with measured values of EW(Li); *iii*) the number of stars selected as candidate members; and *iv*) the number of Li-rich giant outliers

Table 6. Main results for the 42 OCs analysed, indicating, for each cluster, the number of stars from the sample detected in UVES and GIRAFFE; the number of stars with EW(Li) values; the number of stars selected as candidate members (including RV, astrometric and Li members, as well as the final members); and the number of Li-rich giant contaminants.

Cluster[a]	UVES		GIRAFFE		Membership				Li-rich G
	All stars	With Li	All stars	With Li	RV	*Gaia*	Li	Final	outliers
NGC 6530	52	5	1931	1325	470	200	359	343	11
ρ Oph	23	20	288	277	48	29	37	44	2
Trumpler 14	43	11	1859	1045	228	55	165	159	11
Cha I	47	36	660	623	102	54	88	87	6
NGC 2244	8	6	444	385	143	79	123	116	1
NGC 2264	113	70	1740	1539	621	423	507	503	10
λ Ori	116	103	720	675	207	142	163	161	3
Col 197	8	3	401	363	123	86	104	92	7
γ Vel	79	50	1183	1140	...	...	...	234	1
NGC 2232	47	28	1822	1722	750	56	84	68	9
NGC 2547	54	33	423	372	...	...	...	151	0
IC 2391	48	26	386	374	56	27	37	35	6
IC 2602	131	89	1721	1651	309	43	59	55	24
IC 4665	34	30	533	514	233	29	51	33	0
NGC 2451 A/B	90	70	1566	1537	...	...	...	106	10
NGC 6405	21	12	680	486	251	80	53	51	1
Blanco 1	37	31	426	373	142	119	101	98	0
NGC 6067	27	16	753	327	209	126	60	56	0
NGC 6649	6	0	277	62	42	21	4	2	0
NGC 2516	51	32	708	645	460	378	379	376	0
NGC 6709	10	10	720	590	322	71	53	49	10
NGC 6259	16	14	478	264	125	71	39	35	0
NGC 6705	49	31	1017	579	391	313	142	139	0
Berkeley 30	14	13	318	144	78	44	24	24	0
NGC 6281	16	7	304	214	82	38	23	23	1
NGC 3532	67	51	1094	809	518	411	323	384	11
NGC 4815	14	12	204	92	68	50	30	29	0
NGC 6633	57	38	1605	1463	617	35	62	67	9
NGC 2477	11	10	114	0	86	71	9	9	0
Trumpler 23	16	15	165	70	51	41	25	23	0
Berkeley 81	14	14	265	159	69	42	25	24	0
NGC 2355	11	11	197	149	119	129	87	86	0
NGC 6802	13	13	184	69	77	51	36	32	2
NGC 6005	19	19	541	298	174	112	55	49	3
Pismis 18	10	10	134	72	41	24	12	10	0
Melotte 71	9	9	111	0	71	64	4	4	0
Pismis 15	11	11	322	201	91	66	33	31	1
Trumpler 20	29	26	1184	404	451	367	116	104	0
Berkeley 44	7	7	86	73	39	33	31	30	0
NGC 2243	27	27	634	576	469	446	289	289	8
M67	42	36	95	85	109	89	96	96	0

Notes. [a]Regarding the clusters γ Vel, NGC 2547 and NGC 2451 A and B, we directly used the selections obtained by several studies listed in Table 1.

obtained as a parallel result during the membership analysis. Readers are directed to the individual notes of Appendix A, where we offer a detailed and in-depth discussion of the membership analysis for each cluster, as well as commenting on features of interest regarding individual stars in the selection, and comparing our candidate lists with former membership studies. The full tables resulting from our membership analysis, divided into young, intermediate-age and old age ranges, are provided via the CDS, and described in Appendix C. In these tables we list all membership criteria in our analysis and the final selections of candidate members for each of the 42 OCs analysed.

We also show our final selections in the following figures: Fig. 6 shows the EW(Li)-versus-$T_{\rm eff}$ diagrams subdivided into young, intermediate-age, and old clusters. These figures also include for reference the upper envelope of EW(Li) for IC 2602 (35 Myr, in red), the upper and lower envelopes of the Pleiades (78–125 Myr, in grey), and the upper envelope of the Hyades (750 Myr, turquoise). In Fig. 6 we also show the representative average errors in $T_{\rm eff}$ and EW(Li) for all members of the young, intermediate-age and old clusters. These average errors amount to 68 K and 12 mÅ for the young clusters; 69 K and 7 mÅ for the intermediate-age clusters; and 65 K and 8 mÅ for the old

Table 7. Results for the 42 star forming regions and OCs in the sample, indicating, for each cluster: all stars (both UVES and GIRAFFE) from the GES sample and the number of stars detected with measured EW(Li) values, the number of stars selected as candidate members, and Li-rich giant field contaminants.

Cluster	iDR6 stars		Members			Li-rich giants	
	All	With Li	#	%(All)	%(with Li)	#	%(All)
NGC 6530	1983	1330	343	17.3	25.8	11	0.6
ρ Oph	311	297	44	13.8	14.5	2	0.6
Trumpler 14	1902	1056	159	8.4	15.1	11	0.6
Cha I	707	659	87	12.3	13.2	6	0.8
NGC 2244	452	391	116	25.7	29.7	1	0.2
NGC 2264	1853	1609	503	27.1	31.3	10	0.5
λ Ori	836	778	161	19.3	20.7	3	0.4
Col 197	409	366	92	22.5	25.1	7	1.7
γ Vel	1262	1190	234	18.5	19.7	1	0.1
NGC 2232	1869	1750	68	3.6	3.9	9	0.5
NGC 2547	477	405	151	31.7	37.3	0	0.0
IC 2391	434	400	35	8.1	8.8	6	1.4
IC 2602	1852	1740	55	3.0	3.2	24	1.3
IC 4665	567	544	33	5.8	6.1	0	0.0
NGC 2451 A/B	1656	1607	106	6.4	6.6	10	0.6
NGC 6405	701	498	51	7.3	10.2	1	0.1
Blanco 1	463	404	96	20.7	23.8	0	0.0
NGC 6067	780	343	56	7.2	16.3	0	0.0
NGC 6649	283	62	2	0.7	3.2	0	0.0
NGC 2516	759	677	376	49.5	55.5	0	0.0
NGC 6709	730	600	49	6.7	8.2	10	1.4
NGC 6259	494	278	35	7.1	12.6	0	0.0
NGC 6705	1066	610	139	13.0	22.8	0	0.0
Berkeley 30	332	157	24	7.2	15.3	0	0.0
NGC 6281	320	221	23	7.2	10.4	1	0.3
NGC 3532	1145	860	384	33.5	44.7	11	1.0
NGC 4815	218	104	29	13.3	27.9	0	0.0
NGC 6633	1662	1501	67	4.0	4.5	9	0.5
NGC 2477	125	10	9	7.2	90.0	0	0.0
Trumpler 23	165	85	23	13.9	27.1	0	0.0
Berkeley 81	279	173	24	8.6	13.9	0	0.0
NGC 2355	208	160	86	41.4	53.8	0	0.0
NGC 6802	197	82	32	16.2	39.0	2	1.0
NGC 6005	560	317	49	8.8	15.5	3	0.5
Pismis 18	142	82	10	7.0	12.2	0	0.0
Melotte 71	120	9	4	3.4	44.5	0	0.0
Pismis 15	333	211	31	9.3	14.7	1	0.3
Trumpler 20	1213	430	104	8.6	24.2	0	0.0
Berkeley 44	93	80	30	32.3	37.5	0	0.0
NGC 2243	661	603	289	43.7	48.0	8	1.2
M67	131	121	96	73.3	79.3	0	0.0

Notes. Regarding member stars, we provide their percentages with respect to all GES stars and to those with a EW(Li) measurement in the field of each cluster.

clusters. On the other hand, Fig. 7 shows the γ-versus-$T_{\rm eff}$ diagram for the young clusters in our sample, as well as the Kiel diagram for all intermediate-age and old clusters in the sample. Additionally, Appendix B shows all the individual figures for the cluster sample, including both candidate members as well as Li-rich contaminants of interest.

Finally, in Table 7 we show some further results of our membership analysis for the 42 sample clusters. As in Table 6, we show the number of stars in the field of each cluster from the initial iDR6 sample and the number of candidate stars for all clusters, as well as the Li-rich giant contaminants. With these results we derived percentages of the candidate members and outlier contaminants, which can be used to rank the target clusters and different age ranges in terms of the percentage of candidate members and contaminants identified in each case. Regarding the cluster members, these percentages are considered firstly with respect to all stars in the field of each cluster, and also with respect to all stars that present Li in the initial sample. However, we only present percentages for the Li-rich giant outliers with respect to all stars in the field, given that these were selected taking A(Li) and not EW(Li) into account.

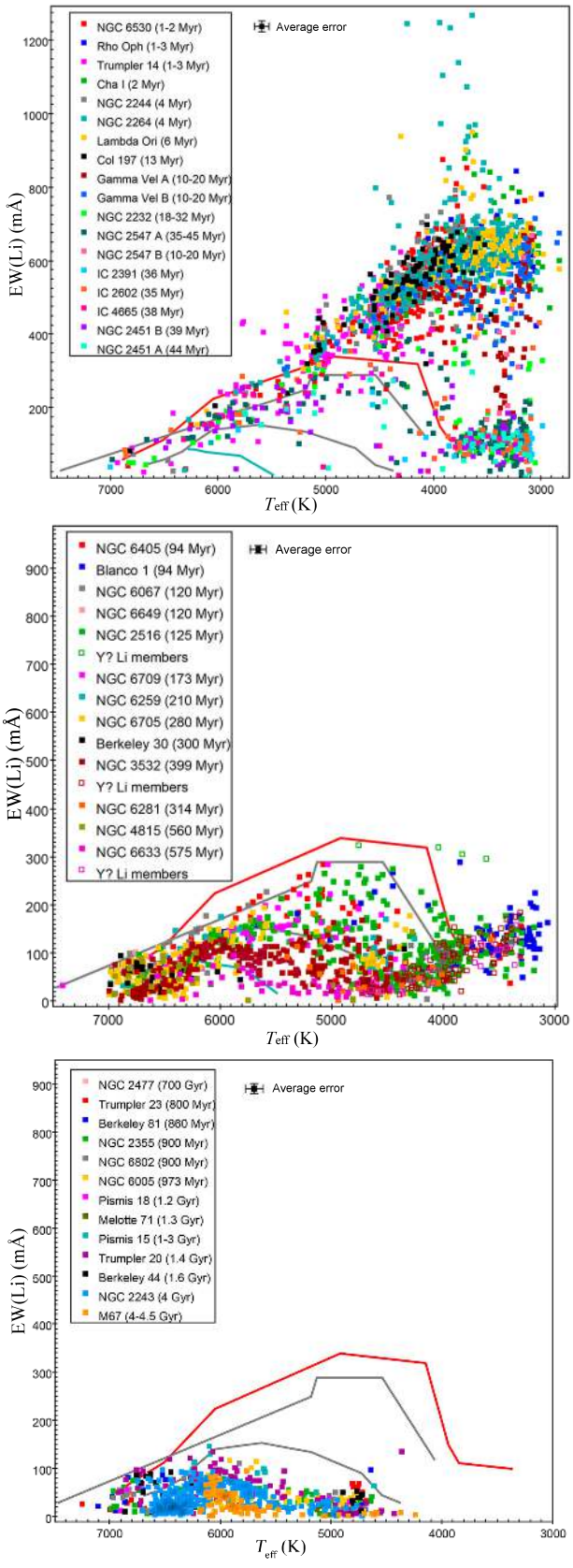

Fig. 6. EW(Li)-versus-$T_{\rm eff}$ diagrams for the candidate members of the young (1–50 Myr; top panel), intermediate-age (50–700 Myr; middle panel), and old clusters (>700 Myr; bottom panel). Open squares indicate improbable EW(Li) values for some members. Average errors in $T_{\rm eff}$ (K) and EW(Li) (mÅ) are also shown. Reference envelopes for IC 2602, Pleiades and Hyades shown as described in Fig. 4.

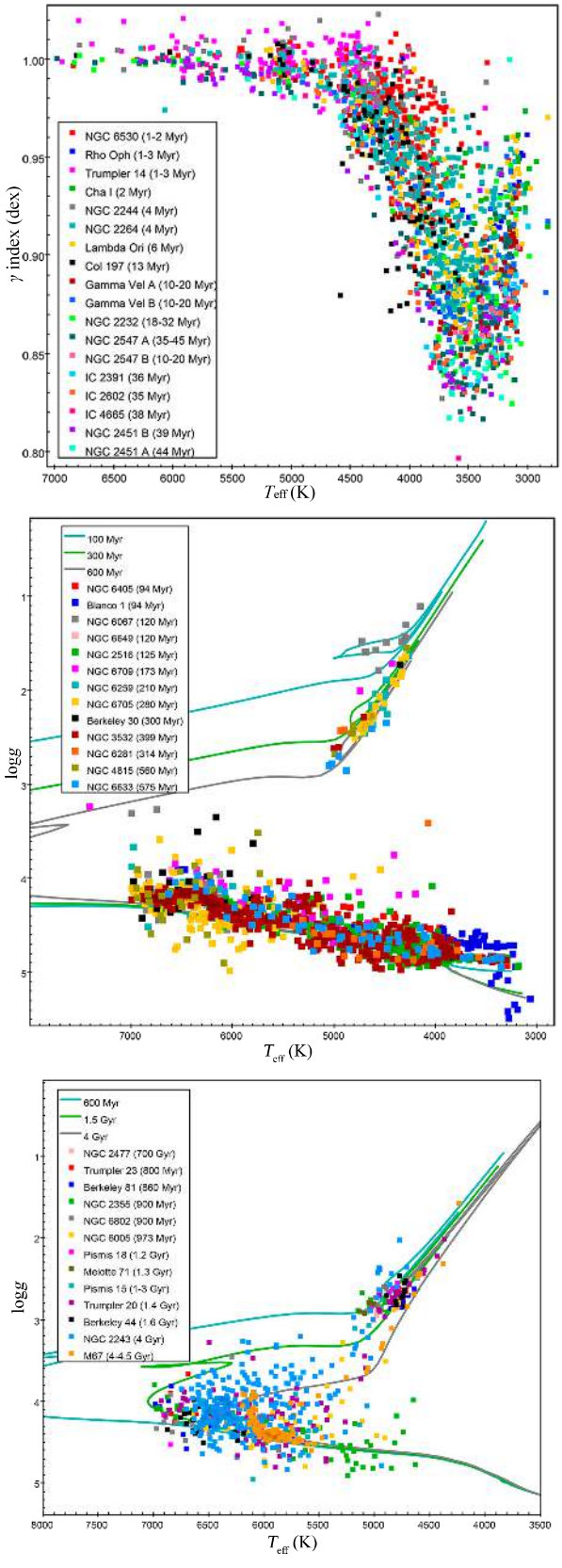

Fig. 7. Gravity index γ as a function of $T_{\rm eff}$ for the members for all young clusters of the sample (top panel), and Kiel diagrams for all intermediate-age and old clusters for the candidate members of the intermediate-age (50–700 Myr; middle panel) and old clusters (>700 Myr; bottom panel). We overplot the PARSEC isochrones in a similar age range, with a metallicity of $Z = 0.019$.

5. Summary

This work is a large-scale project, which we started in Paper I (Gutiérrez Albarrán et al. 2020) and concluded in Paper III (Gutierrez Albarrán et al., in prep.), with the main objective of studying Li as an age indicator and calibrating a Li–age relation for PMS, ZAMS, and early MS FGK late-type stars. With a considerably expanded sample of 42 OCs spanning a wide age range from 1–3 Myr to 4–4.5 Gyr, in the present work we made use of the most recent available GES-derived data provided by iDR6, as well as of the high-precision data provided by *Gaia* EDR3, in order to conduct a thorough membership analysis and obtain updated and expanded selections of candidates for all target clusters. We summarise our analysis and the main results of this work as follows:

With the present work, we considerably enlarged and improved our target sample, with 42 young, intermediate-age and old clusters provided by GES iDR6 at our disposal, as compared to our former sample of 20 clusters using data from GES iDR4 from Paper I. The new homogeneous analysis done in iDR6 also offers marked improvements to both our cluster sample and our consequent analysis, including a significantly larger number of stars measured in the field of many of the clusters, the recalculation of parameters for higher accuracy, and accounting for the contamination of background nebular lines (as detailed in Sect. 2).

We carried out extensive preliminary bibliographical research on each of the 42 sample clusters, compiling a thorough selection of literature data on ages, distances, and reddening values (see Tables 1 and 2 in Sect. 2), as well as RVs (Table 3 in Sect. 3), proper motions, parallaxes (Table 4 in Sect. 3), [Fe/H] metallicity (Table 5 in Sect. 3), previous Li measurements, and numerous existing membership studies (as also presented in Tables 1 and 2, as well as in Appendix A).

We performed exhaustive and detailed membership analyses (see Sect. 3), firstly studying the RV distributions to obtain likely kinematic candidates, and complementing this with a thorough study of the proper motions and parallaxes provided by *Gaia*, a marked improvement in regards to our former analyses in Paper I. Gravity indicators such as $\log g$ and the γ index were helpful in order to discard field giant contaminants and confirm the membership of the astrometric selections, also significantly improved by *Gaia* photometry in CMDs. We complemented all these criteria with a study of the distribution of [Fe/H] metallicity, which helped reinforce our cluster selections and discard further rogue contaminants. Finally, we used Li as a final criterion by plotting the candidates in EW(Li) versus $T_{\rm eff}$ diagrams.

We obtained selections of robust candidates for all 42 sample clusters, some of which had not been previously studied in detail by the GES consortium (see Table 6 in Sect. 4), and we also discuss which individual clusters and age ranges present the highest percentages of members in our target sample in Table 7. All individual figures are displayed in Appendix B, and this paper also includes descriptions for the associated tables of results, described in Appendix C, in which we list the final candidates for all clusters and specify which membership criteria are fulfilled by each of the target stars for each cluster.

We made use of a number of studies from the literature conducted from *Gaia* DR1, DR2, and EDR3 data to do an in-depth assessment of our candidate selections after concluding our membership analysis, typically obtaining coherent results, as we found our lists of cluster members to be in general agreement with these previous GES studies (see Appendix A). In addition, we also fitted the distributions of RV, parallaxes, and [Fe/H] metallicity values of all final cluster selections, as displayed in Tables 3 (for RVs), 4 (for parallaxes), and 5 (for metallicity), obtaining mean values that are consistent with the literature for the majority of clusters, with very few exceptions.

Given their importance for our understanding of stellar Li, as an additional result of our membership analysis we also selected a series of preliminary Li-rich giant outliers for 23 out of the 42 target clusters (see Sect. 3.4, as well as Table 6 in Sect. 4 and Appendix C). Given the scarcity of these objects, we require further confirmation to accept all stars listed as Li-rich giant contaminants in this study.

The selections of cluster candidates obtained by means of recent GES and *Gaia* data can be used by the scientific community in multiple applications, from the calibration of a Li–age relation –the aim of this particular work – to further analysis of (the same or other) cluster members, or the characterisation of a variety of stellar parameters and other areas of interest regarding OCs and the formation and evolution of stars in the Galaxy.

In the companion paper to this work, Paper III, we conclude our calibration of an empirical Li–age relation and obtain a set of empirical Li envelopes for several key ages in our sample. This final paper will also describe our future work.

Acknowledgements. We acknowledge financial support from the Universidad Complutense de Madrid (UCM) and the Agencia Estatal de Investigación (AEI/10.13039/501100011033) of the Ministerio de Ciencia e Innovación and the ERDF "A way of making Europe" through projects PID2019-109522GB-C5[4] and PID2022-137241NBC4[4]. We acknowledge the support from INAF and Ministero dell' Istruzione, dell' Universitá' e della Ricerca (MIUR) in the form of the grant "Premiale VLT 2012". T.B. was supported by grant no. 2018-04857 from the Swedish Research Council. J.I.G.H. acknowledges financial support from the Spanish Ministry of Science, Innovation and Universities (MICIU) under the 2003 Ramón y Cajal program RYC-2013-14875, and also from the Spanish Ministry project MICIU AYA2017-86389-P. E.J.A. acknowledges financial support from the State Agency for Research of the Spanish MCIU through the "Center of Excellence Severo Ochoa" award to the Instituto de Astrofśica de Andalucá (CEX2021- 001131-S). E.M. acknowledges financial support through a "Margarita Salas" postdoctoral fellowship from Universidad Complutense de Madrid (CT18/22), funded by the Spanish Ministerio de Universidades with NextGeneration EU funds. F.J.E. acknowledges support from ESA through the Faculty of the European Space Astronomy Centre (ESAC) – Funding reference 4000139151/22/ES/CM. Based on data products from observations made with ESO Telescopes at the La Silla Paranal Observatory under programme focusID 188.B-3002. These data products have been processed by the Cambridge Astronomy Survey Unit (CASU) at the Institute of Astronomy, University of Cambridge, and by the FLAMES/UVES reduction team at INAF – Osservatorio Astrofisico di Arcetri. These data have been obtained from the GES Data Archive, prepared and hosted by the Wide Field Astronomy Unit, Institute for Astronomy, University of Edinburgh, which is funded by the UK Science and Technology Facilities Council. The results presented here benefit from discussions held during GES workshops and conferences supported by the ESF (European Science Foundation) through the GREAT Research Network Programme. This work has made use of data from the European Space Agency (ESA) mission *Gaia* (`https://www.cosmos.esa.int/gaia`), processed by the *Gaia* Data Processing and Analysis Consortium (DPAC, `https://www.cosmos.esa.int/web/gaia/dpac/consortium`). Funding for the DPAC has been provided by national institutions, in particular the institutions participating in the *Gaia* Multilateral Agreement. This publication makes use of the VizieR database (Ochsenbein et al. 2000) and the SIMBAD database (Wenger et al. 2000), both operated at CDS, Centre de Données astronomiques de Strasbourg, France. This research also made use of the WEBDA database, operated at the Department of Theoretical Physics and Astrophysics of the Masaryk University, and the interactive graphical viewer and editor for tabular data TOPCAT (Taylor 2005). For the analysis of the distributions of RV and metallicity we used RStudio Team (2015). Integrated Development for R. RStudio, Inc., Boston, MA (`http://www.rstudio.com/`). Finally, we would like to thank the anonymous referee for helpful comments and suggestions.

References

Alonso-Santiago, J., Negueruela, I., Marco, A., et al. 2017, MNRAS, 469, 1330
Alonso-Santiago, J., Negueruela, I., Marco, A., et al. 2020, A&A, 644, A136
Arancibia-Silva, J., Bouvier, J., Bayo, A., et al. 2020, A&A, 635, A13
Armstrong, J. J., Wright, N. J., Jeffries, R. D., et al. 2020, MNRAS, 494, 4794
Bailey, J. I., Mateo, M., White, R. J., et al. 2018, MNRAS, 475, 1609
Balachandran, S. 1995, ApJ, 446, 203
Balog, Z., Kiss, L. L., Vinkó, J., et al. 2009, ApJ, 698, 1989
Barrado y Navascués, D. 2004, A&A, 422, 631
Barrado y Navascués, D., Stauffer, J. R., Briceño, C., et al. 2001, ApJS, 134, 103
Barrado, D., Stelzer, B., Morales-Calderón, M., et al. 2011, A&A, 526, A21
Barsony, M., Haisch, K. E., Marsh, K. A., et al. 2012, ApJ, 751, 22
Bayo, A., Barrado, D., Huélamo, N., et al. 2012, A&A, 547, A80
Beccari, G., Boffin, H. M. J., Jerabkova, T., et al. 2018, MNRAS, 481, L11
Binks, A. S., Jeffries, R. D., Sacco, G. G., et al. 2022, MNRAS, 513, 5727
Bonatto, C., & Bica, E. 2010, A&A, 516, A81
Bonito, R., Prisinzano, L., Guarcello, M. G., et al. 2013, A&A, 556, A108
Bonito, R., Prisinzano, L., Venuti, L., et al. 2020, A&A, 642, A56
Bossini, D., Vallenari, A., Bragaglia, A., et al. 2019, A&A, 623, A108
Bouvier, J., Barrado, D., Moraux, E., et al. 2018, A&A, 613, A63
Bragaglia, A., Alfaro, E., Flaccomio, E., et al. 2022, A&A, 659, A200
Bravi, L., Zari, E., Sacco, G. G., et al. 2018, A&A, 615, A37
Bressan, A., Marigo, P., Girardi, L., et al. 2012, MNRAS, 427, 127
Brucalassi, A., Koppenhoefer, J., Saglia, R., et al. 2017, A&A, 603, A85
Buckner, A. S. M., & Froebrich, D. 2014, MNRAS, 444, 290
Cánovas, H., Cantero, C., Cieza, L., et al. 2019, A&A, 626, A80
Cantat-Gaudin, T., Jordi, C., Vallenari, A., et al. 2018, A&A, 618, A93
Cantat-Gaudin, T., Mapelli, M., Balaguer-Núñez, L., et al. 2019, A&A, 621, A115
Cargile, P. A., James, D. J., & Jeffries, R. D. 2010, ApJ, 725, L111
Carlberg, J. K. 2014, AJ, 147, 138
Carraro, G., Geisler, D., Baume, G., et al. 2005, MNRAS, 360, 655
Carrera, R., Bragaglia, A., Cantat-Gaudin, T., et al. 2019, A&A, 623, A80
Casali, G., Magrini, L., Tognelli, E., et al. 2019, A&A, 629, A62
Casamiquela, L., Carrera, R., Balaguer-Núñez, L., et al. 2018, A&A, 610, A66
Casey, A. R., Ruchti, G., Masseron, T., et al. 2016, MNRAS, 461, 3336
Castro-Ginard, A., Jordi, C., Luri, X., et al. 2020, A&A, 635, A45
Conrad, C., Scholz, R. D., Kharchenko, N. V., et al. 2017, A&A, 600, A106
Damiani, F., Prisinzano, L., Micela, G., et al. 2014, A&A, 566, A50
Damiani, F., Klutsch, A., Jeffries, R. D., P., et al. 2017, A&A, 603, A81
Damiani, F., Prisinzano, L., Micela, G., et al. 2019, A&A, 623, A25
de la Torre Rojo, A. 2020, Master's thesis, Universidad Complutense de Madrid, Spain
De Silva, G. M., D'Orazi, V., Melo, C., et al. 2013, MNRAS, 431, 1005
de Wit, W. J., Bouvier, J., Palla, F., et al. 2006, A&A, 448, 189
Dias, W. S., Alessi, B. S., Moitinho, A., et al. 2002, A&A, 389, 871
Dias, W. S., Monteiro, H., Lépine, J. R. D., et al. 2019, MNRAS, 486, 5726
Dib, S., Schmeja, S., & Parker, R. J. 2018, MNRAS, 473, 849
Dobbie, P. D., Day-Jones, A., Williams, K. A., et al. 2012, MNRAS, 423, 2815
Dodd, R. J. 2004, MNRAS, 355, 959
Donati, P., Beccari, G., Bragaglia, A., et al. 2014a, MNRAS, 437, 1241
Donati, P., Cantat Gaudin, T., Bragaglia, A., et al. 2014b, A&A, 561, A94
Ducourant, C., Teixeira, R., Krone-Martins, A., et al. 2017, A&A, 597, A90
Dumont, T., Charbonnel, C., Palacios, A., et al. 2021a, A&A, 654, A46
Dumont, T., Palacios, A., Charbonnel, C., et al. 2021b, A&A, 646, A48
Duque Arribas, C. 2020, Master's thesis, Universidad Complutense de Madrid, Spain
Eigenbrod, A., Mermilliod, J. C., Clariá, J. J., et al. 2004, A&A, 423, 189
Elliott, P., Bayo, A., Melo, C. H. F., et al. 2016, A&A, 590, A13
Esplin, T. L., Luhman, K. L., Faherty, J. K., et al. 2017, AJ, 154, 46
Franciosini, E., & Sacco, G. G. 2011, A&A, 530, A150
Franciosini, E., Sacco, G. G., Jeffries, R. D., et al. 2018, A&A, 616, A12
Franciosini, E., Randich, S., de Laverny, P., et al. 2022a, A&A, 668, A49
Franciosini, E., Tognelli, E., Degl'Innocenti, S., et al. 2022b, A&A, 659, A85
Frasca, A., Biazzo, K., Lanzafame, A. C., et al. 2015, A&A, 575, A4
Friel, E. D., & Janes, K. A. 1993, A&A, 267, 75
Friel, E. D., Donati, P., Bragaglia, A., et al. 2014, A&A, 563, A117
Frinchaboy, P. M., & Majewski, S. R. 2008, AJ, 136, 118
Fritzewski, D. J., Barnes, S. A., James, D. J., et al. 2019, A&A, 622, A110
Fritzewski, D. J., Barnes, S. A., James, D. J., et al. 2020, A&A, 641, A51
Fritzewski, D. J., Barnes, S. A., James, D. J., et al. 2021, A&A, 652, A60
Gaia Collaboration (Brown, A. G. A., et al.) 2016a, A&A, 595, A2
Gaia Collaboration (Prusti, T., et al.) 2016b, A&A, 595, A1
Gaia Collaboration (Babusiaux, C., et al.) 2018a, A&A, 616, A10
Gaia Collaboration (Brown, A. G. A., et al.) 2018b, A&A, 616, A1
Gaia Collaboration (Brown, A. G. A., et al.) 2021, A&A, 649, A1
Gaia Collaboration (Vallenari, A., et al.) 2023, A&A, 674, A1
Galli, P. A. B., Bouy, H., Olivares, J., et al. 2021, A&A, 646, A46
Gao, X. 2018, AJ, 156, 121
Geller, A. M., Latham, D. W., & Mathieu, R. D. 2015, AJ, 150, 97
Gillen, E., Hillenbrand, L. A., Stauffer, J., et al. 2020, MNRAS, 495, 1531
Gilmore, G., Randich, S., Asplund, M., et al. 2012, The Messenger, 147, 25
Gilmore, G., Randich, S., Worley, C. C., et al. 2022, A&A, 666, A120
Gómez Garrido, M. 2015, Master's thesis, Universidad Complutense de Madrid, Spain
Gómez Garrido, M., Montes, D., Gutiérrez Albarrán, M. L., et al. 2017, Highlights on Spanish Astrophysics IX, Proceedings of the XII Scientific Meeting of the Spanish Astronomical Society held on July 18–22, 2016, in Bilbao, Spain
Gutiérrez Albarrán, M. L. 2022, PhD thesis, Universidad Complutense de Madrid, Spain
Gutiérrez Albarrán, M. L., Montes, D., Gómez Garrido, M., et al. 2020, A&A, 643, A71
Hatzidimitriou, D., Held, E. V., Tognelli, E., et al. 2019, A&A, 626, A90
Hayes, C. R., & Friel, E. D. 2014, AJ, 147, 69
Heiter, U., Soubiran, C., Netopil, M., et al. 2014, A&A, 561, A93
Hernández, J., Morales-Calderón, M., Calvet, N., et al. 2010, ApJ, 722, 1226
Hetem, A., & Gregorio-Hetem, J. 2019, MNRAS, 490, 2521
Hobbs, L. M., & Pilachowski, C. 1986, ApJ, 311, L37
Hourihane, A., Francois, P., Worley, C. C., et al. 2023, A&A, 676, A129
Hünsch, M., Randich, S., Hempel, M., et al. 2004, A&A, 418, 539
Ilin, E., Schmidt, S. J., Poppenhäger, K., et al. 2021, A&A, 645, A42
Irwin, J., Hodgkin, S., Aigrain, S., et al. 2007, MNRAS, 377, 741
Jackson, R. J., & Jeffries, R. D. 2010, MNRAS, 407, 465
Jackson, R. J., Jeffries, R. D., Randich, S., et al. 2016, A&A, 586, A52
Jackson, R. J., Jeffries, R. D., Wright, N. J., et al. 2022, MNRAS, 509, 1664
Jacobson, H. R., Friel, E. D., & Pilachowski, C. A. 2011, AJ, 141, 58
Jacobson, H. R., Friel, E. D., Jílková, L., et al. 2016, A&A, 591, A37
Jadhav, V. V., Pennock, C. M., Subramaniam, A., et al. 2021, MNRAS, 503, 236
Jeffries, R. D. 1997, MNRAS, 292, 177
Jeffries, R. D. 2014, EAS Pub. Ser, 65, 289
Jeffries, R. D., James, D. J., & Thurston, M. R. 1998, MNRAS, 300, 550
Jeffries, R. D., Thurston, M. R., & Hambly, N. C. 2001, A&A, 375, 863
Jeffries, R. D., Totten, E. J., Harmer, S., et al. 2002, MNRAS, 336, 1109
Jeffries, R. D., Jackson, R. J., James, D. J., et al. 2009, MNRAS, 400, 317
Jeffries, R. D., Jackson, R. J., Cottaar, M., et al. 2014, A&A, 563, A94
Jeffries, R. D., Jackson, R. J., & Binks, A. S. 2023, MNRAS, 526, 1260
Jones, B. F., Fischer, D., & Soderblom, D. R. 1999, AJ, 117, 330
Joshi, Y. C., Dambis, A. K., Pandey, A. K., et al. 2016, A&A, 593, A116
Juarez, A. J., Cargile, P. A., James, D. J., et al. 2014, ApJ, 795, 143
Kang, W., & Lee, S.-G. 2012, MNRAS, 425, 3162
Kharchenko, N. V., Piskunov, A. E., Röser, S., et al. 2005, A&A, 438, 1163
Kılıçoğlu, T., Monier, R., Richer, J., et al. 2016, AJ, 151, 49
Kiman, R., Faherty, J. K., Cruz, K. L., et al. 2021, AJ, 161, 277
Kounkel, M., & Covey, K. 2019, AJ, 158, 122
Kuhn, M. A., Hillenbrand, L. A., Sills, A., et al. 2019, ApJ, 870, 32
Lanzafame, A. C., Frasca, A., Damiani, F., et al. 2015, A&A, 576, A80
Lim, B., Sung, H., Kim, J. S., et al. 2016, ApJ, 831, 116
Lindegren, L. 2018, Proceedings from the third Gaia DPAC consortium meeting, GAIA-C3-TN-LU-LL-124-01
Lindegren, L., Hernández, J., Bombrun, A., et al. 2018, A&A, 616, A2
Liu, L., & Pang, X. 2019, ApJS, 245, 32
Lodieu, N., de Wit, W. J., Carraro, G., et al. 2011, A&A, 532, A103
López Martí, B., Jiménez-Esteban, F., Bayo, A., et al. 2013, A&A, 556, A144
López-Santiago, J., Montes, D., Fernández-Figueroa, M. J., et al. 2003, A&A, 411, 489
Luhman, K. L., & Muench, A. A. 2008, ApJ, 684, 654
Luhman, K. L., Allen, L. E., Allen, P. R., et al. 2008, ApJ, 675, 1375
Lyubimkov, L. S. 2016, Astrophysics, 59, 411
Magrini, L., Randich, S., Romano, D., et al. 2014, A&A, 563, A44
Magrini, L., Randich, S., Donati, P., et al. 2015, A&A, 580, A85
Magrini, L., Randich, S., Kordopatis, G., et al. 2017, A&A, 603, A2
Magrini, L., Vincenzo, F., Randich, S., et al. 2018, A&A, 618, A102
Magrini, L., Smiljanic, R., Lagarde, N., et al. 2021, The Messenger, 185, 18
Maíz Apellániz, J. 2019, A&A, 630, A119
Manzi, S., Randich, S., de Wit, W. J., et al. 2008, A&A, 479, 141
Martín, E. L., & Montes, D. 1997, A&A, 318, 805
Martos, G., Meléndez, J., Rathsam, A., & Carvalho Silva, G. 2023, MNRAS, 522, 3217
Mel'nik, A. M., & Dambis, A. K. 2017, MNRAS, 472, 3887
Merle, T., Van Eck, S., Jorissen, A., et al. 2017, A&A, 608, A95
Merle, T., Van der Swaelmen, M., Van Eck, S., et al. 2020, A&A, 635, A155

Messina, S., Desidera, S., Lanzafame, A. C., et al. 2011, A&A, 532, A10
Michalska, G. 2019, MNRAS, 487, 3505
Montes, D., López-Santiago, J., Fernández-Figueroa, M. J., et al. 2001, A&A, 379, 976
Mužić, K., Scholz, A., Peña Ramírez, K., et al. 2019, ApJ, 881, 79
Netopil, M., & Paunzen, E. 2013, A&A, 557, A10
Netopil, M., Paunzen, E., Heiter, U., et al. 2016, A&A, 585, A150
Neuhaeuser, R., Torres, G., Sterzik, M. F., et al. 1997, A&A, 325, 647
Ochsenbein, F., Bauer, P., & Marcout, J. 2000, A&AS, 143, 23
Oh, S., Price-Whelan, A. M., Brewer, J. M., et al. 2018, ApJ, 854, 138
Oliveira, J. M., Jeffries, R. D., Devey, C. R., et al. 2003, MNRAS, 342, 651
Overbeek, J. C., Friel, E. D., Donati, P., et al. 2017, A&A, 598, A68
Pace, G., Castro, M., Meléndez, J., et al. 2012, A&A, 541, A150
Pallavicini, R., Randich, S., Giampapa, M., & Cutispoto, G. 1990, The Messenger, 62, 51
Pallavicini, R., Randich, S., & Giampapa, M. S. 1992, A&A, 253, 185
Pallavicini, R., Pasquini, L., & Randich, S. 1997, Mem. Soc. Astron. It., 68, 933
Pallavicini, R., Randich, S., & Sestito, P. 2005, ESA SP, 560, 867
Pang, X., Li, Y., Yu, Z., et al. 2021, ApJ, 912, 162
Pasquini, L., Randich, S., & Pallavicini, R. 1997, A&A, 325, 535
Pasquini, L., Brucalassi, A., Ruiz, M. T., et al. 2012, A&A, 545, A139
Paunzen, E., Heiter, U., Netopil, M., et al. 2010, A&A, 517, A32
Platais, I., Melo, C., Mermilliod, J. C., et al. 2007, A&A, 461, 509
Platais, I., Girard, T. M., Vieira, K., et al. 2011, MNRAS, 413, 1024
Postnikova, E. S., Chupina, N. V., & Vereshchagin, S. V. 2019, INASAN Sci. Rep., 3, 336
Postnikova, E. S., Elsanhoury, W. H., Sariya, D. P., et al. 2020, Res. Astron. Astrophys., 20, 016
Prisinzano, L., Damiani, F., Micela, G., et al. 2005, A&A, 430, 941
Prisinzano, L., Damiani, F., Micela, G., et al. 2007, A&A, 462, 123
Prisinzano, L., Micela, G., Sciortino, S., et al. 2012, A&A, 546, A9
Prisinzano, L., Damiani, F., Micela, G., et al. 2016, A&A, 589, A70
Prisinzano, L., Damiani, F., Kalari, V., et al. 2019, A&A, 623, A159
Prisinzano, L., Damiani, F., Sciortino, S., et al. 2022, A&A, 664, A175
Rain, M. J., Ahumada, J. A., & Carraro, G. 2021, A&A, 650, A67
Randich, S., & Magrini, L. 2021, Front. Astron. Space Sci., 8, 6
Randich, S., Aharpour, N., Pallavicini, R., et al. 1997, A&A, 323, 86
Randich, S., Pallavicini, R., Meola, G., et al. 2001, A&A, 372, 862
Randich, S., Primas, F., Pasquini, L., et al. 2002, A&A, 387, 222
Randich, S., Gilmore, G., & Gaia-ESO Consortium 2013, The Messenger, 154, 47
Randich, S., Tognelli, E., Jackson, R., et al. 2018, A&A, 612, A99
Randich, S., Pasquini, L., Franciosini, E., et al. 2020, A&A, 640, L1
Randich, S., Gilmore, G., Magrini, L., et al. 2022, A&A, 666, A121
Rangwal, G., Yadav, R. K. S., Durgapal, A., et al. 2019, MNRAS, 490, 1383
Richer, H. B., Fahlman, G. G., Rosvick, J., et al. 1998, ApJ, 504, L91
Riello, M., De Angeli, F., Evans, D. W., et al. 2021, A&A, 649, A3
Rigliaco, E., Wilking, B., Meyer, M. R., et al. 2016, A&A, 588, A123
Robrade, J., & Schmitt, J. H. M. M. 2007, A&A, 461, 669
Roccatagliata, V., Sacco, G. G., Franciosini, E., et al. 2018, A&A, 617, A4
Romano, D., Magrini, L., Randich, S., et al. 2021, A&A, 653, A72
Sacco, G. G., Franciosini, E., Randich, S., et al. 2008, A&A, 488, 167
Sacco, G. G., Jeffries, R. D., Randich, S., et al. 2015, A&A, 574, A7
Sacco, G. G., Spina, L., Randich, S., et al. 2017, A&A, 601, A97
Sampedro, L., Dias, W. S., Alfaro, E. J., et al. 2017, MNRAS, 470, 3937
Sestito, P., & Randich, S. 2005, A&A, 442, 615
Siess, L., Dufour, E., & Forestini, M. 2000, A&A, 358, 593
Silaj, J., & Landstreet, J. D. 2014, A&A, 566, A132
Skrutskie, M. F., Cutri, R. M., Stiening, R., et al. 2006, AJ, 131, 1163
Smiljanic, R., Randich, S., & Pasquini, L. 2011, A&A, 535, A75
Smiljanic, R., Korn, A. J., Bergemann, M., et al. 2014, A&A, 570, A122
Smiljanic, R., Franciosini, E., Randich, S., et al. 2016, A&A, 591, A62
Smiljanic, R., Franciosini, E., Bragaglia, A., et al. 2018, A&A, 617, A4
Sneden, C., Bean, J., Ivans, I., Lucatello, S., & Sobeck, J. 2012, Astrophysics Source Code Library [record ascl:1202.009]
Soderblom, D. R. 2010, ARA&A, 48, 581
Soderblom, D. R., Jones, B. F., Balachandran, S., et al. 1993, AJ, 106, 1059
Soderblom, D. R., Hillenbrand, L. A., Jeffries, R. D., et al. 2014, Protostars and Planets VI, eds., H. Beuther, R. S. Klessen, C. P. Dullemond, & T. Henning (Tucson: University of Arizona Press), 219
Soubiran, C., Cantat-Gaudin, T., Romero-Gómez, M., et al. 2018, A&A, 619, A155
Spina, L., Randich, S., Palla, F., et al. 2014a, A&A, 568, A2
Spina, L., Randich, S., Palla, F., et al. 2014b, A&A, 567, A55
Spina, L., Randich, S., Magrini, L., et al. 2017, A&A, 601, A70
Stauffer, J. R., Hartmann, L. W., Prosser, C. F., et al. 1997, ApJ, 479, 776
Subramaniam, A., & Sagar, R. 1999, AJ, 117, 937
Sutherland, W., Emerson, J., Dalton, G., et al. 2015, A&A, 575, A25
Tabernero, H. M., Marfil, E., Montes, D., et al. 2019, A&A, 628, A131
Tang, B., Geisler, D., Friel, E., et al. 2017, A&A, 601, A56
Tautvaišienė, G., Drazdauskas, A., Mikolaitis, Š., et al. 2015, A&A, 573, A55
Taylor, M. B. 2005, ASP Conf. Ser., 347, 29
Terndrup, D. M., Pinsonneault, M., Jeffries, R. D., et al. 2002, ApJ, 576, 950
Torra, F., Castañeda, J., Fabricius, C., et al. 2021, A&A, 649, A10
Umezu, M., & Saio, H. 2000, MNRAS, 316, 307
Vande Putte, D., Garnier, T. P., Ferreras, I., et al. 2010, MNRAS, 407, 2109
Venuti, L., Damiani, F., & Prisinzano, L. 2019, A&A, 621, A14
Vereshchagin, S. V., Tutukov, A. V., & Chupina, N. V. 2019, INASAN Sci. Rep., 3, 302
Wenger, M., Ochsenbein, F., Egret, D., et al. 2000, A&AS, 143, 9
Wright, N. J., Drake, J. J., Mamajek, E. E., et al. 2011, ApJ, 743, 48
Wright, N. J., Jeffries, R. D., Jackson, R. J., et al. 2019, MNRAS, 486, 2477
Yong, D., Liu, F., Ting, Y.-S., et al. 2023, MNRAS, 526, 2181
Zhang, Y., Tang, S.-Y., Chen, W. P., et al. 2020, ApJ, 889, 99

[1] Departamento de Física de la Tierra y Astrofísica and IPARCOS-UCM (Instituto de Física de Partículas y del Cosmos de la UCM), Facultad de Ciencias Físicas, Universidad Complutense de Madrid, 28040, Madrid, Spain
e-mail: mlgutierrez@ucm.es
[2] Centro de Astrobiología (CSIC/INTA), Instituto Nacional de Técnica Aeroespacial, Ctra de Torrejón a Ajalvir, km 4, 28850 Torrejón de Ardoz, Madrid, Spain
[3] Instituto de Astrofísica de Canarias (IAC), 38205 La Laguna, Tenerife, Spain
[4] Universidad de la Laguna, Dept. Astrofísica, 38206 La Laguna, Tenerife, Spain
[5] Hamburger Sternwarte, Gojenbergsweg 112, 21029 Hamburg, Germany
[6] INAF – Osservatorio Astrofisico di Catania, via S. Sofia 78, 95123 Catania, Italy
[7] Università di Catania, Dipartimento di Fisica e Astronomia, Sezione Astrofisica, Via S. Sofia 78, 95123 Catania, Italy
[8] Institut für Astronomie und Astrophysik, Eberhard Karls Universität, Sand 1, 72076 Tübingen, Germany
[9] INAF – Osservatorio Astrofisico di Arcetri, Largo E. Fermi 5, 50125, Firenze, Italy
[10] Nicolaus Copernicus Astronomical Center, Polish Academy of Sciences, ul. Bartycka 18, 00-716 Warsaw, Poland
[11] Observational Astrophysics, Division of Astronomy and Space Physics, Department of Physics and Astronomy, Uppsala University, Box 516, 751 20 Uppsala, Sweden
[12] Institute of Astronomy, University of Cambridge, Madingley Road, Cambridge CB3 0HA, UK
[13] Instituto de Astrofísica de Andalucía (CSIC), Glorieta de la Astronomía s/n, Granada 18008, Spain
[14] Centro de Astrobiología, CSIC-INTA, Camino bajo del castillo s/n, 28692, Villanueva de la Cañada, Madrid, Spain
[15] INAF – Osservatorio Astronomico di Palermo, Piazza del Parlamento, 1, 90134 Palermo, Italy
[16] Lund Observatory, Division of Astrophysics, Department of Physics, Lund University, Box 43, 22100 Lund, Sweden
[17] INAF – Rome Astronomical Observatory (OAR), Via di Frascati, 33, 00044, Monte Porzio Catone, Italy
[18] INAF – Osservatorio Astronomico di Padova, Vicolo dell'Osservatorio 5, 35122 Padova, Italy
[19] School of Physical and Chemical Sciences – Te Kura Matū, University of Canterbury, Private Bag 4800, Christchurch 8140, New Zealand
[20] 114, 10 College Walk, School of Physics and Astronomy, Monash University, Monash, VIC 3800, Australia
[21] European Space Agency (ESA), European Space Research and Technology Centre (ESTEC), Keplerlaan 1, 2201 AZ Noordwijk, The Netherlands
[22] GEPI, Observatoire de Paris, CNRS, Université Paris Diderot, 5 Place Jules Janssen, 92190 Meudon, France
[23] Dipartimento di Fisica e Astronomia, Università di Padova, Vicolo dell'Osservatorio 3, 35122 Padova, Italy

Appendix A: Cluster selections: Individual notes

In this appendix we present an in depth account of each of the 42 clusters in the sample, including general information about the different age estimations of the cluster sample, as well as a detailed discussion on membership analysis and final selections from Sect. 3, especially featuring relevant particular cases, as well as a comparison of the final candidates with a series of studies from the literature. In Paper III, we further comment on particular cases in regards to the study of rotation, activity and metallicity. We additionally refer to the individual figures of Sect. 3 in Appendix B.

Appendix A.1: Star forming regions (age ≤ 6 Myr) and young OCs (age ≤ 50 Myr)

∗ **NGC 6530**

NGC 6530 is a 1–2 Myr star forming region (Prisinzano et al. 2005; Damiani et al. 2019; Wright et al. 2019; Randich et al. 2020; Jackson et al. 2022) associated to the HII region M8 (Lagoon Nebula).

Of the final 359 Li candidates for NGC 6530 we discarded 16 stars according to the following criterion: We decided to discard all stars which we could not analyse using the astrometric and photometric *Gaia* data (be it because there were not *Gaia* data available for those stars, or because said data did not pass the quality indicators) if they were additionally listed as clear non-members by Jackson et al. (2022). All of these 16 stars are listed as clear non-members with a probability of 0.00–0.16, and one of them also has a metallicity value deviating appreciably from the mean of the cluster. As a result of the analysis of NGC 6530 we found 14 strong accreting stars, all of which are Li members and classified as high-probability members (P > 0.90) by Jackson et al. (2022). As for kinematics, 44 stars in our final selection were RV non-members according to the initial 2σ interval, with RVs deviating up to 13.0–15.0 km s^{-1} from the mean of the cluster. We accepted the stars which deviate from the limits established by the 2σ interval by ∼10 km s^{-1} given that they fulfil the rest of membership criteria (especially regarding available *Gaia* data, as well as gravity indicators and lithium) (see Paper I). All of these stars are additionally listed as high-probability members by several studies (e.g, Damiani et al. 2019; Prisinzano et al. 2019; Wright et al. 2019; Jackson et al. 2022). On the other hand, we also accepted as final candidates four stars with no measured RV values in iDR6, due to the fact that they fully fulfil the astrometry criteria (as well as the other criteria), and are also listed as members by these studies (e.g, Damiani et al. 2019; Prisinzano et al. 2019; Wright et al. 2019; Jackson et al. 2022). Finally, regarding metallicity, 26 stars in our final selection are marginal members which deviate moderately from the limits of the initial 3σ membership interval, with values up to 0.40–0.80 dex from the mean of the cluster. As discussed in Sect. 3 (also see Paper I), we accepted these marginal stars as final cluster members, seeing as they fulfil all prior criteria (including the more robust criteria of cinematics and astrometry), and all of these stars are also listed as high-probability members by various studies (e.g, Damiani et al. 2019; Prisinzano et al. 2019; Wright et al. 2019; Jackson et al. 2022). In addition, five of the stars in our final selection additionally present [Fe/H] values which deviate more appreciably from the 3σ limit, up to 0.93–1.68 dex from the cluster mean. As further discussed in both Paper I and the updated analysis presented in the thesis, however, we also listed these stars as final candidates, given that they fully fulfil the rest of criteria, including the more restrictive criteria, and they are all additionally listed as members by Jackson et al. (2022) with P=0.99.

In regards to previous selections, we found the following number of common stars with our selection: 52 stars in Prisinzano et al. (2007) and Prisinzano et al. (2012), 148 in Spina et al. (2017), 255 in Damiani et al. (2019), 320 in Prisinzano et al. (2019), 286 in Wright et al. (2019), and one in Castro-Ginard et al. (2020). Finally, Jackson et al. (2022) includes 331 out of our 343 candidates. Of the remaining 12 stars, 10 of them were not included in their analysis, and two of them are listed with probabilities of 0.26–0.33 (Jackson et al. (2022) considers high-probability members to have P > 0.90 and definite non-members to have P< 0.10). We accepted these two stars given that they fulfilled all of our available membership criteria, and were furthermore included in several other studies (e.g, Damiani et al. 2019; Prisinzano et al. 2019; Wright et al. 2019). As already discussed in Sect. 3.4, we also note that we seem to find some inconsistencies when plotting the Li-rich giant outliers selected in the field of this cluster in the CMD diagram, with a couple of them appearing among the cluster candidates. However, when plotting them in the γ index-versus-$T_{\rm eff}$ diagram the expected clear distinction is found between the non-giant cluster candidates and the Li-rich giant outliers.

∗ **Rho Oph**

The ρ Ophiuchi (ρ Oph) molecular cloud complex, consisting of two major regions of dense gas and dust (L1688 and L1689), is an 1–3 Myr star forming region (Barsony et al. 2012; Rigliaco et al. 2016; Spina et al. 2017; Cánovas et al. 2019; Randich et al. 2020; Kiman et al. 2021; Jackson et al. 2022).

In addition to the final 37 Li members, for ρ Oph we also considered for completeness seven strong accreting stars which presented no values of EW(Li) in the iDR6 file. We also note that one of the stars in our final selection (16270456-2442140) presents a [Fe/H] value which deviates appreciably from the 3σ limit (0.45 dex from the cluster mean). We listed it as a final candidate given that it fully fulfils all the other criteria, and is additionally listed as a member by Cánovas et al. (2019) and Jackson et al. (2022) (with P=0.99). Of the final members in ρ Oph, 29 belong to the star forming region L1688 (Rigliaco et al. 2016), and 15 of them are also strong accretors with Hα10% > 270–300 km s^{-1}. Of these 15 accreting stars, only one (16273311-2441152) does not pass our gravity criteria. This star, with γ=1.022 and A(Li)=3.2, could be listed as a potential Li-rich giant contaminant, but due to the fact that it is also a strong accretor (with Hα10% = 469.13 km s^{-1}, we counted it as a likely member of ρ Oph, also in accordance with Rigliaco et al. (2016) and Jackson et al. (2022). Regarding other membership studies from the literature, Rigliaco et al. (2016) has 42 of our final candidates in their selection, while Ducourant et al. (2017) lists 10 common members, Spina et al. (2017) also lists 10 common stars for ρ Oph, and Cánovas et al. (2019) obtained 35 stars in common with our selection. Finally, we have 42 stars in common with Jackson et al. (2022). The remaining two stars in our selection for ρ Oph were not included in the analysis of Jackson et al. (2022), but are however listed as members by Rigliaco et al. (2016) and fulfil all our membership criteria.

∗ **Trumpler 14**

Trumpler 14 is a 1–3 Myr star forming region (Sampedro et al. 2017; Randich et al. 2020; Jackson et al. 2022) associated to the Carina Nebula, one of the most massive HII regions in the Galaxy. Of the final 165 Li candidates in Trumpler 14 we

discarded six stars we could not analyse using the astrometric and photometric *Gaia* data, and they were additionally listed as non-members by Jackson et al. (2022) (most of them are clear non-members with a probability of 0.00, one of them is listed with P=0.27, but it is similarly discarded). One of these six stars also has a metallicity value deviating appreciably from the mean of the cluster. We also found five strong accreting stars among our final members, all of which are Li members and classified as high-probability members by Jackson et al. (2022). We also note that we discarded an F-type star with an EW(Li) that seemed to be higher than we would expect for a star forming region (150 mÅ). This star had no recorded measurements of either accretion or Hα that could perhaps explain its EW(Li), and it was additionally listed as a non-member by Damiani et al. (2017). Regarding kinematics, five stars in our final selection were RV non-members according to the initial 2σ interval, with RVs deviating up to 13.0–15.0 km s^{-1} from the mean of the cluster. We accepted the stars which deviate from the limits established by the 2σ interval by ∼10 km s^{-1}, given that they fulfil the rest of membership criteria (especially regarding available *Gaia* data, as well as gravity indicators and lithium. All of these stars are additionally listed as high-probability members by Jackson et al. (2022). In addition, we also accepted as final candidates 24 stars with no measured RV values in iDR6, due to the fact that they fully fulfil the astrometry criteria (as well as the other criteria), and are also listed as members by Jackson et al. (2022) with high probabilities in the range of 0.85–1.00. Finally, we also accepted as final cluster candidates 11 marginal members deviating from the 3σ metallicity limit up to 0.26 dex from the mean of the cluster. All of these stars fulfil all other criteria, and 10 of them are listed as high-probability members by Jackson et al. (2022) (with P=0.86–0.99).

Regarding other membership selections from the literature, we found the following number of common stars with our selection: 63 stars in Spina et al. (2014b), as well as 65 in Damiani et al. (2017), 51 stars in Cantat-Gaudin et al. (2018), and one star in Castro-Ginard et al. (2020). Finally, Jackson et al. (2022) includes 153 out of our 159 candidates (the remaining six were not included in their analysis). We also note that Jackson et al. (2022) includes several stars which we initially discarded for not fulfilling our gravity criteria of $\gamma < 1.01$ for non-giants (see Sect. 3.4). The reason for this is that Jackson et al. (2022) considers a less restrictive criterion of $\gamma < 1.33$. We also note that we seem to find some inconsistencies when plotting the Li-rich giant outliers selected in the field of this cluster in the CMD diagram, with eight of them appearing among the cluster candidates. However, when plotting them in the γ index-versus-$T_{\rm eff}$ diagram the expected distinction is found between the non-giant cluster candidates and the Li-rich giant outliers.

∗ Chamaeleon I

Chamaeleon I (Cha I) is a ∼2 Myr star forming region (López Martí et al. 2013; Spina et al. 2014a; Sacco et al. 2015; Randich et al. 2020; Jackson et al. 2022), composed of two subclusters (Luhman et al. 2008; Sacco et al. 2017; Roccatagliata et al. 2018), with a shift in velocity of ∼1 km s^{-1}, and ages in the range of 5–6 Myr and 3–4 Myr, respectively.

Of the final 88 Li candidates for Cha I we discarded two stars: The first one (11080297-7738425) had no *Gaia* data available (thus, astrometry could not be analysed) and its [Fe/H] value deviated appreciably from the mean of the distribution, beyond the extended 3σ membership interval. The second star (11095340-7634255), also a non-member according to metallicity, we considered as a final non-member because we could not analyse this star using the astrometric and photometric *Gaia* data and it was additionally listed as a clear non-member with a probability of 0.00 by Jackson et al. (2022). As a result of the analysis of Cha I we found 35 strong accreting stars, of which only one (11104959-7717517) is not a Li member, probably due to possible veiling suppressing the absorption Li line. We classified this strong accretor as an additional likely member, and it is additionally considered as a member of Cha I by Jackson et al. (2022). We also decided to classify as final cluster members four very young active stars which exhibit little dispersion with respect to the rest of candidates, but also present values of EW(Li) which are slightly larger than in the case of most member stars (841–948 mÅ). Two of them, the ones with the largest EW(Li)s, are additionally strong accretors with Hα10% > 270–300 km s^{-1}, and so their larger EW(Li)s are a potential effect of either accretion-induced enhancement, or, more probably in this case, a result of a strong veiling correction, where derived *EW*s may be too high if the veiling factor is overestimated. For more details on chromospheric activity and accretion mechanisms in regards to Li depletion, we refer the reader to Paper III. We also note that three of the stars in our final selection were RV non-members according to the initial 2σ interval, with RVs deviating up to 3.7–10.2 km s^{-1} from the mean of the cluster. We accepted the stars which deviate from the limits established by the 2σ interval by ∼10 km s^{-1}, given that they fulfil the rest of membership criteria (especially regarding gravity indicators and lithium, as only one of them has available *Gaia* data), and all three of them are additionally listed as candidates by several studies (e.g, Esplin et al. 2017; Sacco et al. 2017; Galli et al. 2021; Jackson et al. 2022). Regarding metallicity, we also accepted seven marginal members (three of which are also strong accreting stars), deviating up to 0.45 dex from the mean of the cluster; as well as one additional star (11091172-7729124) which deviated more appreciably from the 3σ limit (0.80 dex from the cluster mean). All of these stars fulfil all other criteria, and are listed as high-probability members with P=0.99 by Jackson et al. (2022).

Regarding previous selections, we found the following number of common stars with our selection: nine stars in Robrade & Schmitt (2007), 23 in Luhman & Muench (2008), and 47 in López Martí et al. (2013). We found 12 common stars in Spina et al. (2014a), all UVES members in their selection, except for 10555973-7724399 and 11092378-7623207, for which several parameters are not released in the iDR6 catalogue. We also found 88 of our candidate stars in the member list of Esplin et al. (2017), 75 in Sacco et al. (2017), and 66 in Galli et al. (2021). Finally, Jackson et al. (2022) includes 82 out of our 87 candidates (the remaining five were not included in their analysis). Regarding field contaminants, one Li-rich giant (11000515-7623259) is listed in Casey et al. (2016).

∗ NGC 2244

NGC 2244 is a 2–4 Myr star forming region (Michalska 2019; Mužić et al. 2019; Jackson et al. 2022), associated with the Rosette Nebula in the Perseus Arm of the Galaxy.

Of the final 123 Li candidates for NGC 2244, we discarded 11 stars which we could not analyse using the astrometric and photometric *Gaia* data, and which were additionally listed as non-members by Jackson et al. (2022) (all but one are definite non-members with a probability of 0.00, while the remaining one is listed with P=0.29, and is similarly discarded).We also

found 10 strong accreting stars among our final members, and all but one are Li members and classified as high-probability members by Jackson et al. (2022) (the remaining one has no measured EW(Li) in DR6 and is not included in Jackson et al. (2022)). Regarding kinematics, one star in our final selection was a RV non-member according to the initial 2σ interval, with a RV deviating 6.0 km s^{-1} from the mean of the cluster. We accepted it given that it fulfilled the rest of membership criteria, and it was also listed as a high-probability member by Jackson et al. (2022). On the other hand, we also accepted as final candidates nine stars with no measured RV values in iDR6, due to the fact that they fully fulfil the astrometry criteria (as well as the other criteria), and are also listed as members by Jackson et al. (2022) with probabilities in the range of 0.53–0.99. As for metallicity, we accepted 22 marginal members which deviate up to 0.35 dex from the mean of the cluster, and also one additional star (06312952+0454342) deviating more appreciably from the 3σ limit (0.45 dex from the cluster mean). All of these stars fulfil the rest of criteria, and are listed as high-probability members with P=0.99 Jackson et al. (2022). Regarding other membership selections from the literature, we found the following number of common stars with our selection: 78 stars in Cantat-Gaudin et al. (2018), one star in Carrera et al. (2019), and 39 stars in Michalska (2019). Finally, Jackson et al. (2022) includes 114 out of our 116 candidates (the remaining two were not included in their analysis). We also note that we included several stars with a marginal metallicity, deviating slightly from the 2σ interval, as they fulfilled the rest of criteria and were furthermore reinforced by high probabilities listed by Jackson et al. (2022).

∗ **NGC 2264**

NGC 2264 is a 4 Myr star forming region (Jackson et al. 2022), the dominant component of the Mon OB1 association in the Monoceros constellation. Several studies list ages in the 1–5 Myr range (Spina et al. 2017; Cantat-Gaudin et al. 2018; Venuti et al. 2019; Arancibia-Silva et al. 2020; Bonito et al. 2020; Gillen et al. 2020; Randich et al. 2020).

Of the final 507(535) Li candidates for NGC 2264, we discarded 28 stars on the basis of not being able to analyse them using astrometric and photometric *Gaia* data, and all of these 28 stars were additionally listed as non-members by Jackson et al. (2022) (most are clear non-members with a probability of 0.00, while a few are listed with probabilities up to P=0.35, and are similarly discarded). In the analysis of NGC 2264 we found 144 strong accreting stars with Hα10% > 270–300 km s^{-1} among our final members , and a high number of the remaining candidates show considerable values of accretion as well, albeit under that limit. Of these 144 strong accretors, all are Li members and classified as high-probability members by Jackson et al. (2022), except for 22 stars which show higher levels of EW(Li)s than expected (marked as 'Y?' in the table of Appendix C), and two stars which do not appear to be Li members, but are similarly included as final members due to their strong accretion. These two stars furthermore fulfil the rest of our criteria and are included as high probability members by Jackson et al. (2022). As was also discussed earlier with Cha I, we also considered as members all of the 28 strong accretors which present values of EW(Li) notably larger than the rest of candidates (800–1270 mÅ). Furthermore, 20 of them are listed as high probability members by Jackson et al. (2022) and several are also included in several others membership studies (e.g, Lim et al. 2016; Cantat-Gaudin et al. 2018; Maíz Apellániz 2019; Venuti et al. 2019). Also see Paper III for more details on the influence of accretion for this cluster specifically. As for kinematics, three star in our final selection were RV non-members according to the initial 2σ interval, with RVs deviating up to 9.0 km s^{-1} from the mean of the cluster. As in the case of other cluster analyses, we accepted them as final members, as they fulfilled the rest of membership criteria, and were also listed as high-probability members by Jackson et al. (2022). On the other hand, we also accepted as final candidates 22 stars with no measured RV values in iDR6, due to the fact that they fully fulfilled all astrometric criteria (as well as the other criteria), and are also listed as members by Jackson et al. (2022) with probabilities in the range of 0.67–0.99. Finally, we also accepted 12 marginal metallicity members (three of which are also strong accreting stars), deviating from the 3σ limit up to 0.20–0.40 dex from the mean of the cluster. All of these stars fulfil all other criteria, and are listed as high-probability members with P=0.96–0.99 by Jackson et al. (2022).

Regarding previous membership selections from the literature, we found the following number of common stars with our selection in several studies: 197 stars in Jackson et al. (2016), 69 stars in Lim et al. (2016), 130 stars in Spina et al. (2017), 116 stars in Cantat-Gaudin et al. (2018), 198 stars in Maíz Apellániz (2019), and 226 stars in Venuti et al. (2019). Finally, Jackson et al. (2022) includes 479 out of our 503 candidates. Of the remaining candidates in our selection, 21 were not included in their analysis, and the other four (which fully fulfil all our criteria) are listed with probabilities in the range of 0.29–0.38 by Jackson et al. (2022). We also note that we seem to find some inconsistencies when plotting the Li-rich giant outliers selected in the field of this cluster in the CMD diagram, with one of them appearing among the cluster candidates. However, when plotting them in the γ index-versus-$T_{\rm eff}$ diagram the expected distinction is found between the non-giant cluster candidates and the Li-rich giant outliers.

∗ λ **Ori**

λ Ori (Collinder 69) is a young cluster with an age range of 5–12 Myr (Jackson et al. 2022; Binks et al. 2022), the oldest of the associations included in the λ Ori star forming region (Barrado et al. 2011).

Of the final 163 Li candidates we discarded two stars because we were not able to analyse them using astrometric and photometric *Gaia* data, and they were listed as non-members with P=0.00–0.01 by Jackson et al. (2022). In the analysis we also found 34 strong accreting stars among our final candidates. Of these 34 strong accretors, all of them are Li members, and 17 are also listed as high-probability members by Jackson et al. (2022) (the rest are not included in their study). In addition, we list four stars with EW(Li) values slightly larger than the rest of candidates (870–950 mÅ). Similarly to the cases of Cha I and NGC 2264, we consider them as members given that they exhibit little dispersion with respect to the rest of candidates, and we explain their larger apparent values of Li for being young active stars, with high values of both accretion, and in some cases also chromospheric Hα. Two of them, the ones with the largest EW(Li) values, are additionally strong accretors with Hα10% > 270–300 km s^{-1}, and so, once again, their larger EW(Li)s could also be an effect of either accretion-induced enhancement or the result of a strong veiling correction. As for kinematics, 105 stars in our final selection were RV non-members according to the initial 2σ interval, with RVs deviating 7–10 km s^{-1} from the mean of the cluster. As in the case of other cluster analyses, we accepted them as final

members, as they fulfilled the rest of membership criteria, and all stars except for 14 (which are not included in their study) were also listed as high-probability members by Jackson et al. (2022). Regarding previous membership selections from the literature, we found the following number of common stars with our selection in several studies: 10 stars in Sacco et al. (2008), 70 stars in Hernández et al. (2010), 30 stars in Barrado et al. (2011), 16 stars in Franciosini & Sacco (2011), 51 stars in Bayo et al. (2012), and 94 stars in Cantat-Gaudin et al. (2018). Finally, Jackson et al. (2022) includes 116 out of our 161 candidates (the 45 remaining stars were not included in their study).

∗ **Col 197**

Collinder 197 (Col 197 or Cr 197) is a low-population young cluster with an age of 12–14 Myr (Bonatto & Bica 2010; Vande Putte et al. 2010; Sampedro et al. 2017; Dias et al. 2019; Jackson et al. 2022; Romano et al. 2021), embedded in the HII region of Gum 15.

Similarly to other clusters, of the final 104 Li candidates for Col 197 we discarded 11 stars as we were not able to analyse them using astrometric and photometric *Gaia* data, and they were listed as non-members with P=0.00–0.01 by Jackson et al. (2022). We also decided to discard one star, in spite of fulfilling all our criteria, for being listed as a non-member by both Cantat-Gaudin et al. (2018) and Jackson et al. (2022). In addition, we also accepted as final candidates six stars with no measured RV values in iDR6, due to the fact that they fully fulfil the astrometry criteria (as well as the other criteria), and are also listed as members by Jackson et al. (2022) with probabilities in the range of 0.70–1.00. In the analysis we also found 11 strong accreting stars among our final candidates. Of these 11 strong accretors, all of them are Li members, and eight are also listed as members by Jackson et al. (2022). Finally, we also accepted 10 marginal metallicity members (one of which is also a strong accretor), deviating from the 3σ limit up to 0.38–0.50 dex from the mean of the cluster. All of these stars fulfil all other criteria, and are listed as members by Cantat-Gaudin et al. (2018) and/or Jackson et al. (2022) (in the case of 5 of these stars, with P=0.99).

Regarding previous membership selections from the literature, we found 79 common stars in Cantat-Gaudin et al. (2018), and Jackson et al. (2022) includes 65 out of our 92 candidates. Of the remaining candidates in our selection, eight stars were not included in their study, and in an untypical way in all our membership comparisons with this work, we found the remaining 19 stars listed as non-members with P=0.00–0.02. All of these 19 stars seem to fulfil all of our criteria, including *Gaia*, so we did not discard them from our final selection, but the disagreement is worth noting, even more so considering that this is the only cluster in our sample of 42 clusters whose final RV mean estimation additionally does not agree with the values given by the literature.

∗ **Vela OB2 association: γ Velorum and NGC 2547**

The γ Velorum (γ Vel) and NGC 2547 clusters are two of the PMS clusters around the Vela OB2 association (γ^2 Vel), each of them composed of two kinematically distinct populations. The age of both γ Vel A and B is typically listed as 10–20 Myr, with γ Vel A being 1–2 Myr older than γ Vel B (e.g., Jeffries et al. 2014; Spina et al. 2014b; Frasca et al. 2015; Sacco et al. 2015, 2017; Spina et al. 2017; Beccari et al. 2018; Franciosini et al. 2018; Armstrong et al. 2020; Jackson et al. 2022). The age of NGC 2547 is listed as either 35–45 Myr (with Jeffries et al. (2023) recently obtaining an age of $39.2^{+1.6}_{-1.3}$ Myr), or a slightly younger range of 20–35 Myr. NGC 2547 B is younger than NGC 2547 A, and coeval with γ Vel, with an age of 10–20 Myr (e.g., Oliveira et al. 2003; Soderblom et al. 2014; Sacco et al. 2017; Spina et al. 2017; Beccari et al. 2018; Randich et al. 2018; Bossini et al. 2019; Jackson et al. 2022; Pang et al. 2021; Romano et al. 2021).

The cluster membership selections for both γ Vel and NGC 2547 consist of 234 stars in γ Vel (99 in γ Vel A and 84 in γ Vel B, as well as 51 additional candidate stars that are not associated to a specific population), and 151 stars in NGC 2547 (138 in NGC 2547 A and 13 in NGC 2547 B). As mentioned in Sect. 2, for this study we used the membership selections obtained by a series of former studies in the literature: Regarding γ Vel, we first used Jeffries et al. (2014), the study specifying the members of γ Vel A and B, as well as a series of other GES studies (Damiani et al. 2014; Spina et al. 2014b; Frasca et al. 2015; Prisinzano et al. 2016; Cantat-Gaudin et al. 2019; Jackson et al. 2022). For NGC 2547 we similarly used several membership studies from the literature, some of which list the membership probabilities of each candidate to Pop. A/B Sacco et al. (2015); Randich et al. (2018); Cantat-Gaudin et al. (2018), while others do not Spina et al. (2017); Jackson et al. (2022). *Gaia* studies Randich et al. (2018), Cantat-Gaudin et al. (2018) and Jackson et al. (2022) offer updated membership probabilities for γ Vel A Jackson et al. (2022) and NGC 2547 (all three of them). Randich et al. (2018) listed a series of new members with respect to Sacco et al. (2015). Although their membership probabilities for each population are generally consistent with each other, a small number of stars were associated with different populations in Sacco et al. (2015) and Randich et al. (2018). In this case, we adopted the membership from Randich et al. (2018), as this is the most recent study of the two. For NGC 2547 we also compared the member stars in Sacco et al. (2015), Cantat-Gaudin et al. (2018) and Randich et al. (2018) with the candidate members in Bravi et al. (2018). For all our adopted candidates, Bravi et al. (2018) found high probabilities, namely ranging from 60 to 100%, of being RV members of the cluster. Finally, Jackson et al. (2022) offer updated probabilities for both clusters, and we decided to also prioritize the membership probabilities of this work with respect to earlier studies, for those cases were they might appear to disagree.

While we mainly used the membership lists offered by the aforementioned works, we also note that we did make use of the *Gaia* EDR3 data to analyse the proper motions, parallaxes and the position in the CMD for all stars marked as members for γ Vel and NGC 2547, in order to improve the final selections. We thus discarded a series of stars which deviated appreciably from the locus of the rest of members in the *pmra*-versus-*pmdec* diagram, as well as those stars which proved to be parallax non-members, and those which also deviated appreciably from the rest in the CMDs. As to field contaminants, we also find two of the γ Vel Li-rich giants in our list (J08095783-4701385 and J08102116-4740125), as well as one of the Li-rich giants from NGC 2547 (J08110403-4852137), in Casey et al. (2016). Another one, (J08110403-4658057) in γ Vel, is listed in Smiljanic et al. (2018).

∗ **NGC 2232**

NGC 2232 is a young cluster in Monoceros with an estimated age range of 18–38 Myr, with the most recent studies veering towards younger ages in the 18–25 Myr range (Liu & Pang 2019; Jackson et al. 2022; Pang et al. 2021; Romano et al. 2021; Binks et al. 2022). Jeffries et al. (2023) recently obtained an age of $29.3^{+1.2}_{-1.0}$ Myr.

Of the final 68 Li candidates for NGC 2232 we discarded 16 stars, listed as non-members with P=0.00–0.01 by Jackson et al. (2022), and not including any astrometric or photometric *Gaia* data. One of them additionally has [Fe/H] value deviating appreciably from the mean of the cluster, beyond the extended 3σ membership interval. In our final selection we note as a particular case a star with a EW(Li) value which is higher than the rest of candidates (841–948 mÅ), but without exhibiting a large dispersion with respect to the rest of the candidates. We consider it as a final member given that it fulfilled the other criteria as well as being listed in several studies as a candidate of the cluster (Cantat-Gaudin et al. 2018; Jackson et al. 2022; Binks et al. 2022). As for metallicity, we accepted one marginal member deviating 0.24 dex from the mean of the cluster, as it fulfilled all other criteria, and is listed as a high-probability member with P=0.98 by Jackson et al. (2022). Regarding previous membership selections from the literature, we found 46 stars in common with Cantat-Gaudin et al. (2018), as well as 49 stars in Pang et al. (2021), and 58 stars in Binks et al. (2022). Finally, Jackson et al. (2022) includes 56 out of our 68 candidates (the remaining stars were not included in their study, except for one which was listed with P=0.30).

∗ **IC 2391**

IC 2391 is an open cluster in the constellation Vela, with an age in the 20–60 Myr range (e.g., Stauffer et al. 1997; Randich et al. 2001; Barrado y Navascués 2004; Platais et al. 2007; Smiljanic et al. 2011; De Silva et al. 2013). Bossini et al. (2019) gave an age of 36 ± 2 Myr using *Gaia* data, while LDB estimates result in an age range of 50–58 Myr, and Jeffries et al. (2023) recently proposed an age of $60.1^{+26.8}_{-9.2}$ Myr.

Of the final 37 Li candidates for IC 2391, we discarded two stars from the final member selection. These stars could not be analysed with any *Gaia* data (gravity, RV and Li were the only criteria available), and they were additionally classified as non-members with a probability of 0.00 by Jackson et al. (2022). We also note that we added one star as part of our final selection which initially was a RV non-member according to the initial 2σ interval, with a RV deviating 6.5 km s^{-1} from the mean of the cluster. We accepted it as it deviated by less than 10 km s^{-1} from the mean RV, fulfilled the rest of criteria and is listed as a member by Jackson et al. (2022). Finally, we accepted a marginal metallicity member deviating 0.18 dex from the mean of the cluster, as well as one additional star (08384138-5255039) which deviated more appreciably from the 3σ limit (0.30 dex from the cluster mean). Both of these stars fulfil all other criteria, and are listed as members by several studies (e.g, Randich et al. 2018; Bravi et al. 2018; Jackson et al. 2022).

Regarding previous selections, we found the following number of common candidates in the membership lists of these non-GES studies: 19 stars in Barrado y Navascués et al. (2001) and Barrado y Navascués (2004); three stars in Randich et al. (2001); four stars in Dodd (2004); six stars in Platais et al. (2007), Messina et al. (2011) and De Silva et al. (2013); and three stars in Elliott et al. (2016). We also refer to Gómez Garrido (2015) and Gómez Garrido et al. (2017) for a membership study of this cluster, alongside IC 2602 and IC 4665. Regarding GES studies, we firstly found four common stars in Spina et al. (2017) and 14 stars in Bravi et al. (2018). The latter study derived RV membership probabilities and lists of candidate members for this cluster (alongside IC 2602, IC 4665 and NGC 2547) using iDR4 data. Comparing our final selection of 35 members with the list of 53 candidate stars of Bravi et al. (2018), we find 30 kinematic candidates and 14 final members in common (all of the common members stars have high RV membership probabilities of at least 0.95, except for two stars in the 0.7–0.9 range). We note that, for many stars Bravi et al. (2018) used values of EW(Li) and/or $T_{\rm eff}$ which were derived from one of the WG12 nodes and do not appear in our sample. As a result, we excluded these stars from our membership analysis and only consider those stars in Bravi et al. (2018) with EW(Li) values in our iDR6 sample. Our mean RV and σ for IC 2391 also agree with the estimates in Bravi et al. (2018) (see Table 3). Finally, a series of more recent studies using both GES and *Gaia* data also list updated membership probabilities for IC 2391 (Cantat-Gaudin et al. 2018; Randich et al. 2018; Jackson et al. 2022; Pang et al. 2021). We have 28 common stars as members with Randich et al. (2018), as well as 24 stars with Cantat-Gaudin et al. (2018), 29 with Jackson et al. (2022) (the remaining six were not included in their analysis), and 23 with Pang et al. (2021). As we mention in Sect. 3.3, in this study we relied more heavily on Jackson et al. (2022), the most extensive and one of the most recent studies using both GES and *Gaia* data. Thus, we decided to discard as a final member a marginal star according to our analysis given that Jackson et al. (2022) listed it as a non-member, even though Randich et al. (2018) considered it a candidate. To finish, for completeness we also mention here a series of recent studies that used *Gaia*-DR2 data to study the spacial-kinematic distribution and cluster membership of IC 2391 (Postnikova et al. 2019, 2020; Vereshchagin et al. 2019).

∗ **IC 2602**

IC 2602 is an open cluster in the constellation Carina, with an age of 35 ± 1 Myr according to Bossini et al. (2019), while previous studies found ages ranging from 30–67 Myr (Randich et al. 1997; Stauffer et al. 1997; Randich et al. 2001; Smiljanic et al. 2011; Jackson et al. 2022; Pang et al. 2021; Romano et al. 2021). Ages in the range of 46–53 Myr were also derived from the LDB method (Dobbie et al. 2012; Jeffries et al. 2023), and Jeffries et al. (2023) proposed an slightly older estimation of $45.8^{+4.7}_{-3.3}$ Myr for this cluster.

Of the final 59 Li candidates for IC 2602, we discarded four stars from the final member selection. Two of them were also discarded via the criteria of RV and metallicity. In addition, similarly to other clusters, all four of these stars could not be analysed with any *Gaia* data (gravity, RV, Li, and sometimes metallicity were the only criteria available), and they were additionally classified as non-members with a probability of 0.00 by Jackson et al. (2022) (all four stars were also listed as non-members by Randich et al. (2018)). Finally, we accepted two marginal metallicity members, deviating moderately from the 3σ limit (0.30–0.40 dex from the mean of the cluster), both fulfilling all other criteria. One of them (10452826-6413450) is also listed as a high-probability member with P=0.99 by Jackson et al. (2022).

Comparing our selection with former studies, we found three stars in common with non-GES Randich et al. (2001), and we also reinforced our membership selection with 28 additional members of IC 2602 with measured EW(Li)s listed by this study. We also made use of 44 additional members with EW(Li) measurements from Jeffries et al. (2009). All these member stars which were not measured by GES were of particular interest to construct the empirical lithium envelope for IC 2602 (with the envelope of Montes et al. (2001) as a base) as well, especially in the region of the LDB (Lithium Depletion Boundary, see Paper III). We also refer to Gómez Garrido (2015) and Gómez Garrido et al. (2017) for a membership study of this cluster, alongside

IC 2391 and IC 4665. Regarding GES studies, we firstly found 11 common stars in Spina et al. (2017), as well as 55 kinematic candidates and 27 final members in common with the list of 101 candidates in Bravi et al. (2018). As in the case of IC 2391, many of the stars in Bravi et al. (2018) have no EW(Li) values in the iDR6 sample, and therefore we excluded them in our own membership analysis.The mean RV and σ derived in Bravi et al. (2018) for IC 2602 are also in agreement with the ones obtained in this paper. As for GES studies that include *Gaia* data, we have 36 common stars listed as members with Randich et al. (2018), as well as 29 stars with Cantat-Gaudin et al. (2018), and 49 with Jackson et al. (2022) (the remaining six were not included in their analysis).

∗ **IC 4665**

IC 4665 is an open cluster in the constellation Ophiuchus. Bossini et al. (2019) calculated an age of 38 ± 3 Myr for this cluster, in agreement with the 35–43 Myr range reported in several studies (Martín & Montes 1997; Jeffries et al. 2001; Jackson et al. 2022; Pang et al. 2021; Romano et al. 2021). However, while they also cite an LDB age of ∼32 Myr, Jeffries et al. (2023) recently obtained a slightly older age of $52.9^{+6.8}_{-5.2}$ Myr for this cluster, proposing that the published LDB age should be interpreted as a lower limit.

Of the final 51 Li candidates for IC 4665, we discarded 18 stars from the final member selection. Similarly to the case of other clusters, all of these stars could not be analysed with any *Gaia* data, and they were all classified as non-members by Jackson et al. (2022) (15 stars with a probability of 0.00, the remaining three in the potential but not definite non-member range of 0.17-0.49). Randich et al. (2018) also lists seven of these 18 stars as non-members (the rest were not considered in their analysis).

Regarding previous selections, we found the following number of common candidates in the membership lists of these non-GES studies: six stars in de Wit et al. (2006) and Jeffries et al. (2009); 11 stars in Manzi et al. (2008); and 17 stars in Lodieu et al. (2011). We also reinforced our membership selection with 23 additional members of IC 4665 with measured EW(Li)s listed by Manzi et al. (2008). We also refer to Gómez Garrido (2015) and Gómez Garrido et al. (2017) for a membership study of this cluster, alongside IC 2391 and IC 2602. As for GES studies, we found 15 common stars in Spina et al. (2017), as well as 30 kinematic candidates and 19 final members in common with the list of 122 candidates in Bravi et al. (2018). Our mean RV and σ are also consistent with the previous estimates in this work. Finally, regarding GES studies that include *Gaia* data, we have 11 common stars listed as members with Randich et al. (2018), as well as 16 stars with Cantat-Gaudin et al. (2018), 23 stars with Pang et al. (2021), and 29 candidate stars in common with Jackson et al. (2022). In this latter comparison, three out of the remaining four stars were not included in the analysis of citejackson2021, and the other one was listed with a probability of 0.14, but seeing as it fully fulfilled all our criteria, including *Gaia* astrometry, we accepted it as a final member. In spite of using the same data sets and very similar membership criteria, it is probable that the reason for these individual deviations between our two analyses originated from the existing differences regarding, for example, criteria limits or the weight of the factors implicated in the decision to accept or discard stars (especially if they seem to be marginal stars according to the individual membership criteria) as final candidates.

∗ **NGC 2451 A and B**

NGC 2451 A and NGC 2451 B are two open clusters projected along the same line of sight. The age of both NGC 2547 A and B is generally listed in the 50–80 Myr range (e.g., Balog et al. 2009; Netopil & Paunzen 2013; Silaj & Landstreet 2014; Randich et al. 2018; Franciosini et al. 2022b; Jackson et al. 2022; Pang et al. 2021), while individual ages are also listed, such as the estimations of Bossini et al. (2019), who calculated an age of 44 ± 2 Myr for NGC 2547 A and 39 ± 1 for NGC 2547 B. Thus, the nearer cluster NGC 2547 A seems to be slightly older than the more distant cluster NGC 2547 B Hünsch et al. (2004).

The cluster membership selections for both NGC 2451 A and NGC 2451 B consist of 42 stars in NGC 2451 A and 64 stars in NGC 2451 B. For this study we used the membership selections obtained by a series of former studies in the literature: Silaj & Landstreet (2014) only gives a candidate list for NGC 2451 A, while the rest include final member lists for both NGC 2451 A and NGC 2451 B (indicated as 'A' and 'B' in the table of Appendix C) (Spina et al. 2017; Randich et al. 2018; Cantat-Gaudin et al. 2018; Jackson et al. 2022). *Gaia* studies Randich et al. (2018), Cantat-Gaudin et al. (2018) and Jackson et al. (2022) offer updated membership probabilities for NGC 2451 A and NGC 2451 B. Although their membership probabilities for each population are generally consistent with each other, a small number of stars were considered as members by Randich et al. (2018) and Cantat-Gaudin et al. (2018) but were listed as definite non-members in Jackson et al. (2022). In these cases, we adopted the membership from Jackson et al. (2022), as this is the most recent study. As seen with other clusters, we decided to prioritize the membership probabilities of Jackson et al. (2022) with respect to earlier studies, for those cases were they might appear to disagree. While we mainly used the membership lists offered by the aforementioned works, we also note that we did make use of the *Gaia* EDR3 data to analyse the proper motions, parallaxes and the position in the CMD for all stars marked as members for NGC 2451 A/B, in order to improve the final selections. We thus discarded a series of stars which deviated appreciably from the locus of the rest of members in the *pmra*-versus-*pmdec* diagram, as well as those stars which proved to be parallax non-members, and those which also deviated appreciably from the rest in the CMDs. Most of these discarded stars were also listed as non-members by Jackson et al. (2022), in contrast to them being considered as members by earlier studies, which reinforced our decision to discard them on the basis of our astrometric criteria.

Appendix A.2: Intermediate-age clusters (age= 50–700 Myr)

∗ **NGC 6405**

NGC 6405 (also known as M6) is a 80–100 Myr cluster (Kılıçoğlu et al. 2016; Netopil et al. 2016; Gao 2018; Jackson et al. 2022), located between the local arm and the Sagittarius arm of the Galaxy.

Of the final 53 Li candidates for NGC 6405, we discarded two stars: one of them, additionally listed as a clear non-member by Jackson et al. (2022), we could not analyse using the astrometric and photometric *Gaia* data. The remaining one was similarly listed as a non-member by both Cantat-Gaudin et al. (2018) and Jackson et al. (2022), and it was also a marginal non-member according to our parallax criterion. We also accepted four marginal metallicity members, deviating from the 3σ limit up to 0.35 dex from the mean of the cluster. All of these stars fulfil all other criteria, and are listed as high-probability

members with P=0.89–0.99 by Jackson et al. (2022). Regarding other membership selections from the literature, we found 46 stars in common with Cantat-Gaudin et al. (2018), and 45 star in Gao (2018). Jackson et al. (2022) includes 50 out of our 51 candidates. The remaining one is listed with P=0.28. Seeing as it fully fulfilled all our criteria, including *Gaia* astrometry, we accepted it as a final member.

∗ **Blanco 1**

Blanco 1 is a cluster located towards the South Galactic Pole, with an age in the range 90–150 Myr (Gillen et al. 2020; Zhang et al. 2020; Jackson et al. 2022; Pang et al. 2021; Romano et al. 2021). Bossini et al. (2019) calculated an age estimation of 94 ± 5 Myr, while studies based on the LDB method give slighter higher ages: 114 ± 10 Myr (Juarez et al. 2014) and 132 ± 24 Myr Cargile et al. (2010). On the other hand, Jeffries et al. (2023) recently proposed a younger age of $73.5^{+12.9}_{-6.9}$ Myr for this cluster.

Of the final 101 Li candidates for Blanco I, we discarded three stars because we were not able to analyse them using astrometric and photometric *Gaia* data, and they were listed as non-members with P=0.00 by Jackson et al. (2022). As for kinematics, nine stars in our final selection were RV non-members according to the initial 2σ interval, with RVs deviating 4–8 km s^{-1} from the mean of the cluster. As in the case of other cluster analyses, we accepted them as final members, and all stars were also listed as high-probability members by Jackson et al. (2022). On the other hand, we also accepted as final candidates two stars with no measured RV values in iDR6, due to the fact that they fully fulfil the astrometry criteria (as well as the other criteria), and are also listed as members by several studies (Platais et al. 2011; Zhang et al. 2020; Jackson et al. 2022). Finally, we also accepted seven marginal metallicity members, deviating from the 3σ limit up to 0.16 dex from the mean of the cluster. All of these stars fulfil all other criteria, and are listed as high-probability members by Jackson et al. (2022), with P=0.99–1.00.

Regarding previous membership selections from the literature, we found 58 stars in common with Platais et al. (2011), one star in Juarez et al. (2014), and 80 stars in Zhang et al. (2020). Finally, Jackson et al. (2022) includes 92 out of our 98 candidates. Four of the remaining ones were not included in their study, one is listed with P=0.37, and the last one is listed as a non-member with P=0.00. The latter two stars fully fulfil all our membership criteria, so we accepted them as final members. As in the case of IC 4665, it is probable that the reason for these individual deviations between our two analyses originated from the existing differences regarding criteria limits or the weight of the factors implicated in the decision to accept or discard stars.

∗ **NGC 6067**

NGC 6067 is an open cluster superimposed on the Norma star cloud, with an age in a 60–150 Myr range, with the most recent studies citing ages of 100–120 Myr (Frinchaboy & Majewski 2008; Netopil et al. 2016; Alonso-Santiago et al. 2017; Magrini et al. 2018; Rangwal et al. 2019; Randich et al. 2020; Jackson et al. 2022; Romano et al. 2021).

Of the final 60 Li candidates for NGC 6067, we discarded four stars with no astrometric and photometric *Gaia* data, further listed as non-members with P=0.00 (for two stars) and P=0.19–0.36 by Jackson et al. (2022). As for kinematics, two stars in our final selection were RV non-members according to the initial 2σ interval, with RVs deviating 13–14 km s^{-1} from the cluster mean. Listed as high-probability members by Jackson et al. (2022) and fulfilling the rest of criteria, we accepted them as final members. Regarding metallicity, we also accepted six marginal members (deviating up to 0.20 dex from the mean of the cluster), as well as one additional star (16130269-5408556) which fulfilled all criteria except for metallicity, deviating more appreciably from the 3σ limit (0.36 dex from the cluster mean). All of these stars are further listed as high-probability members by Jackson et al. (2022), with P=0.97–0.99. As for previous membership selections from the literature, we found three stars in common with Frinchaboy & Majewski (2008), eight stars in Alonso-Santiago et al. (2017), and 42 stars in Cantat-Gaudin et al. (2018). Jackson et al. (2022) includes all 56 of our final candidates.

∗ **NGC 6649**

NGC 6649 is a heavily-reddened ($E(B-V)$=1.43 ± 0.05 Myr) open cluster located in the first Galactic quadrant with an age in a 50–126 Myr range, close to the age of the Pleiades, with the most recent studies citing ages of 120 Myr (Kharchenko et al. 2005; Dib et al. 2018; Liu & Pang 2019; Alonso-Santiago et al. 2020; Jackson et al. 2022).

Of the final 3 Li candidates for NGC 6649, we discarded one star with no astrometric and photometric *Gaia* data, also listed as a non-member with P=0.00 by Jackson et al. (2022). As for kinematics, one star in our final selection was a RV non-member according to the initial 2σ interval, with a RV value deviating 10 km s^{-1} from the mean of the cluster. Similarly to other clusters in this case, we accepted it as a final member, and it is also listed as a high-probability member by Jackson et al. (2022). Regarding previous membership selections from the literature, we found no stars in common with Cantat-Gaudin et al. (2018), and one star out of our two final candidates in common with Jackson et al. (2022) (the other one was not included in their study).

∗ **NGC 2516**

NGC 2516 is an open cluster in the southern constellation of Carina. The age of 251 ± 3 Myr in Bossini et al. (2019) is older than the previous age estimates ranging from 110 to 150 Myr (e.g., Jacobson et al. 2016; Magrini et al. 2017; Fritzewski et al. 2020; Randich et al. 2020; Dumont et al. 2021b; Franciosini et al. 2022b; Jackson et al. 2022; Binks et al. 2022).

Of the final 379(383) Li candidates for NGC 2516, we discarded seven stars which we were not able to analyse using astrometric and photometric *Gaia* data, and all of them were further listed as non-members with P=0.00–0.10 by Jackson et al. (2022). The four stars we classified as possible Li members (marked as 'Y?' in the table of Appendix C) present values of EW(Li) slightly larger than the rest of candidates (300–325 mÅ), especially regarding what we could expect from the age of the cluster. However, they do not exhibit appreciable dispersion with respect to the other members, all four stars fulfil the rest of membership criteria, and all of them are also listed as high probability members by Jackson et al. (2016), and so we accepted them as final members of the cluster. As well as possible scatter due to errors in the measures, we could also explain the higher observable values of EW(Li) of these stars considering the fact that they also exhibit either higher values of rotation and/or chromospheric activity, and thus, a potential slower rate of Li depletion (see more on rotation and activity in regards to Li depletion in Paper III, where we analyse in detail the dependence with several parameters). As for kinematics, 23 stars in our final selection were RV non-members according to the initial 2σ interval, with RVs deviating 5–8 km s^{-1} from the mean of the cluster. Fulfilling the rest of cirteria and listed as high-probability members with

P=0.99–1.00 by Jackson et al. (2022), we accepted all of these stars as members. In addition, we accepted as final members 63 marginal metallicity members, deviating 0.12–0.30 dex from the mean of the cluster, as well as eight additional stars with values which deviate more appreciably from the 3σ limit, up to 0.40 dex from the cluster mean. As with prior clusters, all of these stars fulfil the rest of criteria and are also listed as members by several studies (Randich et al. 2018; Cantat-Gaudin et al. 2018). Finally, all but one of these stars are further listed as high-probability members by Jackson et al. (2022), with P=0.98–1.00.

Regarding previous membership selections from the literature, we found the following number of common stars with our selection in a series of both non-GES and GES studies: Firstly, we found 326 stars in Jeffries et al. (2001), 25 stars in Terndrup et al. (2002), 55 stars in Irwin et al. (2007), 44 stars in Jackson & Jeffries (2010), six stars in Wright et al. (2011), and two stars in Heiter et al. (2014). As for GES studies, we found 56 common stars in Jacobson et al. (2016), 15 stars in Jackson et al. (2016), 13 stars in Magrini et al. (2017), 49 stars in Bailey et al. (2018), 210 stars in Cantat-Gaudin et al. (2018), 332 stars in Randich et al. (2018), and 226 stars in Fritzewski et al. (2019). Finally, Jackson et al. (2022) includes 373 out of our 379 candidates (the remaining six stars were not included in their analysis). We also note that, in order to further reinforce the membership of the stars in the field of this cluster, we also made use of the additional non-GES members with EW(Li) values of Jeffries et al. (1998).

∗ **NGC 6709**

NGC 6709 is an open cluster situated towards the center of the Galaxy in the constellation Aquila, with an age in a 150–190 Myr range (Subramaniam & Sagar 1999; Vande Putte et al. 2010; Jackson et al. 2022; Romano et al. 2021). Bossini et al. (2019) calculated an age estimation of 173 ± 34 Myr.

Of the final 53 Li candidates for NGC 6709, we discarded four stars with no astrometric and photometric *Gaia* data, all four of them also listed as non-members with P=0.00 by Jackson et al. (2022). Regarding previous membership selections from the literature, we found 45 stars in common with Cantat-Gaudin et al. (2018), and Jackson et al. (2022) includes 46 out of our 49 of final candidates. Of the remaining three, two stars were not included in their study, and the last one is listed with P=0.31. Given that said star fully fulfils our membership criteria, including astrometry, we included it in our final selection. We also note that we seem to find some inconsistencies when plotting the Li-rich giant outliers selected in the field of this cluster in the CMD diagram, with two of them, for example, appearing very close among the non-giant cluster candidates. However, when plotting them in the Kiel diagram the expected distinction is found between the non-giant cluster candidates and the Li-rich giant outliers.

∗ **NGC 6259**

NGC 6259 is an open cluster with an age of 210 Myr (Sampedro et al. 2017; Magrini et al. 2018; Casali et al. 2019; Randich et al. 2020; Jackson et al. 2022).

Of the final 39 Li candidates for NGC 6259, we discarded four stars with no astrometric or photometric data, additionally listed as non-members with P=0.00 by Jackson et al. (2022). We also accepted two marginal metallicity members (deviating up to 0.28 dex from the mean of the cluster), which fulfilled all other criteria and were listed as members by Jackson et al. (2022). Regarding previous membership selections from the literature, we found 20 stars in common with Cantat-Gaudin et al. (2018), and 34 out of our 35 members in Jackson et al. (2022). The remaining star in our final selection is listed in the latter study with P=0.32. Seeing as it fully fulfils all our membership criteria, we accepted it as a final member.

∗ **NGC 6705**

NGC 6705 (also known as M11) is a rich open cluster in the constellation Scutum, with an estimated age of 280–300 Myr (Jacobson et al. 2016; Magrini et al. 2017; Randich et al. 2020; Jackson et al. 2022; Romano et al. 2021).

Of the final 142 Li candidates for NGC 6705, we discarded three stars with no photometric or astrometric data, also listed as non-members by Jackson et al. (2022). As for kinematics, eight stars in our final selection were RV non-members according to the initial 2σ interval, with RVs deviating up to 10–13 km s^{-1} from the mean of the cluster. Also listed as high-probability members by Jackson et al. (2022), as in the case of other clusters, we accepted all of these stars as final members. In addition, we also accepted 14 marginal metallicity members (deviating up to 0.30–0.40 dex from the mean of the cluster), which fulfilled the rest of criteria, as well as one additional star (18504954-0614585) which fulfilled all criteria except for $\log g$ and metallicity, deviating appreciably from the starting 3σ limit (0.95 dex from the cluster mean). All of these stars are further listed as high-probability members by Jackson et al. (2022), with P=0.99–1.00.

Comparing our final selection with existing membership studies from the literature for this cluster, we found the following number of common stars with a number of studies: Firstly, we found 21 common stars in Magrini et al. (2014), as well as 27 stars in Tautvaišienė et al. (2015) and Jacobson et al. (2016), 15 stars in Sampedro et al. (2017) and Magrini et al. (2017), and 44 stars in Cantat-Gaudin et al. (2018) and 11 in Casamiquela et al. (2018). Finally, Jackson et al. (2022) includes 136 out of our final 139 candidates (the remaining three stars in our selection were not included in their study).

∗ **Berkeley 30**

Berkeley 30 is an open cluster with an age of 300–313 Myr (Kharchenko et al. 2005; Sampedro et al. 2017; Jackson et al. 2022; Romano et al. 2021).

Among the final 24 Li candidates for this cluster, we included one marginal metallicity member (deviating 0.20 dex from the mean of the cluster), as well as two stars with [Fe/H] values deviating more appreciably from the 3σ limit (0.83 dex from the cluster mean). All three of them are additionally listed as members by Cantat-Gaudin et al. (2018), and by Jackson et al. (2022), with P=0.94–0.99. Regarding previous membership selections from the literature, we found five stars in common with Cantat-Gaudin et al. (2018), and Jackson et al. (2022) includes all 24 of our final candidates.

∗ **NGC 6281**

NGC 6281 is an open cluster with an age of 314–316 Myr (Dias et al. 2002; Joshi et al. 2016; Sampedro et al. 2017; Jackson et al. 2022).

Among the final 24 Li candidates for NGC 6281, we accepted as a final candidate one star, listed as a high-probability member by Jackson et al. (2022), in spite of being a RV non-member according to the initial 2σ interval, with a RV value deviating 5 km s^{-1} from the mean of the cluster. Regarding previous membership selections from the literature, we found the following number of stars in common with several studies: Firstly, we found two stars in common with Frinchaboy & Majewski (2008) and Heiter et al. (2014), as well as 19 common stars in Cantat-Gaudin et al. (2018). Finally, Jackson et al. (2022) includes all 23 of our final candidates.

∗ **NGC 3532**

NGC 3532 is a very rich southern open cluster in a crowded Galactic field in Carina. Intermediate in age between the Pleiades (78–125 Myr) and the Hyades (750 Myr), it has an age estimate of 399 ± 5 Myr according to Bossini et al. (2019), while other studies give an age range of 300–399 Myr (Dobbie et al. 2012; Fritzewski et al. 2019; Jackson et al. 2022; Romano et al. 2021).

Of the final 323 Li candidates for NGC 3532, we discarded a small number of stars according to the following criteria: Firstly, we discarded seven stars which we were not able to analyse using astrometric and photometric *Gaia* data, and which were further listed as non-members by Jackson et al. (2022). We also discarded one SB2 star, as well as another star we also could not analyse with astrometric criteria and deviated appreciably in the Kiel diagram. Lastly, we discarded two final stars with no *Gaia* data analysis available which was marked as a non-member by Fritzewski et al. (2019). As for kinematics, we note that 42 stars in our final selection were RV non-members according to the initial 2σ interval, with RVs deviating up to 8–11 km s^{-1} from the mean of the cluster. As in the case of other cluster analyses, we accepted all of them as final members, and all 42 stars were also listed as high-probability members by Jackson et al. (2022). Regarding metallicity, we accepted as final candidates 76 marginal members (deviating up to 0.48 dex from the mean of the cluster), as well as two additional stars which deviate more appreciably from the 3σ limit, up to 0.83 dex from the cluster mean. All of these stars fulfil all other criteria, and are further listed as members by several studies (e.g., Cantat-Gaudin et al. 2018; Fritzewski et al. 2019, 2021), with all but eight of these stars being also considered as high-probability members by Jackson et al. (2022), with P=0.98–1.00.

Regarding previous membership selections from the literature, we found the following number of stars in common with these studies: Firstly, we found one star in common with Heiter et al. (2014), as well as 310 stars in Cantat-Gaudin et al. (2018), 216 stars in Fritzewski et al. (2019), 27 stars in Hetem & Gregorio-Hetem (2019), and 132 stars in Fritzewski et al. (2021). Finally, Jackson et al. (2022) includes 382 out of our 384 final candidates (the remaining two stars in our final selection were not included in their study).

We will now discuss the 72 stars that we classified as possible Li members, marked as 'Y?' in the table of Appendix C and represented as open squares in all EW(Li)-versus-$T_{\rm eff}$ diagrams to differentiate them from the rest of the candidates (see Appendix B). These 72 stars are late-K and M-type stars with $T_{\rm eff} < 4100$ K, and all of them consistently present values of EW(Li) which are considerably larger than we would expect for KM stars in NGC 3532, a cluster with an age of 300–399 Myr. However, similarly to other clusters such as NGC 6633 (see below), the apparently overestimated EW(Li) values of these stars can be explained by taking into account the inherent difficulty of obtaining accurate Li measurements for KM type stars in this age range: At low temperatures ($T_{\rm eff} \leq 4250$), the *EW*s can be thought of as pseudo-*EW*s derived by integrating over an interval which depends on $v\sin i$ values, and so they include several additional components. As a result, Li measurements for this age range do not go to zero even when Li would already be depleted, and they furthermore actually increase with decreasing $T_{\rm eff}$ as the additional components become stronger (Gilmore et al. 2022; Franciosini et al. 2022a; Randich et al. 2022). And, while we see such *EW*s for KM stars very clearly in intermediate-age clusters such as NGC 3532 and NGC 6633, all clusters reaching such low $T_{\rm eff}$s can show this effect, starting with younger clusters such as NGC 2547 A and NGC 2451 A/B.

Given that the EW(Li) values of these stars are for these reasons not truly representative of the age of this cluster, we decided not to take them into account when creating the empirical envelope for this cluster (see Paper III). However, we also consider all these stars to be robust members of NGC 3532, given that i) They do not exhibit appreciable dispersion with respect to each other or the other members, making it highly improbable for all 93 stars are spurious outliers; ii) All of them consistently fulfil the rest of membership criteria (including kinematics, astrometry, gravity and metallicity criteria); and iii) All of them are listed as high probability members by Jackson et al. (2016) with P=0.97–1.00, and several appear as candidates in other studies as well (Cantat-Gaudin et al. 2018; Fritzewski et al. 2019, 2021).

Another factor with which we could potentially explain some of the higher EW(Li) values for these stars involves the study of their levels of rotation and activity. It is possible to explain higher observable values of EW(Li) considering the fact that they might exhibit either higher values of rotation and/or higher values of chromospheric activity, as we already saw in the case of clusters such as NGC 2516, where undepleted members due to magnetic activity were found both in the literature and possibly in our final selection as well (see above). Due to the Li-rotation and Li-activity anti-correlations, these stars would consequently deplete lithium in a slower rate than their less active and/or slower rotating counterparts, thus exhibiting higher values of EW(Li) as a result. Studies such as Pallavicini et al. (1990) concluded that, while less common, this effect can also be observed in K-type stars in older clusters with intermediate ages between the Pleiades (78–125 Myr) and the Hyades (750 Myr), such as both NGC 3532 (399 Myr) and NGC 6633 (575 Myr).

This cluster does indeed include a series of K-type stars exhibiting high rotation and chromospheric activity, and thus, some of these faster rotators and the more active stars could have consequently depleted Li more slowly, resulting in higher EW(Li)s than would be expected for late K-type stars at this age. However, while this may be a factor for some of the 93 KM stars here discussed, not all of them exhibit sufficiently high rotations and activity to be able to explain their observable Li as a consequence of these effects, many of them actually being among the slowest rotating stars in the final selection for this cluster. And so, for clusters such as NGC 3532 and NGC 6633 (see below), we believe that the most probable explanation for the *EW*s of KM members points to the GES measurement process detailed above.

∗ **NGC 4815**

NGC 4815 is a heavily populated open cluster in the constellation of Musca, with an age of 500–570 Myr (Friel et al. 2014; Jacobson et al. 2016; Magrini et al. 2017, 2018; Jackson et al. 2022).

Similarly to our analysis of others clusters in the sample, of the final 30 Li candidates we discarded one star for not being able to analyse it using astrometric and photometric *Gaia* data, and because it was additionally listed as a non-member by Jackson et al. (2022). As for kinematics, we accepted five stars in our final selection (also listed as high-probability members by Jackson et al. (2022)) as final members in spite of being RV non-members, with RVs deviating up to 14 km s^{-1} from the mean of the cluster. Regarding previous membership selections from the literature, we found the following number of stars in common with several studies: Firstly, we found five stars in common with Friel et al. (2014), Magrini et al. (2014), Tautvaišienė et al. (2015) and Jacobson et al. (2016), as well as three common stars in Magrini et al. (2017), and seven stars

in Cantat-Gaudin et al. (2018). Finally, Jackson et al. (2022) includes all 29 of our final candidates. We also note that two of the final candidates in our sample (12572442-6455173 and 12575818-6459323) show higher values of EW(Li) compared to the other candidates, showing more dispersion with respect to the rest of the cluster members as well. Fulfilling the rest of criteria, these stars seem to be Li-rich (non-giant) members, and are included as candidates of the cluster by a series of previous studies (Magrini et al. 2014; Tautvaišienė et al. 2015; Jacobson et al. 2016; Jackson et al. 2022).

∗ **NGC 6633**

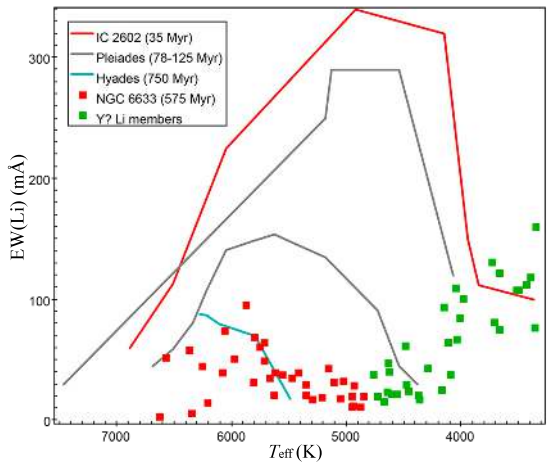

Fig. A.1. EW(Li)-versus-$T_{\rm eff}$ diagram showing the final candidate selection (red squares) for NGC 6633, a 575 Myr-old intermediate-age cluster. In green squares we mark a series of late-K and M stars with considerably higher values of EW(Li) than would be expected for this cluster, but still listed as final candidates of the cluster.

NGC 6633 is an open cluster in the constellation Ophiuchus. The age estimations for this cluster span an age range of 575–773 Myr (e.g., Umezu & Saio 2000; Jeffries et al. 2002; Sestito & Randich 2005; Jacobson et al. 2016; Magrini et al. 2017). While Bossini et al. (2019) gave an estimation of 773^{+50}_{-10} Myr (older than the age of the Hyades, 750 Myr), we have here adopted the younger estimation of 575 Myr in Jackson et al. (2022).

Of the final 62 Li candidates for NGC 6633, we discarded 14 stars with no astrometric and photometric *Gaia* data, further listed as non-members by Jackson et al. (2022). Regarding kinematics and astrometry, we note that both the RV and parallax distributions for NGC 6633 revealed a large contaminant population in the middle of the distribution, which could not be discarded with the aid of the 2σ clipping procedure (as we have done in the case of the remaining 41 clusters in the sample to identify contaminants in the tails of the distribution). The presence of this contaminant population significantly affected the mean RV and mean parallax rendered by the Gaussian fits, and also gave very high final dispersions even after the final convergence of the clipping procedure was reached. When comparing the final fits with the literature values (see Tables 3 and 4), we saw that taking all the contaminant RVs and parallaxes in the middle of the distributions into consideration caused the mean RV and parallax to deviate considerably from the reference estimates for this cluster and effectively affected the final cluster candidate selection well. For this reason, we decided to manually filter out this contaminant population before re-analysing the RV and parallax distributions. In this way, we obtained mean values fully consistent with the literature estimations. This step was vital in order to obtain a probable final list of candidate members for this cluster, seeing as we found that some of the stars in the contaminant population even seemed to fulfil the rest of criteria in spite of clearly not being part of NGC 6633 according to the kinematic and astrometric distributions (which is why kinematics and astrometry are the first criteria applied and the most restrictive in our analysis).

Regarding previous membership selections from the literature, we found the following number of stars in common with these studies: Firstly, we found seven stars in common with Heiter et al. (2014), as well as eight stars in Jacobson et al. (2016), six stars in Magrini et al. (2017), 24 stars in Sampedro et al. (2017), 22 stars in Cantat-Gaudin et al. (2018), and 32 stars in Randich et al. (2018). Finally, Jackson et al. (2022) includes only 19 out of our 67 final candidates, and all the remaining stars in our final selection were not included in their study. We also note that we reinforced the membership of our final selection by making use of the additional members with EW(Li) in Jeffries (1997), Heiter et al. (2014), Magrini et al. (2017), and Sampedro et al. (2017). Finally, regarding non-members, one of the Li-rich giants in our list (J18265248+0627259) is listed in Smiljanic et al. (2018).

For these cluster we have classified 19 stars as possible Li members, marked as 'Y?' in the table of Appendix C and indicated as open squares in all EW(Li)-versus-$T_{\rm eff}$ diagrams to differentiate them from the rest of the candidates (see Sect. 4 and Appendix B). As showcased in Fig. A.1, these stars are late K and M type stars with $T_{\rm eff}$ < 4800–5000 K, and all of them consistently present values of EW(Li) which are considerably larger than we would expect for KM stars in NGC 6633 (575–630 Myr). As such, we decided not to take any of these 19 stars into account when creating the empirical envelope for this cluster. We here refer to the detailed discussion in the individual note of NGC 3532, another intermediate-age cluster that notably showed the same issue with a larger number of stars, showcasing higher Li values than would be expected for KM member stars as a result of the GES measurement process to obtain EW(Li)s at very low temperatures. Similarly to NGC 3532, we consider all these 19 stars to be robust cluster members, consistently fulfilling the rest of membership criteria, with six of them listed as high probability members by Jackson et al. (2016) with P=0.87–1.00 (the rest of them were not included in their study), and several appearing as candidates in other studies as well (Cantat-Gaudin et al. 2018; Randich et al. 2018). Even though we believe that this factor cannot fully explain the higher *EW*s of all of these 19 stars, we also note that some of them also exhibit high rotation (the iDR6 sample for this cluster does not offer any values of Hα), and these faster rotators certainly could have consequently depleted Li more slowly, resulting in somewhat higher EW(Li)s.

Regarding the age of NGC 6633, we note that the age estimations for this cluster vary depending on the study, spanning an age range of 575–773 Myr: from 600–630 Myr (Sestito & Randich 2005; Jacobson et al. 2016; Magrini et al. 2017), to the estimation of 773^{+50}_{-10} Myr by Bossini et al. (2019) (older than the age of the Hyades, 750 Myr), to 575 Myr in the recently published paper by Jackson et al. (2022) (younger than the age of the Hyades). On the other hand, Umezu & Saio (2000) and Jeffries et al. (2002) considered a very similar age to the Hyades for NGC 6633, and concluded that the lower metallicity of this cluster, −0.10–−0.01 dex (Jeffries et al. 2002; Jacobson et al. 2016; Magrini et al. 2018), was a factor that could explain why the EW(Li) envelope for NGC 6633 lied above

the Hyades, and thus, the fact that, according to the study, Li was being depleted at a slower pace in the case of NGC 6633. We personally interpreted the dependence of Li depletion with cluster metallicity differently, as we adopted an appreciably younger age of 575 Myr for NGC 6633, as reported by Bossini et al. (2019) making use of *Gaia* DR2 data. We believe that this younger age is in agreement with our final selection for this cluster, and explain the fact that its upper Li envelope lies slightly above the Hyades due to NGC 6633 being younger by at least 150 Myr, and not as a result of being more metal-poor. We thus suggest that the metallicity of NGC 6633 has no observable effect on the position of its Li envelope in comparison to the envelope for the Hyades cluster as these clusters do not seem to be coeval.

Appendix A.3: Old clusters (age > 700 Myr)

∗ **NGC 2477**

NGC 2477 is one of the richest open clusters in the Southern sky with an age of 0.7–1.0 Gyr (Gao 2018; Rain et al. 2021).

Among the nine Li candidates for NGC 2477, we note that we accepted as a final candidate one star with no measured RV in iDR6, due to the fact that it fully fulfilled the astrometry criteria (as well as the other criteria), and was also listed as a member by Cantat-Gaudin et al. (2018). We also accepted one marginal metallicity member (07521722-3831323) deviating 0.20 dex from the mean of the cluster, as it fulfilled all other criteria, and is listed as a member by Cantat-Gaudin et al. (2018). Regarding previous membership selections from the literature, we found three stars in common with Eigenbrod et al. (2004), 10 stars in Cantat-Gaudin et al. (2018), and seven stars in Jadhav et al. (2021). We note that this is one of the three clusters out of our sample of 42 clusters which is not included in Jackson et al. (2022).

∗ **Trumpler 23**

Trumpler 23 is a well-populated open cluster with an age of about 800 Myr (Jacobson et al. 2016; Magrini et al. 2017, 2018; Overbeek et al. 2017; Jackson et al. 2022).

Of the final 25 Li candidates for Trumpler 23, we discarded two stars with no astrometric and photometric *Gaia* data, further listed as non-members with P=0.00 by Jackson et al. (2022). As for kinematics, we also listed two stars as final candidates, RV non-members according to the initial 2σ interval, with RVs deviating up to 6 km s^{-1} from the mean of the cluster, but fulfilling the rest of criteria and further listed as high-probability members by Jackson et al. (2022). Regarding previous membership selections from the literature, we firstly found nine stars in common with Jacobson et al. (2016), as well as 10 stars in Magrini et al. (2017) and Overbeek et al. (2017), and 14 stars in Sampedro et al. (2017). Finally, Jackson et al. (2022) includes all 23 of our final candidates. We note that, in spite of being listed as a non-member by Overbeek et al. (2017), we considered the UVES star 16004025-5329439 as a candidate of Trumpler 23, as opposed to a Li-rich giant non-member, given that this star fulfilled all our membership criteria, and was listed as a member by several studies, such as Magrini et al. (2017) and Jackson et al. (2022).

∗ **Berkeley 81**

Berkeley 81 (also known as Br 81 or Be 81) in an open cluster with an age of 0.75–1 Gyr (Donati et al. 2014a; Jacobson et al. 2016; Magrini et al. 2017, 2018; Jackson et al. 2022; Romano et al. 2021).

Similarly to other clusters in this range, of the final 25 Li candidates for Berkeley 81, we discarded one star with no astrometric or photometric *Gaia* data (further listed as a non-member by Jackson et al. (2022)). We also considered one UVES Li-rich giant star (19014498-0027496) as an additional candidate instead of a giant contaminant, not only because it fulfilled all of our membership criteria, but also because other studies (Jacobson et al. 2016; Magrini et al. 2017) considered it to be a member of this cluster. As for kinematics, two stars in our final selection were RV non-members according to the initial 2σ interval, with RVs deviating 11 km s^{-1} from the mean of the cluster. Also listed as high-probability members by Jackson et al. (2022) and fulfilling all other criteria, we accepted them as candidates. In addition, we also accepted one star (19013633-0024141), listed as a member with P=0.99 by Jackson et al. (2022) and fulfilling all criteria except for metallicity, as it deviates more appreciably from the 3σ limit (0.43 dex from the cluster mean). On the other hand, another star we discarded for deviating appreciably from the [Fe/H] of the cluster, as it was not included in any study, and we also could not analyse this star using astrometry. Regarding previous membership selections from the literature, we firstly found seven stars in common with Magrini et al. (2015), as well as 13 stars in Jacobson et al. (2016) and Magrini et al. (2017), 10 stars in Sampedro et al. (2017), and three stars in Cantat-Gaudin et al. (2018). Finally, Jackson et al. (2022) includes all 24 of our final candidates.

∗ **NGC 2355**

NGC 2355 is an open cluster in the outer part of the Galactic disc with an age of 0.8–1 Gyr (Kharchenko et al. 2005; Sampedro et al. 2017; Jackson et al. 2022; Romano et al. 2021).

Of the final 87 Li candidates for NGC 2355, we discarded one star, listed as a non-member by Jackson et al. (2022) and with no astrometric or photometric data available, as well as not fulfilling the gravity criteria. As for kinematics, 23 stars in our final selection were RV non-members according to the initial 2σ interval, with RVs deviating up to 6–8 km s^{-1} from the mean of the cluster. Fulfilling the rest of membership criteria, and also listed as high-probability members by Jackson et al. (2022) with P=0.99–1.00, we accepted them as candidates as in the case of other clusters. Regarding metallicity, we accepted 10 marginal members, as well as two stars which fulfilled all criteria except for metallicity, deviating more appreciably from the 3σ limit (up to 0.25 dex from the cluster mean). All of these stars are further listed as high-probability members by Jackson et al. (2022), with P=1.00. Regarding previous membership selections from the literature, we found 64 stars in common with Cantat-Gaudin et al. (2018), and Jackson et al. (2022) includes 84 of our 86 final candidates (the remaining two stars in our selection were not included in their study).

∗ **NGC 6802**

NGC 6802 is an inner disc open cluster in the constellation Fuchs, with an age of 0.9–1.0 Gyr (Jacobson et al. 2016; Magrini et al. 2017; Tang et al. 2017; Magrini et al. 2018; Jackson et al. 2022; Romano et al. 2021).

Of the final 36 Li candidates for NGC 6802, we firstly discarded four stars listed as non-members by Jackson et al. (2022) and without any astrometric or photometric *Gaia* data available. As for kinematics, we accepted six stars in our final selection which were RV non-members according to the initial 2σ interval, listed as high-probability members by Jackson et al. (2022) with P=0.94–0.99 and fulfilling all criteria except for the fact that their RVs deviated up to 4–17 km s^{-1} from the mean of

the cluster. We also note that the final selection of this cluster includes a couple of stars which present values of EW(Li) slightly larger than the rest of candidates (112–113 mÅ). These two stars fulfil the rest of membership criteria, and one of them is also listed as a high probability member by Jackson et al. (2016) (the other one is not included in their study), and so we accepted them as final members of the cluster. Furthermore, we can also explain the higher observable values of EW(Li) of these stars considering the fact that they potentially experimented a lower rate of Li depletion due to them exhibiting values of rotation that are in the middle of the scale for this cluster (also see Paper III). Regarding previous membership selections from the literature, we found the following stars in common with several studies: Firstly, we found eight common stars with Jacobson et al. (2016) and Magrini et al. (2017), as well as 10 stars in Sampedro et al. (2017), 18 stars in Tang et al. (2017), and five common stars in Cantat-Gaudin et al. (2018). Jackson et al. (2022) includes 31 of our 32 final candidates (the remaining star in our selection was not included in their study). Finally, one of the Li-rich giants in our list (J19304281+2016107) is also listed in Casey et al. (2016).

∗ **NGC 6005**

NGC 6005 is a Southern open cluster in the constellation Norma with an age of 0.97–1.20 Gyr (Jacobson et al. 2016; Magrini et al. 2017; Bossini et al. 2019; Jackson et al. 2022). Bossini et al. (2019) calculated an age of 973 ± 4 Myr for this cluster.

Of the final 55 Li candidates for NGC 6005, we discarded five stars which we were not able to analyse using astrometric and photometric *Gaia* data, and were further listed as non-members by Jackson et al. (2022). We also discarded another star which fulfilled all criteria except for metallicity. In contrast to our decision to accept stars as final candidates if they fulfil the rest of criteria apart from metallicity or $\log g$, especially the more restrictive astrometric criteria, in this case we discarded it from the final selection on the basis of not being able to analyse it with *Gaia* data, and additionally for not being included by Jackson et al. (2022). As for kinematics, we accepted two stars which were RV non-members according to the initial 2σ interval, with RVs deviating up to 7–11 km s^{-1} from the mean of the cluster, but fulfilled all other criteria and were also listed as members of the cluster by Jackson et al. (2022) with P=0.90–0.91. We also note that the final selection of this cluster includes three stars which, even while presenting values of EW(Li) slightly larger than the rest of candidates (102–118 mÅ), fulfil the rest of membership criteria, are listed as high probability members by Jackson et al. (2016), and could also be experiencing a slower rate of Li depletion caused by rotation values that are in the middle of the scale for this cluster. Finally, we also accepted eight marginal members (deviating up to 0.30–0.50 dex from the mean of the cluster), as they fulfilled all other criteria, and are listed as high-probability members by Jackson et al. (2022), with P=0.90–0.99.

Regarding previous membership selections from the literature, we found the following stars in common with several studies: Firstly, we found 12 common stars with Jacobson et al. (2016), as well as seven stars in Magrini et al. (2017), 11 stars in Sampedro et al. (2017), and 12 common stars in Cantat-Gaudin et al. (2018). Jackson et al. (2022) includes all 49 of our final candidates. As already discussed in Sect. 3.4, we also note that we seem to find some inconsistencies when plotting the Li-rich giant outliers selected in the field of this cluster in the CMD diagram, with all three of them appearing among the non-giant cluster candidates. However, when plotting them in the Kiel diagram the expected distinction is found between the non-giant cluster candidates and the Li-rich giant outliers.

∗ **Pismis 18**

Pismis 18 is a Southern open cluster with an age of 1.2 Gyr (Jacobson et al. 2016; Magrini et al. 2017, 2018; Jackson et al. 2022).

Of the final 12 Li candidates for Pismis 18, we firstly accepted one star in our final selection which fulfilled all criteria listed as a member of the cluster by Jackson et al. (2022) with P=0.98, but was a RV non-member according to the initial 2σ interval, with a RV deviating up to 6 km s^{-1} from the mean of the cluster. We also discarded two stars with no astrometric and photometric *Gaia* data available, further listed as non-members by Jackson et al. (2022). Regarding previous membership selections from the literature, we found the following stars in common with several studies: Firstly, we found five common stars with Jacobson et al. (2016), as well as three stars in Magrini et al. (2017), and all of our 10 stars are listed in Hatzidimitriou et al. (2019). Jackson et al. (2022) also includes all 10 of our final candidates.

∗ **Melotte 71**

Melotte 71 (also known as Mel 71) is an open cluster between the inner and outer disc. Bossini et al. (2019) calculated an age of 1294 ± 89 Myr for this cluster, while Netopil et al. (2016) listed an age of 0.7 Gyr.

Regarding previous membership selections from the literature for Melotte 71, we found three stars in common with Sampedro et al. (2017), and four common stars in Cantat-Gaudin et al. (2018). We note that this is one of the three clusters out of our sample of 42 clusters which is not included in Jackson et al. (2022).

∗ **Pismis 15**

Pismis 15 is an open cluster with an age of 1.3 Gyr (Carraro et al. 2005; Kharchenko et al. 2005; Sampedro et al. 2017; Liu & Pang 2019; Jackson et al. 2022).

Among the final 33 Li candidates for Pismis 15, we accepted a star which fulfilled all criteria except for metallicity, deviating more appreciably from the 3σ limit (0.66 dex from the cluster mean). This star is further listed as a member by Jackson et al. (2022), with P=0.99. We also discarded two stars with no astrometric or photometric *Gaia* data, listed as non-members by Jackson et al. (2022). We also note that the final selection of this cluster includes eight stars which present values of EW(Li) slightly larger than the rest of candidates (92–147 mÅ), albeit without exhibiting appreciable dispersion with respect to the other members, fulfilling the rest of membership criteria, and also being listed as high probability members by Jackson et al. (2016) with P=0.98–0.99. Furthermore, a couple of these stars also exhibit high values of rotation according to the range observed for this cluster. The effects of rotation could thus also explain the higher values of EW(Li) of these stars, as we could explain them as members of Pismis 15 exhibiting a slightly slower rate of Li depletion as a result of being faster rotators. Regarding previous membership selections from the literature, we found five common stars with Sampedro et al. (2017), as well as 15 stars in Cantat-Gaudin et al. (2018). Jackson et al. (2022) includes all 31 of our final candidates.

∗ **Trumpler 20**

Trumpler 20 is an open cluster located towards the Galactic centre, with an age of 1.4–1.8 Gyr (Donati et al. 2014b; Jacobson et al. 2016; Magrini et al. 2017; Jackson et al. 2022; Romano et al. 2021).

Of the final 116 Li candidates for Trumpler 20, we firstly discarded 12 stars, listed as non-members by Jackson et al. (2022), with no astrometric *Gaia* data available; as well as another star which fulfilled all criteria except for metallicity (but lacked *Gaia* data), and was listed as a definite non-member by Jackson et al. (2022). As for kinematics, we accepted five stars, all of them listed as members of the cluster by Jackson et al. (2022) with P=0.87–0.98, albeit being RV non-members according to the initial 2σ interval, with RVs deviating up to 10 km s^{-1} from the mean of the cluster. As for metallicity, we also accepted 10 marginal members (deviating up to 0.20–0.40 dex from the mean of the cluster). All of these stars fulfilled the rest of criteria, and all are further listed as members by Jackson et al. (2022), with P=0.87–0.99.

Thee final selection for this cluster also includes a number of stars which present values of EW(Li) somewhat larger than the rest of candidates (90–120 mÅ), albeit without showing an appreciable dispersion with respect to the other members, and also fulfilling all other criteria, and listed as high probability members by Jackson et al. (2016) with P=0.89–.99. Furthermore, we may also explain the higher observable values of EW(Li) of several of these stars seeing as they also exhibit values of rotation that are in the middle and high end of the scale for this cluster, thus potentially making them cluster members that have experienced a slower rate of Li depletion as a result (see Paper III). Finally, we also find one star (12400449-6036566) which also exhibits a high EW(Li) (137 mÅ) and stands apart from the rest of the candidates. We listed this star as a Li-rich candidate of the cluster. This star fulfilled the rest of our criteria, and it is also listed as a Li-rich member by Smiljanic et al. (2016).

Regarding previous membership selections from the literature, we found the following stars in common with several studies: Firstly, we found 97 common stars with Donati et al. (2014b), as well as 23 stars in Tautvaišienė et al. (2015), 23 stars in Jacobson et al. (2016), 23 stars in Smiljanic et al. (2016), 17 stars in Magrini et al. (2017), 31 stars in Sampedro et al. (2017), and 42 stars in Cantat-Gaudin et al. (2018). Finally, Jackson et al. (2022) includes all but one of our 104 final candidates. The remaining star in our selection fulfils all of our criteria in spite of being listed as a non-member in Jackson et al. (2022). Once again, the reason for these individual deviations between our two analyses probably originates from the existing differences regarding criteria limits or the weight of the factors implicated in the decision to accept or discard stars as final candidates.

∗ **Berkeley 44**

Berkeley 44 (also known as Br 44) is an open cluster with a dense background field and an age of 1.4–1.6 Gyr (Hayes & Friel 2014; Jacobson et al. 2016; Magrini et al. 2017, 2018; Jackson et al. 2022; Romano et al. 2021).

Of the final 31 Li candidates for Berkeley 44, we discarded one star which we could not analyse with *Gaia* astrometric data, also listed as a non-member by Jackson et al. (2022). On the other hand, we accepted five stars, listed as members of the cluster by Jackson et al. (2022) with P=0.86–0.99 and fulfilling all other critera, which were RV non-members according to the initial 2σ interval, with RVs deviating up to 3–4 km s^{-1} from the mean of the cluster. We also accepted one marginal metallicity member (deviating 0.29 dex from the mean of the cluster), as it fulfilled all other criteria and is listed as a high-probability member by Jackson et al. (2022), with P=1.00. Regarding previous membership selections from the literature, we found the following stars in common with several studies: Firstly, we found three common stars with Jacobson et al. (2016) and Magrini et al. (2017), as well as eight stars in Sampedro et al. (2017), and 20 stars in Cantat-Gaudin et al. (2018). Finally, Jackson et al. (2022) includes all 30 of our final candidates.

∗ **NGC 2243**

NGC 2243 is a rich open cluster in the constellation of Canis Major, with an age in the range of 3.8–4.4 Gyr (Richer et al. 1998; Jacobson et al. 2011; Heiter et al. 2014; Magrini et al. 2017, 2018; Jackson et al. 2022; Romano et al. 2021). NGC 2243 is one of the most metal-poor clusters known, with a [Fe/H] value of -0.38 ± 0.04 dex (Magrini et al. 2017, 2018). We note that for the individual figures of this cluster (see Appendix B), due to the low metallicity of this cluster we considered PARSEC isochrones with Z=0.006 instead of the usual near-solar metallicity of Z=0.019 we used for the rest of the clusters in our sample.

Regarding kinematics, 36 stars in our final selection for NGC 2243 were RV non-members according to the initial 2σ interval, with RVs deviating up to 8 km s^{-1} from the mean of the cluster. As in the case of other cluster analyses, we accepted both of them as final members, and both stars were also listed as members of the cluster by Jackson et al. (2022) with P=0.93–1.00. We also accepted 13 marginal metallicity members (deviating up to 0.50 dex from the mean of the cluster), as well as three additional stars which deviated more appreciably from the 3σ limit (up to 0.60–0.80 dex from the cluster mean). All of these stars fulfilled all other criteria and all but one are further listed as high-probability members by Jackson et al. (2022), with P=0.99–1.00.

Regarding previous membership selections from the literature, we found the following stars in common with several studies: Firstly, we found nine common stars with Jacobson et al. (2011), as well as one star in Heiter et al. (2014), 13 stars in Magrini et al. (2017), 42 stars in Sampedro et al. (2017), and 178 stars in Cantat-Gaudin et al. (2018). Finally, Jackson et al. (2022) includes all but one of our 289 of our final candidates (the remaining star in our selection was not included in their study). Given that NGC 2243 and M67 are very close age-wise, we also note that we additionally made use of the Li envelope created by our candidate selection for M67 (see Paper III, as well as former M67 attested members, to help confirm the membership of our selection for NGC 2243. We also note that we seem to find some inconsistencies when plotting the Li-rich giant outliers selected in the field of this cluster in the CMD diagram, with five of them appearing among the non-giant cluster candidates. However, when plotting them in the Kiel diagram the expected distinction is found between the non-giant cluster candidates and the Li-rich giant outliers.

∗ **M67**

M67 (also known as Messier 67 or NGC 2682) is an open cluster in the constellation of Cancer, with an age in the range of 3.6–4.5 Gyr, an age close to that of the Sun (Balachandran 1995; Richer et al. 1998; Pallavicini et al. 2005; Sestito & Randich 2005).

Eight stars in our final selection for M67 were RV non-members according to the initial 2σ interval, with RVs deviating up to 4–9 km s^{-1} from the mean of the cluster, but were accepted as final members and also listed as definite candidates by

Jackson et al. (2022) with P=0.99. We also accepted one marginal metallicity member (08511748+1145225), which deviates 0.14 dex from the cluster mean but fulfilled all other criteria, also being listed as a high-probability member by Jackson et al. (2022), with P=1.00. Regarding previous membership selections from the literature, we found the following stars in common with several studies: Firstly, we found 65 common stars with Pace et al. (2012), as well as 50 stars in Pasquini et al. (2012), two stars in Carlberg (2014), 65 stars in Geller et al. (2015), 55 stars in Brucalassi et al. (2017), 74 stars in Sampedro et al. (2017), 29 stars in Jadhav et al. (2021), and seven stars in Ilin et al. (2021). Finally, Jackson et al. (2022) includes all 96 of our final candidates. We also note that in order to reinforce the membership of our GES selection we made use of several lists of M67 candidates from a series of non-GES studies (Hobbs & Pilachowski 1986; Balachandran 1995; Pallavicini et al. 1997; Pasquini et al. 1997; Jones et al. 1999; Randich et al. 2002).

Appendix B: Cluster membership analysis: Individual figures

This appendix includes individual figures for several membership criteria discussed in Sect. 3, for all 42 clusters in the sample. For the final selection of candidate members in each cluster, we show the final RV distribution and parallax distributions, the *pmra*-versus-*pmdec* proper motions diagram, the *Gaia* CMD, the γ-versus-$T_{\rm eff}$ and/or Kiel diagrams, and the EW(Li)-versus-$T_{\rm eff}$ diagram. When available, strong accreting members and Li-rich giant contaminants are further plotted alongside the candidate members. Also shown in all EW(Li)-versus-$T_{\rm eff}$ diagrams are the upper envelope of EW(Li) for IC 2602 (35 Myr, red), the upper and lower envelopes of the Pleiades (78–125 Myr, grey), and the upper envelope of the Hyades (750 Myr, turquoise).

Appendix B.1: NGC 6530

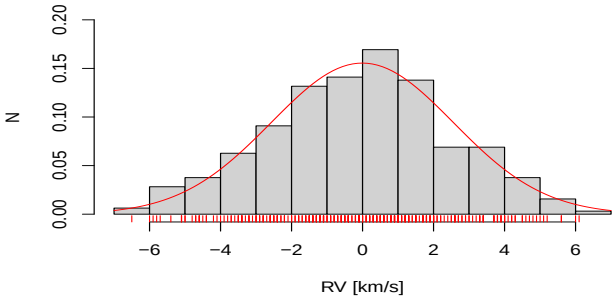

Fig. B.1. RV distribution for NGC 6530.

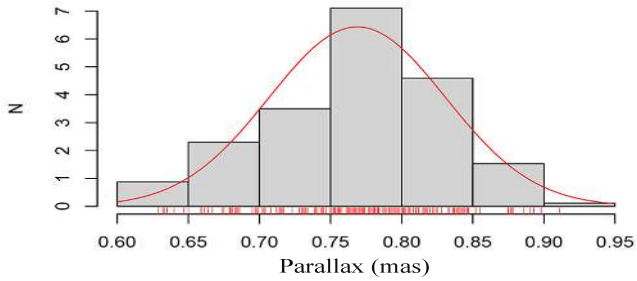

Fig. B.2. Parallax distribution for NGC 6530.

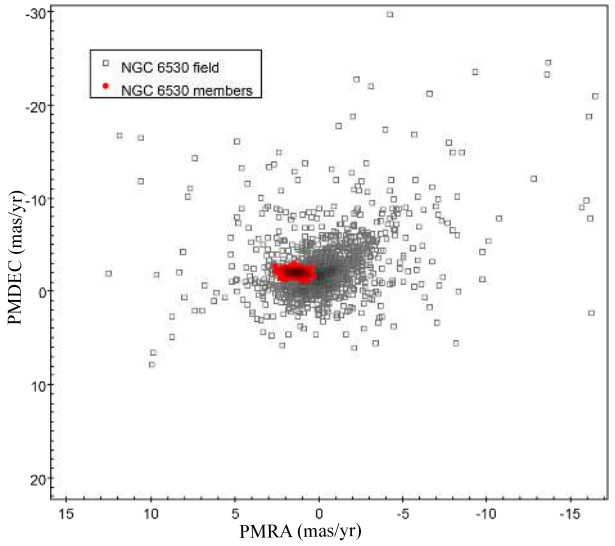

Fig. B.3. PMs diagram for NGC 6530.

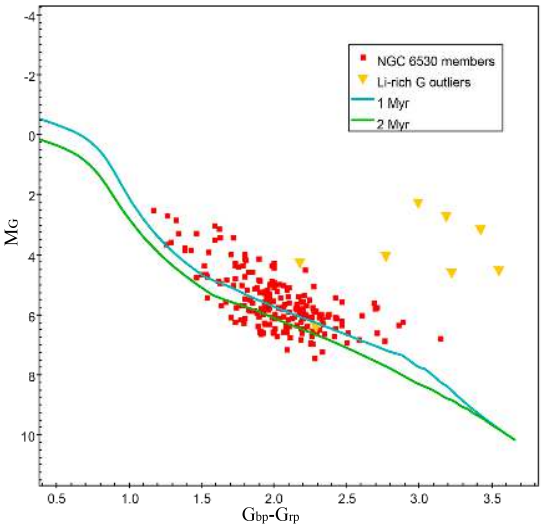

Fig. B.4. CMD for NGC 6530.

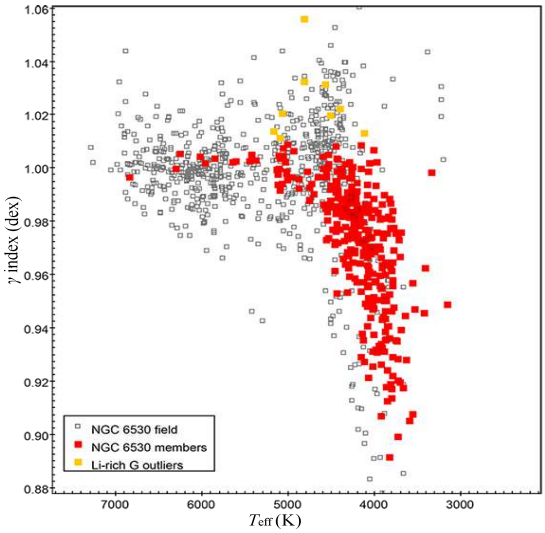

Fig. B.5. γ index-versus-$T_{\rm eff}$ diagram for NGC 6530.

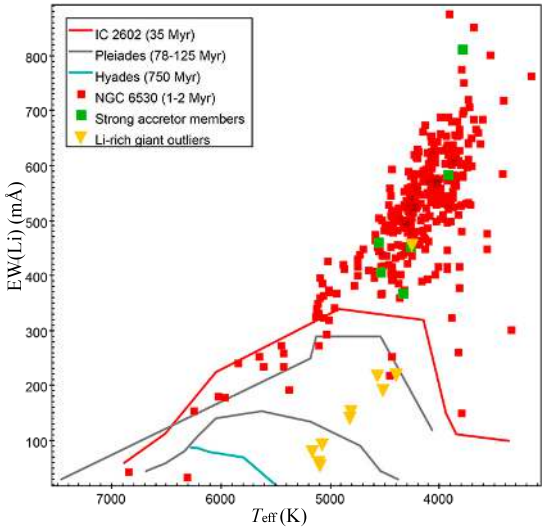

Fig. B.6. EW(Li)-versus-$T_{\rm eff}$ diagram for NGC 6530.

Appendix B.2: Rho Oph

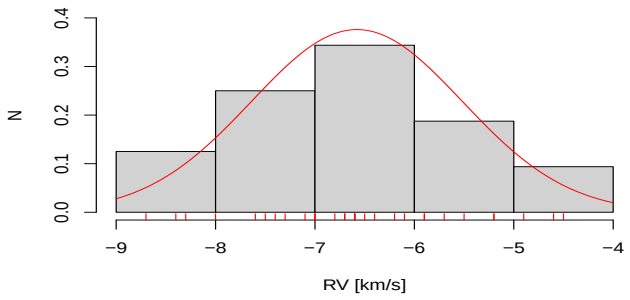

Fig. B.7. RV distribution for Rho Oph.

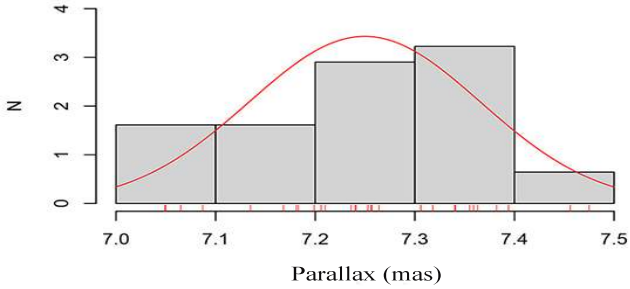

Fig. B.8. Parallax distribution for ρ Oph

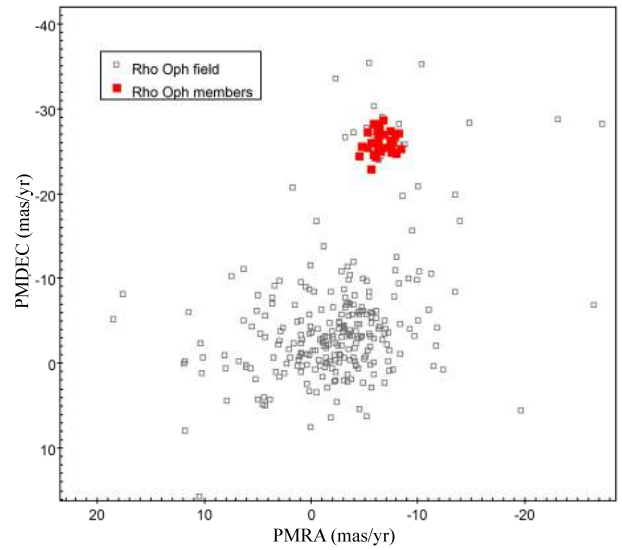

Fig. B.9. PMs diagram for ρ Oph.

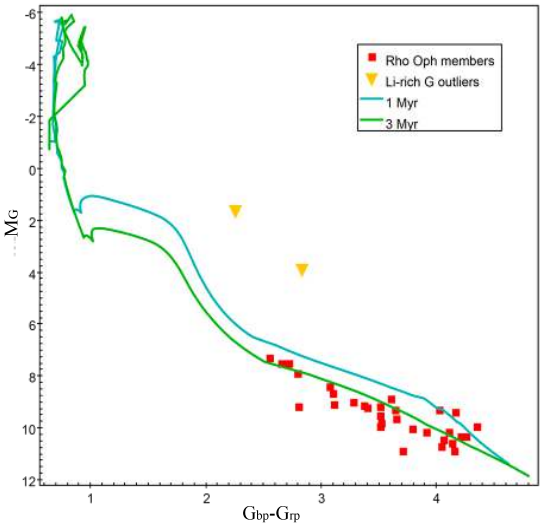

Fig. B.10. CMD for ρ Oph.

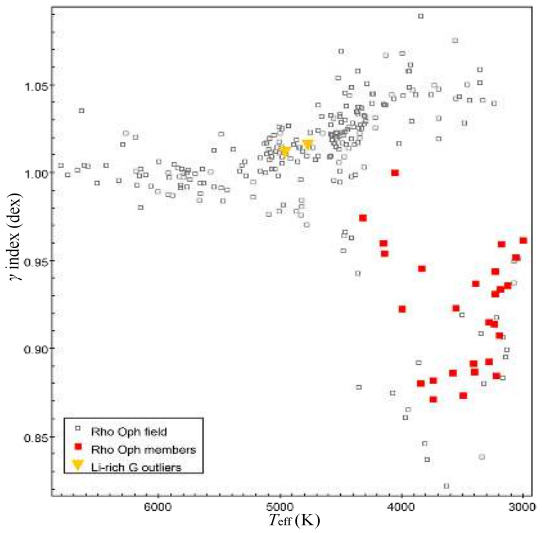

Fig. B.11. γ index-versus-$T_{\rm eff}$ diagram for ρ Oph.

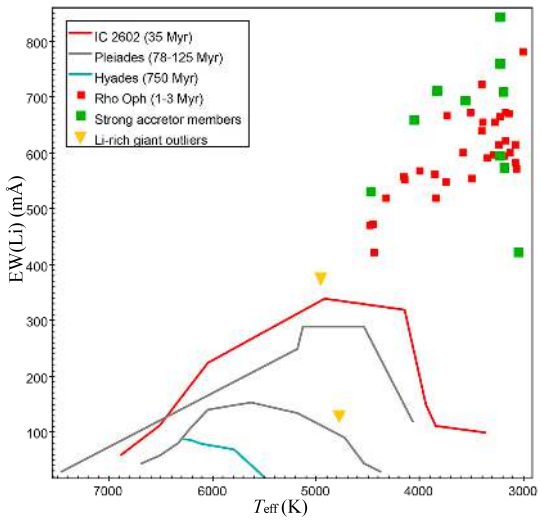

Fig. B.12. EW(Li)-versus-$T_{\rm eff}$ diagram for ρ Oph.

Appendix B.3: Trumpler 14

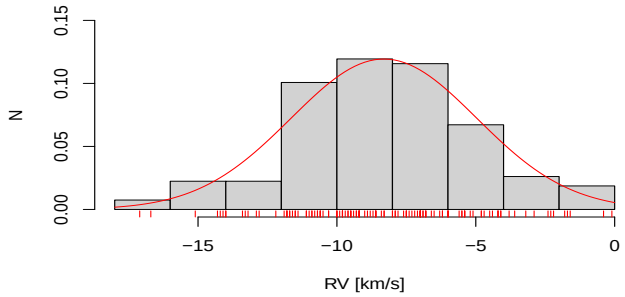

Fig. B.13. RV distribution for Trumpler 14.

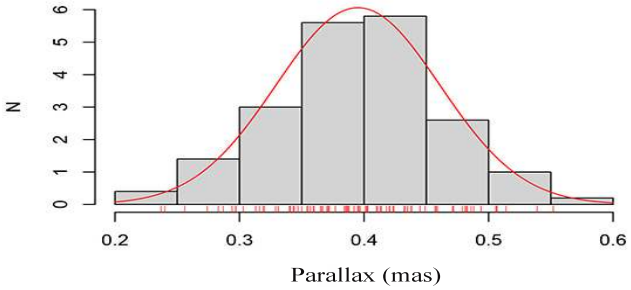

Fig. B.14. Parallax distribution for Trumpler 14.

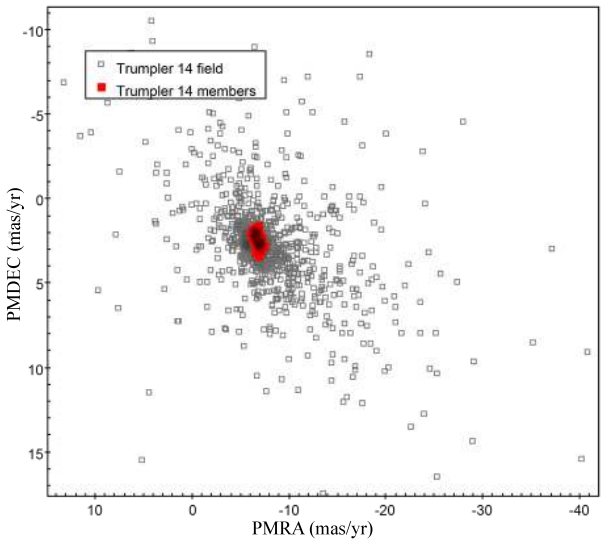

Fig. B.15. PMs diagram for Trumpler 14.

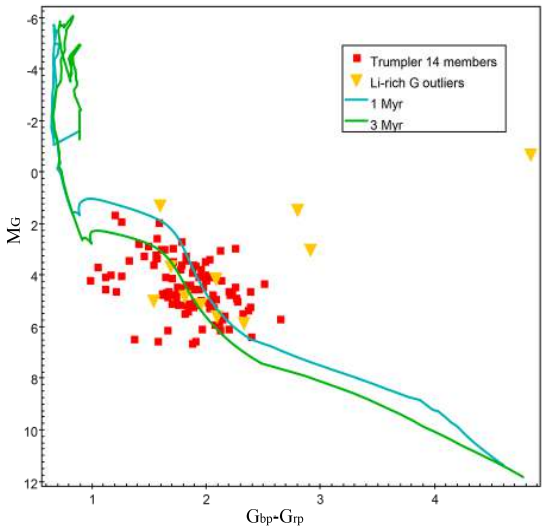

Fig. B.16. CMD for Trumpler 14.

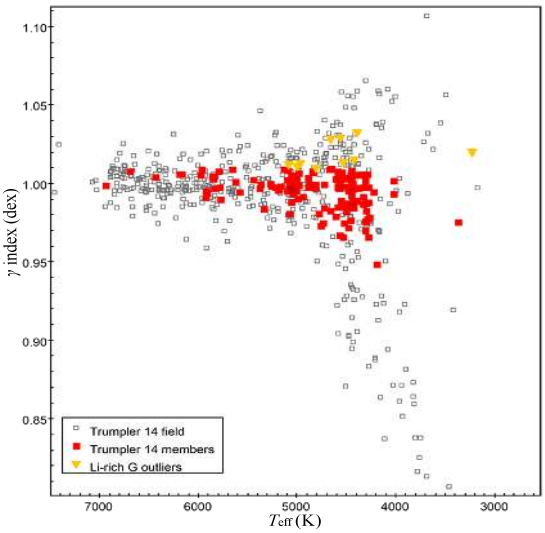

Fig. B.17. γ index-versus-$T_{\rm eff}$ diagram for Trumpler 14.

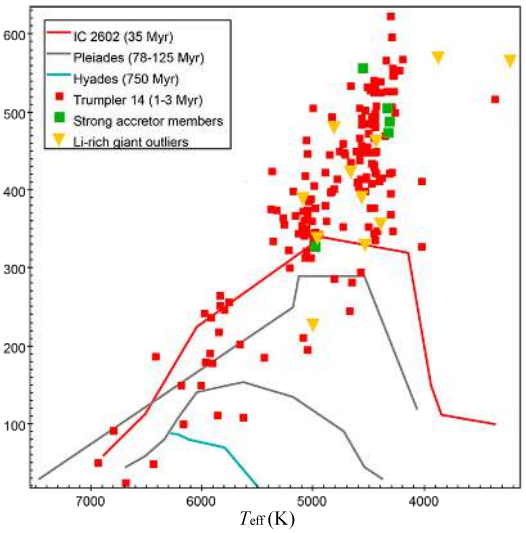

Fig. B.18. EW(Li)-versus-$T_{\rm eff}$ diagram for Trumpler 14.

Appendix B.4: Cha I

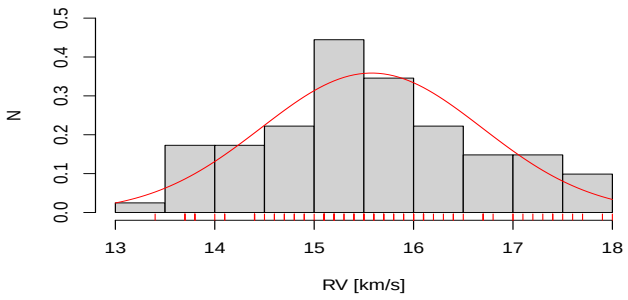

Fig. B.19. RV distribution for Cha I.

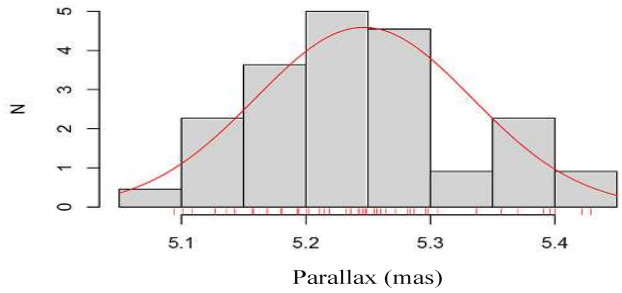

Fig. B.20. Parallax distribution for Cha I.

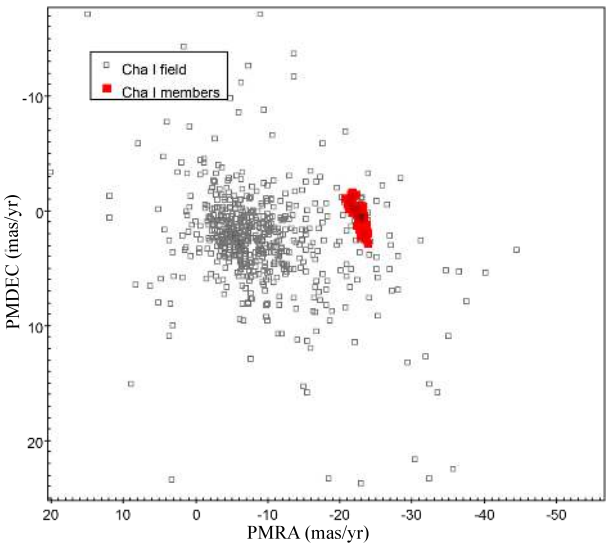

Fig. B.21. PMs diagram for Cha I.

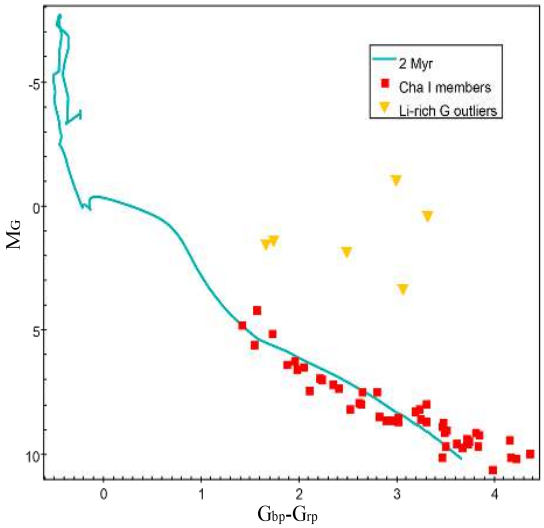

Fig. B.22. CMD for Cha I.

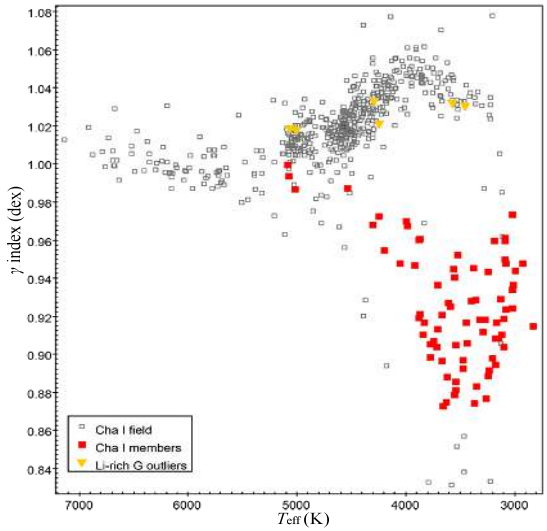

Fig. B.23. γ index-versus-$T_{\rm eff}$ diagram for Cha I.

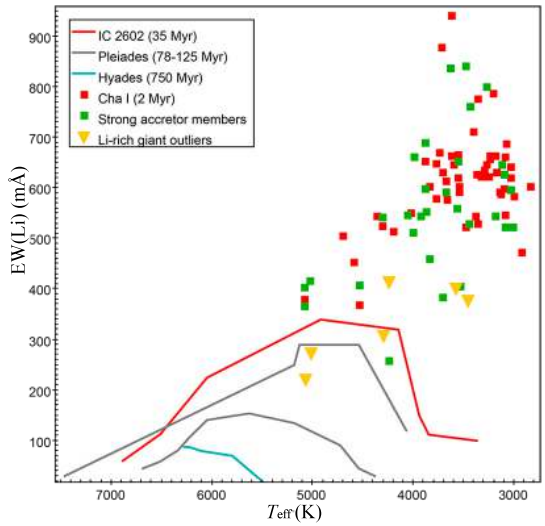

Fig. B.24. EW(Li)-versus-$T_{\rm eff}$ diagram for Cha I.

Appendix B.5: NGC 2244

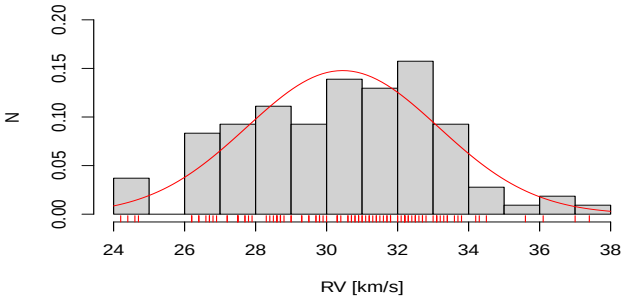

Fig. B.25. RV distribution for NGC 2244.

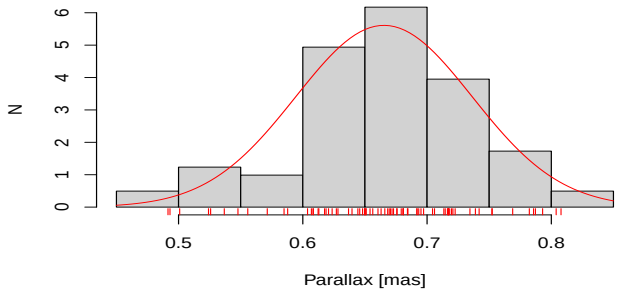

Fig. B.26. Parallax distribution for NGC 2244.

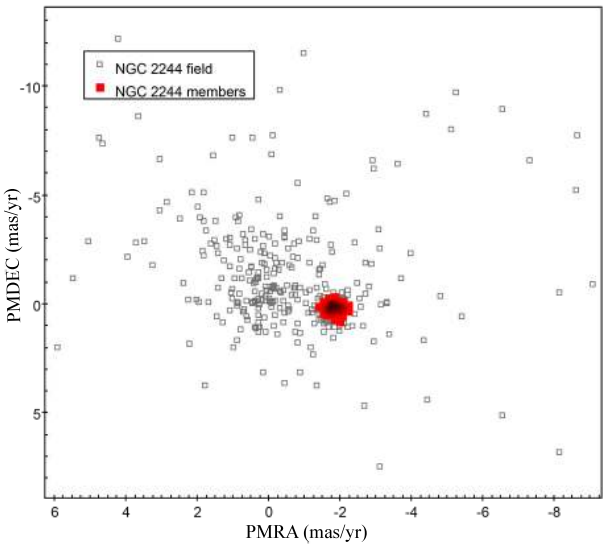

Fig. B.27. PMs diagram for NGC 2244.

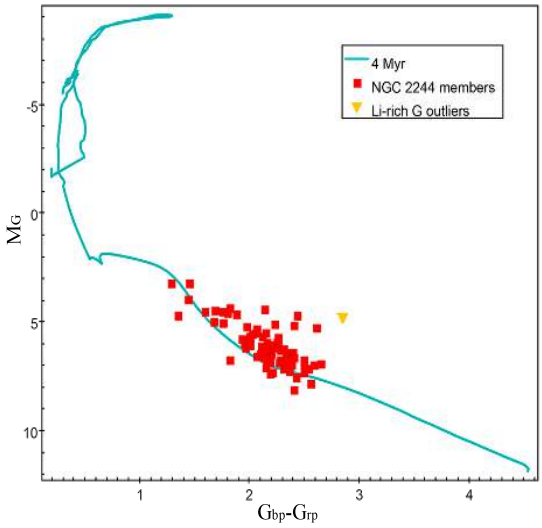

Fig. B.28. CMD for NGC 2244.

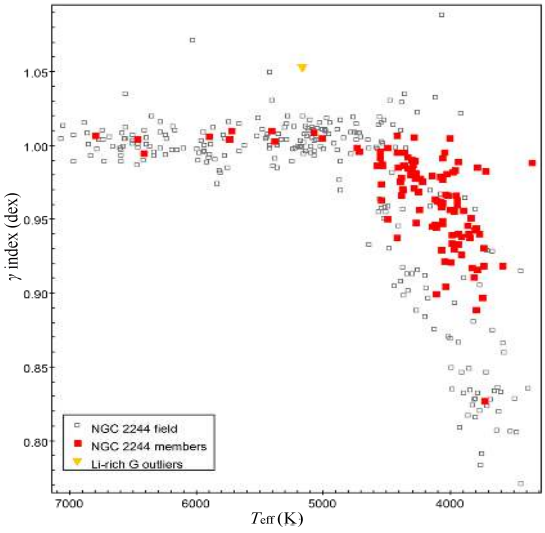

Fig. B.29. γ index-versus-$T_{\rm eff}$ diagram for NGC 2244.

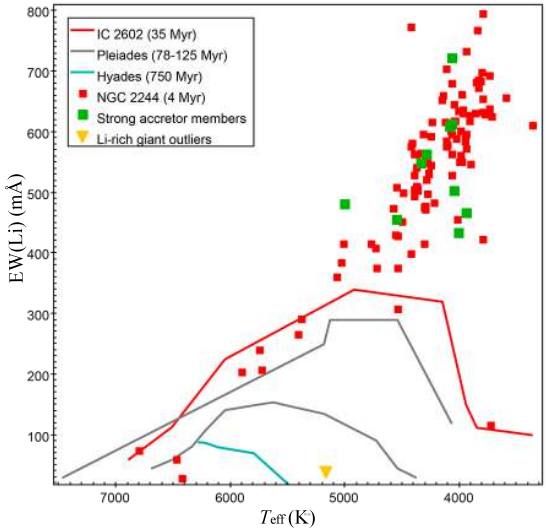

Fig. B.30. EW(Li)-versus-$T_{\rm eff}$ diagram for NGC 2244.

Appendix B.6: NGC 2264

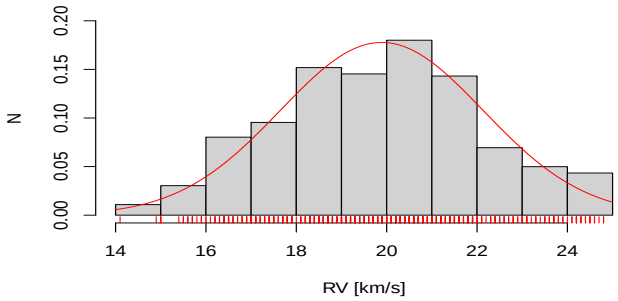

Fig. B.31. RV distribution for NGC 2264.

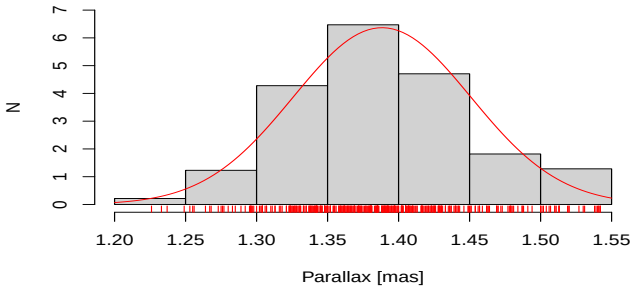

Fig. B.32. Parallax distribution for NGC 2264.

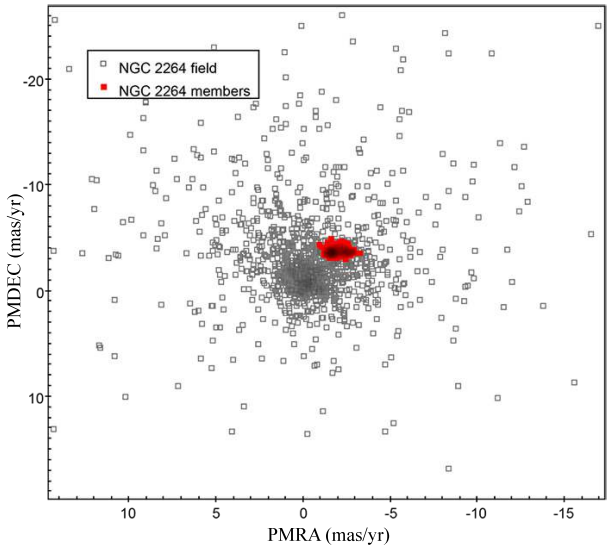

Fig. B.33. PMs diagram for NGC 2264.

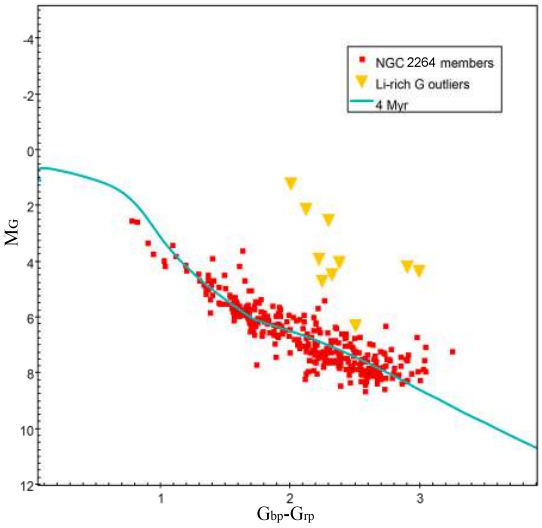

Fig. B.34. CMD for NGC 2264.

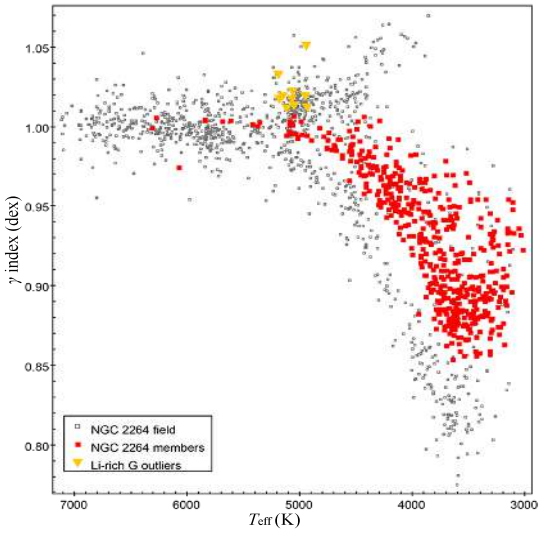

Fig. B.35. γ index-versus-$T_{\rm eff}$ diagram for NGC 2264.

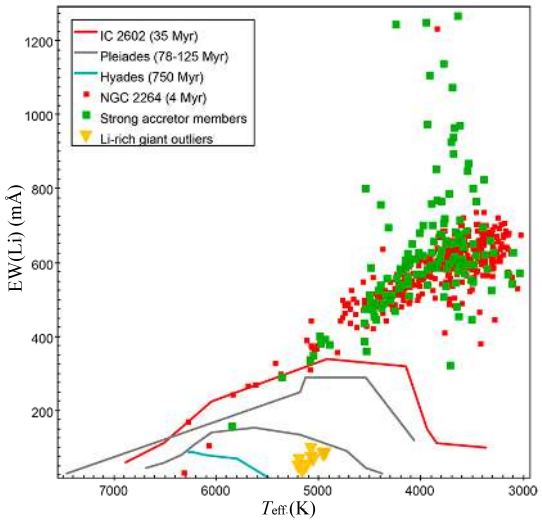

Fig. B.36. EW(Li)-versus-$T_{\rm eff}$ diagram for NGC 2264.

Appendix B.7: λ Ori

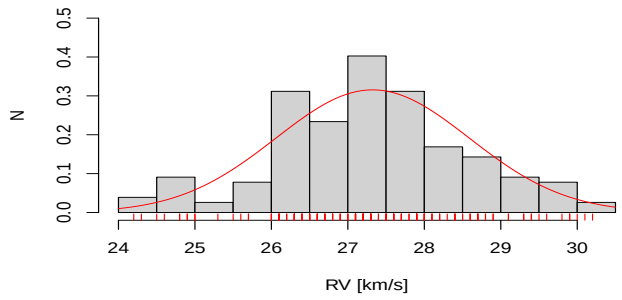

Fig. B.37. RV distribution for λ Ori.

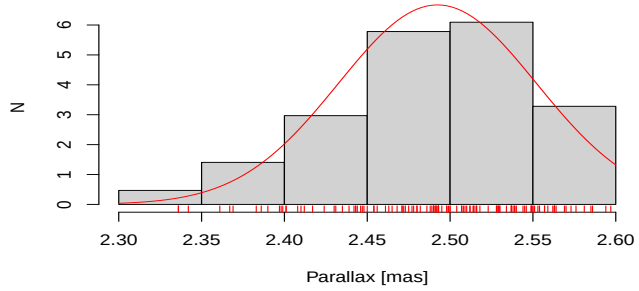

Fig. B.38. Parallax distribution for λ Ori.

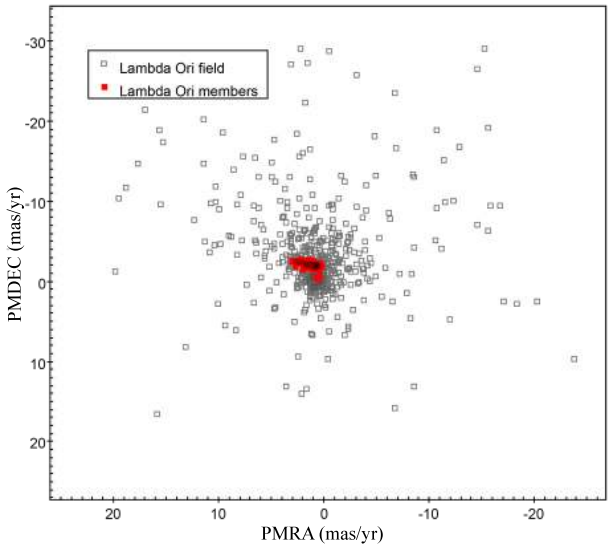

Fig. B.39. PMs diagram for λ Ori.

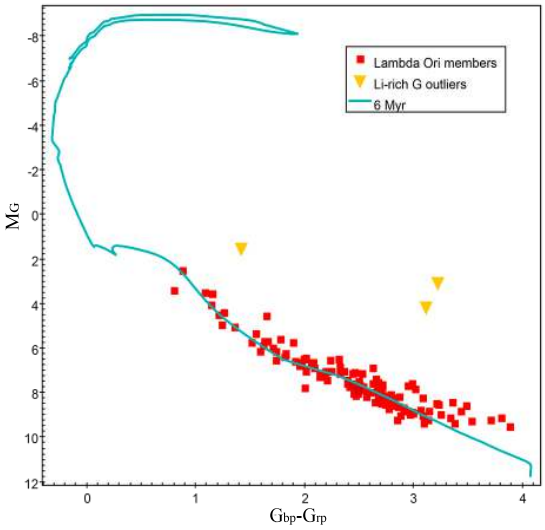

Fig. B.40. CMD for λ Ori.

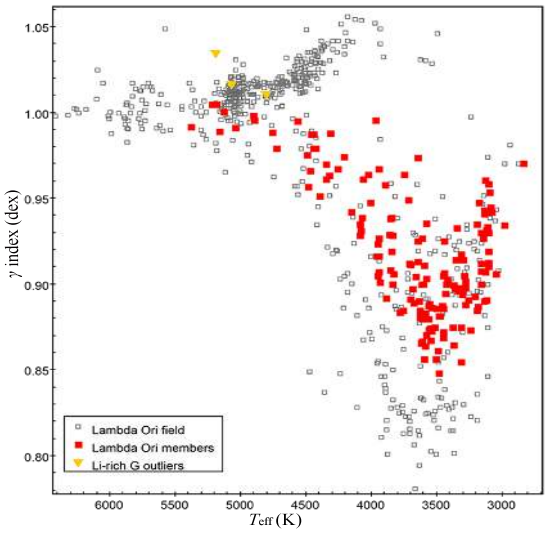

Fig. B.41. γ index-versus-$T_{\rm eff}$ diagram for λ Ori.

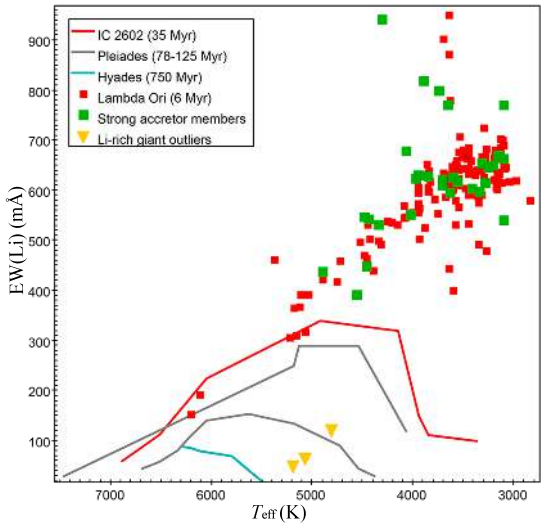

Fig. B.42. EW(Li)-versus-$T_{\rm eff}$ diagram for λ Ori.

Appendix B.8: Col 197

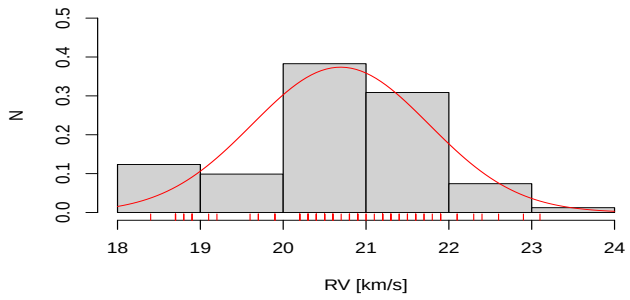

Fig. B.43. RV distribution for Col 197.

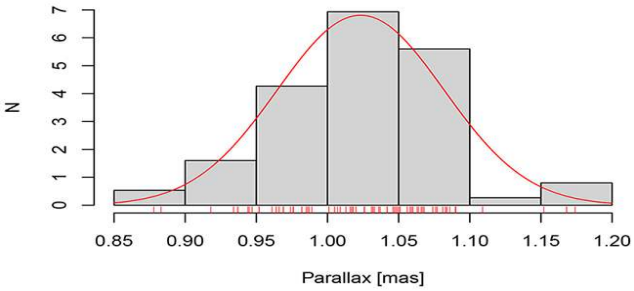

Fig. B.44. Parallax distribution for Col 197.

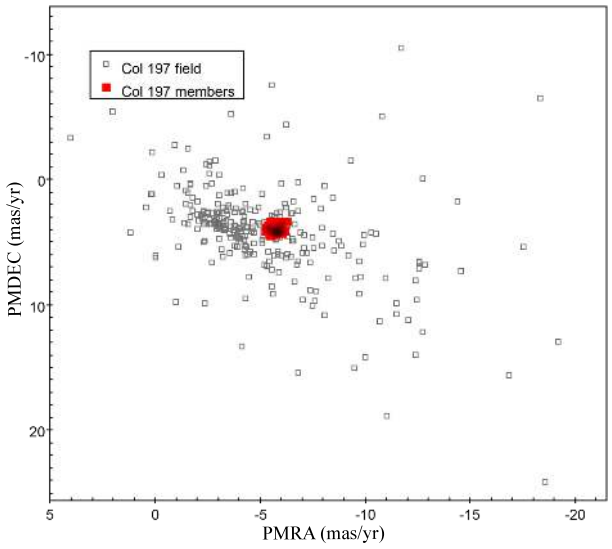

Fig. B.45. PMs diagram for Col 197.

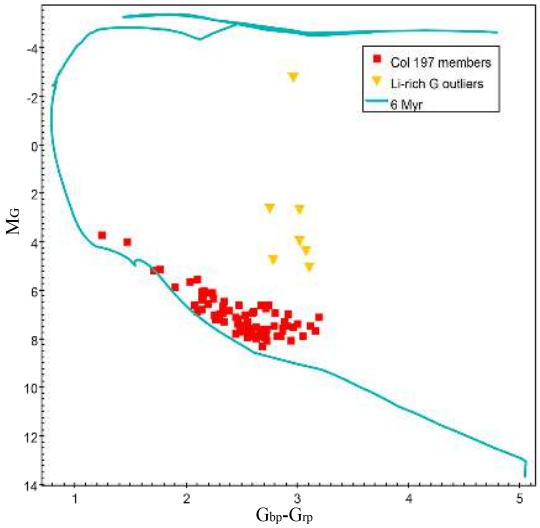

Fig. B.46. CMD for Col 197.

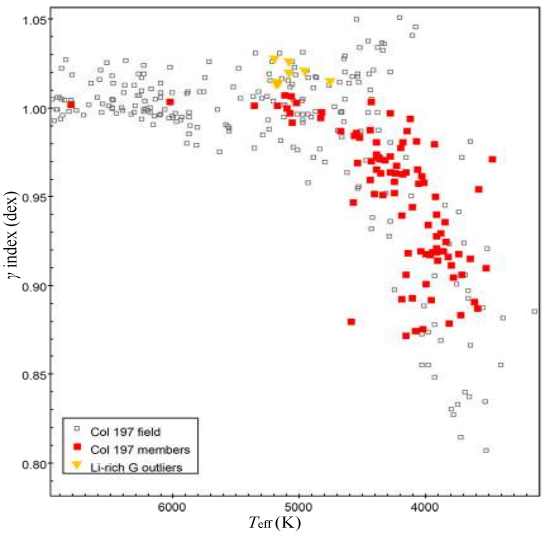

Fig. B.47. γ index-versus-$T_{\rm eff}$ diagram for Col 197.

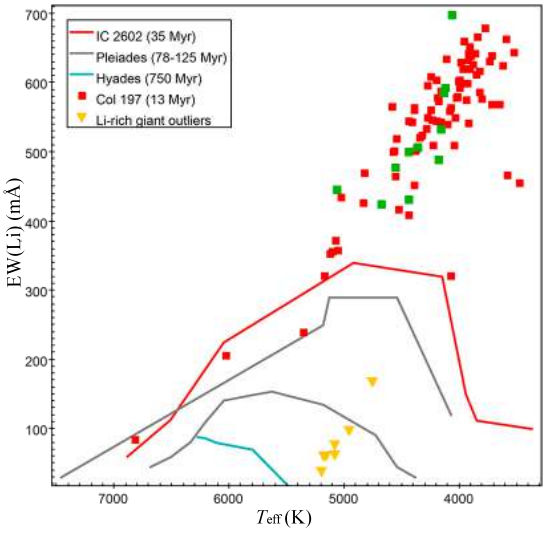

Fig. B.48. EW(Li)-versus-$T_{\rm eff}$ diagram for Col 197.

Appendix B.9: γ Vel

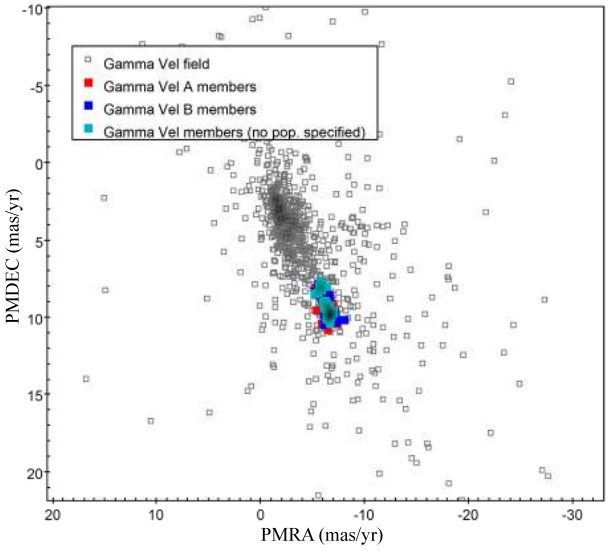

Fig. B.49. PMs diagram for γ Vel.

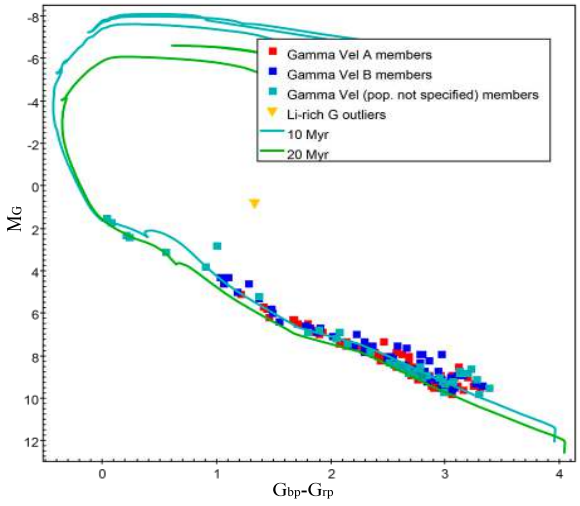

Fig. B.50. CMD for γ Vel.

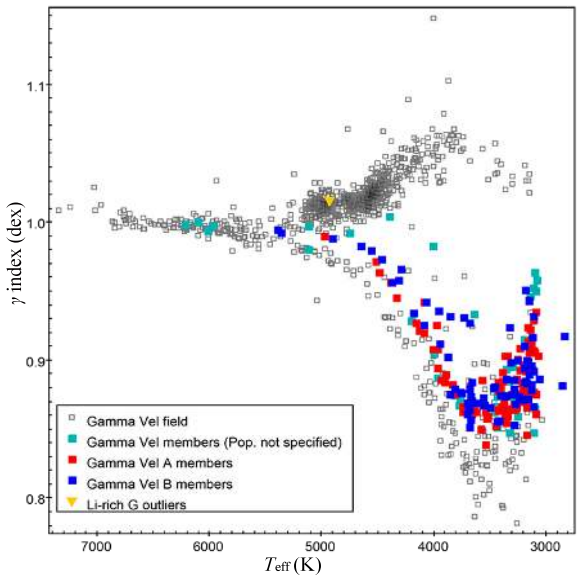

Fig. B.51. γ index-versus-$T_{\rm eff}$ diagram for γ Vel.

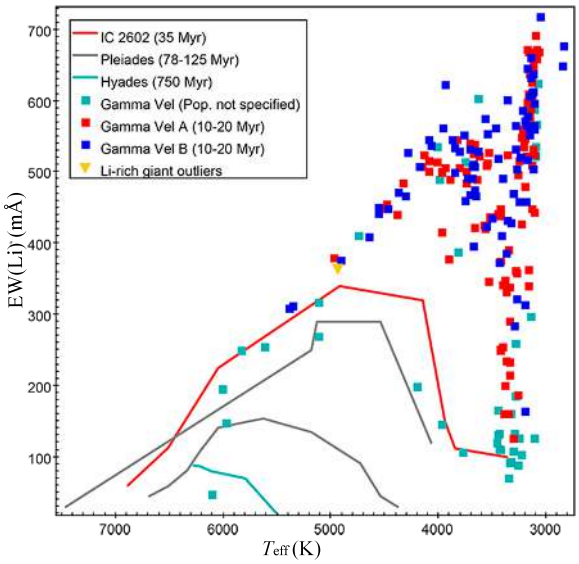

Fig. B.52. EW(Li)-versus-$T_{\rm eff}$ diagram for γ Vel.

Appendix B.10: NGC 2232

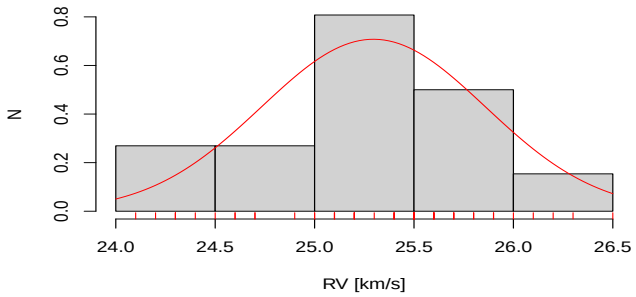

Fig. B.53. RV distribution for NGC 2232.

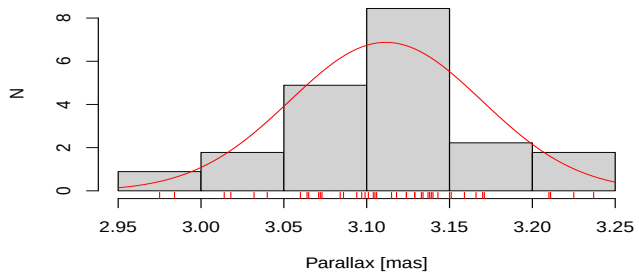

Fig. B.54. Parallax distribution for NGC 2232.

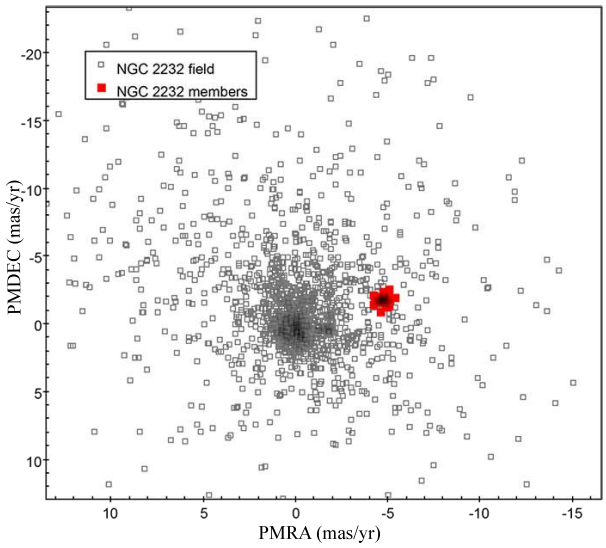

Fig. B.55. PMs diagram for NGC 2232.

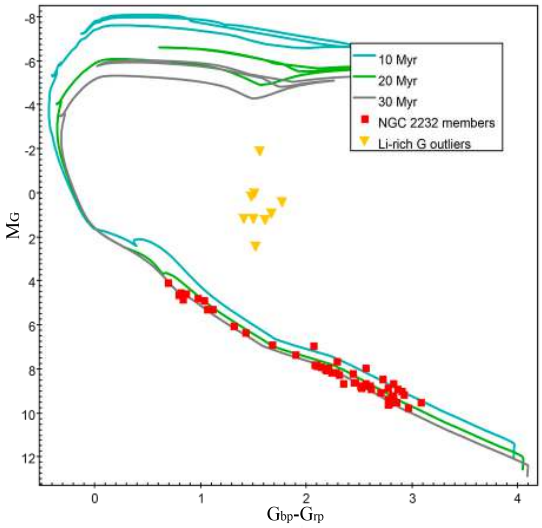

Fig. B.56. CMD for NGC 2232.

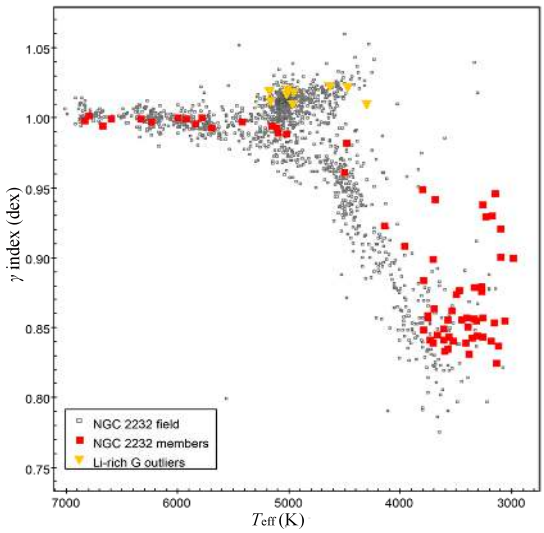

Fig. B.57. γ index-versus-$T_{\rm eff}$ diagram for NGC 2232.

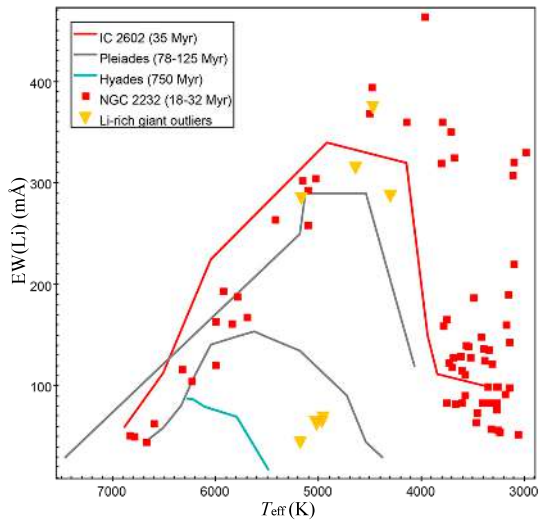

Fig. B.58. EW(Li)-versus-$T_{\rm eff}$ diagram for NGC 2232.

Appendix B.11: NGC 2547

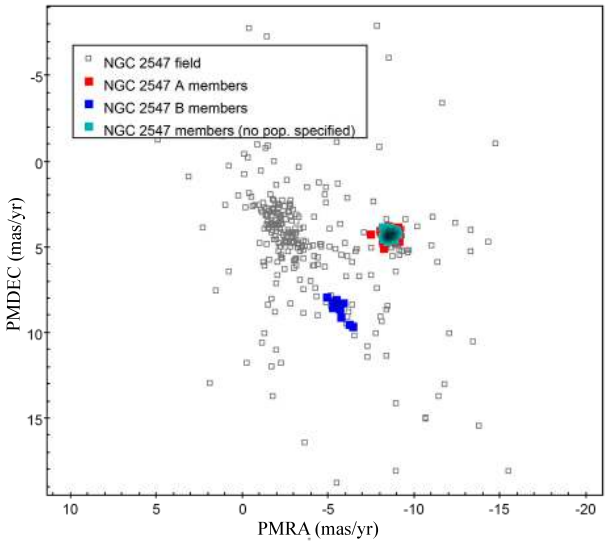

Fig. B.59. PMs diagram for NGC 2547.

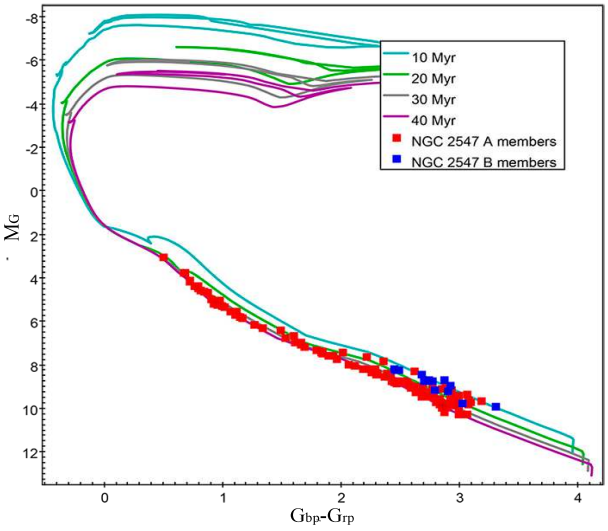

Fig. B.60. CMD for NGC 2547.

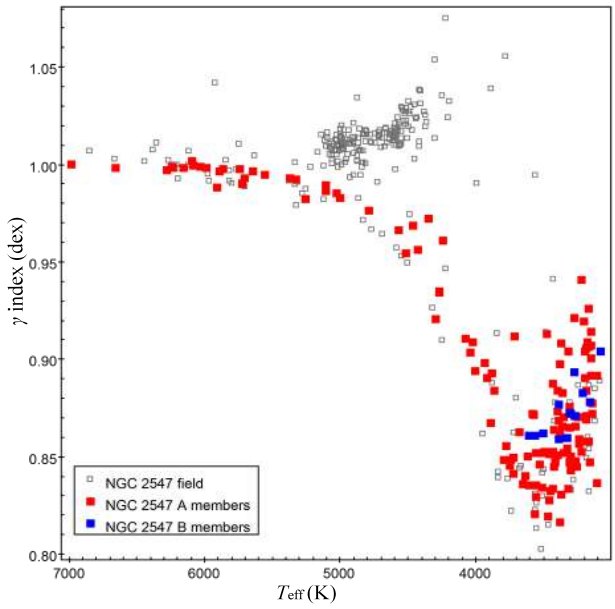

Fig. B.61. γ index-versus-$T_{\rm eff}$ diagram for NGC 2547.

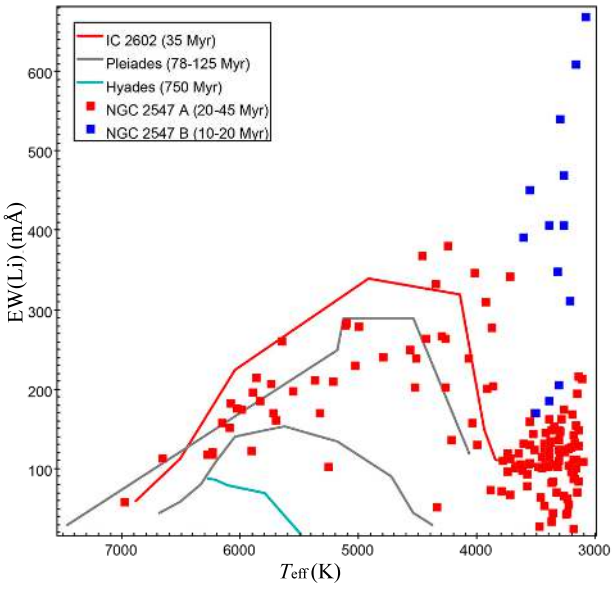

Fig. B.62. EW(Li)-versus-$T_{\rm eff}$ diagram for NGC 2547.

Appendix B.12: IC 2391

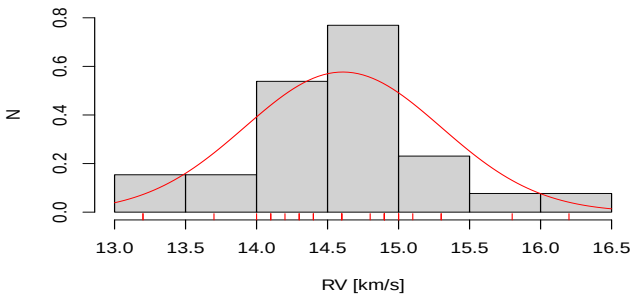

Fig. B.63. RV distribution for IC 2391.

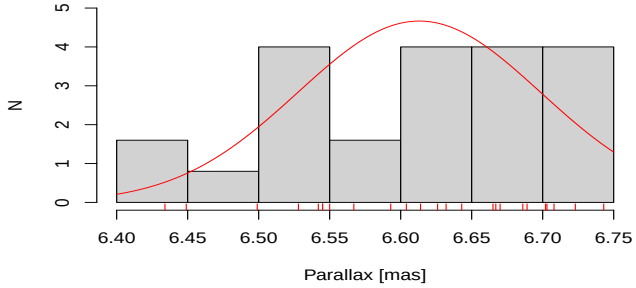

Fig. B.64. Parallax distribution for IC 2391.

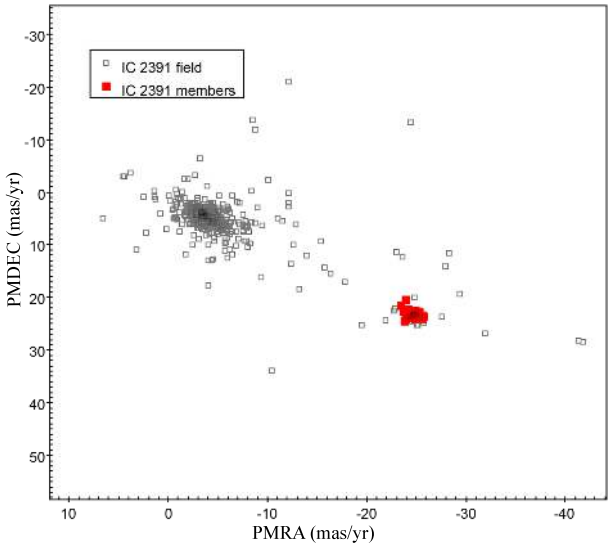

Fig. B.65. PMs diagram for IC 2391.

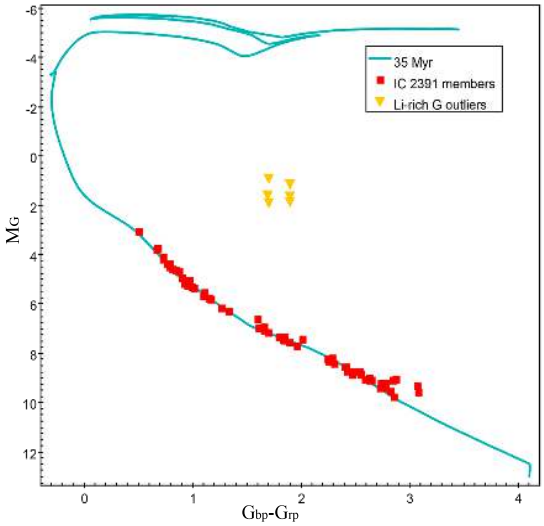

Fig. B.66. CMD for IC 2391.

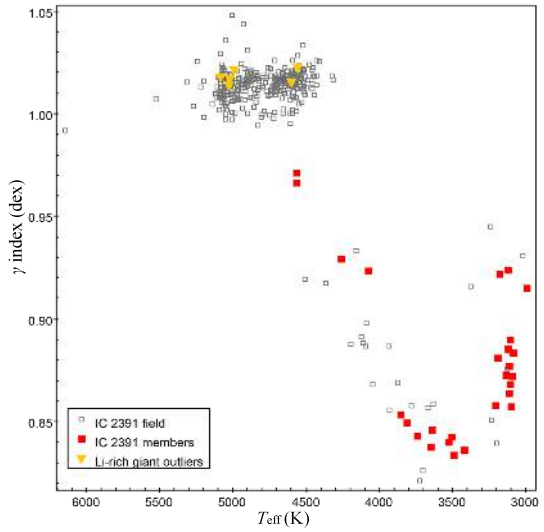

Fig. B.67. γ index-versus-$T_{\rm eff}$ diagram for IC 2391.

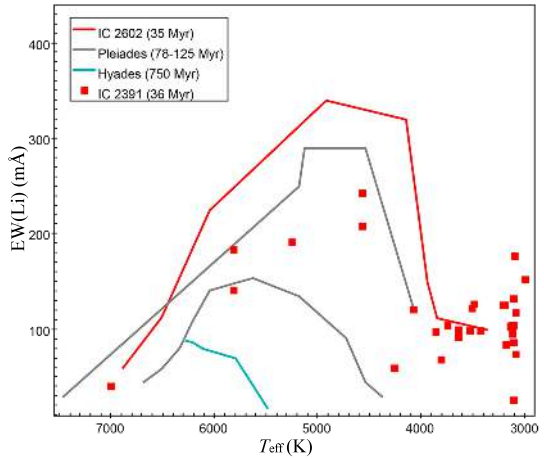

Fig. B.68. EW(Li)-versus-$T_{\rm eff}$ diagram for IC 2391.

Appendix B.13: IC 2602

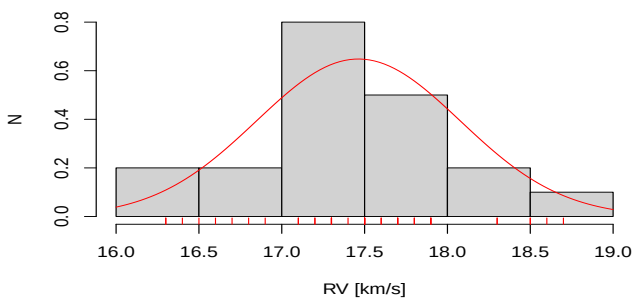

Fig. B.69. RV distribution for IC 2602.

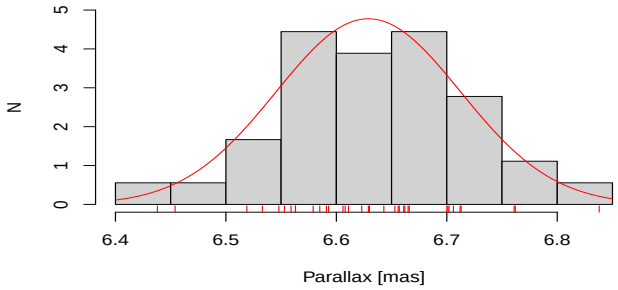

Fig. B.70. Parallax distribution for IC 2602.

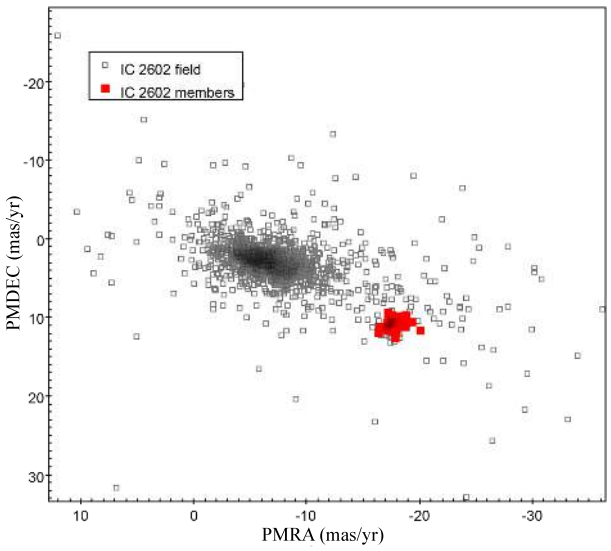

Fig. B.71. PMs diagram for IC 2602.

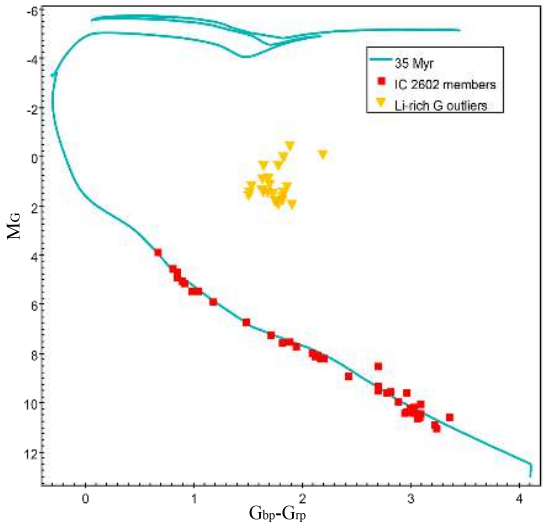

Fig. B.72. CMD for IC 2602.

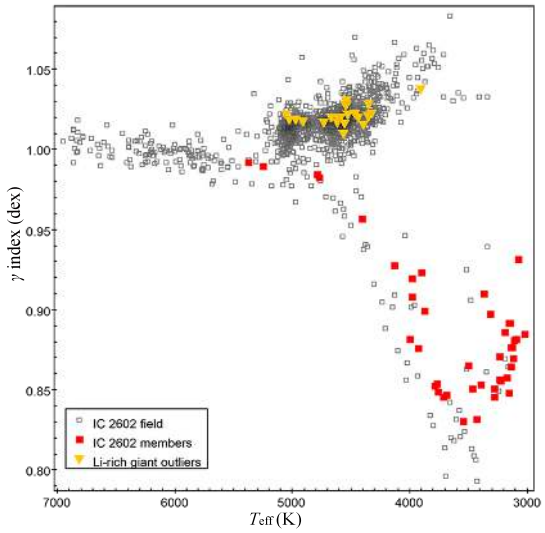

Fig. B.73. γ index-versus-$T_{\rm eff}$ diagram for IC 2602.

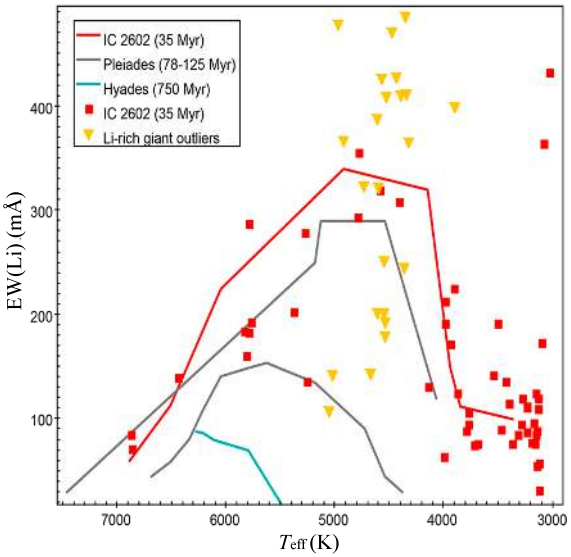

Fig. B.74. EW(Li)-versus-$T_{\rm eff}$ diagram for IC 2602.

Appendix B.14: IC 4665

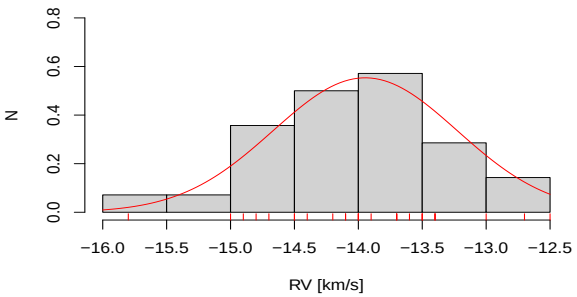

Fig. B.75. RV distribution for IC 4665.

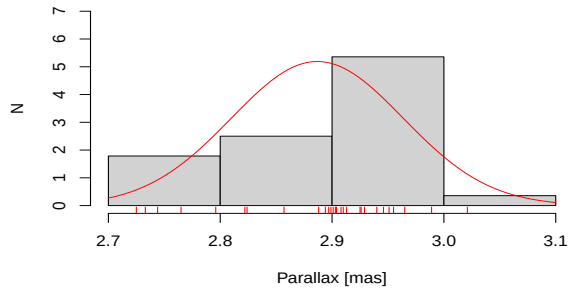

Fig. B.76. Parallax distribution for IC 4665.

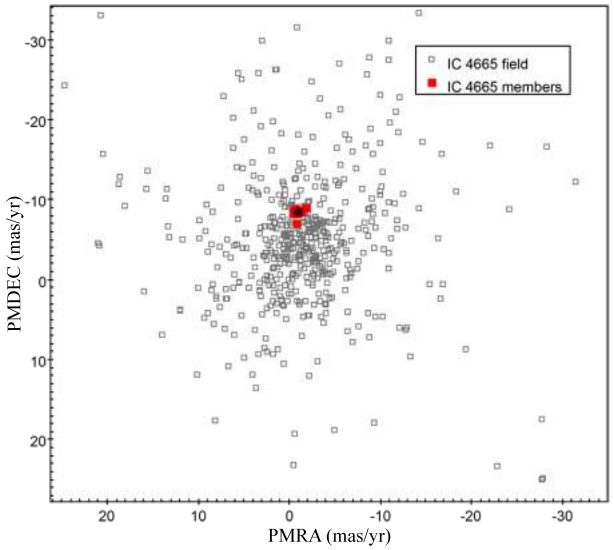

Fig. B.77. PMs diagram for IC 4665.

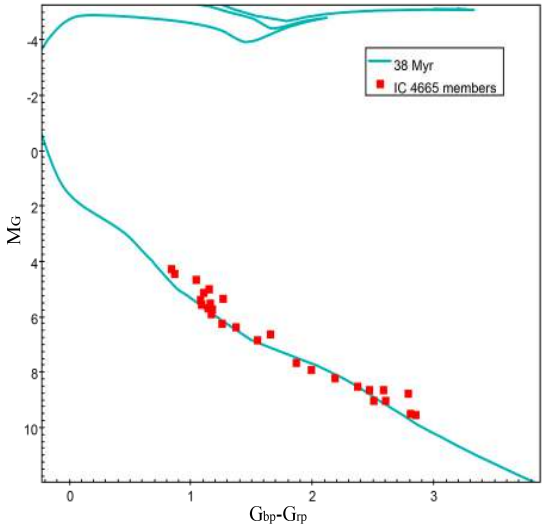

Fig. B.78. CMD for IC 4665.

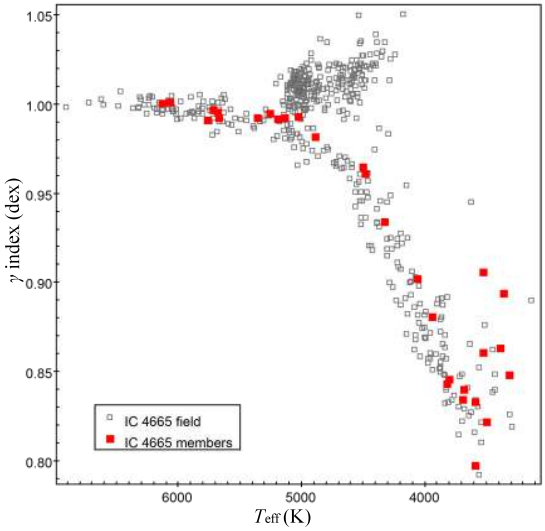

Fig. B.79. γ index-versus-$T_{\rm eff}$ diagram for IC 4665.

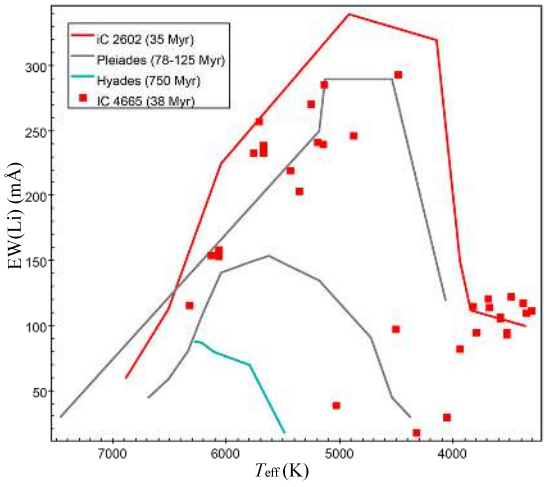

Fig. B.80. EW(Li)-versus-$T_{\rm eff}$ diagram for IC 4665.

Appendix B.15: NGC 2451

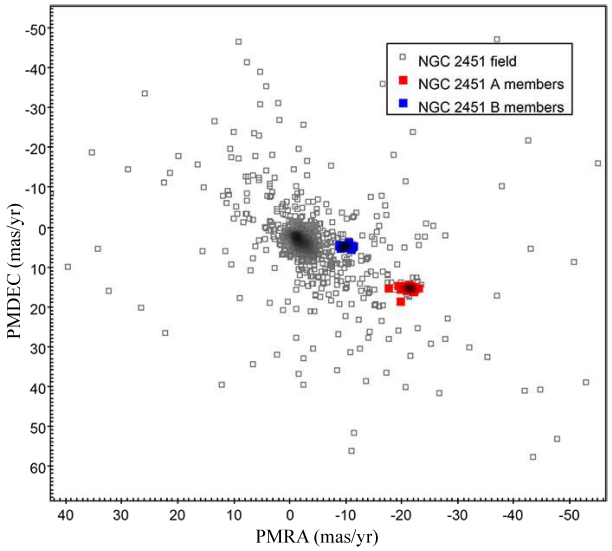

Fig. B.81. PMs diagram for NGC 2451.

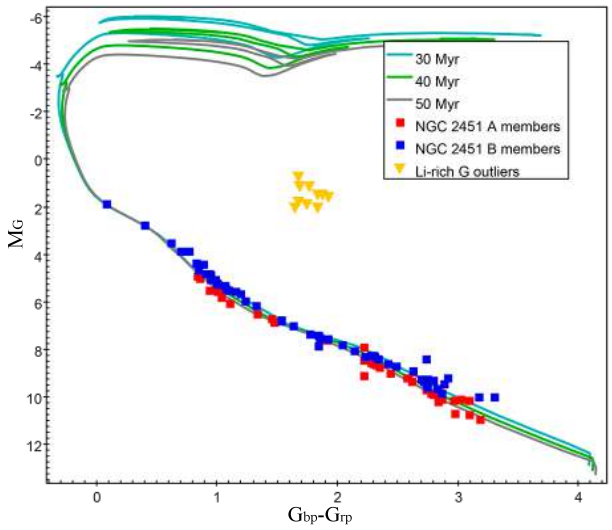

Fig. B.82. CMD for NGC 2451.

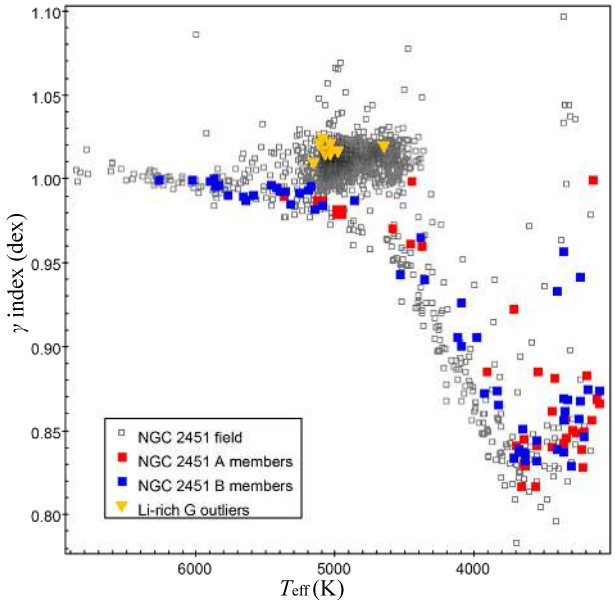

Fig. B.83. γ index-versus-$T_{\rm eff}$ diagram for NGC 2451.

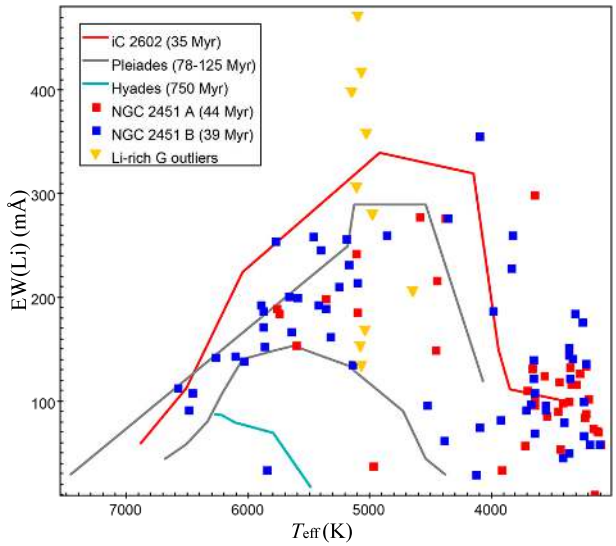

Fig. B.84. EW(Li)-versus-$T_{\rm eff}$ diagram for NGC 2451.

Appendix B.16: NGC 6405

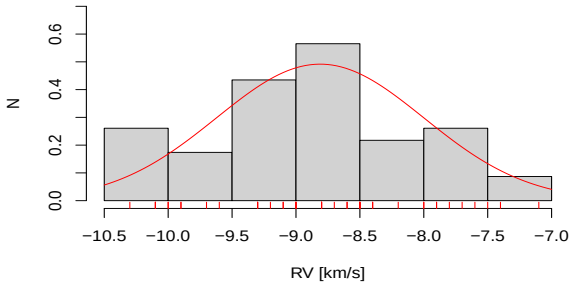

Fig. B.85. RV distribution for NGC 6405.

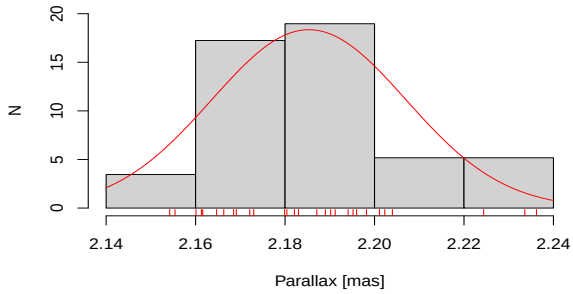

Fig. B.86. Parallax distribution for NGC 6405.

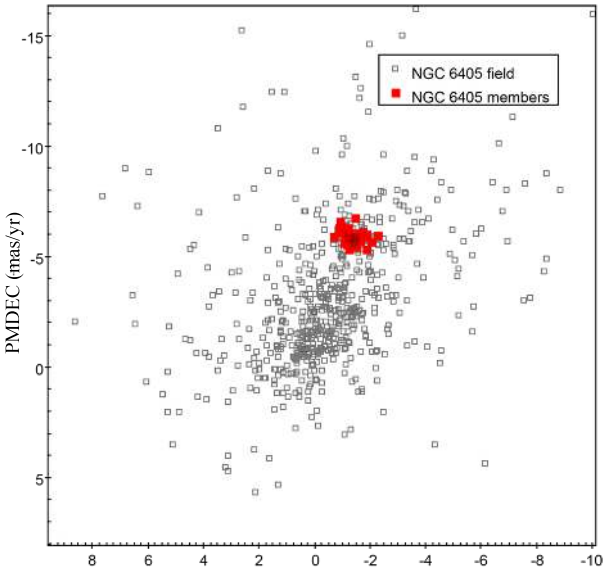

Fig. B.87. PMs diagram for NGC 6405.

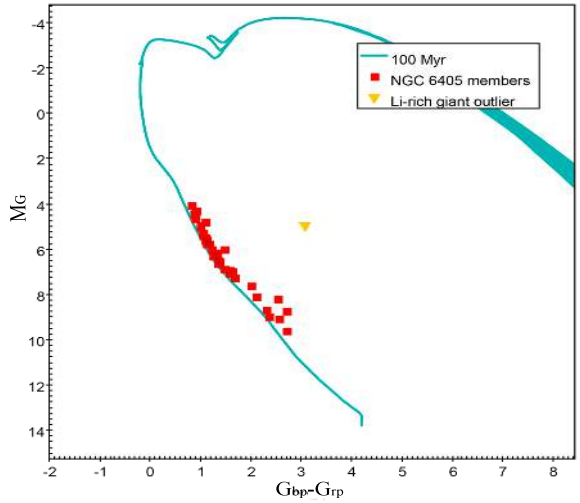

Fig. B.88. CMD for NGC 6405.

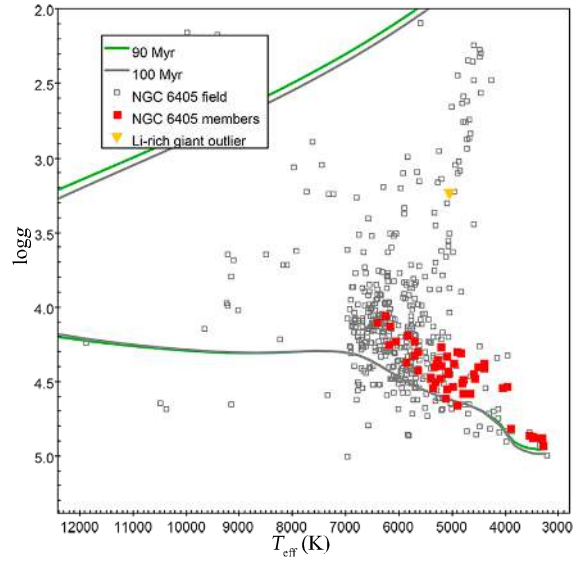

Fig. B.89. Kiel diagram for NGC 6405.

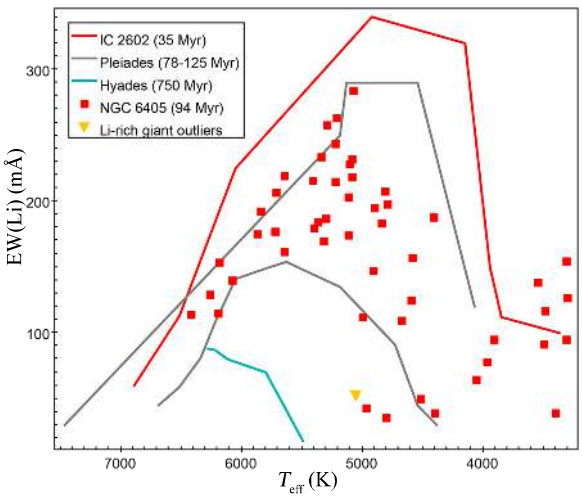

Fig. B.90. EW(Li)-versus-$T_{\rm eff}$ diagram for NGC 6405.

Appendix B.17: Blanco 1

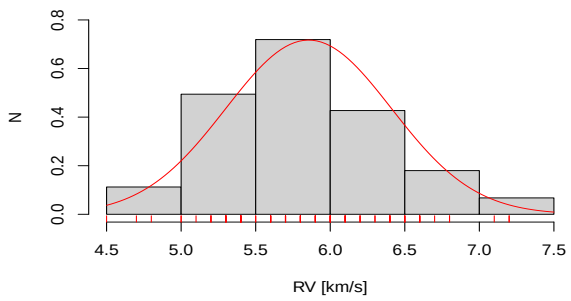

Fig. B.91. RV distribution for Blanco 1.

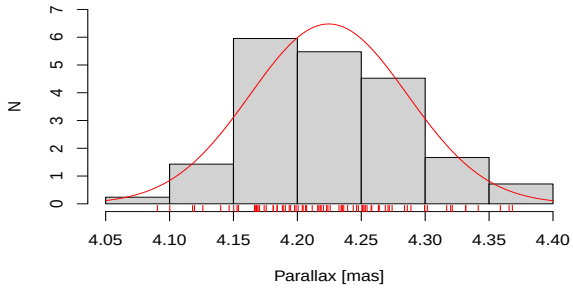

Fig. B.92. Parallax distribution for Blanco 1.

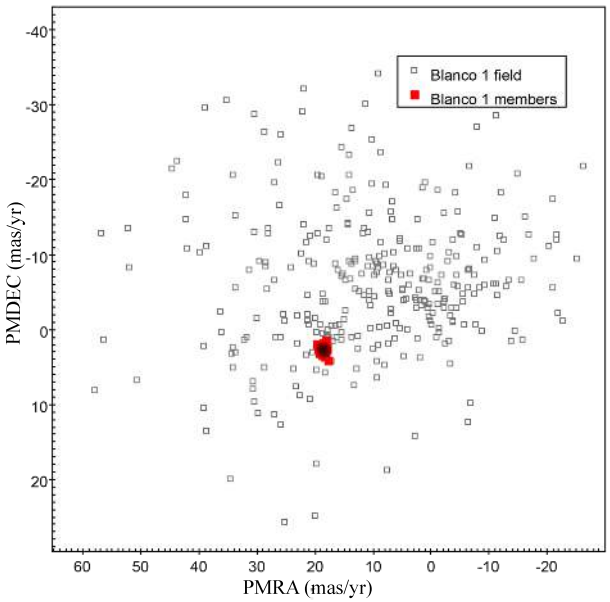

Fig. B.93. PMs diagram for Blanco 1.

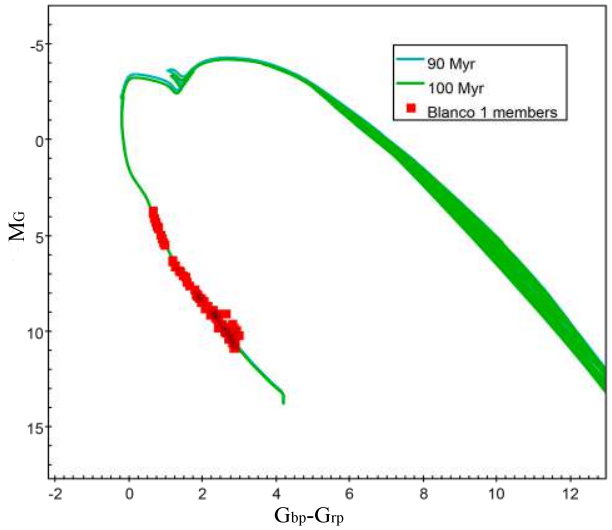

Fig. B.94. CMD for Blanco 1.

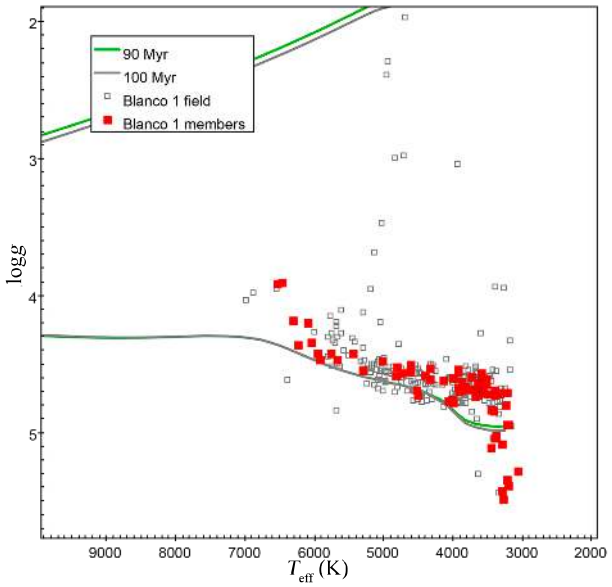

Fig. B.95. Kiel diagram for Blanco 1.

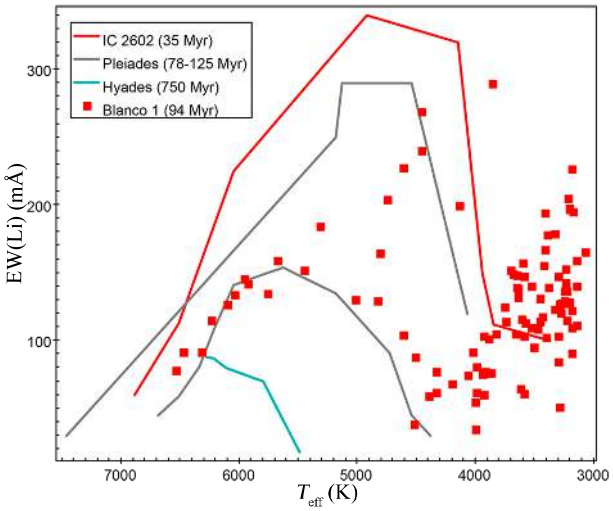

Fig. B.96. EW(Li)-versus-$T_{\rm eff}$ diagram for Blanco 1.

Appendix B.18: NGC 6067

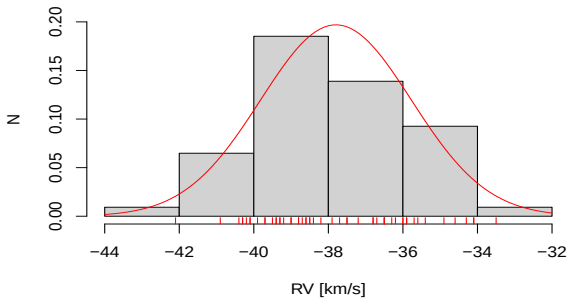

Fig. B.97. RV distribution for NGC 6067.

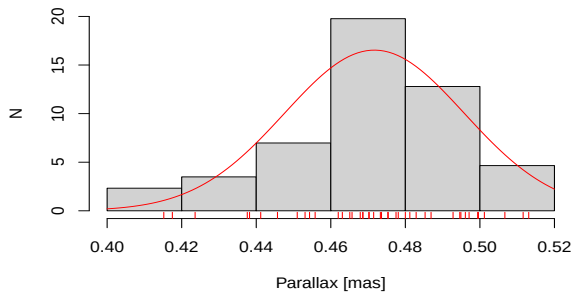

Fig. B.98. Parallax distribution for NGC 6067.

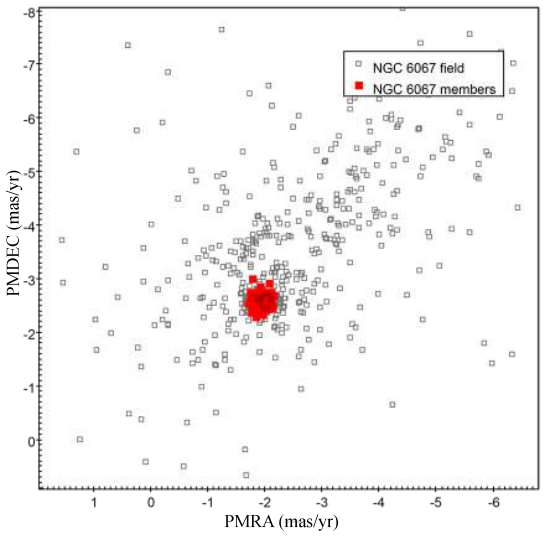

Fig. B.99. PMs diagram for NGC 6067.

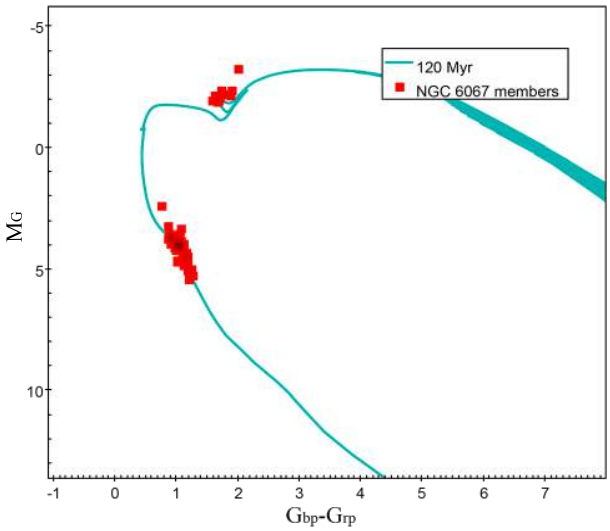

Fig. B.100. CMD for NGC 6067.

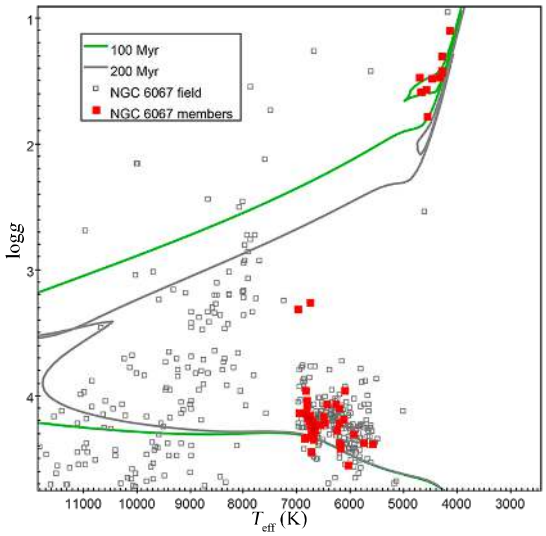

Fig. B.101. Kiel diagram for NGC 6067.

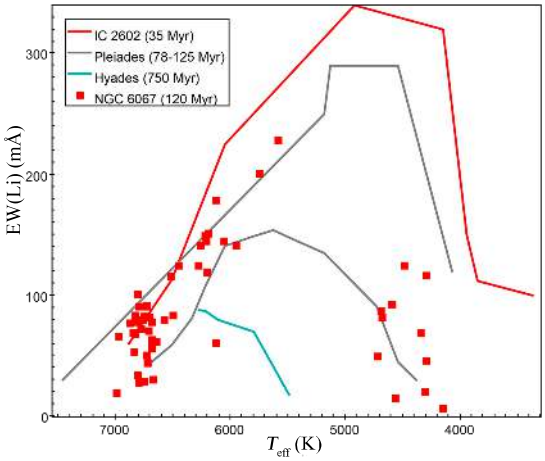

Fig. B.102. EW(Li)-versus-$T_{\rm eff}$ diagram for NGC 6067.

Appendix B.19: NGC 6649

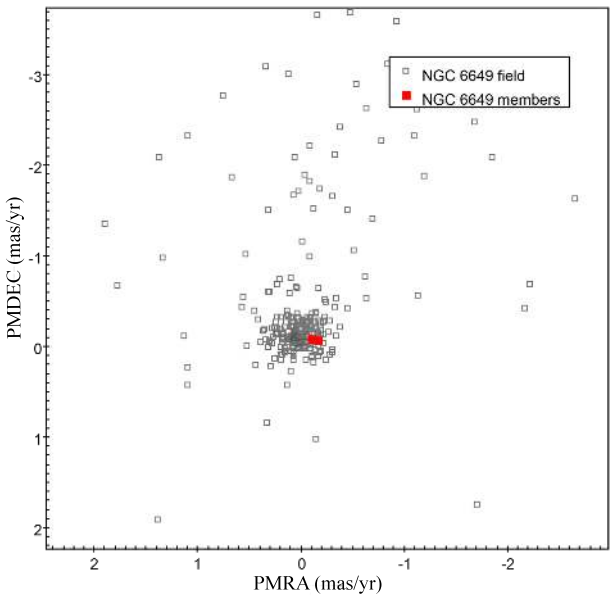

Fig. B.103. PMs diagram for NGC 6649.

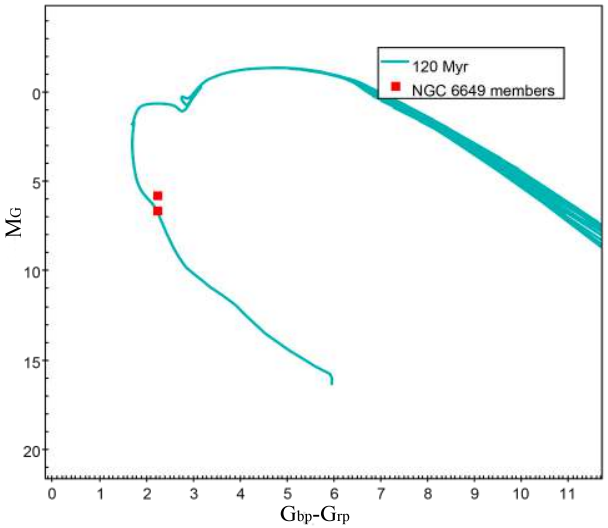

Fig. B.104. CMD for NGC 6649.

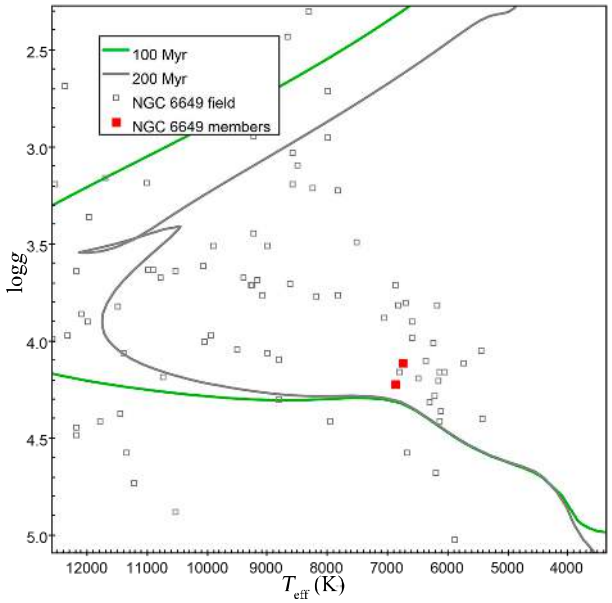

Fig. B.105. Kiel diagram for NGC 6649.

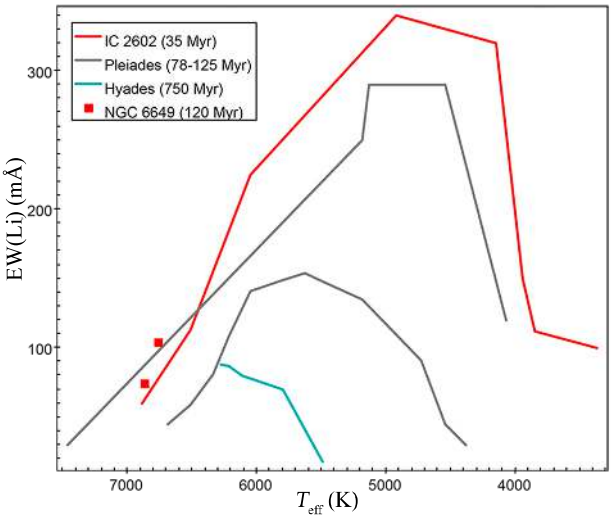

Fig. B.106. EW(Li)-versus-$T_{\rm eff}$ diagram for NGC 6649.

Appendix B.20: NGC 2516

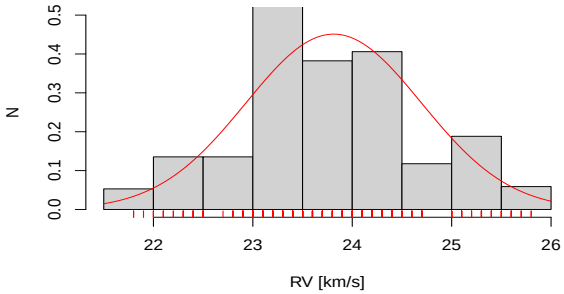

Fig. B.107. RV distribution for NGC 2516.

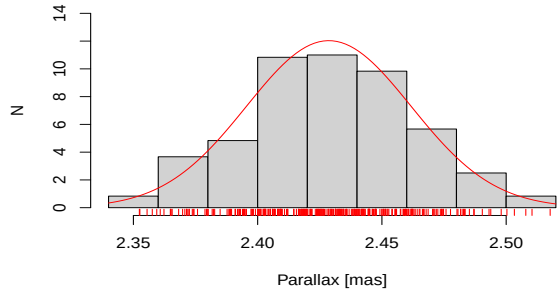

Fig. B.108. Parallax distribution for NGC 2516.

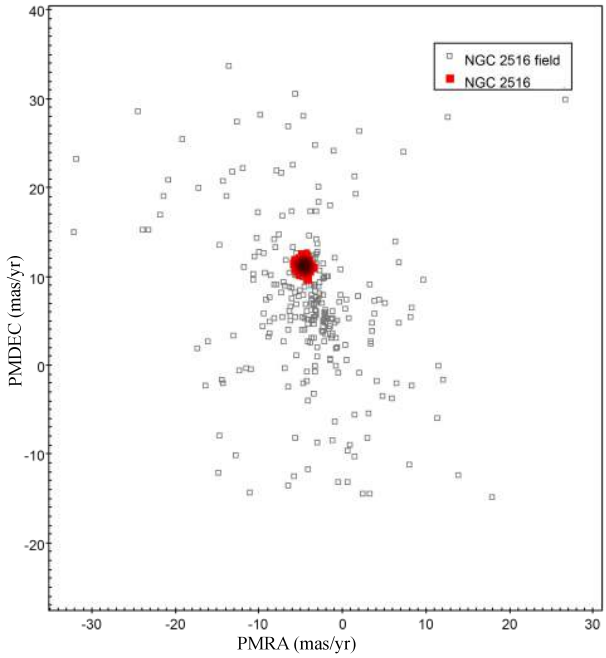

Fig. B.109. PMs diagram for NGC 2516.

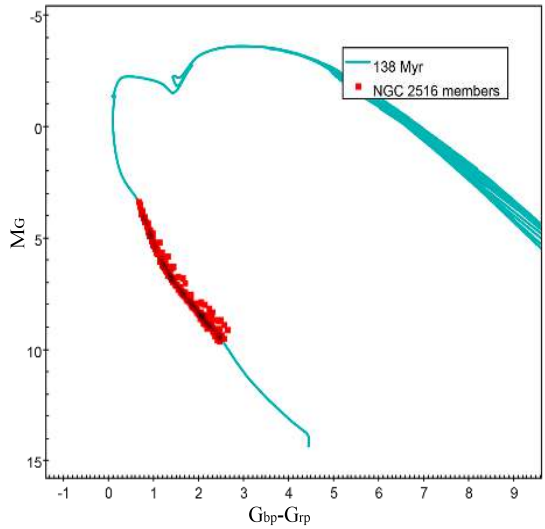

Fig. B.110. CMD for NGC 2516.

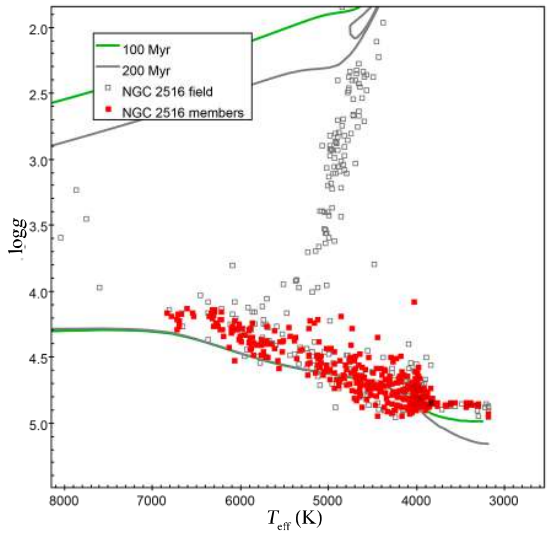

Fig. B.111. Kiel diagram for NGC 2516.

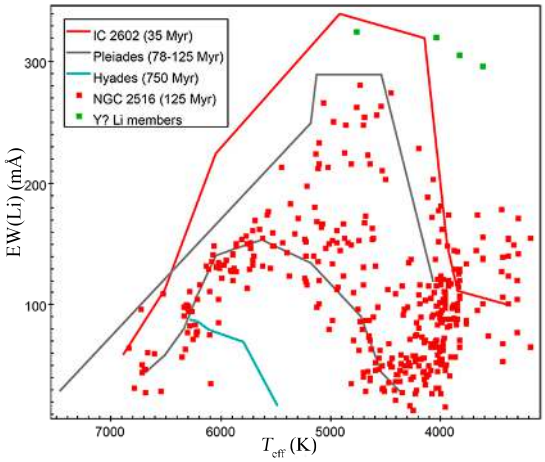

Fig. B.112. EW(Li)-versus-$T_{\rm eff}$ diagram for NGC 2516.

Appendix B.21: NGC 6709

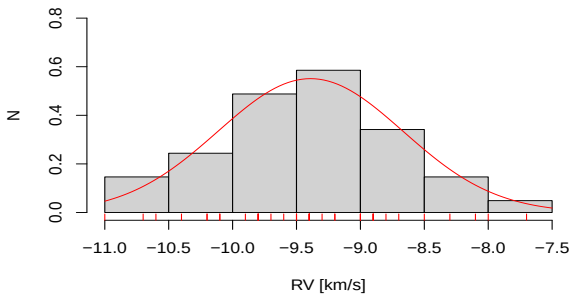

Fig. B.113. RV distribution for NGC 6709.

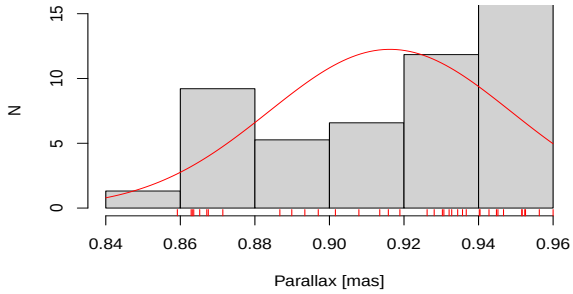

Fig. B.114. Parallax distribution for NGC 6709.

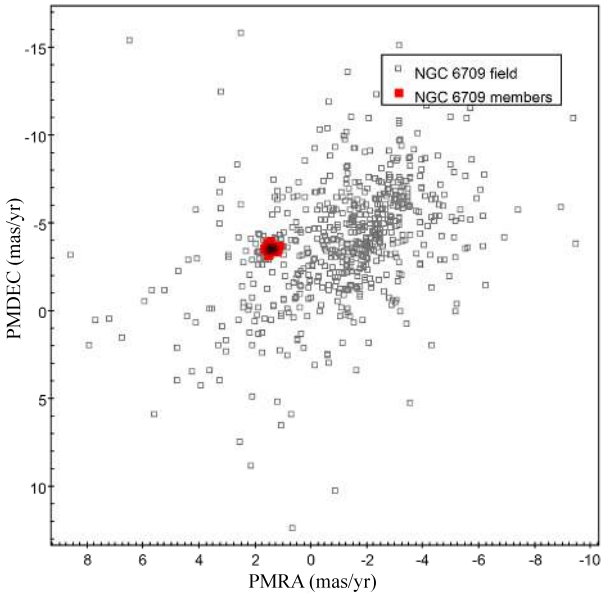

Fig. B.115. PMs diagram for NGC 6709.

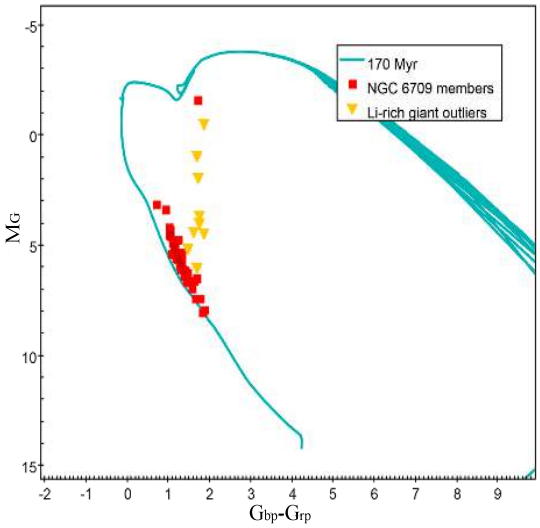

Fig. B.116. CMD for NGC 6709.

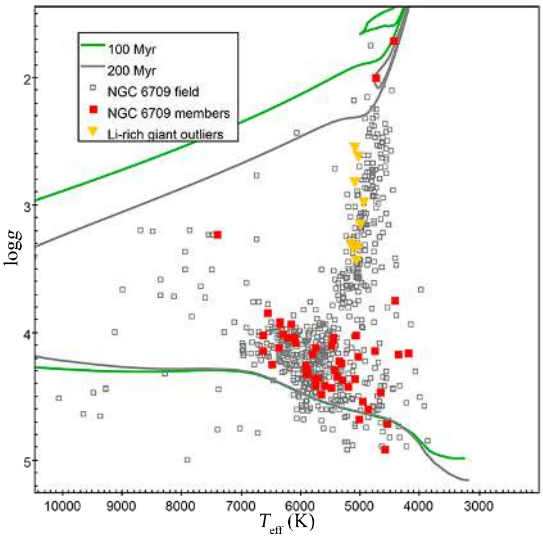

Fig. B.117. Kiel diagram for NGC 6709.

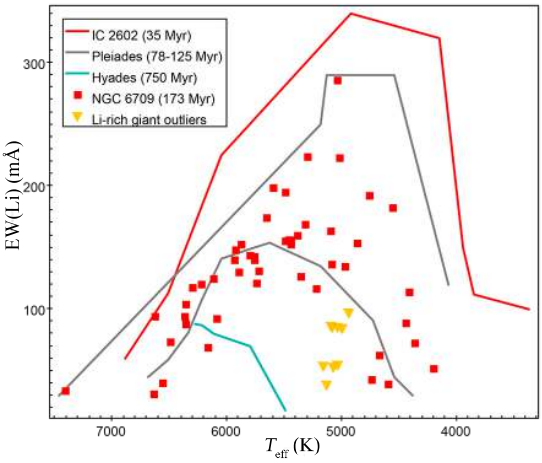

Fig. B.118. EW(Li)-versus-$T_{\rm eff}$ diagram for NGC 6709.

Appendix B.22: NGC 6259

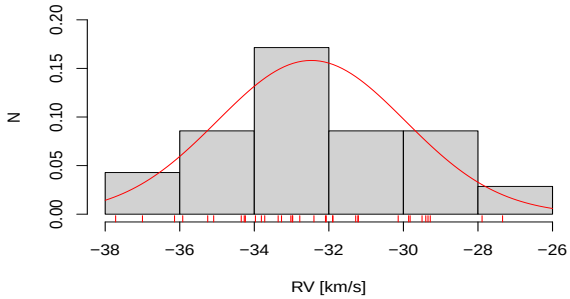

Fig. B.119. RV distribution for NGC 6259.

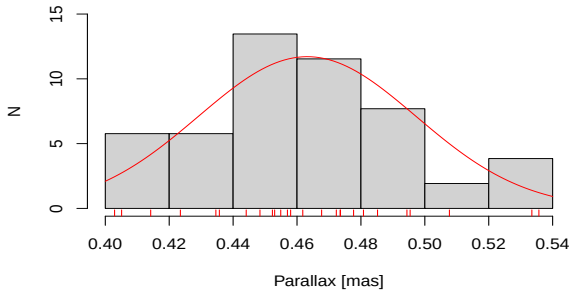

Fig. B.120. Parallax distribution for NGC 6259.

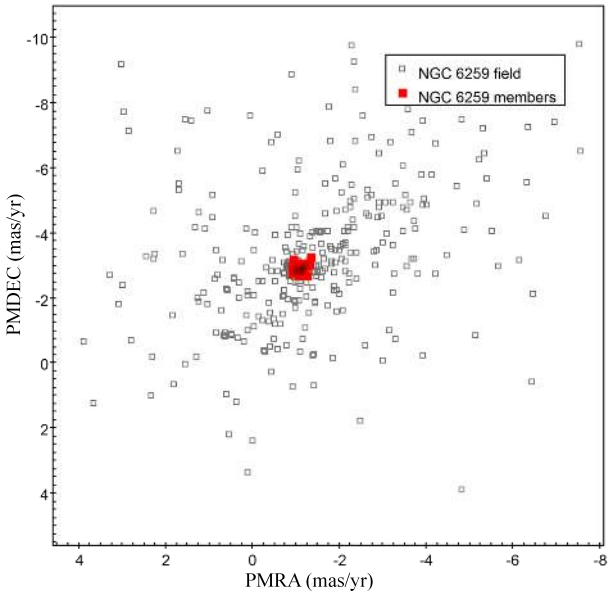

Fig. B.121. PMs diagram for NGC 6259.

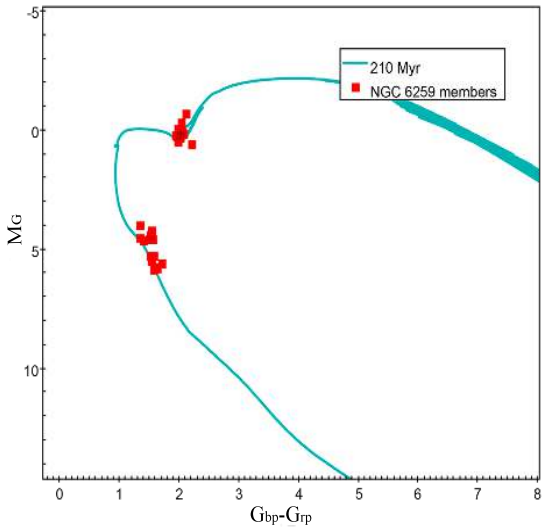

Fig. B.122. CMD for NGC 6259.

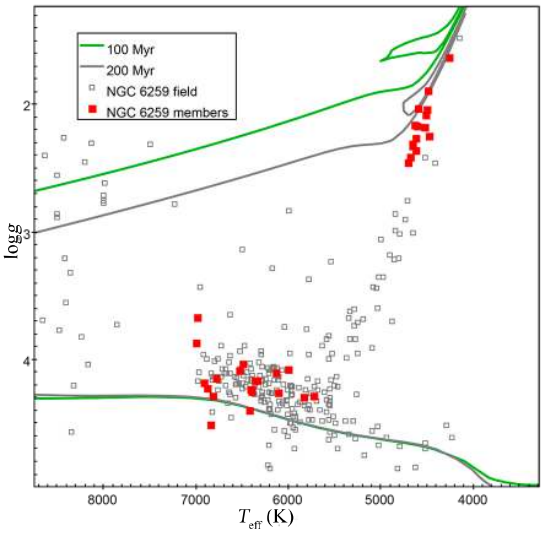

Fig. B.123. Kiel diagram for NGC 6259.

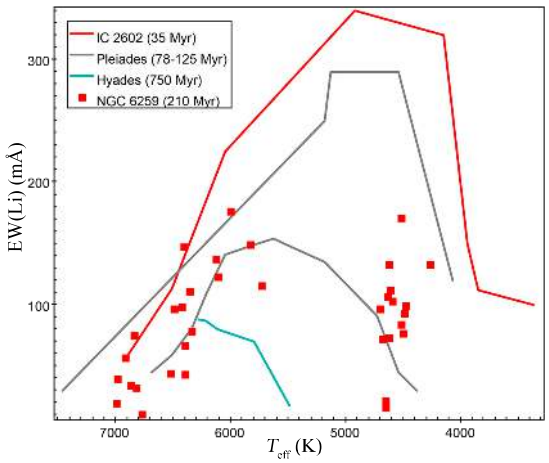

Fig. B.124. EW(Li)-versus-$T_{\rm eff}$ diagram for NGC 6259.

Appendix B.23: NGC 6705

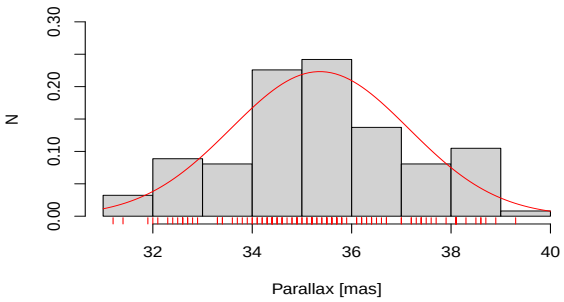

Fig. B.125. RV distribution for NGC 6705.

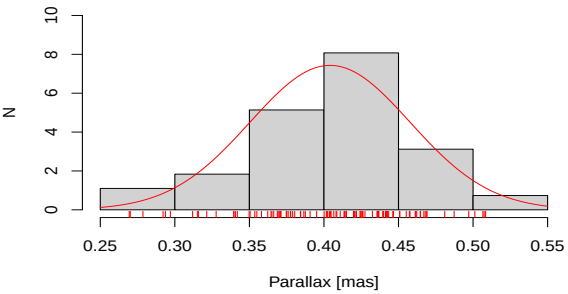

Fig. B.126. Parallax distribution for NGC 6705.

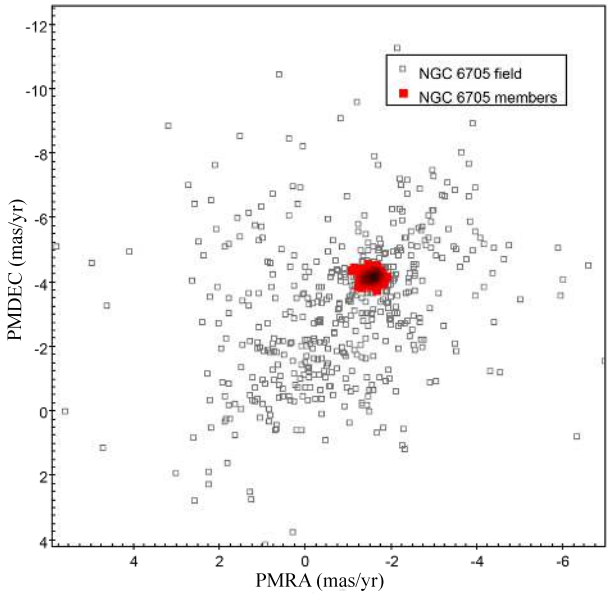

Fig. B.127. PMs diagram for NGC 6705.

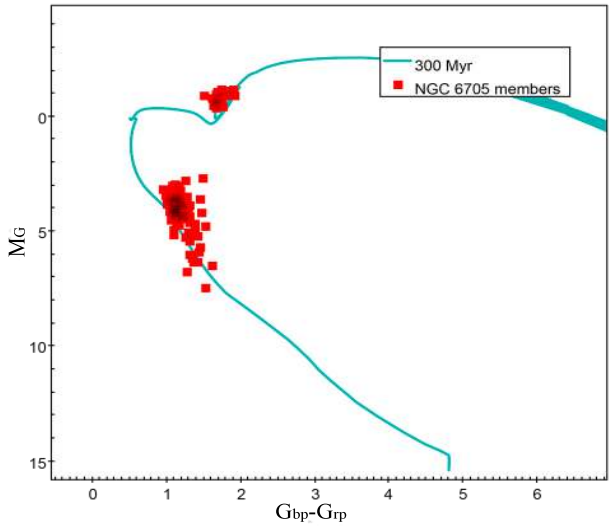

Fig. B.128. CMD for NGC 6705.

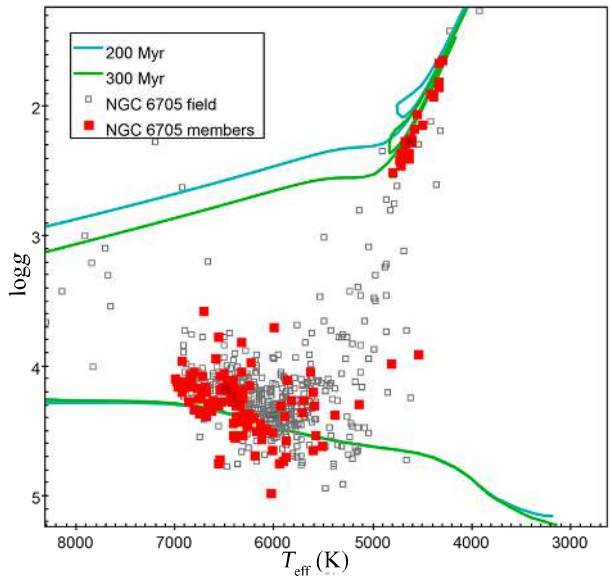

Fig. B.129. Kiel diagram for NGC 6705.

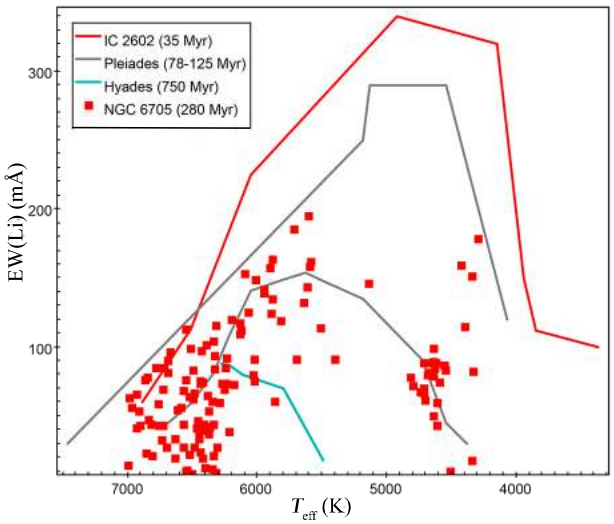

Fig. B.130. EW(Li)-versus-$T_{\rm eff}$ diagram for NGC 6705.

Appendix B.24: Berkeley 30

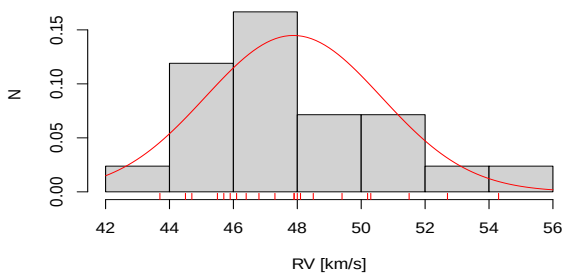

Fig. B.131. RV distribution for Berkeley 30.

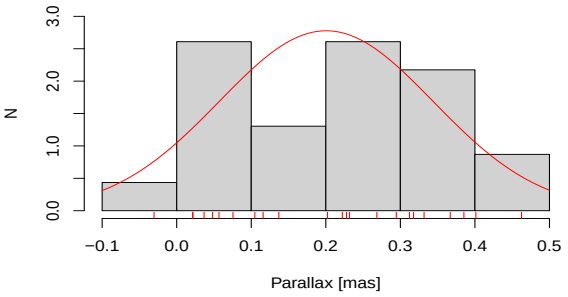

Fig. B.132. Parallax distribution for Berkeley 30.

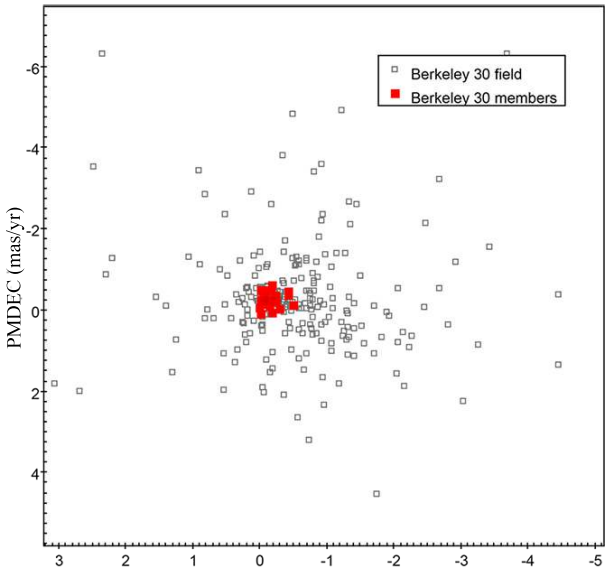

Fig. B.133. PMs diagram for Berkeley 30.

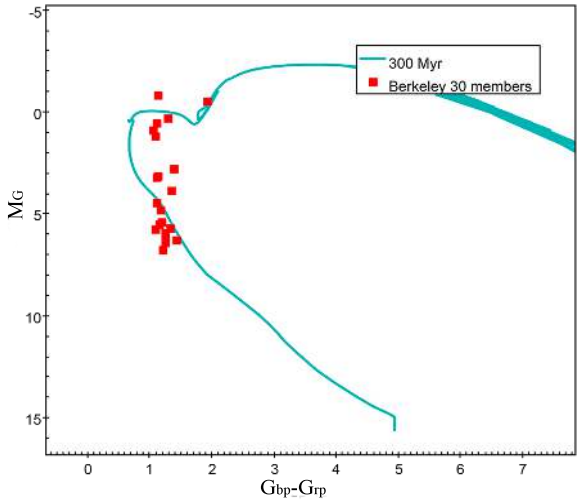

Fig. B.134. CMD for Berkeley 30.

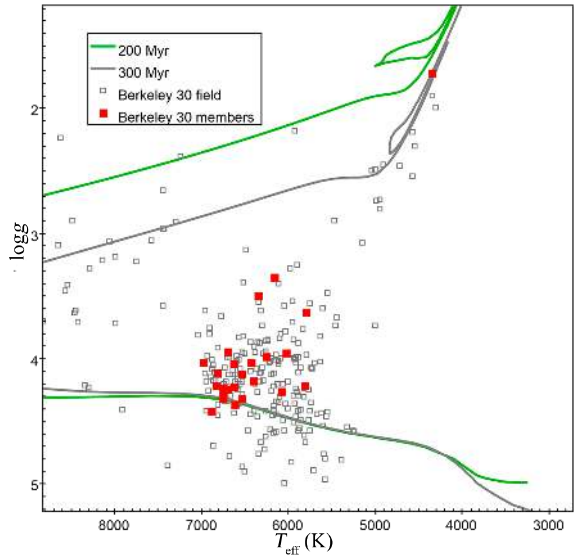

Fig. B.135. Kiel diagram for Berkeley 30.

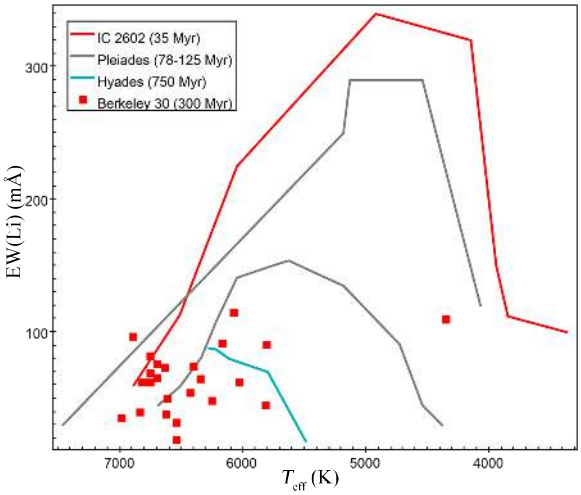

Fig. B.136. EW(Li)-versus-$T_{\rm eff}$ diagram for Berkeley 30.

Appendix B.25: NGC 6281

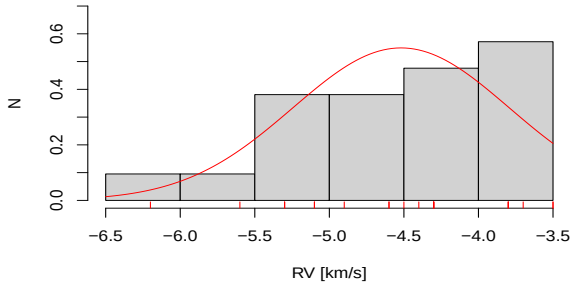

Fig. B.137. RV distribution for NGC 6281.

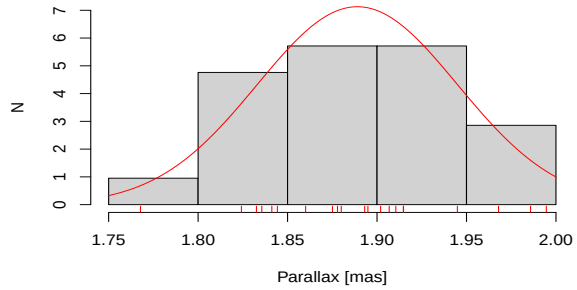

Fig. B.138. Parallax distribution for NGC 6281.

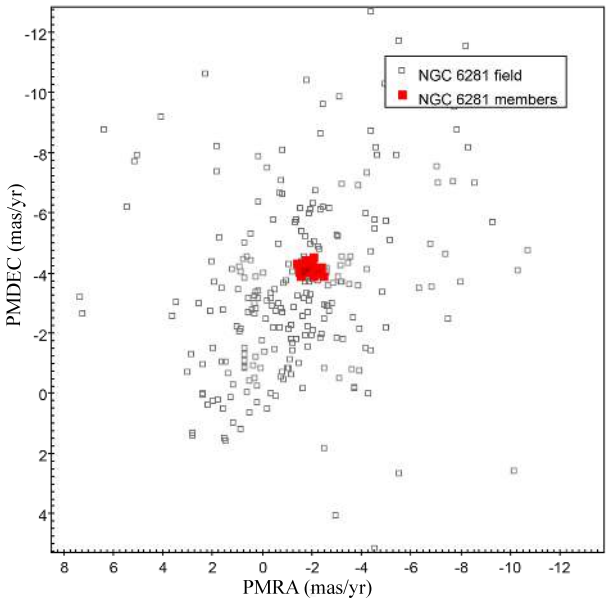

Fig. B.139. PMs diagram for NGC 6281.

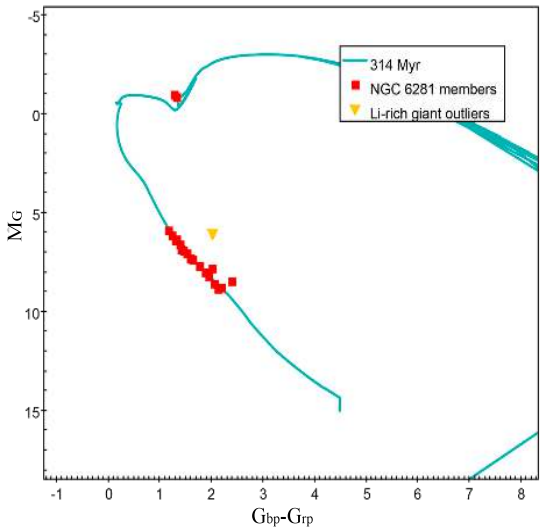

Fig. B.140. CMD for NGC 6281.

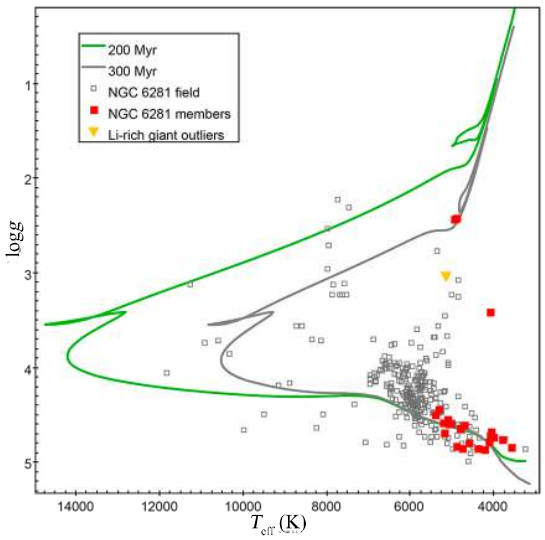

Fig. B.141. Kiel diagram for NGC 6281.

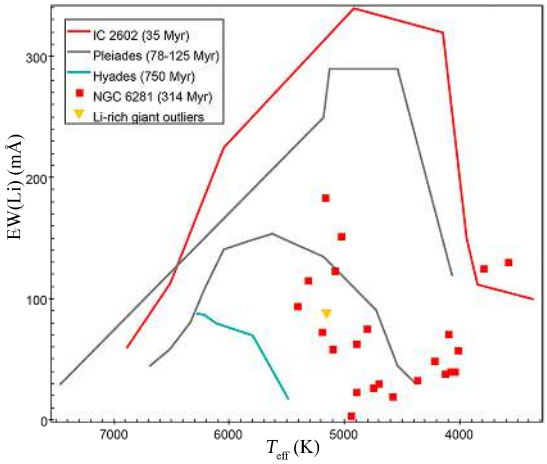

Fig. B.142. EW(Li)-versus-$T_{\rm eff}$ diagram for NGC 6281.

Appendix B.26: NGC 3532

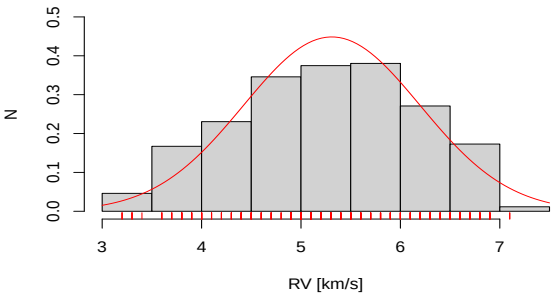

Fig. B.143. RV distribution for NGC 3532.

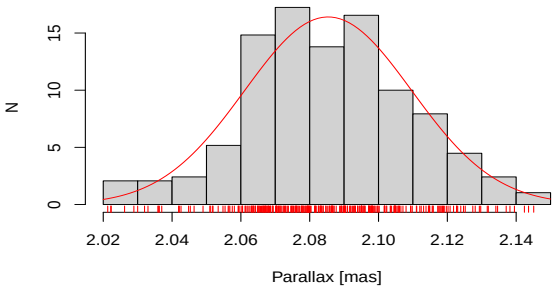

Fig. B.144. Parallax distribution for NGC 3532.

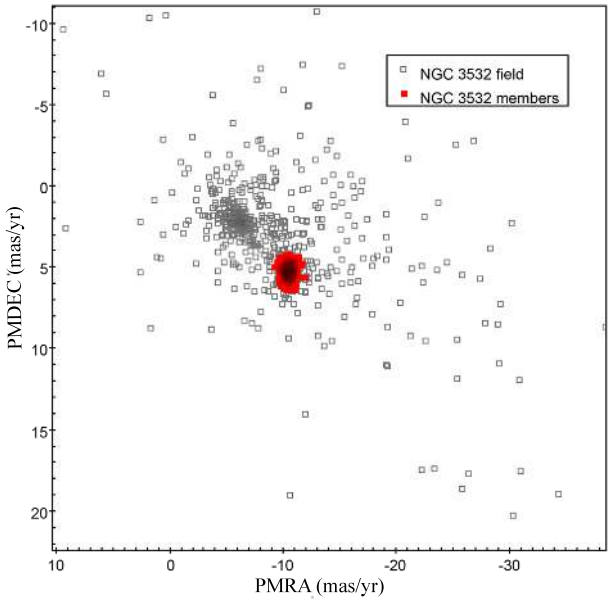

Fig. B.145. PMs diagram for NGC 3532.

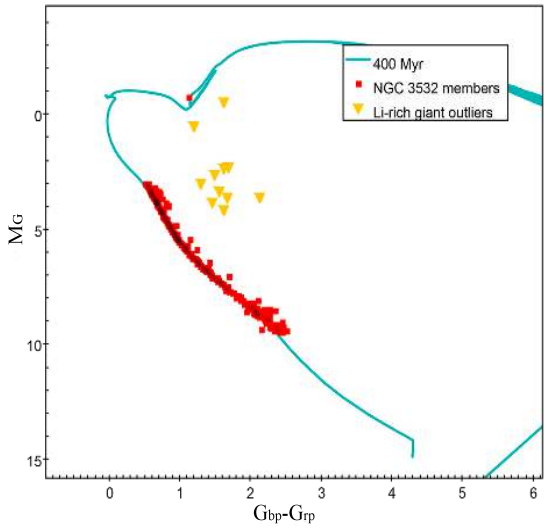

Fig. B.146. CMD for NGC 3532.

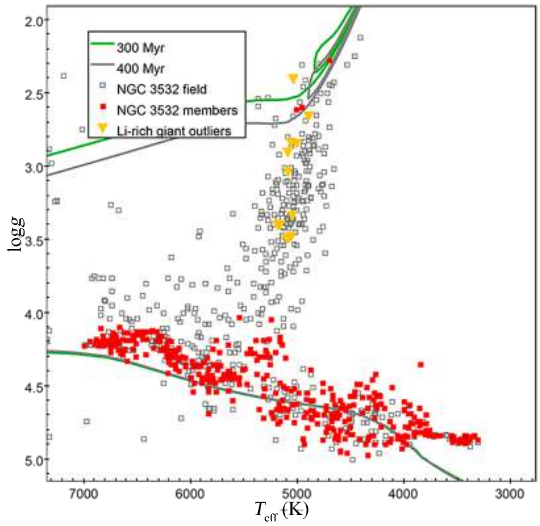

Fig. B.147. Kiel diagram for NGC 3532.

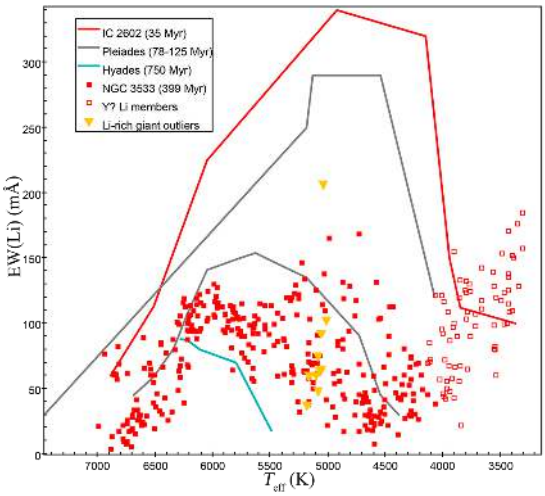

Fig. B.148. EW(Li)-versus-$T_{\rm eff}$ diagram for NGC 3532.

Appendix B.27: NGC 4815

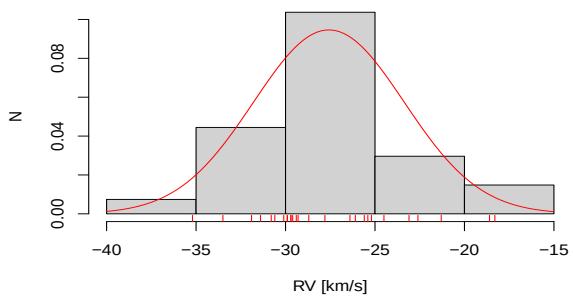

Fig. B.149. RV distribution for NGC 4815.

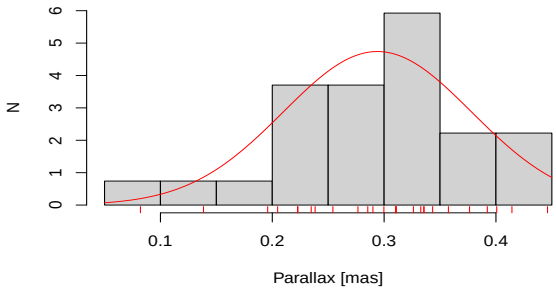

Fig. B.150. Parallax distribution for NGC 4815.

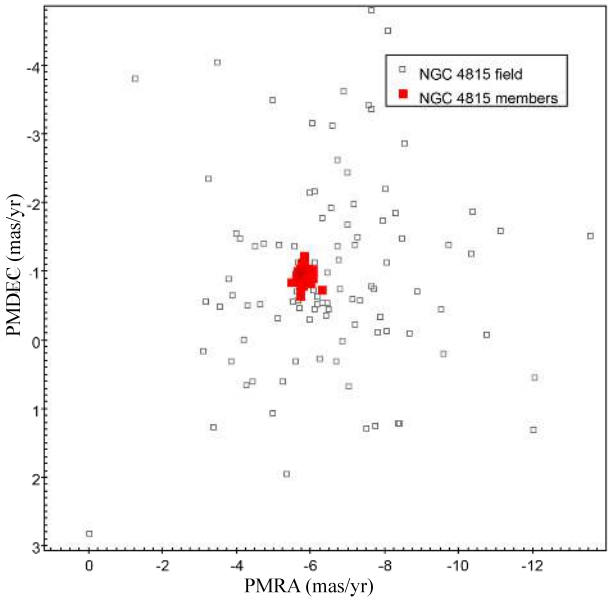

Fig. B.151. PMs diagram for NGC 4815.

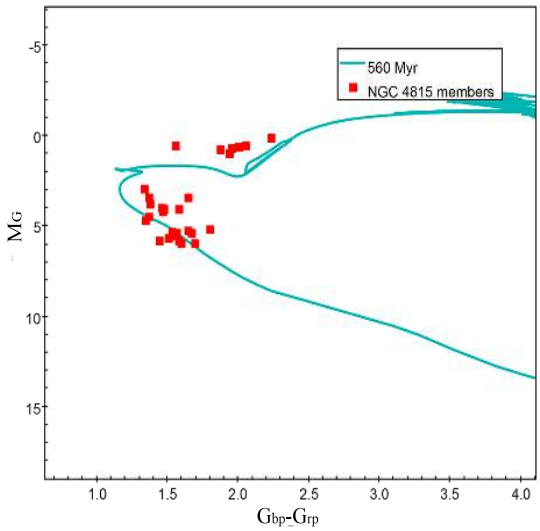

Fig. B.152. CMD for NGC 4815.

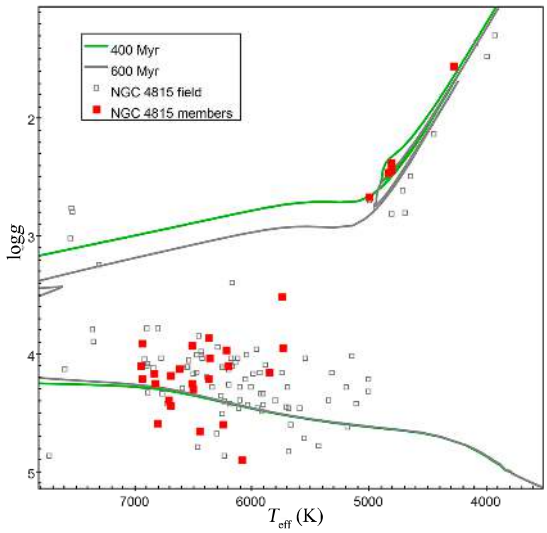

Fig. B.153. Kiel diagram for NGC 4815.

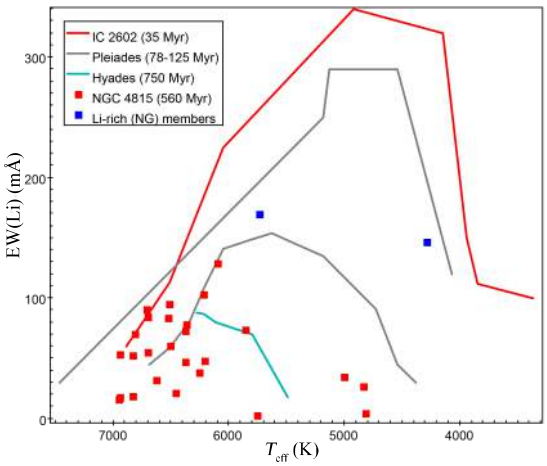

Fig. B.154. EW(Li)-versus-$T_{\rm eff}$ diagram for NGC 4815.

Appendix B.28: NGC 6633

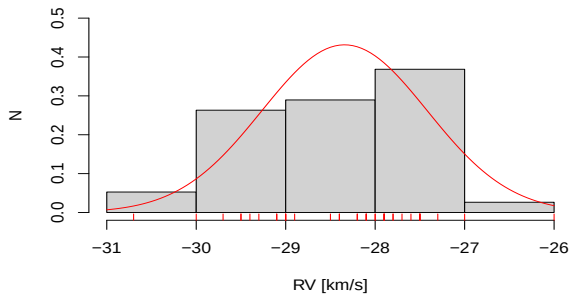

Fig. B.155. RV distribution for NGC 6633.

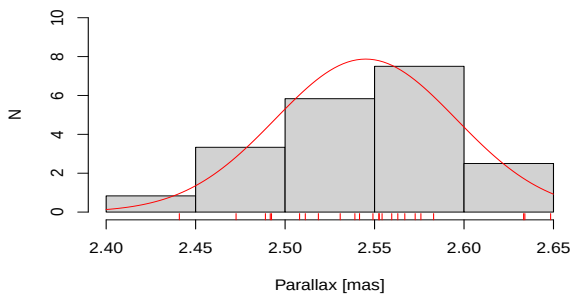

Fig. B.156. Parallax distribution for NGC 6633.

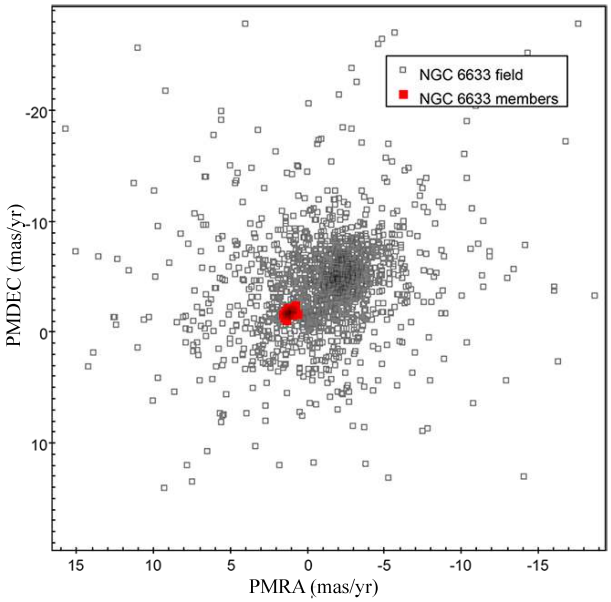

Fig. B.157. PMs diagram for NGC 6633.

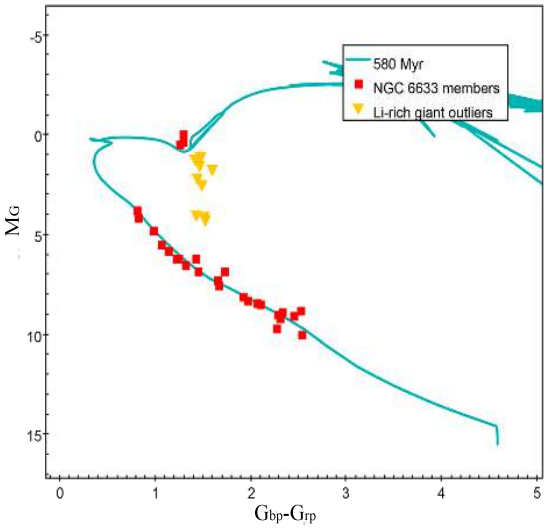

Fig. B.158. CMD for NGC 6633.

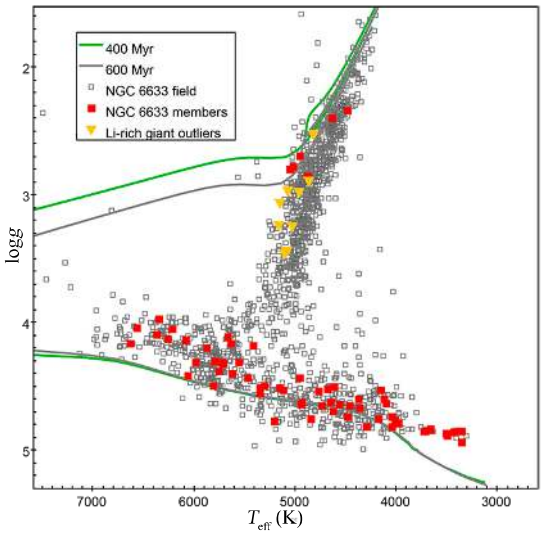

Fig. B.159. Kiel diagram for NGC 6633.

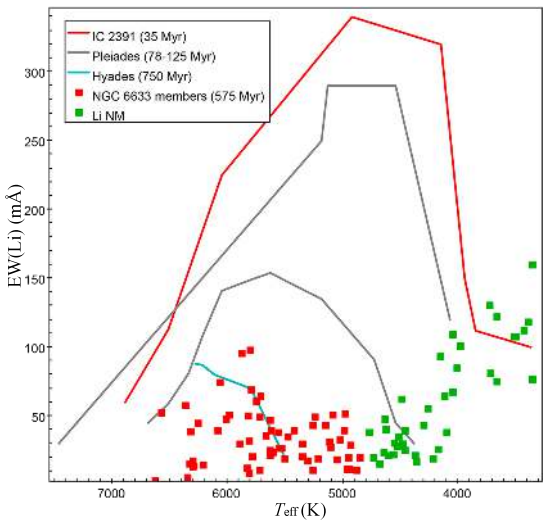

Fig. B.160. EW(Li)-versus-$T_{\rm eff}$ diagram for NGC 6633.

Appendix B.29: NGC 2477

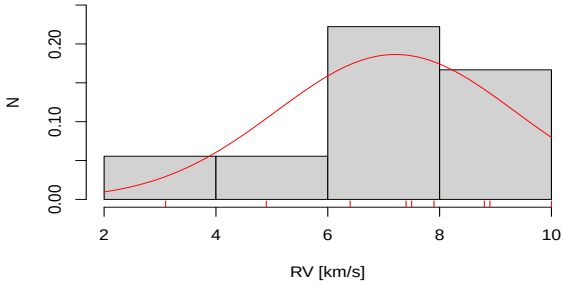

Fig. B.161. RV distribution for NGC 2477.

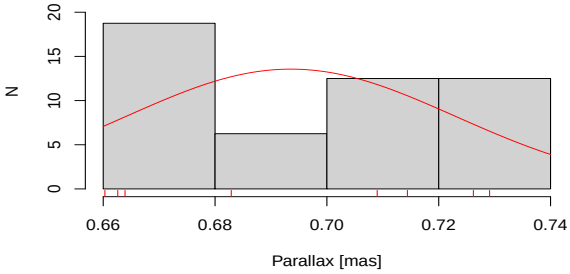

Fig. B.162. Parallax distribution for NGC 2477.

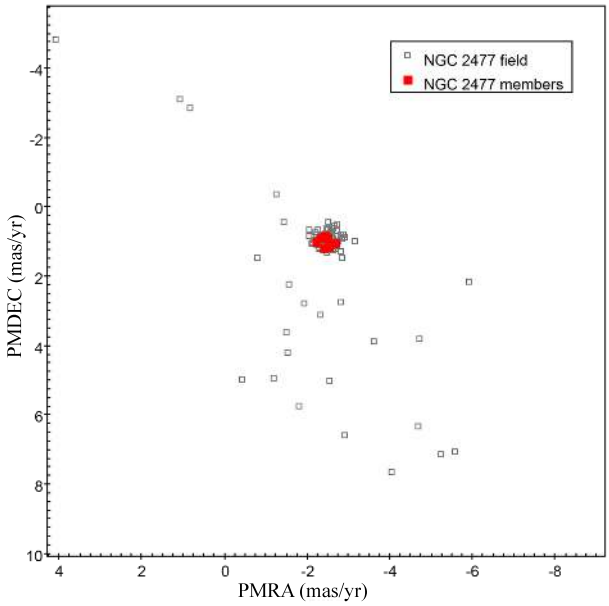

Fig. B.163. PMs diagram for NGC 2477.

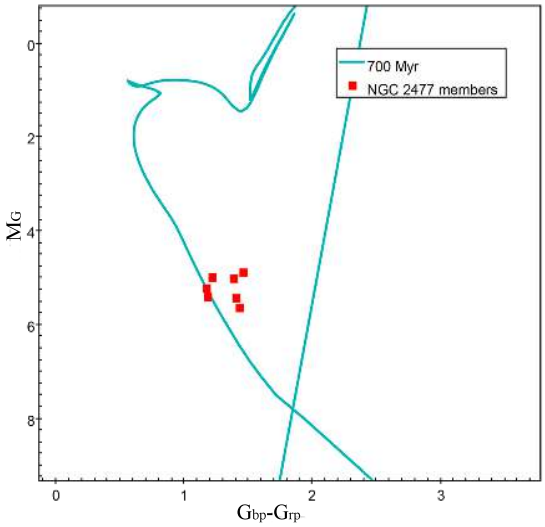

Fig. B.164. CMD for NGC 2477.

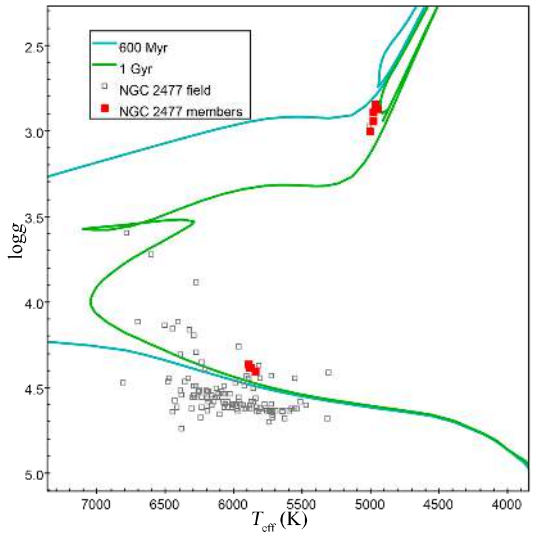

Fig. B.165. Kiel diagram for NGC 2477.

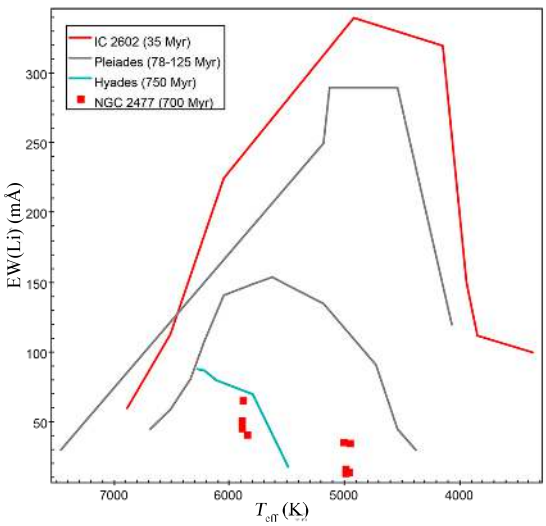

Fig. B.166. EW(Li)-versus-$T_{\rm eff}$ diagram for NGC 2477.

Appendix B.30: Trumpler 23

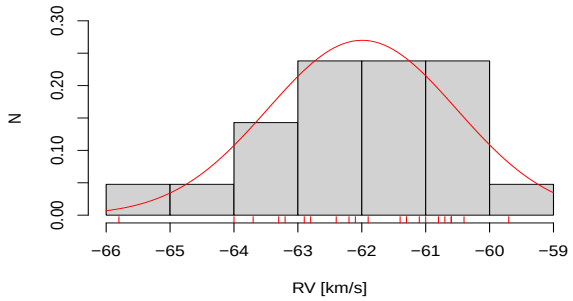

Fig. B.167. RV distribution for Trumpler 23.

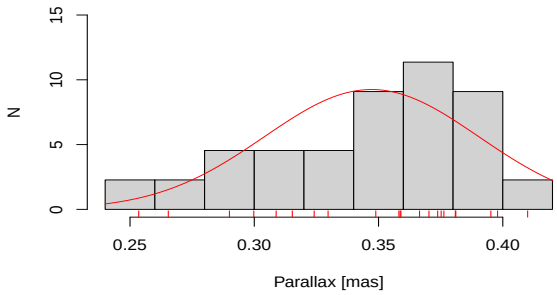

Fig. B.168. Parallax distribution for Trumpler 23.

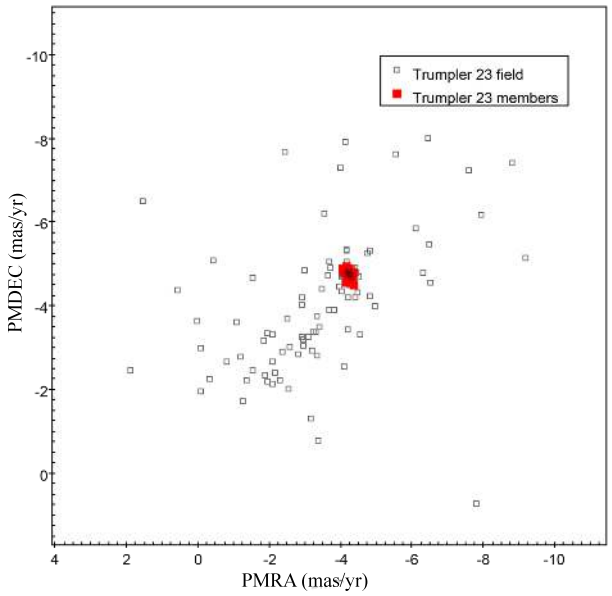

Fig. B.169. PMs diagram for Trumpler 23.

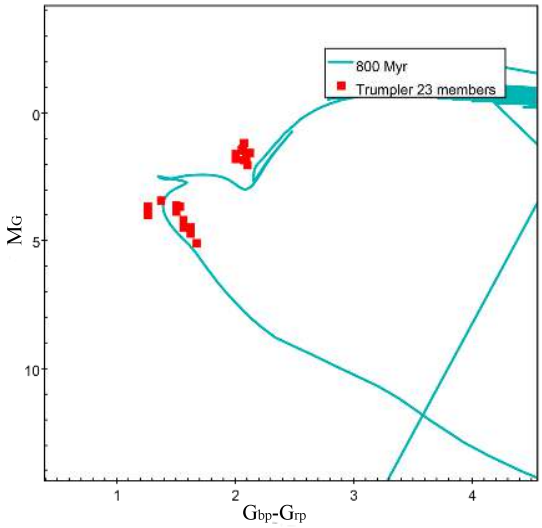

Fig. B.170. CMD for Trumpler 23.

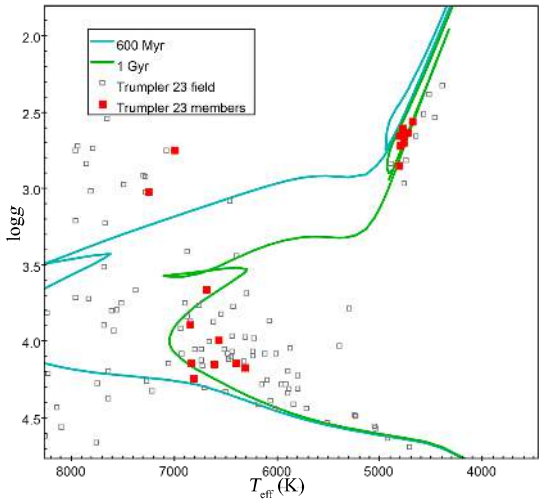

Fig. B.171. Kiel diagram for Trumpler 23.

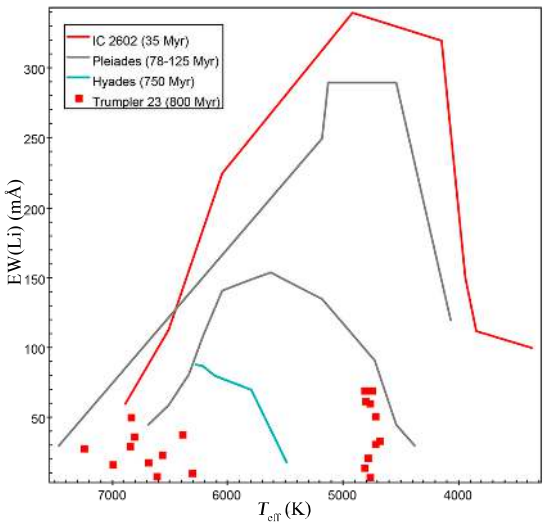

Fig. B.172. EW(Li)-versus-$T_{\rm eff}$ diagram for Trumpler 23.

Appendix B.31: Berkeley 81

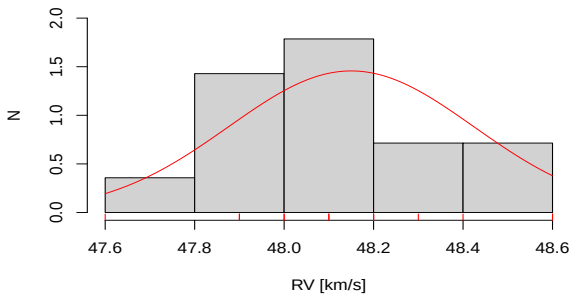

Fig. B.173. RV distribution for Berkeley 81.

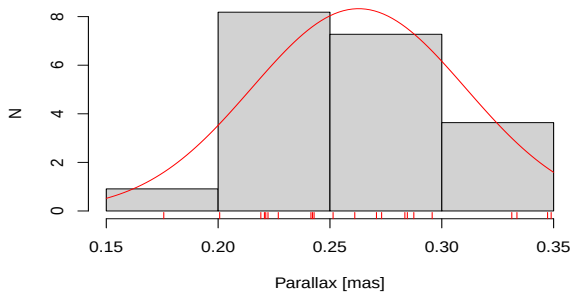

Fig. B.174. Parallax distribution for Berkeley 81.

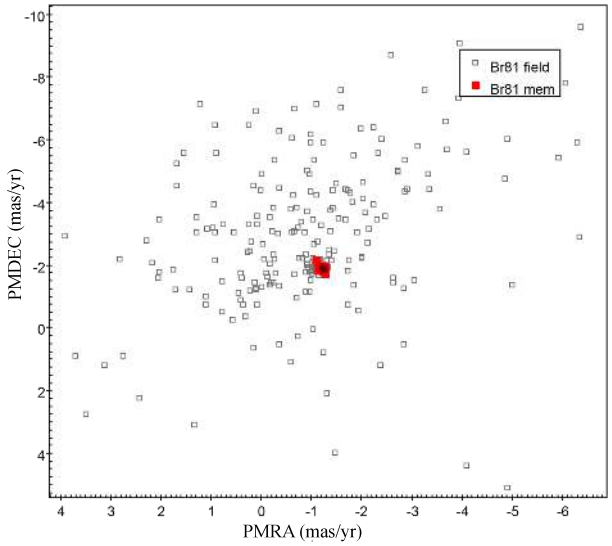

Fig. B.175. PMs diagram for Berkeley 81

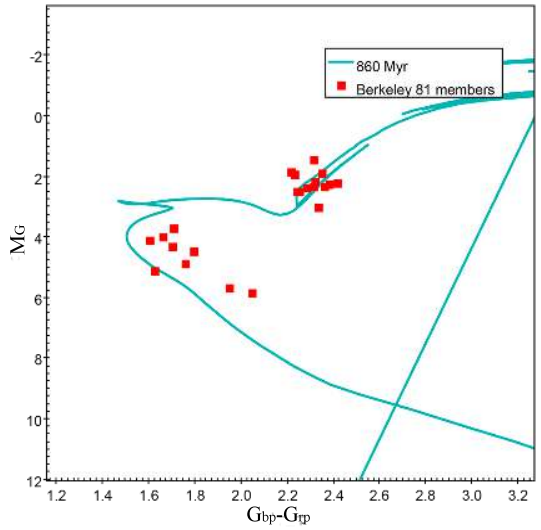

Fig. B.176. CMD for Berkeley 81.

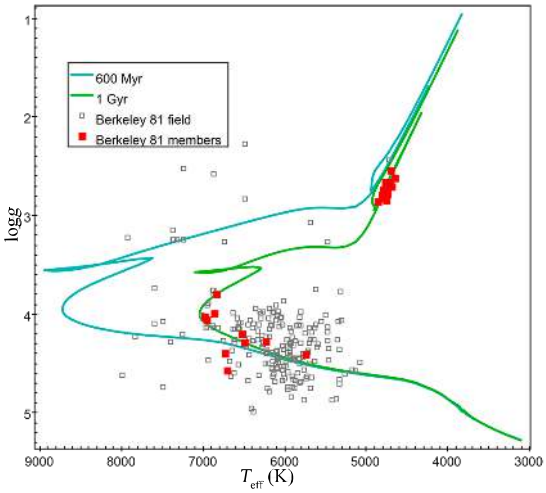

Fig. B.177. Kiel diagram for Berkeley 81.

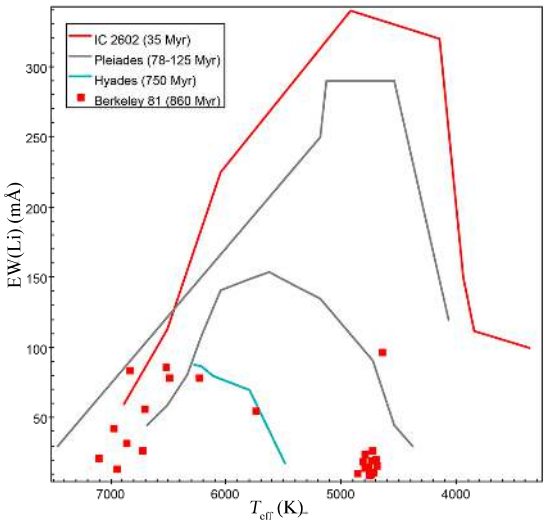

Fig. B.178. EW(Li)-versus-$T_{\rm eff}$ diagram for Berkeley 81.

Appendix B.32: NGC 2355

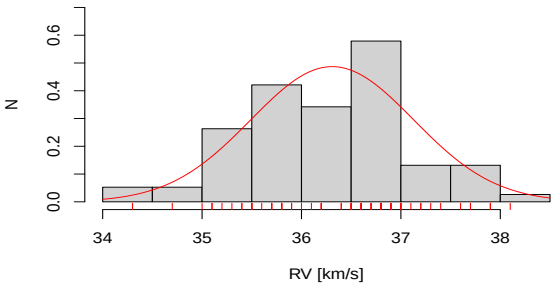

Fig. B.179. RV distribution for NGC 2355.

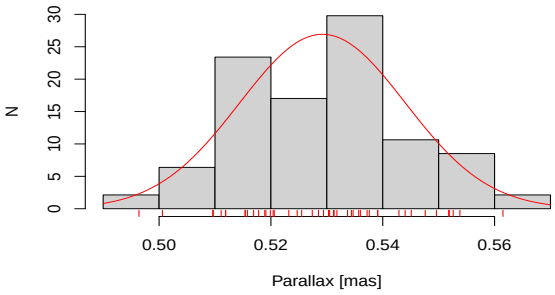

Fig. B.180. Parallax distribution for NGC 2355.

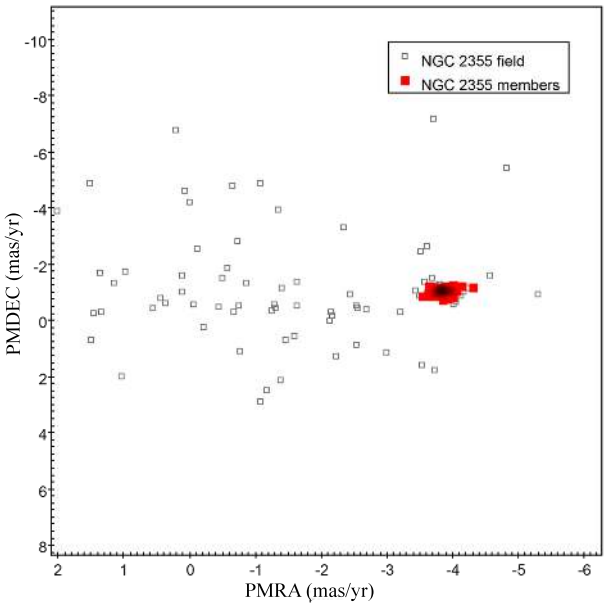

Fig. B.181. PMs diagram for NGC 2355.

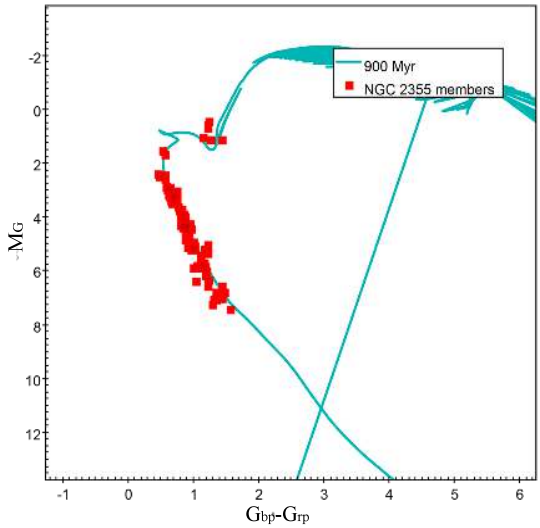

Fig. B.182. CMD for NGC 2355.

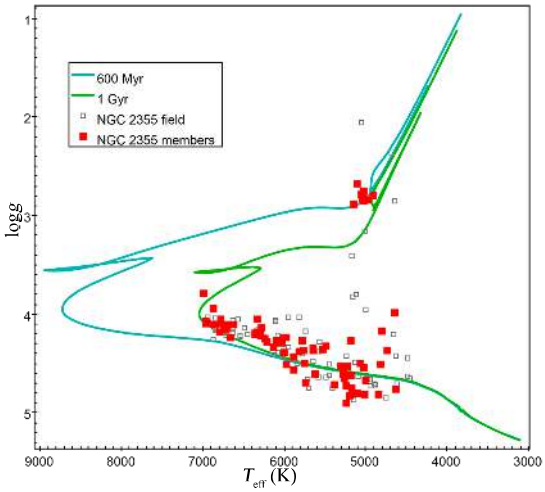

Fig. B.183. Kiel diagram for NGC 2355.

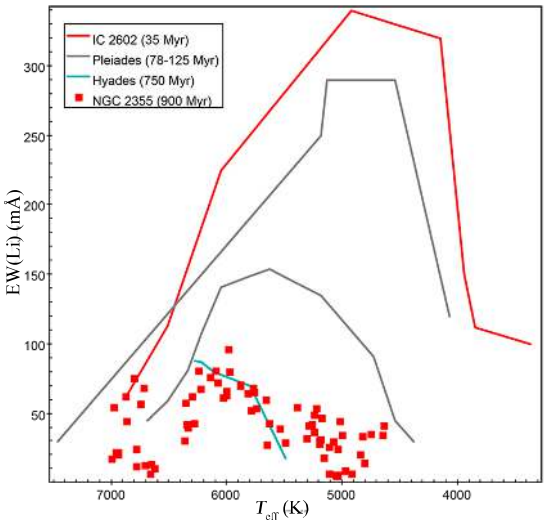

Fig. B.184. EW(Li)-versus-$T_{\rm eff}$ diagram for NGC 2355.

Appendix B.33: NGC 6802

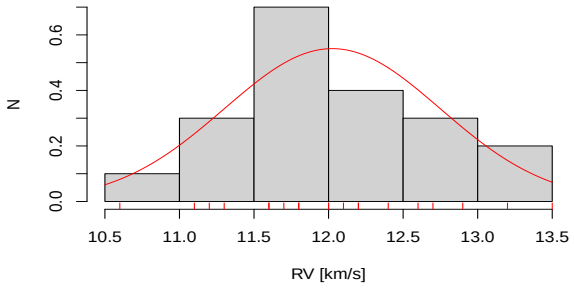

Fig. B.185. RV distribution for NGC 6802.

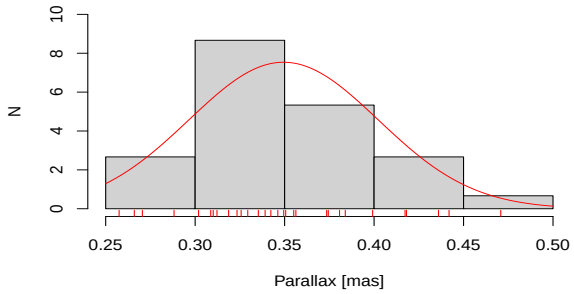

Fig. B.186. Parallax distribution for NGC 6802.

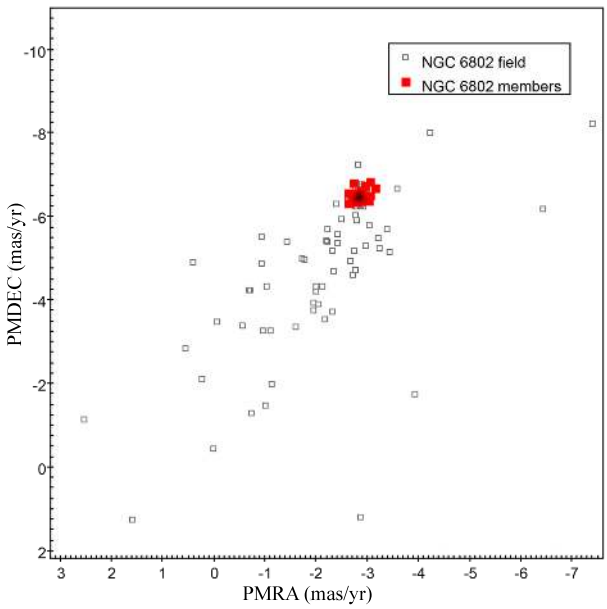

Fig. B.187. PMs diagram for NGC 6802.

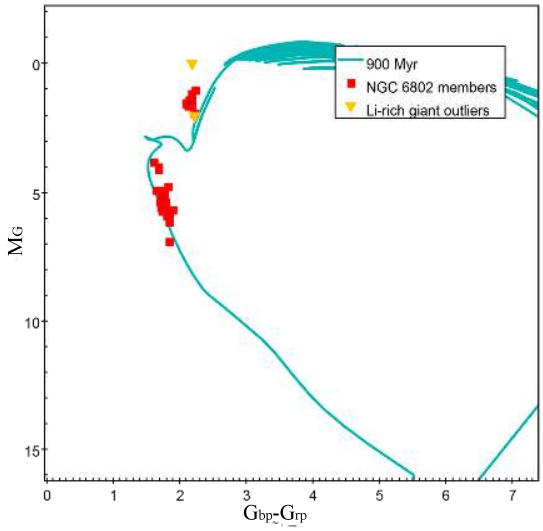

Fig. B.188. CMD for NGC 6802.

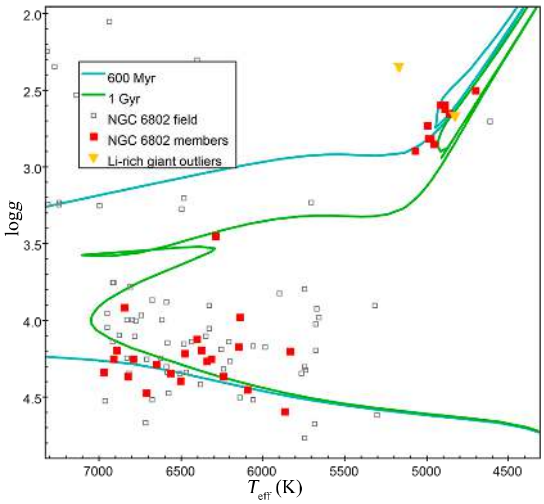

Fig. B.189. Kiel diagram for NGC 6802.

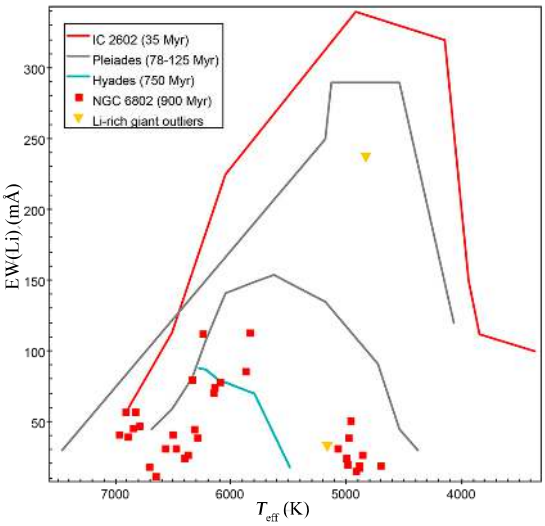

Fig. B.190. EW(Li)-versus-$T_{\rm eff}$ diagram for NGC 6802.

Appendix B.34: NGC 6005

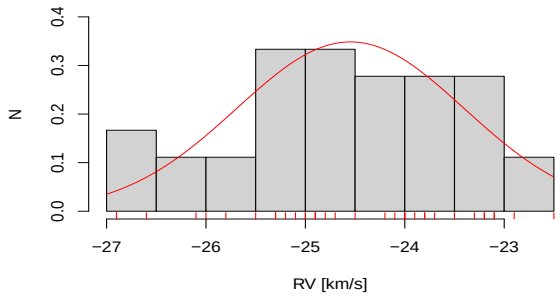

Fig. B.191. RV distribution for NGC 6005.

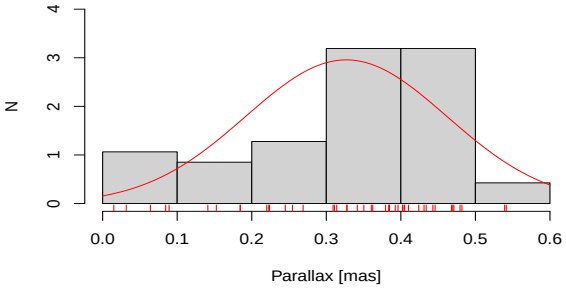

Fig. B.192. Parallax distribution for NGC 6005.

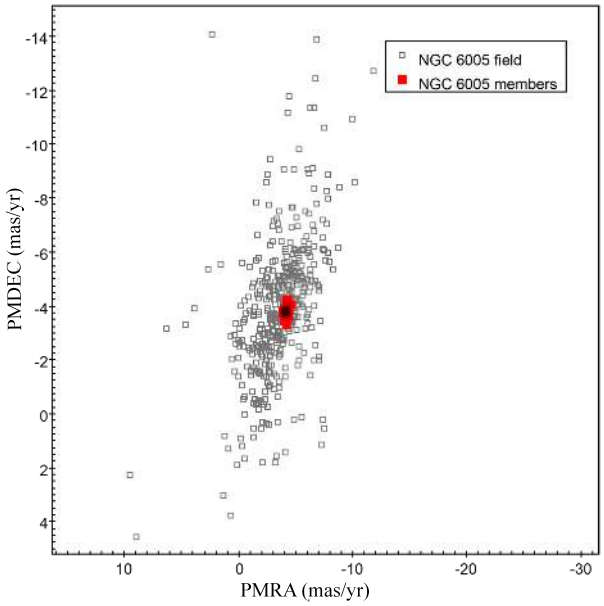

Fig. B.193. PMs diagram for NGC 6005.

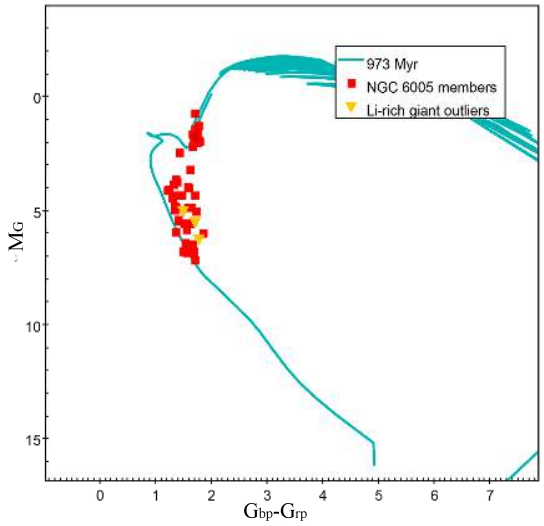

Fig. B.194. CMD for NGC 6005.

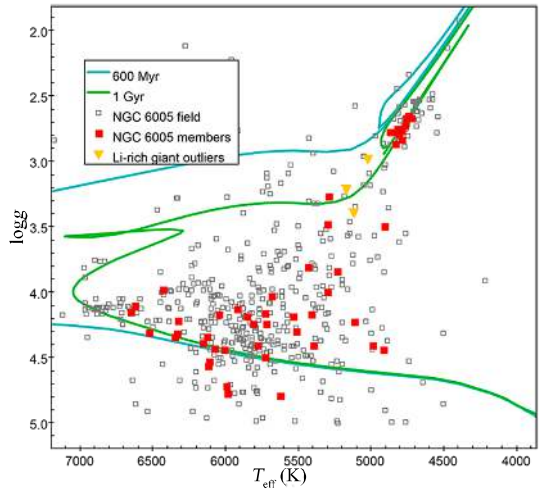

Fig. B.195. Kiel diagram for NGC 6005.

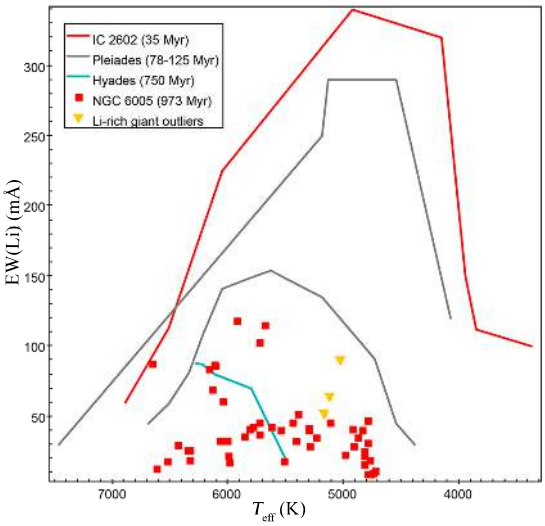

Fig. B.196. EW(Li)-versus-$T_{\rm eff}$ diagram for NGC 6005.

Appendix B.35: Pismis 18

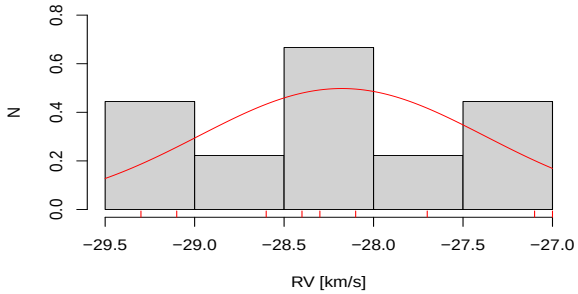

Fig. B.197. RV distribution for Pismis 18.

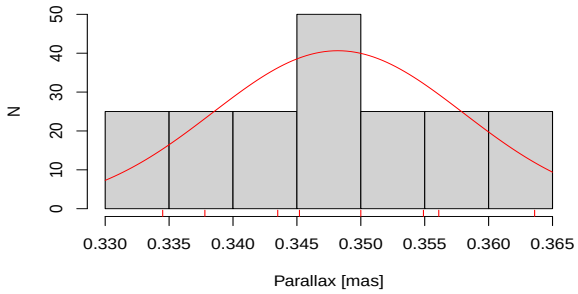

Fig. B.198. Parallax distribution for Pismis 18.

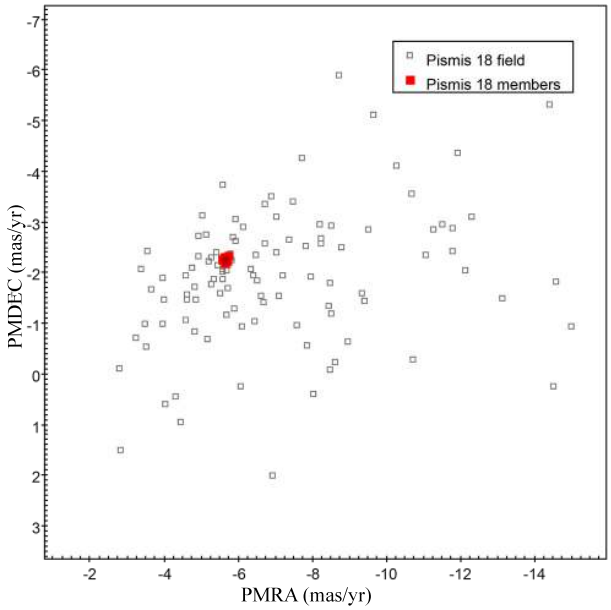

Fig. B.199. PMs diagram for Pismis 18.

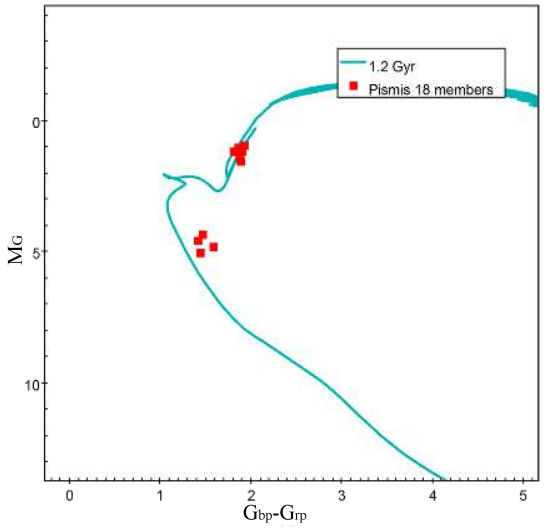

Fig. B.200. CMD for Pismis 18.

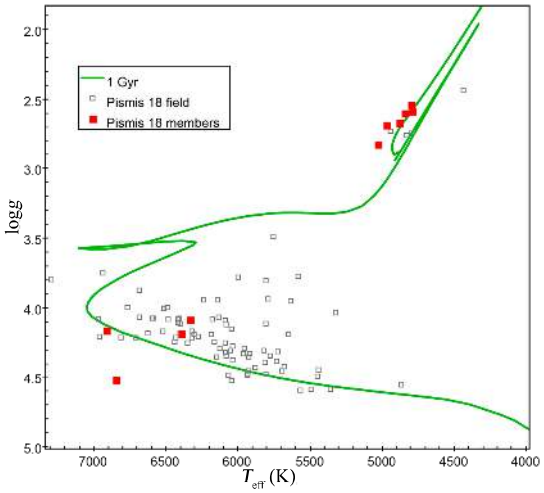

Fig. B.201. Kiel diagram for Pismis 18.

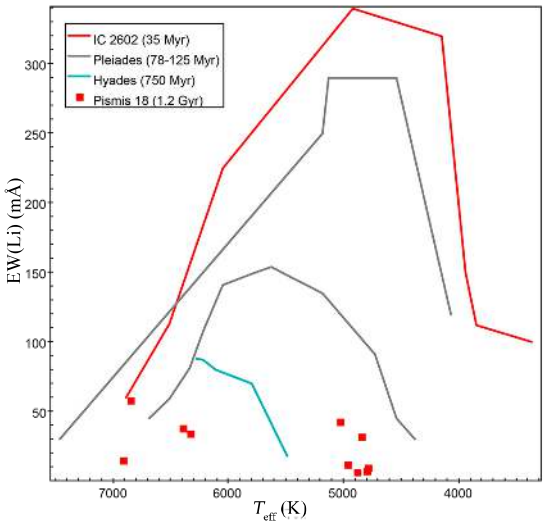

Fig. B.202. EW(Li)-versus-$T_{\rm eff}$ diagram for Pismis 18.

Appendix B.36: Melotte 71

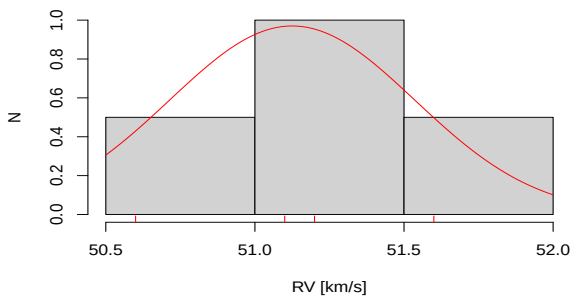

Fig. B.203. RV distribution for Melotte 71.

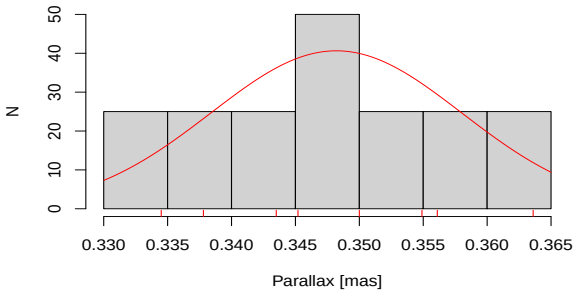

Fig. B.204. Parallax distribution for Melotte 71.

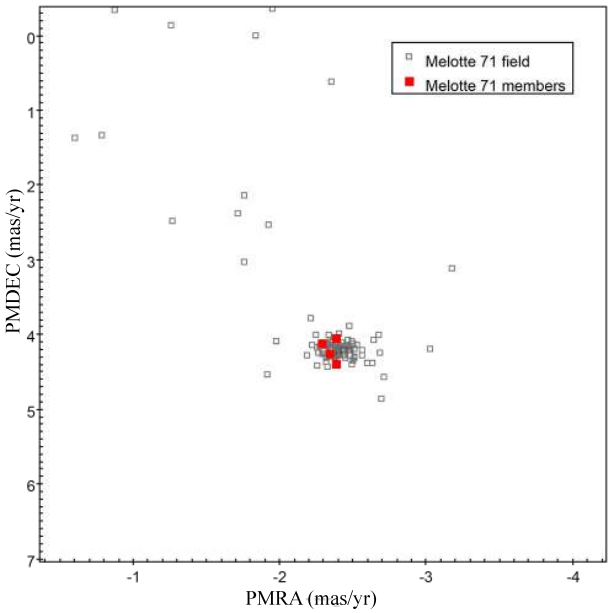

Fig. B.205. PMs diagram for Melotte 71.

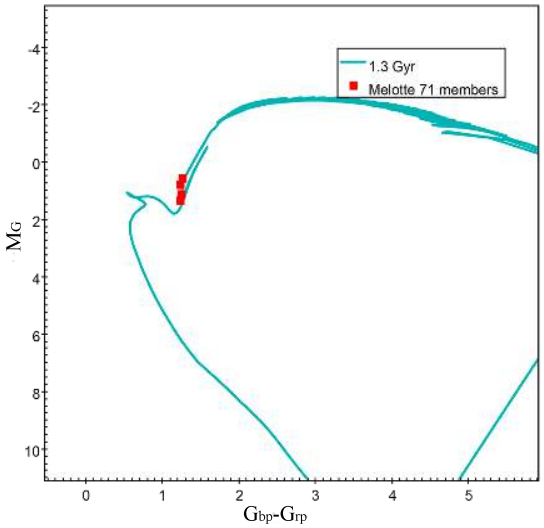

Fig. B.206. CMD for Melotte 71.

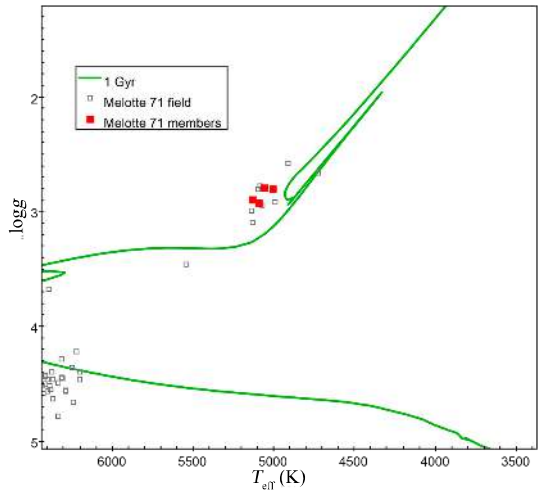

Fig. B.207. Kiel diagram for Melotte 71.

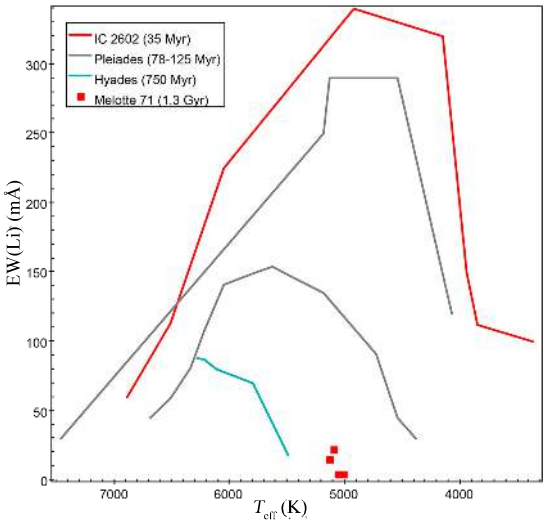

Fig. B.208. EW(Li)-versus-$T_{\rm eff}$ diagram for Melotte 71.

Appendix B.37: Pismis 15

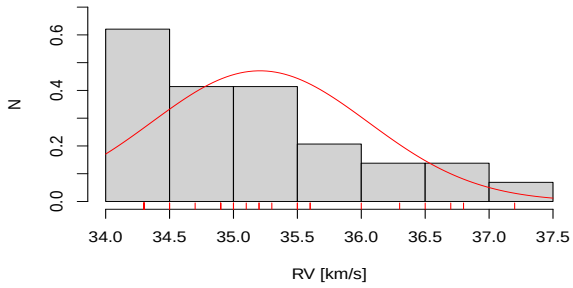

Fig. B.209. RV distribution for Pismis 15.

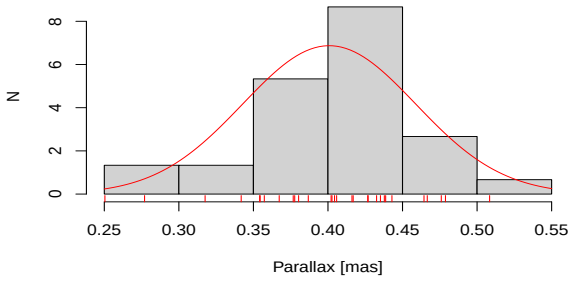

Fig. B.210. Parallax distribution for Pismis 15.

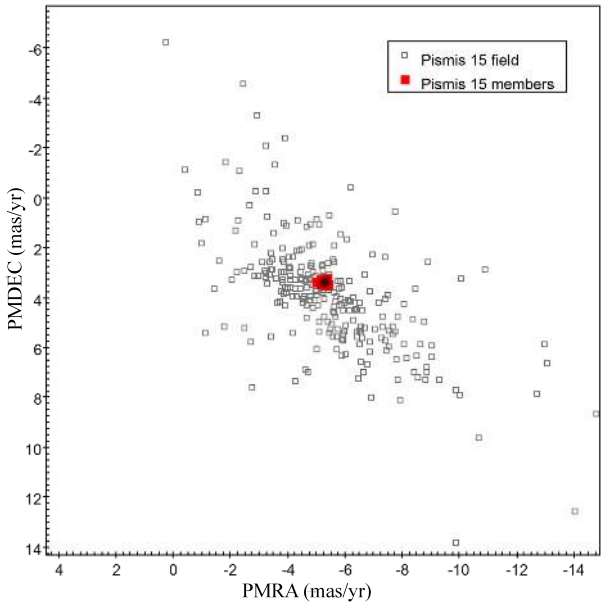

Fig. B.211. PMs diagram for Pismis 15.

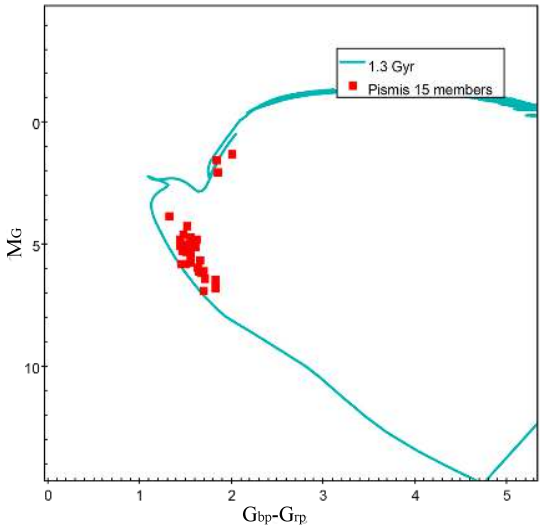

Fig. B.212. CMD for Pismis 15.

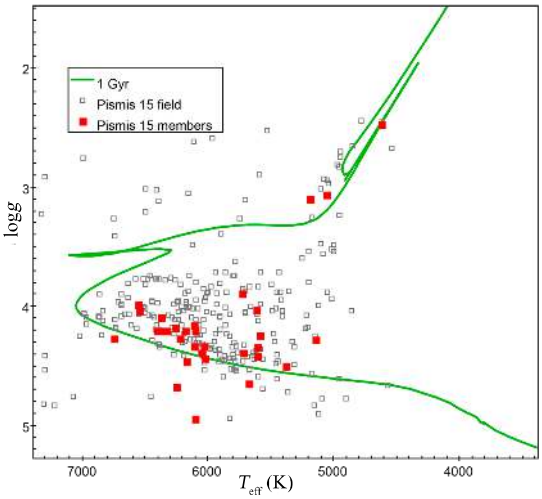

Fig. B.213. Kiel diagram for Pismis 15.

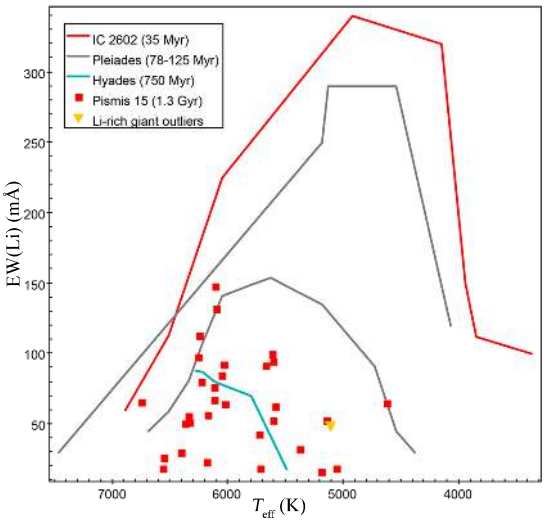

Fig. B.214. EW(Li)-versus-$T_{\rm eff}$ diagram for Pismis 15.

Appendix B.38: Trumpler 20

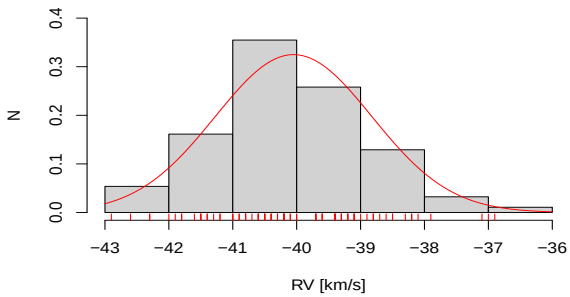

Fig. B.215. RV distribution for Trumpler 20.

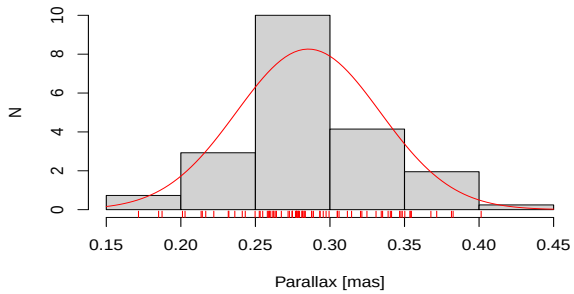

Fig. B.216. Parallax distribution for Trumpler 20.

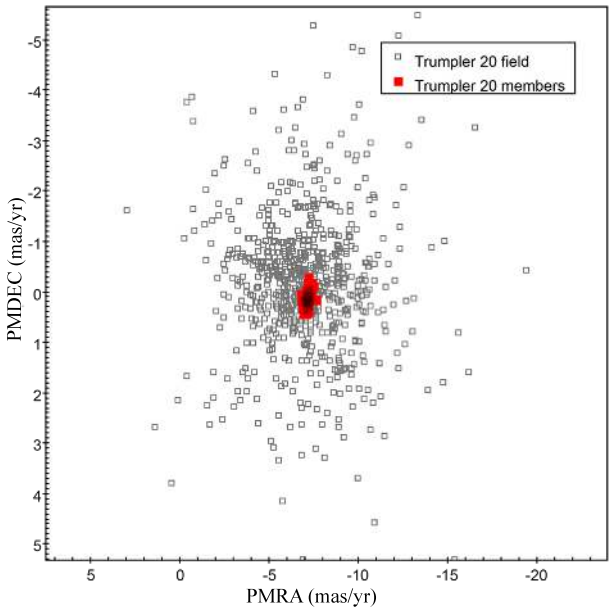

Fig. B.217. PMs diagram for Trumpler 20.

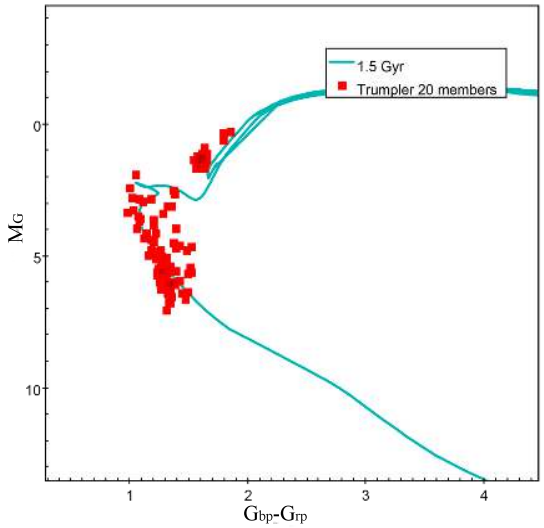

Fig. B.218. CMD for Trumpler 20.

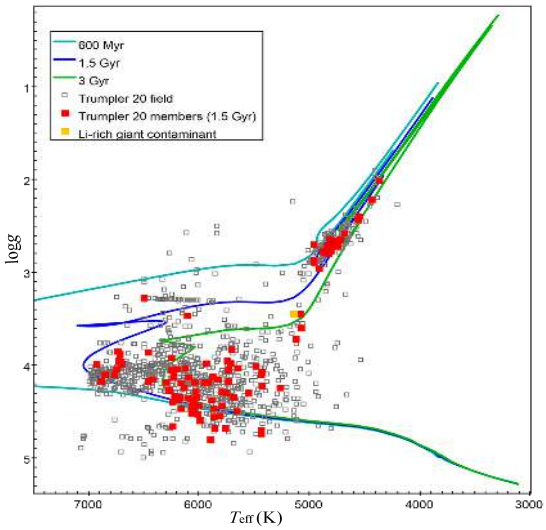

Fig. B.219. Kiel diagram for Trumpler 20.

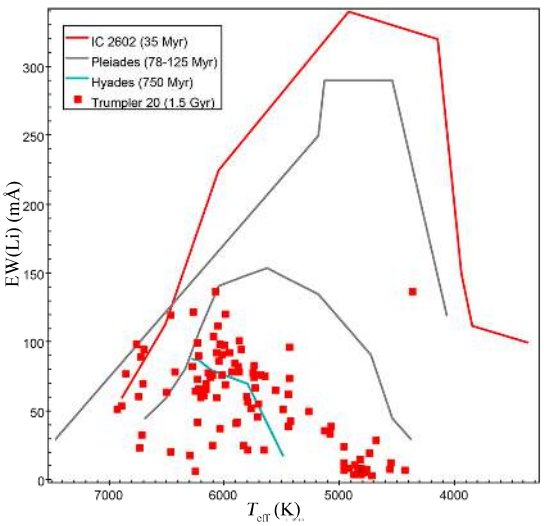

Fig. B.220. EW(Li)-versus-$T_{\rm eff}$ diagram for Trumpler 20.

Appendix B.39: Berkeley 44

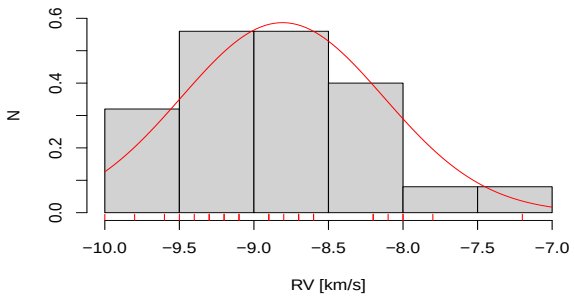

Fig. B.221. RV distribution for Berkeley 44.

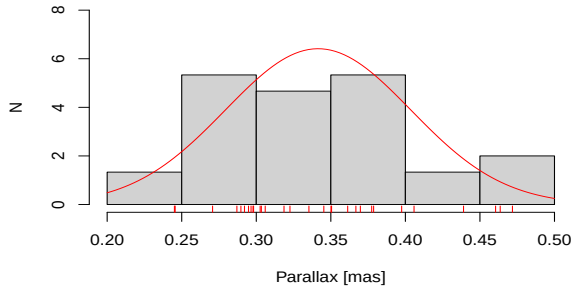

Fig. B.222. Parallax distribution for Berkeley 44.

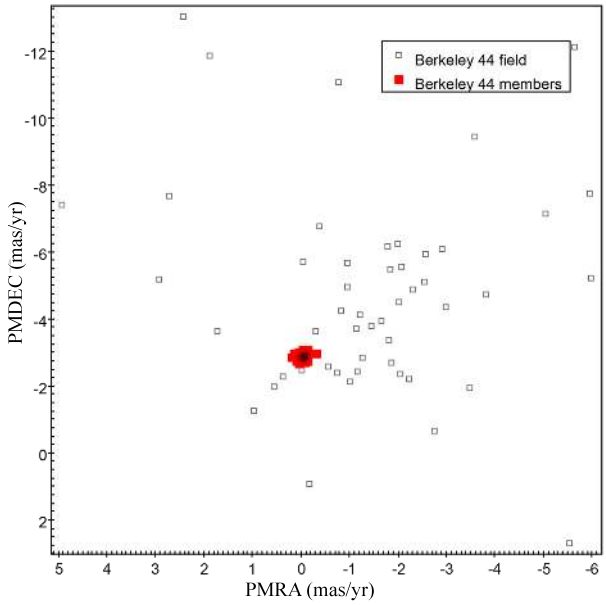

Fig. B.223. PMs diagram for Berkeley 44.

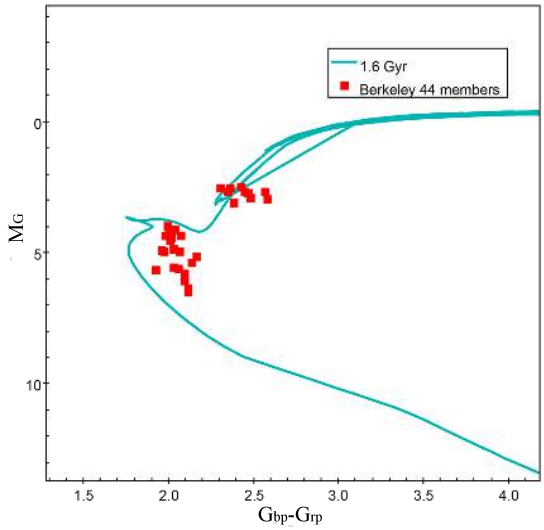

Fig. B.224. CMD for Berkeley 44.

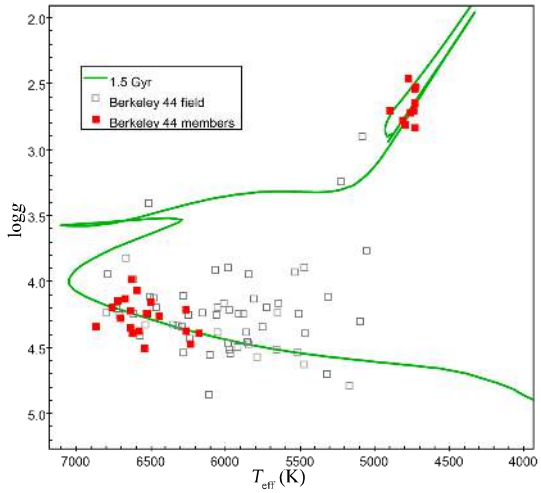

Fig. B.225. Kiel diagram for Berkeley 44.

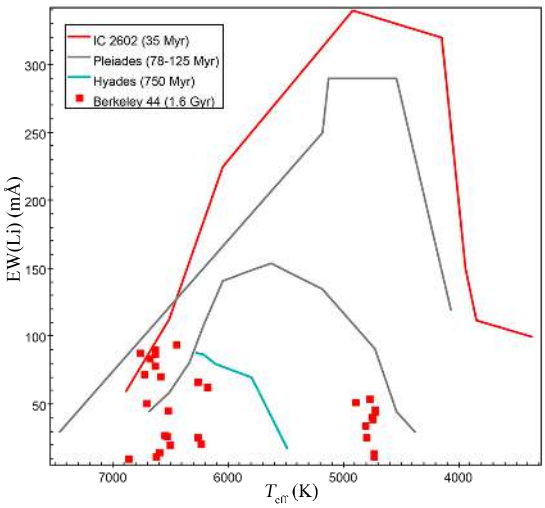

Fig. B.226. EW(Li)-versus-$T_{\rm eff}$ diagram for Berkeley 44.

Appendix B.40: NGC 2243

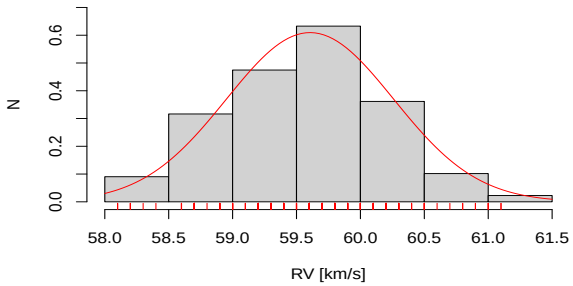

Fig. B.227. RV distribution for NGC 2243.

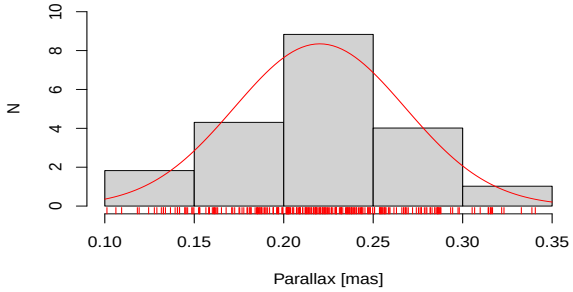

Fig. B.228. Parallax distribution for NGC 2243.

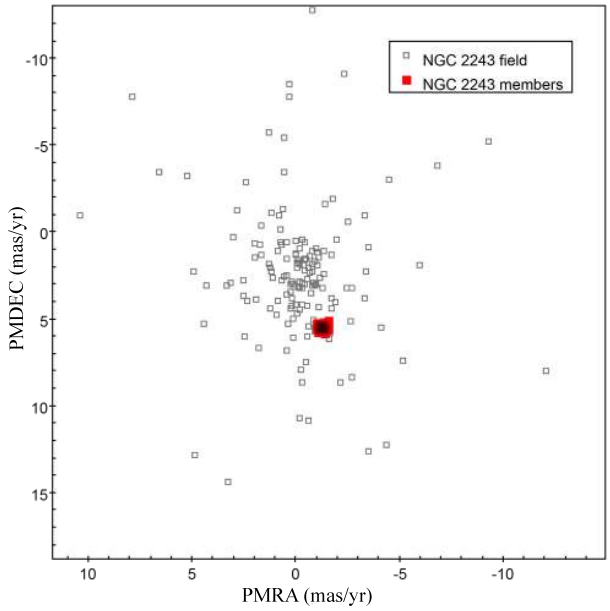

Fig. B.229. PMs diagram for NGC 2243.

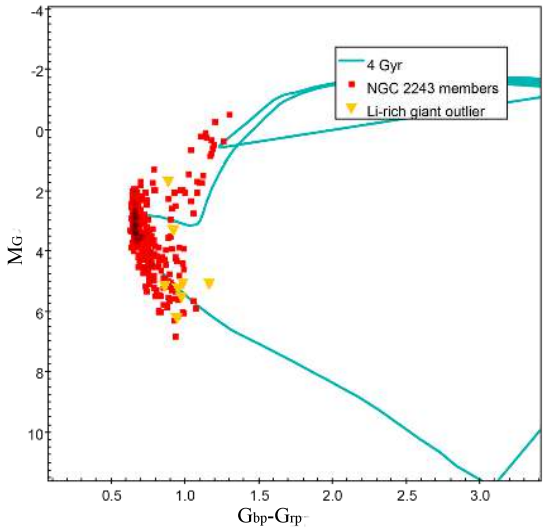

Fig. B.230. CMD for NGC 2243.

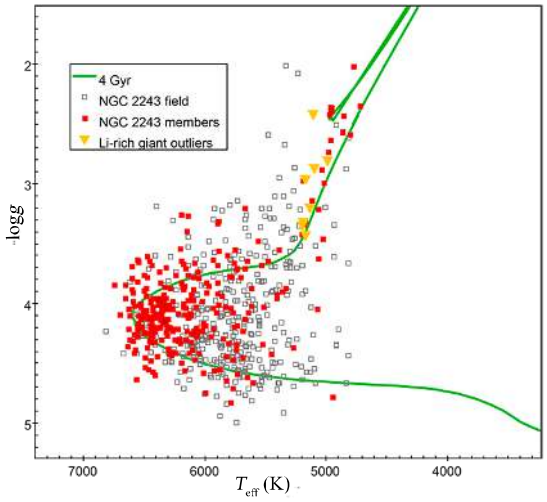

Fig. B.231. Kiel diagram for NGC 2243.

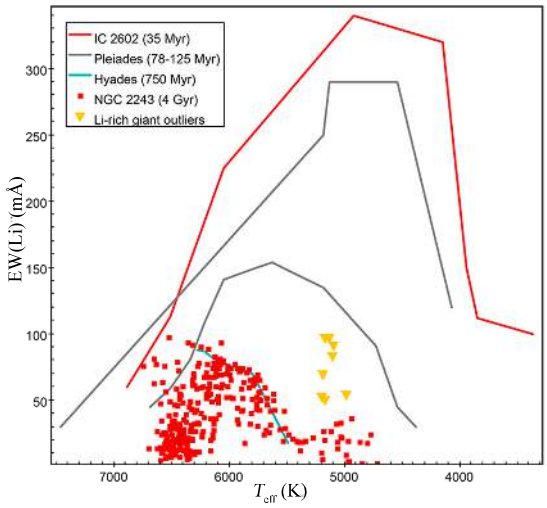

Fig. B.232. EW(Li)-versus-$T_{\rm eff}$ diagram for NGC 2243.

Appendix B.41: M67

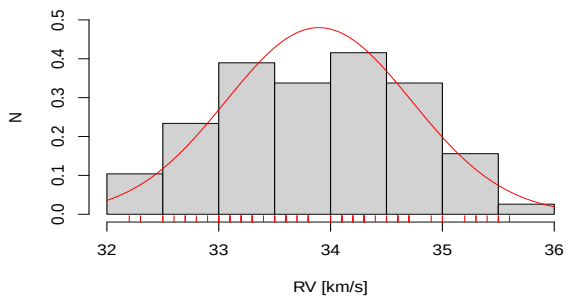

Fig. B.233. RV distribution for M67.

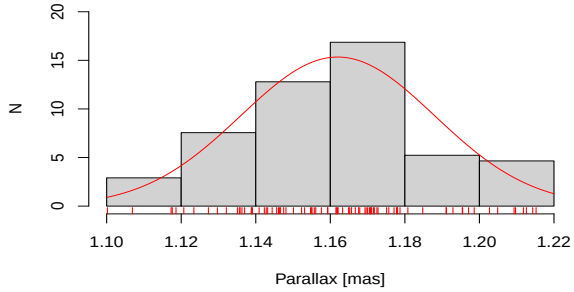

Fig. B.234. Parallax distribution for M67.

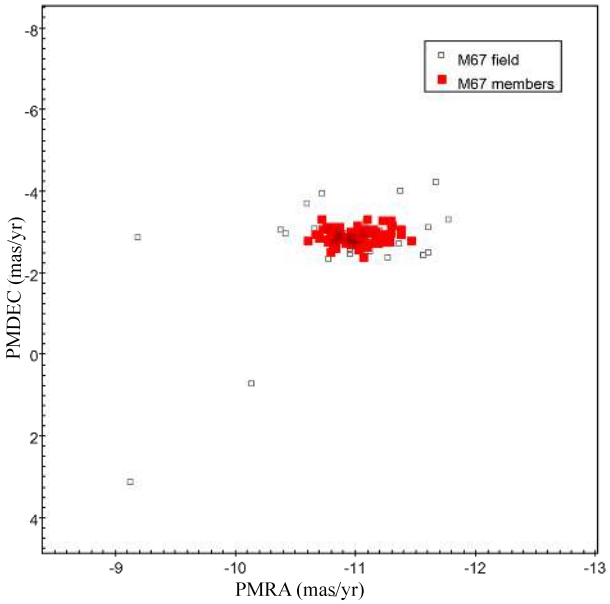

Fig. B.235. PMs diagram for M67.

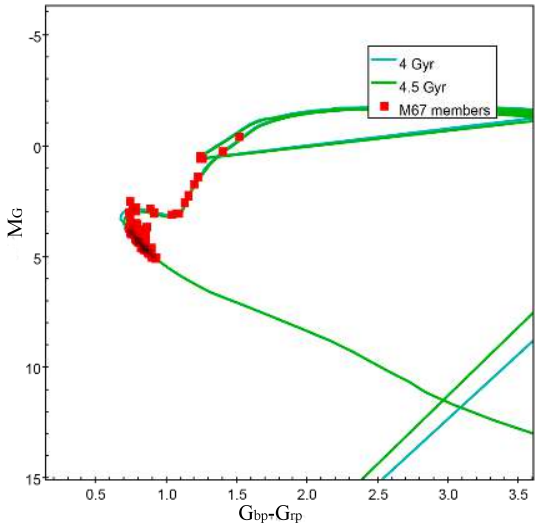

Fig. B.236. CMD for M67.

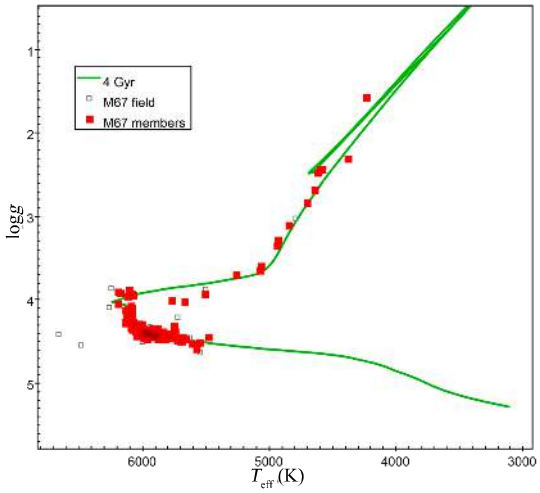

Fig. B.237. Kiel diagram for M67.

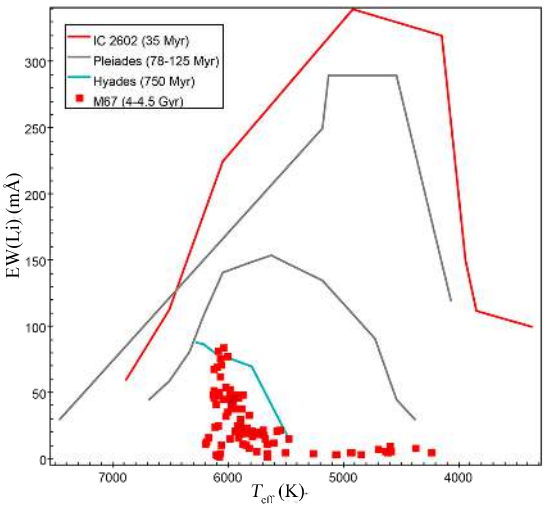

Fig. B.238. EW(Li)-versus-$T_{\rm eff}$ diagram for M67.

Appendix C: Cluster membership and final selections: Long tables

This appendix describes the long tables containing all the parameters from GES and *Gaia* which we have used throughout this work, as well as the tables summarizing the membership analysis of Sect. 3 and the final cluster selections for each of the 42 clusters in the sample. The full tables for all sample clusters are available in electronic form at the CDS. The columns for each table are described as follows:

Table C.1. GES parameters (see the exemplified Tables C.4 and C.5 for cluster NGC 2516).

Column name	Description
CNAME	GES object name from coordinates
RA	Right ascension in J2000 (hrs)
DEC	Declination in J2000 (deg)
VRAD	Radial velocity (km s^{-1})
E_VRAD	Error in radial velocity (km s^{-1})
VSINI	$v\sin i$ rotational velocity (km s^{-1})
E_VSINI	Error in $v\sin i$ (km s^{-1})
TEFF	Effective temperature $T_{\rm eff}$ (K)
E_TEFF	Error in $T_{\rm eff}$ (K)
TEFF_IRFM	Infrared photometric temperature (K)[(a)]
E_TEFF_IRFM	Error in infrared photometric temperature (K)
LOGG	log$g$ surface gravity (dex)[(b)]
E_LOGG	Error in log$g$ (dex)
GAMMA	γ index[(c)] (dex)
E_GAMMA	Error in γ index (dex)
FEH	[Fe/H] metallicity (dex)
E_FEH	Error in [Fe/H] metallicity (dex)
EWC_LI	Blends-corrected values of EW(Li) (mÅ)
E_EWC_LI	Error in EW(Li) (mÅ)
LIM_EWC_LI	Flag for blends-corrected EW(Li) error[(d)]
EW_LI_UNVEIL	The primarily-used veiling-corrected values of EW(Li) (mÅ)
E_EW_LI_UNVEIL	Error in EW(Li) (mÅ)
LIM_EW_LI_UNVEIL	Flag for veiling-corrected EW(Li) errors[(d)]
LI1	A(Li) neutral Li abundances in logϵ(X) (dex)
E_LI1	Error in A(Li) (dex)
EW_HA_ACC	Hα EW: accretion (Å)
E_EW_HA_ACC	Error in Hα EW: accretion (Å)
HA10	Hα10%, width of the Hα emission line at 10% peak intensity (km s^{-1})
E_HA10	Error in Hα10% (km s^{-1})
EW_HA_CHR	Hα chromospheric activity (Å)
E_EW_HA_CHR	Error in Hα chromospheric activity (Å)

Notes. [(a)]Not shown in Table C.4, primarily measured for young clusters. [(b)]Used in this work for intermediate-age and old clusters. [(c)]The empirical gravity indicator defined by Damiani et al. (2014) and used in the case of the young clusters. [(d)]0=no flag necessary; 1 = EW(Li) corrected by blends contribution using models; 2 = EW(Li) measured separately — Li line resolved, UVES only; and 3=Upper limit — no error for EW(Li) is given.

Table C.2. *Gaia* parameters and P_{rot} measurements (see the exemplified Tables C.6 and C.7 for cluster NGC 2516).

Column name	Description
CNAME	GES object name from coordinates
parallax	π parallax (mas)
parallax_error	Error in parallax (mas)
pmra	*pmra*, PM in RA (mas yr^{-1})
pmra_error	Error in *pmra* (mas yr^{-1})
pmdec	*pmdec*, PM in DEC (mas yr^{-1})
pmdec_error	Error in *pmdec* (mas yr^{-1})
ruwe	RUWE renormalized unit weight error
phot_g_mean_mag	G photometric band (mag)
phot_bp_mean_mag	$G_{\rm BP}$ photometric band (mag)
phot_rp_mean_mag	$G_{\rm RP}$ photometric band (mag)
phot_g_mean_mag_error	Error in G photometric band (mag)
phot_bp_mean_mag_error	Error in $G_{\rm BP}$ photometric band (mag)
phot_rp_mean_mag_error	Error in $G_{\rm RP}$ photometric band (mag)
bp_rp	Obtained *Gaia* G_{bp-rp} colour index (mag)
Mg	Obtained absolute magnitude $M_{\rm G}$ (mag)
Prot	P_{rot} measurements, when available (d)

Table C.3. Membership analysis and candidate selections (see the exemplified Table C.8 for cluster NGC 2516).

Column name	Description
CNAME	GES object name from coordinates
RV_mem	Membership: *RV*
PM_mem	Membership: Proper motions
Parallax_mem	Membership: Parallax
CMD_mem	Membership: CMD
logg_mem	Membership: *logg* (intermediate-age and old clusters)
gamma_mem	Membership: γ index (young clusters)
Met_mem	Membership: [Fe/H] metallicity
Li_mem	Membership: *EW*(Li)
Cantat_Gaudin_2018	Members from Cantat-Gaudin et al. (2018) [a]
Randich_2018	Members from Randich et al. (2018) [a]
Jackson_2021_MEM3D	Members from Jackson et al. (2022) [a], [b]
Jackson_2021_MEMQG	Members from Jackson et al. (2022) [a], [c]
Final	Final candidate members [d]
Particular_cases	Final column listing particular cases [e]

Notes. [a]Additional columns, whenever possible, listing candidates according to relevant *Gaia* studies from the literature. [b]Jackson et al. (2022) — MEM3D refers to the membership using the full data set. [c]Jackson et al. (2022) — MEMQC refers to the probability computed using data set filtered to remove targets with suspect *Gaia* data. [d]'Y'=members; 'n'=Non-members. [e]Particular cases include the Li-rich giant outliers (listed as 'Li-rich G'), strong accretors ('Strong accretor'), and the SB1 and SB2 binary stars ('SB1' and 'SB2') listed by GES iDR6 and Merle et al. (2017, 2020).

Table C.4. NGC 2516 GES parameters (I)[(a)].

CNAME	RA (hrs)	DEC (deg)	RV (km s^{-1})	$v$sin$i$ (km s^{-1})	$T_{\rm eff}$ (K)	log g (dex)	γ (dex)	[Fe/H]
07515457-6047568	117.98	-60.80	6.8 ± 0.4	11.1 ± 1.2	4369 ± 76	4.90 ± 0.18	0.920 ± 0.009	0.00 ± 0.09
07515966-6047220	118.00	-60.79	25.8 ± 0.3	< 7.0	4233 ± 78	4.69 ± 0.18	0.907 ± 0.005	0.06 ± 0.10
07520129-6043233	118.01	-60.72	14.5 ± 0.8	...	...	...	0.830 ± 0.023	...
07520389-6050116	118.02	-60.84	25.5 ± 0.3	< 7.0	4256 ± 76	4.90 ± 0.18	0.892 ± 0.005	0.05 ± 0.09
07521002-6044245	118.04	-60.74	25.5 ± 0.3	< 7.0	4153 ± 76	4.74 ± 0.18	0.893 ± 0.005	0.00 ± 0.09
07521382-6047151	118.06	-60.79	24.2 ± 0.3	< 7.0	3993 ± 77	4.75 ± 0.18	0.861 ± 0.007	-0.02 ± 0.10
07521911-6039241	118.08	-60.66	-7.4 ± 0.5	14.6 ± 2.5	3189 ± 96	4.95 ± 0.23	0.824 ± 0.015	-0.38 ± 0.09
07522464-6043006	118.10	-60.72	-4.1 ± 0.6	15.5 ± 2.6	3845 ± 77	4.56 ± 0.18	0.876 ± 0.014	-0.14 ± 0.09
07523060-6049134	118.13	-60.82	23.4 ± 0.4	< 7.0	3444 ± 108	4.88 ± 0.24	0.812 ± 0.012	-0.29 ± 0.09
07523629-6046405	118.15	-60.78	31.2 ± 0.5	< 7.0	3883 ± 107	4.85 ± 0.24	0.815 ± 0.013	-0.08 ± 0.08
07524604-6039537	118.19	-60.66	23.7 ± 0.3	< 7.0	4141 ± 76	4.76 ± 0.18	0.888 ± 0.005	0.00 ± 0.09
07525994-6053288	118.25	-60.89	23.4 ± 0.3	10.0 ± 1.1	4053 ± 76	4.92 ± 0.18	0.844 ± 0.008	-0.03 ± 0.10
07530001-6042137	118.25	-60.70	5.7 ± 0.4	9.0 ± 1.2	3921 ± 77	4.69 ± 0.18	0.856 ± 0.009	-0.01 ± 0.10
07530057-6048094	118.25	-60.80	24.1 ± 0.3	9.0 ± 1.0	3913 ± 75	4.80 ± 0.18	0.838 ± 0.007	-0.08 ± 0.09
07530259-6050259	118.26	-60.84	28.4 ± 1.0	84.3 ± 1.3	...	...	0.962 ± 0.004	...
07531031-6046400	118.29	-60.78	23.3 ± 0.4	13.3 ± 1.2	3623 ± 110	4.87 ± 0.23	0.830 ± 0.012	-0.27 ± 0.09
07531177-6041390	118.30	-60.69	23.4 ± 0.4	8.4 ± 1.3	3841 ± 108	4.84 ± 0.23	0.836 ± 0.010	-0.11 ± 0.09
07531326-6043422	118.31	-60.73	3.6 ± 0.3	< 7.0	3972 ± 77	4.79 ± 0.18	0.858 ± 0.007	0.01 ± 0.09
07532107-6058131	118.34	-60.97	22.4 ± 0.5	10.5 ± 1.1	3879 ± 108	4.85 ± 0.23	0.838 ± 0.014	-0.08 ± 0.09
07532163-6102129	118.34	-61.04	23.5 ± 0.4	9.3 ± 1.6	3620 ± 108	4.84 ± 0.23	0.826 ± 0.011	-0.22 ± 0.09
...	...	...	...	...	...	...	...	...
...	...	...	...	...	...	...	...	...
...	...	...	...	...	...	...	...	...

Notes. [(a)]This is a truncated table showing the first 20 rows.

Table C.5. NGC 2516 GES parameters (II)[(a)].

CNAME	EW(Li) (blends-corrected) (mÅ)	*EW*(Li) error flag	EW(Li) (veiling-corrected) (mÅ)	EW(Li) error flag [c]	*A*(Li) (dex)	Hα (accretion) (Å)	Hα10% (km s^{-1})	Hα (activity) (Å)
07515457-6047568	< 22	3	< 22	3	< 0.2	...	...	...
07515966-6047220	...	...	75 ± 5	0	0.6 ± 0.1	0.82 ± 0.07	94.81 ± 1.79	1.78 ± 0.14
07520129-6043233	...	...	108 ± 24	0	...	...	...	...
07520389-6050116	< 13	3	13 ± 6	0	< -0.4	...	...	0.78 ± 0.09
07521002-6044245	...	...	39 ± 6	0	-0.1 ± 0.3	0.16 ± 0.07	106.61 ± 6.58	0.92 ± 0.09
07521382-6047151	...	...	86 ± 7	0	0.4 ± 0.2	0.19 ± 0.11	119.19 ± 9.95	1.08 ± 0.14
07521911-6039241	...	...	127 ± 15	0	< -1.0	...	...	...
07522464-6043006	...	...	84 ± 15	0	0.0 ± 0.3	0.42 ± 0.32	...	1.71 ± 0.35
07523060-6049134	...	...	128 ± 13	0	-0.7 ± 0.5	0.76 ± 0.14	...	1.61 ± 0.16
07523629-6046405	...	...	117 ± 14	0	0.4 ± 0.3	...	...	0.18 ± 0.16
07524604-6039537	...	...	35 ± 6	0	-0.3 ± 0.4	0.25 ± 0.07	96.33 ± 2.59	1.22 ± 0.12
07525994-6053288	...	...	70 ± 8	0	0.4 ± 0.2	0.26 ± 0.09	114.25 ± 33.15	1.12 ± 0.16
07530001-6042137	...	...	80 ± 9	0	0.2 ± 0.2	...	...	0.09 ± 0.07
07530057-6048094	...	...	57 ± 8	0	-0.2 ± 0.3	...	...	0.49 ± 0.08
07530259-6050259	...	...	< 9	3	...	0.45 ± 0.11	241.81 ± 37.44	1.51 ± 0.13
07531031-6046400	...	...	98 ± 13	0	-0.3 ± 0.5	1.47 ± 0.19	97.84 ± 3.38	2.59 ± 0.21
07531177-6041390	...	...	126 ± 10	0	0.5 ± 0.2	0.22 ± 0.11	92.52 ± 2.90	1.13 ± 0.16
07531326-6043422	...	...	74 ± 7	0	0.2 ± 0.2	...	...	0.08 ± 0.07
07532107-6058131	...	...	129 ± 14	0	0.6 ± 0.2	1.99 ± 0.27	132.89 ± 10.14	3.46 ± 0.35
07532163-6102129	...	...	101 ± 12	0	-0.5 ± 0.6	2.14 ± 0.19	119.94 ± 6.70	3.28 ± 0.36
...	...	...	...	...	...	...	...	...
...	...	...	...	...	...	...	...	...
...	...	...	...	...	...	...	...	...

Notes. [(a)]This is a truncated table showing the first 20 rows.

Table C.6. NGC 2516 *Gaia* parameters[(a)].

CNAME	π (mas)	*pmra* (mas yr^{-1})	*pmdec* (mas yr^{-1})	RUWE error	G (mag)	G_{BP} (mag)	G_{RP} (mag)	G_{BP-RP} (mag)	M_G (mag)
07515457-6047568	2.560 ± 0.027	-5.73 ± 0.04	10.74 ± 0.03	1.0	15.752 ± 0.003	16.573 ± 0.004	14.868 ± 0.004	1.71	7.79
07515966-6047220	2.435 ± 0.032	-3.93 ± 0.04	11.10 ± 0.04	1.0	15.965 ± 0.003	16.848 ± 0.006	15.037 ± 0.004	1.81	7.90
07520129-6043233	2.111 ± 0.061	-24.60 ± 0.09	28.61 ± 0.08	1.0	17.420 ± 0.003	18.653 ± 0.017	16.347 ± 0.006	2.31	9.04
07520389-6050116	2.462 ± 0.028	-4.19 ± 0.04	11.49 ± 0.03	1.0	15.928 ± 0.003	16.807 ± 0.005	15.012 ± 0.004	1.79	7.88
07521002-6044245	2.403 ± 0.032	-4.83 ± 0.04	11.49 ± 0.04	1.1	16.087 ± 0.003	16.998 ± 0.006	15.149 ± 0.004	1.85	7.99
07521382-6047151	2.457 ± 0.042	-4.62 ± 0.06	10.61 ± 0.05	1.0	16.604 ± 0.003	17.642 ± 0.008	15.599 ± 0.005	2.04	8.56
07521911-6039241	3.613 ± 0.073	-16.21 ± 0.11	2.75 ± 0.09	1.0	17.731 ± 0.003	19.182 ± 0.020	16.564 ± 0.006	2.62	10.52
07522464-6043006	3.367 ± 0.357	-1.59 ± 0.50	0.76 ± 0.45	6.0	17.814 ± 0.003	18.607 ± 0.016	16.330 ± 0.006	2.28	10.45
07523060-6049134	2.401 ± 0.068	-4.60 ± 0.10	11.72 ± 0.08	1.0	17.514 ± 0.003	18.877 ± 0.024	16.376 ± 0.006	2.50	9.42
07523629-6046405	1.731 ± 0.063	-3.34 ± 0.09	-0.66 ± 0.10	0.9	17.441 ± 0.003	18.664 ± 0.022	16.370 ± 0.006	2.29	8.63
07524604-6039537	2.443 ± 0.030	-3.98 ± 0.04	10.94 ± 0.04	1.0	16.127 ± 0.003	17.047 ± 0.007	15.183 ± 0.005	1.86	8.07
07525994-6053288	2.500 ± 0.045	-4.32 ± 0.06	11.44 ± 0.06	1.0	16.696 ± 0.003	17.794 ± 0.009	15.666 ± 0.005	2.13	8.69
07530001-6042137	2.030 ± 0.043	-14.78 ± 0.06	13.56 ± 0.06	1.1	16.685 ± 0.003	17.722 ± 0.009	15.687 ± 0.004	2.03	8.22
07530057-6048094	2.441 ± 0.048	-4.25 ± 0.07	10.88 ± 0.07	1.1	16.779 ± 0.003	17.899 ± 0.008	15.711 ± 0.005	2.19	8.72
07530259-6050259	2.435 ± 0.028	-4.12 ± 0.04	10.96 ± 0.04	1.0	15.852 ± 0.003	16.709 ± 0.006	14.935 ± 0.006	1.77	7.78
07531031-6046400	2.531 ± 0.060	-3.41 ± 0.09	12.14 ± 0.09	0.9	17.420 ± 0.003	18.765 ± 0.022	16.297 ± 0.006	2.47	9.44
07531177-6041390	2.328 ± 0.049	-4.75 ± 0.07	12.04 ± 0.07	1.0	17.006 ± 0.003	18.124 ± 0.012	15.956 ± 0.006	2.17	8.84
07531326-6043422	2.142 ± 0.037	-2.38 ± 0.05	7.98 ± 0.06	1.0	16.508 ± 0.003	17.506 ± 0.008	15.521 ± 0.004	1.99	8.16
07532107-6058131	2.412 ± 0.048	-4.36 ± 0.07	11.44 ± 0.06	1.0	16.858 ± 0.003	18.016 ± 0.014	15.795 ± 0.005	2.22	8.77
07532163-6102129	2.392 ± 0.053	-4.02 ± 0.07	11.32 ± 0.08	1.0	17.175 ± 0.003	18.430 ± 0.017	16.080 ± 0.006	2.35	9.07
...	...	...	...	...	...	...	...	...	...
...	...	...	...	...	...	...	...	...	...
...	...	...	...	...	...	...	...	...	...

Notes. [(a)]This is a truncated table showing the first 20 rows.

Table C.7. NGC 2516 P_{rot} measurements[(a)].

CNAME	P_{rot} (d) Irwin et al. (2007)	P_{rot} (d) Wright et al. (2011)	P_{rot} (d) Jackson et al. (2016)	P_{rot} (d) Fritzewski et al. (2020)
07515457-6047568	...	...	...	...
07515966-6047220	...	...	...	...
07520129-6043233	...	...	...	...
07520389-6050116	...	...	...	...
07521002-6044245	...	...	...	...
07521382-6047151	...	...	...	...
07521911-6039241	...	...	...	...
07522464-6043006	...	...	...	...
07523060-6049134	...	...	...	...
07523629-6046405	...	...	...	...
07524604-6039537	...	...	...	...
07525994-6053288	5.66	...	5.66	5.66
07530001-6042137	...	...	...	...
07530057-6048094	11.61	...	11.61	11.61
07530259-6050259	...	...	4.58	...
07531031-6046400	...	...	2.52	...
07531177-6041390	4.58	...	4.58	4.58
07531326-6043422	...	...	...	...
07532107-6058131	2.52	...	2.52	2.52
07532163-6102129	2.34	...	2.34	2.34
...	...	...	...	...
...	...	...	...	...
...	...	...	...	...

Notes. [(a)]This is a truncated table showing the first 20 rows.

Table C.8. NGC 2516 membership analysis and selection[(a)].

CNAME	Membership							Cantat-Gaudin et al (2018)	Randich et al (2018)	Jackson et al (2021)		Final members	Particular cases
	γ	RV	PMs	π	CMD	[Fe/H]	EW(Li)			MEM3D	MEMQG		
07515457-6047568	N	…	…	…	…	…	…	…	N	0.5901	0.5542	n	…
07515966-6047220	Y	Y	Y	Y	Y	Y	Y	Y	Y	0.9991	0.9991	Y	…
07520129-6043233	N	…	…	…	…	…	…	…	Y	0	0	…	…
07520389-6050116	Y	Y	Y	Y	Y	Y	Y	Y	Y	0.9997	0.9997	Y	…
07521002-6044245	Y	Y	Y	Y	Y	Y	Y	Y	Y	0.9998	0.9998	Y	…
07521382-6047151	Y	Y	Y	Y	Y	Y	Y	N	Y	0.9999	0.9999	Y	…
07521911-6039241	N	…	…	…	…	…	…	…	N	0	0	n	…
07522464-6043006	N	…	…	…	…	…	…	…	N	0	-1	n	…
07523060-6049134	Y	Y	Y	Y	Y	Y	Y	…	Y	0.9999	0.9999	Y	…
07523629-6046405	N	…	…	…	…	…	…	…	Y	0	0	n	…
07524604-6039537	Y	Y	Y	Y	Y	Y	Y	Y	Y	0.9999	0.9999	Y	…
07525994-6053288	Y	Y	Y	Y	Y	Y	Y	…	Y	1	1	Y	…
07530001-6042137	N	…	…	…	…	…	…	…	N	0	0	n	…
07530057-6048094	Y	Y	Y	Y	Y	Y	Y	…	Y	0.9999	1	Y	…
07530259-6050259	N	…	…	…	…	…	…	Y	Y	0.9967	0.9971	…	…
07531031-6046400	Y	N	…	…	…	…	…	…	Y	0.99	0.9854	n	…
07531177-6041390	Y	Y	Y	Y	Y	Y	Y	…	Y	0.9998	0.9999	Y	…
07531326-6043422	N	…	…	…	…	…	…	…	N	0	0	n	…
07532107-6058131	Y	Y	Y	Y	Y	Y	Y	…	Y	0.9999	0.9999	Y	…
07532163-6102129	Y	Y	Y	Y	Y	Y	Y	Y	Y	0.9999	0.9999	Y	…
…	…	…	…	…	…	…	…	…	…	…	…	…	…
…	…	…	…	…	…	…	…	…	…	…	…	…	…
…	…	…	…	…	…	…	…	…	…	…	…	…	…

Notes. [(a)]This is a truncated table showing the first 20 rows.